



**Meiner Familie**

---

## Danksagung

An dieser Stelle möchte ich all jenen danken, die mich im Rahmen dieser Diplomarbeit begleitet haben. Ganz aufrichtig möchte ich mich bei meinem Betreuer, Assoc. Prof. Dipl.-Ing. Dr.techn. Roland Fischer für seine fachliche und auch persönliche Unterstützung bedanken. Ein großes Dankeschön widme ich dir auch für die Gespräche abseits der Chemie!

Besonderen Dank möchte ich auch allen Kommilitonen und Kommilitoninnen am Institut für Anorganische Chemie widmen, im speziellen Dipl.-Ing. Thomas Hafner, Dipl.-Ing. Judith Biedermann und MSc. Stefan Stadlbauer, die durch ihre fachliche Expertise und ihre Menschlichkeit einen großen Beitrag zur Untermauerung dieser Diplomarbeit leisteten. Außerdem möchte ich ein großes Dankeschön an Ing. Barbara Seibt, Astrid Falk und Monika Filzwieser richten, deren organisatorischen und auch forschungsspezifischen Anstrengungen ein starkes Fundament am IfAC bilden.

Für die firmenseitige Betreuung am Materials Center Leoben möchte ich auch einen besonderen Dank bei Dr. Barbara Kosednar-Legenstein und Dr. Günther Maier geltend machen, ebenso bei Clemens Kreamsner für die kurzfristige Einschulung und stetige Hilfe in Origin. In weiterer Folge möchte ich Anke Steinberger von AT&S für die Bereitstellung von Information und Material danken.

Ein aufrichtiges Danke widme ich auch meinen Freunden, die mich in den letzten fünf Jahren des Studium begleitet und unterstützt haben. Ein besonderes Danke auch an Carina, für alles.

Für die Geduld meiner Eltern während meines langjährigen Weges zum akademischen Abschluss über den Umweg eines zweiten Bildungsweges möchte ich mich auch bedanken. Ein außerordentlicher Dank gebührt auch Hildegard Birke und Anna Halla für die unterschiedlichsten Unterstützungen in der Heimat.

---

## Statutory Declaration

I declare that I have authored this thesis independently, that I have not used other than the declared sources / resources, and that I have explicitly indicated all material which has been quoted either literally or by content from the used sources. The text document uploaded to TUGRAZonline is identical to the present master's thesis.

## Eidesstattliche Erklärung

Ich erkläre an Eides statt, dass ich die vorliegende Arbeit selbstständig verfasst, andere als die angegebenen Quellen/Hilfsmittel nicht benutzt, und die den benutzten Quellen wörtlich und inhaltlich entnommenen Stellen als solche kenntlich gemacht habe. Das in TUGRAZonline hochgeladene Textdokument ist mit der vorliegenden Masterarbeit identisch.

Graz 16.02.2018

Date, Datum

Barbara Steiner

Signature, Unterschrift

---

## Abstract

Electronic devices are of essential necessity for human beings. The rising demand for high-performance electronics yields stronger efforts concerning bottom-down processes and subsequently higher knowledge about lifetime assessment and quality ensurance for microelectronics as well as for high-voltage applications. Target of this thesis is to gain information about diffusion of gaseous and aqueous species, preferably oxygen and water, in glass reinforced epoxy resin cores, causing certain fatal failures in printed circuit boards. By designing and fabricating a multi purpose custom built diffusion cell, several valuable data sets will be recorded, providing associate industrial partners information to tighten their knowledge about the "Conductive Anodic Filament" (CAF), which is a not yet very well known error occuring in circuit boards. Since the demand for electronically powered cars raises continuously, the PCB-manufacturers are forced to provide insulated circuitry packages of voltages beyond 500 V - associated electronic dropouts could tremendously endanger the economic success of the manufacturer in charge. Beyond ascertaining penetrant's rate of diffusion by gravimetical analysis, the electrokinetic potential analysis ( $\zeta$ -potential) might offer knowledge about materials surface chemistry, which in reverse conclusion enforces the theoretical approaches towards conductive anodic filament.

---

## Kurzfassung

Die Elektronik ist aus heutiger Sicht ein nicht mehr wegzudenkendes Grundbedürfnis der Menschheit. Der steigende Bedarf an Hochtechnologie im Bereich der Elektronik erfordert enervierende Anstrengungen zugunsten der Miniaturisierung (Nanometerbereich) dieser Elemente, welche jedoch starken Einfluss auf die Lebensdauer und die daran gebundene Qualitätssicherung ausübt. Im Zuge dieser Diplomarbeit sollen Informationen über die schadensbeschleunigenden Auswirkungen der Diffusion gasförmiger und wässriger Medien in glasverstärkten Epoxidharz-Komposit-Materialien gemessen und evaluiert werden. Zur Bestimmung der Permeabilität soll zudem eine Messzelle entwickelt werden, die über die Kapazitäten verfügt, unter hermetischen Bedingungen eine Vielzahl an Evaluierungsmethoden zu gestatten. Diese Messdaten sollen in ausgewerteter Form Aufschluss über die Entstehung des leitenden anodischen Filament-Wachstums ("CAF - Conductive Anodic Filament") in Leiterplatten geben. Dieses sich latent evolvierende Filament innerhalb einer Leiterplatte bewirkt irreversible und gefährliche Ausfälle elektronischer Geräte. Durch die starke Nachfrage in der E-Mobilität sind Leiterplattenhersteller gezwungen, ihre Produkte an die leistungstechnischen Grenzen von über 500 V zu treiben - dadurch assoziierte Ausfälle in der Elektronik äußerten sich in einer existenzgefährdenden Causa für den entsprechenden Dienstleister. Um weitere Parameter über die Entstehung von CAF zu generieren, werden neben der im Mittelpunkt stehenden gravimetrischen Diffusions-Bestimmung die elektrokinetischen Potentiale ( $\zeta$ -Potentiale) der Materialien gemessen. Diese sollen Aufschluss über die Oberflächenchemie des Komposits geben, um in weiterer Folge kombinatorische Effekte für die Entstehung des CAF zu liefern.

# Content

Acknowledgement . . . . .	I
Statutory Declaration . . . . .	II
Abstract . . . . .	III
Kurzfassung . . . . .	IV
<b>1 Theoretical Aspects</b>	<b>1</b>
1.1 Diffusion . . . . .	1
1.2 Adsorption . . . . .	6
1.3 Drying Agents . . . . .	8
1.4 Gravimetical Analysis . . . . .	9
1.5 Electrokinetic Potential . . . . .	11
1.6 Electronics - Construction and Design . . . . .	14
1.6.1 Electronic Components . . . . .	14
1.6.2 Printed Circuit Boards . . . . .	15
1.7 Conductive Anodic Filament . . . . .	21
1.8 Mean-Time-To-Failure Formula (MTTF) . . . . .	38
1.9 Cooperative Studies . . . . .	40
1.9.1 Oxygen Transmission Rate - Joanneum Research . . . . .	40
1.9.2 Surface Insulation Resistance Measurements - Joanneum Research	41
1.9.3 Simulation of Influencing Parameters on the Electric Field - Ma- terials Center Leoben . . . . .	45
<b>2 Experimental Section</b>	<b>47</b>
2.1 Introduction - Research Focus . . . . .	47
2.1.1 Matter of Interest . . . . .	48
2.2 Development of an Evaluation Environment . . . . .	49
2.2.1 Diffusion Cell . . . . .	50
2.2.2 IR-Diffusion Cell . . . . .	52
2.2.3 Fabrication of Rapid Analysis Cells . . . . .	54
2.3 Analyte's Preparation . . . . .	55
2.3.1 Primary Analyte - GREC's . . . . .	55

2.3.1.1	1566/1570 Core Preparation . . . . .	55
2.3.1.2	Pre-Drying the GREC Cores . . . . .	55
2.3.1.3	Blank Preparation . . . . .	56
2.3.2	Secondary Analyte - Drying Agents . . . . .	56
2.3.2.1	Desiccant Selection . . . . .	57
2.4	Process of Data Evaluation . . . . .	58
2.4.1	Execution of Gravimetric Analysis . . . . .	58
2.4.2	Execution of Electrokinetic Potential Analysis . . . . .	62
2.5	Alternative Experiments and Studies for Permeability Detection . . . . .	65
<b>3</b>	<b>Results and Discussion</b>	<b>67</b>
3.1	Results' Abstract . . . . .	67
3.1.1	Gravimetric Analysis . . . . .	67
3.1.2	Electrokinetic Potential Analysis . . . . .	72
3.2	Indication Methods . . . . .	73
3.3	Pre-Drying Cores . . . . .	74
3.4	Adsorption Test . . . . .	76
3.5	Measurement Series . . . . .	77
3.5.1	Description of Abbreviations . . . . .	78
3.5.2	Preliminary Phase I - Drying Agent Improvement . . . . .	79
3.5.2.1	(R1566 <sup>100 μm</sup> - H <sub>2</sub> O)@Cell <sup>(0L, 1U'O<sub>2</sub>, 2U, 3U, 4U)</sup> - P <sub>4</sub> O <sub>10</sub> - PA 6.6 - 60 °C . . . . .	79
3.5.2.2	(R1566 <sup>100 μm</sup> - H <sub>2</sub> O)@Cell <sup>(0L, 1U'O<sub>2</sub>, 2U, 3U, 4U)</sup> - MgSO <sub>4</sub> - PA 6.6 - 60 °C . . . . .	80
3.5.2.3	(R1566 <sup>100 μm</sup> - H <sub>2</sub> O)@Cell <sup>(0L, 1U'Al, 2U, 3U, 4U)</sup> - MS 4 Å - PA 6.6 - 60 °C . . . . .	82
3.5.3	Preliminary Phase II - Insulation Enhancement . . . . .	83
3.5.3.1	(R1570 <sup>100 μm</sup> - H <sub>2</sub> O)@Cell <sup>(0L, 1o'Cu200μm, 2U, 3U, 4U)</sup> - MS 4 Å - PA 6.6 - 60 °C . . . . .	84
3.5.3.2	(R1570 <sup>Cu200 μm</sup> - H <sub>2</sub> O)@Cell <sup>(0L'sld, 1U'sld, 2U'sld, 3U, 4U)</sup> - MS 4 Å - PA 6.6 - 60 °C . . . . .	85
3.5.3.3	(R1570 <sup>Cu200 μm</sup> - H <sub>2</sub> O)@Cell <sup>(0L, 1U, 2U, 3U'sld, 4U'sld)</sup> - MS 4 Å - PA 6.6 - 60 °C . . . . .	86
3.5.3.4	(R1570 <sup>100 μm</sup> - H <sub>2</sub> O)@Cell <sup>(0L, 1U'Cu200μm, 2U, 3U, 4U)'sld</sup> - MS 4 Å - PA 6.6 - 60 °C . . . . .	87
3.5.3.5	(R1570 <sup>100 μm</sup> - H <sub>2</sub> O)@Cell <sup>(0L, 1U'Cu200 μm, 2U, 3U, 4U)'sld</sup> - MS 4 Å - SSCs - 60 °C . . . . .	88



3.5.3.6	(R1570 <sup>100 μm</sup> - H <sub>2</sub> O)@Cell <sup>(0U'd, 1U'O<sub>2</sub>'d, 2U'h, 3U'Cu200 μm'h, 4U'h)</sup> 'sld - MS 4 Å - SSCs - 60 °C . . . . .	89
3.5.4	Blank Evaluation . . . . .	90
3.5.4.1	(Aluminum <sup>H<sub>2</sub>O</sup> )@Cell <sup>(0L, 1U, 2U, 3U, 4L)</sup> 'sld - MS 4 Å - SSCs - 60 °C . . . . .	90
3.5.5	Final Phase - Adsorption Data Evaluation . . . . .	92
3.5.5.1	(R1570 <sup>100 μm</sup> - pH 7.15)@Cell <sup>(0L, 1U, 2U, 3U, 4L)</sup> 'sld - MS 4 Å - SSCs - 60 °C . . . . .	93
3.5.5.2	(R1566 <sup>100 μm</sup> - pH 7.15)@Cell <sup>(0L, 1U, 2U, 3U, 4L)</sup> 'sld - MS 4 Å - SSCs - 60 °C . . . . .	94
3.5.5.3	(R1570 <sup>100 μm</sup> - C <sub>8</sub> H <sub>5</sub> KO <sub>4</sub> @ pH 4.01)@Cell <sup>(0L, 1U, 2U, 3U, 4L)</sup> 'sld - MS 4 Å - SSCs - 60 °C . . . . .	95
3.5.5.4	(R1566 <sup>100 μm</sup> - C <sub>8</sub> H <sub>5</sub> KO <sub>4</sub> @ pH 4.01)@Cell <sup>(0L, 1U, 2U, 3U, 4L)</sup> 'sld - MS 4 Å - SSCs - 60 °C . . . . .	96
3.5.5.5	(R1570 <sup>100 μm</sup> - Na <sub>2</sub> B <sub>4</sub> O <sub>7</sub> +NaOH @ pH 9.00)@Cell <sup>(0L, 1U, 2U, 3U, 4L)</sup> 'sld - MS 4 Å - SSCs - 60 °C . . . . .	97
3.5.5.6	(R1566 <sup>100 μm</sup> - Na <sub>2</sub> B <sub>4</sub> O <sub>7</sub> +NaOH @ pH 9.00)@Cell <sup>(0L, 1U, 2U, 3U, 4L)</sup> 'sld - MS 4 Å - SSCs - 60 °C . . . . .	98
3.5.6	Reference Matter Evaluation . . . . .	99
3.5.6.1	(PET <sup>250 μm</sup> - H <sub>2</sub> O)@Cell <sup>(0L, 1U, 2U, 3U, 4L)</sup> 'sld - MS 4 Å - SSCs - 60 °C . . . . .	99
3.5.6.2	(MCE-DT <sup>40 μm</sup> - H <sub>2</sub> O)@RACell <sup>(0U, 1U, 2U, 3U, 4U)</sup> - MS 4 Å - SCGC - 22 °C . . . . .	100
3.6	Electrokinetic Potential Analysis . . . . .	101
3.6.1	R1566WN/R1570 - Blank Evaluation . . . . .	102
3.6.2	Industrial Chemicals Treatment . . . . .	103
3.6.2.1	Chemisch Kupfer - Kupferprozess (chemCu) . . . . .	103
3.6.2.2	Galvanisch Kupfer - Kupferprozess (galvCu) . . . . .	103
3.6.2.3	Etch Bath - Photo Process (CuCl <sub>2</sub> ) . . . . .	104
3.6.3	Standard Chemicals Treatment . . . . .	105
3.6.3.1	Hydrogen Peroxide (H <sub>2</sub> O <sub>2</sub> ) . . . . .	105
3.6.3.2	Sulphuric Acid (H <sub>2</sub> SO <sub>4</sub> ) . . . . .	106
3.6.3.3	Sodium Hydroxide (NaOH) . . . . .	107
3.7	ATIR Spectra Analysis . . . . .	109
3.7.1	IR - Industrial Chemicals . . . . .	112
3.7.2	IR - Standard Chemicals . . . . .	114
3.7.3	IR - Conclusion . . . . .	115

3.8	Permeability Detection by an electrochemical Method . . . . .	117
3.8.1	SEM/EDX Images . . . . .	117
3.8.2	Voltage/Current Specification . . . . .	122
<b>4</b>	<b>Conclusion and Outlook</b>	<b>124</b>
<b>5</b>	<b>Appendix</b>	<b>126</b>
5.1	Development of Supply Tools . . . . .	127
5.2	Troubleshooting - Drawbacks and Opportunities . . . . .	129
5.3	Guides . . . . .	131
5.3.1	Gravimetrical Analysis . . . . .	131
5.3.2	Elektrokinetic Analysis . . . . .	135
5.4	Data and Tables . . . . .	145
5.4.1	Drying Agents . . . . .	145
5.5	Pictures/Images . . . . .	147
5.5.1	CAF . . . . .	147
5.5.2	Diffusion Cell . . . . .	149
5.6	Engineering Drawings . . . . .	151
	<b>Bibliography</b>	<b>155</b>
	<b>Figures</b>	<b>158</b>
	<b>Tables</b>	<b>166</b>

## Abbreviations

ALT	Accelerated Life Test
AMEO	3-Aminopropyltriethoxysilane
ATIR	Attenuated Total Infrared Reflection
AT&S	Austria Technologie & Systemtechnik Aktiengesellschaft
BT	Bismaleimide Triazine (Epoxy Substrate) <sup>[41]</sup>
CE	Cyanate Esters (Epoxy Substrate) <sup>[41]</sup>
CEM-3	A Substrate Similar to G-10 Except With Chopped Glass <sup>[41]</sup>
JR	Joanneum Research
COMET	Competence Center for Excellent Technologies
CTE	Coefficient of Thermal Expansion
DAG	Drying Agent
DC	Direct Current
DGEBA	Diglycidyl Ether Bisphenol A
DHPDOPO	10-Dihydro-9-Oxa-10-Phosphaphenanthrene-10-Oxide
DICY	Dicyandiamide
EC	Ethyl Cellulose
ECM	Electrochemical Migration
EDL	Electrical Double Layer
EIS	Electrochemical Impedance Spectroscopy
ESI	Erich Schmid Institute
FFG	Forschungsförderungsgesellschaft
FR-4	Common Epoxy Matrix For PCB Fabrication
G-10	A non-fire Retardant Epoxy/Woven Glass Material <sup>[41]</sup>
Gravibox	Measuring Container including Drying Agent
GRE	Glass Reinforced Epoxy Resin Composite
GREC	Glass Reinforced Epoxy Resin Composite Core
HASL	Hot Air Soldering Leveling
HAST	Highly Accelerated Stress Test
IEP	Isoelectric Point
IPC	Institute of Printed Circuit Boards
IR	Infrared
IUPAC	International Union of Pure and Applied Chemistry
JR	Joanneum Research Materials
LOD	Limit of Detection

---

MC-2	A Blended Polyester and Epoxy Matrix with Woven Glass Face Sheets, and a Chopped Glass Core <sup>[41]</sup>
MCE-DT	Mixed Cellulose Ester - Dialysis Tube
MCL	Materials Center Leoben
mil	milli-inch (25.4 $\mu\text{m}$ )
Milli-Q	Ultrapure Water Of Type-1 (ISO 3696)
MS 4 Å	Molecular Sieve 4 Ångström
MTTF	Mean-Time-to-Failure
SHE	Standard Hydrogen Electrode
non-PTH	Non-Plated Through-hole Connection
OTR	Oxygen Transmission Rate
PC	Poly Carbonate
PCB	Printed Circuit Board
PE	Poly Ethylene
PET	Polyethylene Terephthalate
PI	Polyimide/Woven Glass <sup>[41]</sup>
PMMA	Polymethylmetacrylate
Prepreg	A Sheet Of Core Material Impregnated With A Synthetic Resin, Such As Epoxy Or Polyimide
PTH	Plated Through-hole Connection
PWB	Printed Wiring Board
RH	Relative Humidity
RT	Room Temperature
SEM	Scanning Electron Microscopy
sld	Sealed
SCGC	Sealed Chemicals Glass Container
SE	Solid Electrolyte
SEI	Solid Electrolyte Interface
SIR	Surface Insulation Resistance
SSCs	Stainless Steel Countersink
T <sub>g</sub>	Glass Transition Temperature
THF	Tetrahydrofuran
TBAI	Tetrabutyl Ammonium Iodide
TBBPA	Tetrabromobisphenol A
TUG	Technische Universtität Graz

---

# 1 Theoretical Aspects

This chapter will reveal theoretical aspects of the corresponding objectives which were executed in the practical period of this diploma thesis. The well-established literature deserves to be mentioned, even if it is retained to be a brief summary. Substantially emphasis is focused on the theory of ionic migration (electrochemical migration, ECM), which is a matter of diffusion. Both, dendritic growth and CAF are ECM associated processes. Dendritic growth is a simple electrochemical process, in which metal becomes soluble at the anode, yielding positively charged metal ions that migrate the substrate to finally re-deposit on the cathode, forming treelike dendrites. In CAF formation, metal either gets dissolved at the anode forming metal ions but early deposits by forming insoluble salts and negatively charged complexes in the presence of water and halide ions. A CAF therefore differs from dendritic growth by emanating from the anode instead of growing on the opposite electrode as native metal (see section "1.7", p. 21). CAF is a key issue for the certification of printed circuit boards and thus, priority is lead into the theory about this ECM mechanism to occur.

## 1.1 Diffusion

In the materials engineering, diffusion attained significant attention in the past. It is a major term when it comes to surface hardening for mechanical elements like gear wheels or other parts which have to hold a rigid hull at a flexible core. For example, centuries ago the Japanese earned mastery in blacksmithing high performance blades called Katana. It is crafted from a high carbon steel and processed to the favor of superior hardness at paramount flexibility properties, just by abstracting and introducing carbon by thermoforming steps. Today, diffusion plays an important role in the food industry. It is of major interest, that whether packaging material diffuse into the nutriment nor the nutriment diffuse through the encapsulating material. In many situations it is of concern to prevent oxygen and water uptake in foods. Furthermore, in the electronic industries it is necessary to avoid diffusion and absorption of moisture into integrated circuitries. In many terms within technology, diffusion can be both, a gift and a major issue, since on the one hand it can be controlled but on the other

hand it always takes place, provided a concentration gradient is present. For example everyone knows that leaving a sparkling beverage CO<sub>2</sub> (e.g. mineral water or coke) in a warm environment, gas solubility in the solution is decreased and it "effuses" out of the bottle, making the beverage dreary. Even for photographers it is a problem. Over time, in minor amounts moisture diffuses into an expensive lens. When photographing outside on chilly days, i.e. in winter, the encapsulated water condenses and this may cause lens fungus. To focus back again to the related topic, moisture permeability is assumed to have a strong impact for the formation of failures in electronic devices. Especially the CAF mechanism is a sensitive issue, which is getting some attention in this thesis.

Diffusion describes a process of the spontaneous intermixing of matter, which not only includes the net flux of ions, atoms, molecules, electrons, holes et cetera as a result of random motions. The driving forces associated to this process refer to a concentration gradient and temperature. While the random motion of atoms or molecules (Brownian motion) is familiar when thinking about the dispersion of smoke in still air, the dispersion of an ink drop in water or the classical experiment of the intermixing of superposed water to a lower iodine solution. While this seems to be legit in terms of emancipated atoms/molecules or particles in the micro-, meso- and macroscopical scale, in solid matter like polymers, crystalline structures and metals the atoms are confined to their specific location within their lattice sites. Everyday practice proves, that the latter are not strictly stuck to their position within the material. If a solid substance A is plated onto a block of a contrary part of substance B and the couple is heated, the concentration gradient enforced by elevated temperature causes interdiffusion to occur.<sup>[2, 9, 39]</sup> The prominent formula which is describing the associated dependencies of this process is called Fickian law (1.1):

$$J = -D \frac{dc}{dx} \tag{1.1}$$

where

$J$  : diffusion flux (number of atoms of type A diffusing across an unit of area of surface per second) [m<sup>-2</sup> s<sup>-1</sup>]

$D$  : diffusion coefficient [m<sup>2</sup> s<sup>-1</sup>]

$dc/dx$  : gradient in concentration  $c$  of A atoms in the  $x$  direction [m<sup>-4</sup>]

A simpler expression of the diffusion flux:

$$J = \frac{m}{At} \tag{1.2}$$

where

$J$  : Diffusion flux (e.g. mass or number of atoms [ $\text{g m}^{-2} \text{s}^{-1}$ ])

$m$  : Mass (molecular M) [kg]

$A$  : Cross-sectional area [ $\text{m}^2$ ]

$t$  : Elapsed diffusion time [ $\text{m}^{-4}$ ]

If the diffusion flux does not change with time, a steady-state condition is given. This denotes a diffusion of linear concentration profile, which is characterized by constant concentrations on both sides. It is therefore selfexplaining that in a nonsteady-state diffusion the flux and the concentration gradient at some particular point in a solid matter vary with time, a net accumulation or depletion of the diffusing species is the result.

$$D = D_0 \exp\left(-\frac{Q_d}{RT}\right) \tag{1.3}$$

where

$D$  : Diffusion flux (number of atoms of type A diffusing across an unit of area of surface per second) [ $\text{m}^{-2} \text{s}^{-1}$ ]

$D_0$  : Pre-exponential term (material related constant) [ $\text{m}^2 \text{s}^{-1}$ ]

$Q_d$  : Activation energy [ $\text{m}^{-4}$ ]

$R$  : Gas constant [ $8.3144 \text{ J mol}^{-1} \text{ K}^{-1}$ ]

$T$  : Temperature (absolute) [K]

With this brief introduction to the very elementals of diffusion the following pages will proceed with a specific overview to diffusion-related literature. This thesis focuses on glass reinforced epoxy resin composites, in which the permeation of contaminants, i.e. moisture, is of great relevance. Since only the penetrants are known, but not the materials' composition itself, the abundance of information this work can give access to is limited. What surely can be basically expected from the amorphous polymer is, that it should:

1. be electrically insulating
2. be easily fabricated to the favor of application
3. be highly impervious to the penetration of moisture and other contaminants

4. be able to form strong adhesive bonds with the wires and SMDs
5. exhibit mechanical and chemical stability for a rational lifetime
6. be simple in manufacture and installation
7. have a coefficient of thermal expansion which is similar to related mountings
8. be cost efficient
9. be fire resistant and flame retardant

Callister et al<sup>[9]</sup> provides a simple table (Fig.1.1) to the properties an IC material should exhibit.

	<i>Epoxy Resins</i>	<i>Silicones</i>	<i>Polyurethanes</i>	<i>Polysulphides</i>
Dielectric strength	Good	Good	Good	Good
Elastic modulus	High	Low	Wide range	Low
Tensile strength	High	Low	Wide range	—
Precursor viscosity	Low	Low	Low	High
Adhesion to package	Excellent	Poor (to ceramics)	Good	Good
Moisture diffusion rate	High	High	Low	Very low

Fig. 1.1: Properties of polymers used for package encapsulation.<sup>[9]</sup>

This figure already gives a hint for the common use of epoxy resins in PCB fabrication, though, moisture diffusion is rated to be high. Since absolute data are not outlined, one can hardly quantify what is meant by "high", unless this table is for packaging material, not specifically for PCBs, though. For the permeability rates of the materials obtained from AT&S refer to chapter "3.5" on p. 77. For more details it is recommended to refer to the primary literature denoted.

As aforementioned, the insulation material is a single layer of an etched GREC, which in a sandwich construction will yield a printed circuit board after several fabrication steps. The penetration of contaminants in such has a great impact to the substrates' lifetime, it is therefore of major concern to find relationship between ad- and absorbed particles (i.e. delocalized metal ions, cavities of water et cetera) foreign to the epoxy and the time to failure a devices' functionality. With the parameters gained by this permeability study, one attribute of a so called mean-time-to-failure formula (MTTF, i.e. a mathematical assessment of an average lifetime a device is presumed to provide) should be solvable. In the measurements that were carried out (see results on p. 67), the diffusion fluxes of the materials to be investigated were ascertained at



different conditions.

Closing this section with a quotation<sup>[29]</sup> will reveal a theory about mechanisms of the penetrant passing through the material.

"The diffusivity of a dilute penetrant in an amorphous polymer matrix is governed by the penetrant size and interactions with the polymer as well as by the shape, size, connectivity, and time scales of thermal rearrangement of unoccupied space within the polymer. In a high-temperature melt ( $T \gg T_d$ ), openings among chains that are capable of accommodating the penetrant undergo rapid redistribution in space. One can envision that the penetrant is "carried along" by density fluctuations caused by the thermal motion of surrounding chains. In the free-volume picture liquid-state diffusion, one could envision that a penetrant molecule resides in a certain position of the polymer matrix until the motion of surrounding chains, modified by the penetrant's presence, leads to the formation a cavity, at a distance commensurate with the penetrant's diameter, into which the penetrant can move. After the move, the cavity in which the penetrant was originally accommodated is closed. A succession of such small random moves of the penetrant constitutes diffusion. In this high-temperature melt limit, formation of a cavity of sufficient size to accommodate the penetrant can be viewed as the rate-controlling step for a move. The time scale between moves is thus set by the relaxation time of density fluctuations on the length scale of the penetrant diameter within the polymer matrix. At temperatures below  $T_g$  on the other hand, one would expect the molecular picture of diffusive jumps to be substantially different. The distribution of open spaces within the configurationally arrested glassy matrix is more or less permanent (long-lived). One can envision a network of preexisting cavities, the magnitude and shape of which fluctuates somewhat with thermal motion and is modulated by the possible presence of a penetrant molecule. A dilute penetrant spends most of its time rattling within a cavity and occasionally jumps from cavity to cavity through a "window" that opens instantaneously via fluctuations in "soft" regions (i.e., regions of lower density or enhanced molecular mobility) between the cavities. The overall diffusivity in the glass would thus depend on the distribution of distances and connectivities among the cavities as well as on the magnitude and distribution of rate constants governing the infrequent jumps of the penetrant between adjacent cavities."<sup>[29]</sup>

## 1.2 Adsorption

Adsorption per definition (IUPAC) describes the "increase in the concentration of a substance at the interface of a condensed and a liquid or gaseous layer owing to the operation of surface forces." The term should not to be confused with absorption (common use in flue gas desulfurization plants), in which an absorbate, i.e. a gas (e.g.  $\text{SO}_x$ ) is absorbed by i.e. a liquid (absorbent, e.g. aqueous  $\text{Ca}(\text{OH})_2$ ). Both, ad- and absorption are encompassed by the term sorption. The vice-versa processes are called desorption.

Adsorption is mainly divided into physi- and chemisorption. While in physisorption the bondings are related to van der Waals forces ( $\Delta_{ad}H_{\text{H}_2\text{O}}^\circ = -59 \text{ kJ mol}^{-1}$ ), in chemisorption strong chemical bondings (usually covalent) are operative.<sup>[3]</sup> The adsorption process depends on

1. chemical nature of the adsorbate
2. chemical nature of the adsorbent
3. surface accessibility (structure and chemistry) of the adsorbent
4. partial pressure of the adsorbate
5. presence of competitive adsorbates
6. temperature (isothermal)

The extent of surface coverage in adsorption is normally expressed as the fractional coverage  $\theta$  (1.4):

$$\theta = \frac{\text{number of adsorption sites occupied}}{\text{number of adsorption sites available}} \quad (1.4)$$

The formula is often expressed in terms of the volume of adsorbate adsorbed by:

$$\theta = \frac{V}{V_\infty} \quad (1.5)$$

$\theta$  : fractional coverage [1]

$V$  : volume [ $\text{m}^3$ ]

$V_\infty$  : volume of complete layer coverage [ $\text{m}^3$ ]

The rate of adsorption  $d\theta/dt$  describes the rate of change of surface coverage and can be determined by evaluating the change of fractional coverage with time. Commonly

gravimetry is utilized to ascertain the increase of mass within time. This method was primarily used for the determination of the permeation of water through the membrane, which should subsequently give the expression  $d\theta/dt = J = -D \cdot dc/dx$ . The measurements and results in this thesis are in respect to Formula 1.2.

While the environmental gas and the adsorbed gas are in dynamic equilibrium, the fractional coverage of the surface is associated with the pressure of the overlying gas. The relationship between the variation of  $\theta$  and pressure at constant temperature is called the adsorption isotherm. The Langmuir isotherm, which describes an equilibrium between reactants ad- and desorbing the substrate is based on three assumptions<sup>[3]</sup>:

1. adsorption cannot proceed beyond monolayer coverage
2. all sites are equivalent and the surface is uniform (that is, the surface is perfectly flat on a microscopic scale)
3. the ability of a molecule to adsorb at a give site is independent of the occupation of neighbouring sites (that is, there are no interactions between adsorbed molecules)

Consequently, if equilibrium reigns, no net change is observable and solving for  $\theta$  gives the Langmuir isotherm<sup>[3]</sup>:

$$\theta = \frac{Kp}{1 + Kp} \quad (1.6) \quad K = \frac{k_a}{k_d} \quad (1.7)$$

### 1.3 Drying Agents

Drying agents are chemical substances which are tending to ad- and absorb water in significant amounts to their own physical mass. The theory which involves the encapsulation of water into cavities or onto surfaces of the desiccant is inherently linked to the above-mentioned section "Adsorption". In this section, some properties of drying agents as well as their possibilities will be discussed.

Drying agents are hygroscopic substances which allow, i.e. the reduction of humidity of environmentally air or the drying of other gasses or materials. To mention some important examples, calcium chloride ( $\text{CaCl}_2$ ), phosphorous pentoxide ( $\text{P}_4\text{O}_{10}$ ) and sodium sulfate ( $\text{Na}_2\text{SO}_4$ ) are prominent in several drying applications. The aforementioned  $\text{P}_4\text{O}_{10}$  achieves quite maximal drying effects of air, becomes ineffective after forming an aqueous layer of derivatives of polyphosphorous species.<sup>[35]</sup> While drying capacity denotes the mass of absorbent the absorbate is capable to bind and store, the desiccant efficiency is related to the species of absorbent to be bound in a reasonable manner. On p.145 a table enlists many desiccants and provides further information (physisorption, chemisorption) to their possible applications.

## 1.4 Gravimetric Analysis

As one of the simplest quantitative methods in analytical investigation the analytical balance is estimated to be one of the historically oldest measurement methods. The recorded history of gravimetry goes back to Egypt 5000 BC - in the following millenniums the word "bilanx" arose from the Latin, which means "two pans".<sup>[37]</sup> The oldest known balances were discovered in Asia and Egypt. For instance, it is conveyed, that in the old Babylonia already a governmental supervising measurement office existed. As analytical references, they used stones and rocks in the shape of sacred animals. Some centuries later, copper and brass found relevance for the application as a mass standard. The oldest normalized mass pieces were parts of cylindrical shape, found in tombs in Naqada, the upper Egypt, estimated to be 5000 years in age. It is of common knowledge, that balances were the most important devices for the price evaluation of materialistic goods such as valueable metals. And not without reason today's certain balances are referred to it as gold balances.<sup>[23]</sup> To leave the historical part, a short discussion about weighing masses will be held.

Even the peoples BC knew, that there is a correlation of the visual and physical appearance of an item or substance to the afford of moving or bearing it. At least they had knowledge about the volume and the mass it contains, furthermore the ancient mathematical faculties introduced the relationship between both, which is known to be the density. To sum this up, mass is a product of the physical volume and the substances' density, yielding the following equation:

$$m = V \cdot \rho \tag{1.8}$$

where

$m$  : Mass [g]

$V$  : Volume [m<sup>3</sup>]

$\rho$  : Density [g m<sup>3</sup>]

The beam balance is the most prominent construction everyone should know, where the lever rule is describing the mathematical definition:

$$m_1 \cdot l_1 = m_2 \cdot l_2 \tag{1.9}$$

where

$m_1$  : Mass to the left of the pivotal point [g]

$m_2$  : Mass to the right of the pivotal point [g]

$l_1$  : Length of the lever left to the pivotal point [m]

$l_2$  : Length of the lever right to the pivotal point [m]

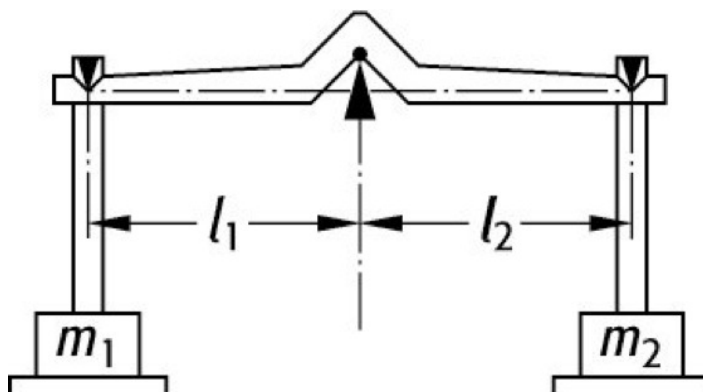


Fig. 1.2: The scheme of a beam balance showing the levers bearing their masses, being in equilibrium around the pivot.<sup>[38]</sup>

In the following eras, different variantes of the balances were developed, just to mention some, the crane weigher, the inclination balance and the spring balance (19. century), followed by the eletromechanical balances, predominantly used in the 20. century and beyond.<sup>[23]</sup>

In this thesis, gravimetrical analysis is the method to determine both the initial mass of a pre-dried drying agent and the mass of water that attaches to the desiccant over a period of time. By subtracting the latter from the tara mass, the uptake of the aqueous species will be obtained.

## 1.5 Electrokinetic Potential

The paragraphs, pictures and even styles in this section are almost exclusively cited and adopted from "The ZETA Guide - Thomas Luxbacher - Anton Paar® GmbH".<sup>[26]</sup>

Firstly observed in 1809 by Ferdinand Friedrich Reuss the migration of colloidal clay particles is assumed to be the point of origin for electrokinetic potential analysis. The electrokinetic potential, also known as zeta potential allows the determination of the charging behavior at surfaces and interfaces, respectively. Its main application, at least when looking to the majority of scientific papers, is in the characterization of solid-liquid interfaces. It is utilized in many cases, i.e. in evaluating the efficiency of membranes and filters, to rate the biocompatibility of biomaterials or how to treat semiconductors (wafers) towards hydrophilicity/hydrophobicity. It allows to get an idea of the swelling of natural and man-made fibers as well as the rinsing and washing capability of detergents and properties of cosmetics.

In theory, the electrochemical double layer (EDL) is used to describe the charging behavior (surfaces charges that nullifies themselves at the isoelectric point, abbreviated by IEP) at solid-liquid interfaces and therefore the definition of the zeta potential is stated.

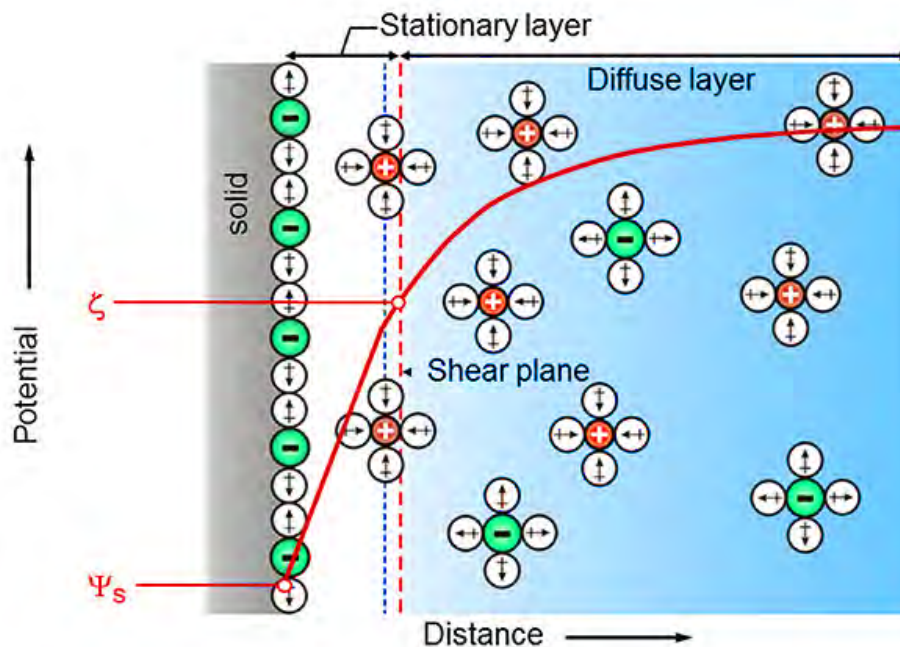


Fig. 1.3: A model of the electrochemical double layer showing the solid-liquid interface and the corresponding potentials.<sup>[26]</sup>

In the presence of an aqueous solution, a particular surface charge is formed on on

the interface solid-liquid. The latter provokes a charge distribution of the available ions being in solution. As a result, an associated surface potential arise which decays with increasing distance from solid surface. This EDL model states, that in between a stationary immobile and a diffuse mobile layer of counterions a compensation of the surface charge occurs.

To summarize, the EDL is a model which defines the zetapotential as an electrical potential at the shear plane which separates a stationary layer and a mobile layer of charges. Thus the zeta potential allows the evaluation of the charging behavior at solid-liquid interfaces. In this system the surface charge is generated by two major mechanisms, which is acid-base reactions of surface functional groups and adsorption of ions. The dependences on which the zeta potential is relying on are shown in the following table.

Table 1.2: Several properties affecting the zeta potential at the solid-liquid interface.<sup>[26]</sup>

<b>Liquid Properties</b>	<b>Solid Properties</b>	<b>Other</b>
pH Value	size	measuring time
ionic strength	porosity	temperature
additive concentration	electronic conductance	material swelling
	surface roughness	

With respect to table 1.2 and the materials studied in this thesis, it is necessary to note that the pH value is the most important parameter that affects the zeta potential. The measurement solution is successively titrated to reveal the corresponding curves and furthermore the isoelectric point (IEP). This point is an important value of the pH dependence of the surface potential, where the zeta potential is assumed to be 0 mV. At this voltage, charge equalization can be assumed. As the IEP is a valuable information in characterizing surface behavior, it will later on utilized to state observations of the GREC membranes. It is important to note that hydrophobic surfaces that exclude surface functional groups that have the same IEP at pH 4 in common, regardless of their chemical composition. This is either true for technical polymers. The table below exhibit some pH-related IEPs, offering surface behavior information.



Table 1.4: Illustration of isoelectric points at different pK- and zeta potentials, revealing surface type behavior.<sup>[26]</sup>

Surface Behavior	IEP	$\zeta_{plateau}$ [mV]	pK
acidic	2.8	-57	2.7
amphoteric	7.0	-34	7.4
basic	8.8	+38	8.6

With this knowledge, adequate measurement curves associated to table 1.4 might look like those depicted in Fig. 3.5.

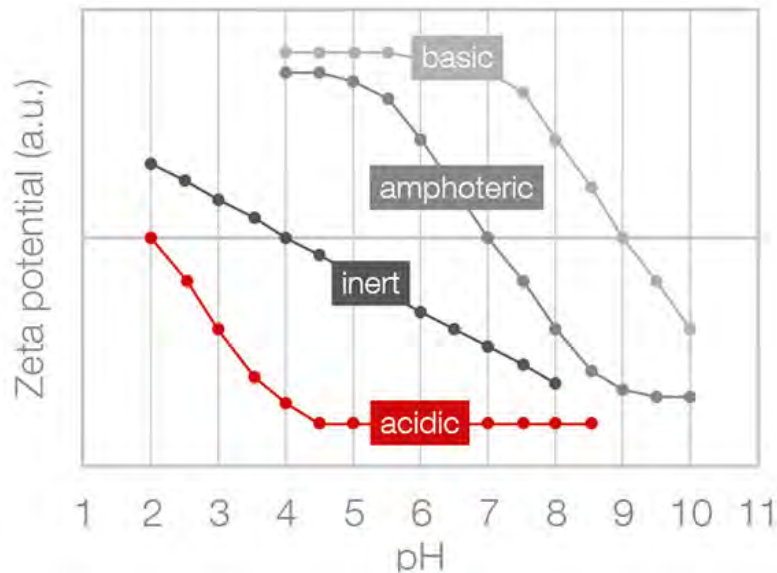


Fig. 1.4: Visualization of hypothetical slopes for acidic (IEP @ pH 2), inert (IEP @ pH 4), amphoteric (IEP @ pH 7) and basic (IEP @ pH 9) surface behaviors.<sup>[26]</sup>

The zeta potentials obtained during the experimental phase were measured to gain information about surface functional groups that may be added, supported or enhanced by chemicals applied in fabrication steps. These possible binding sites provide locations of interest for the diffusion of water to occur, which subsequently results in ad- and absorption effects that must be prevented. Comprising all the facts recently discussed, the measurements taken during this thesis will be reviewed on p. 101.

For the associated measurement principle as well as for further information to zeta potential analysis refer to "The ZETA Guide - Thomas Luxbacher - Anton Paar<sup>®</sup> GmbH".<sup>[26]</sup>

## 1.6 Electronics - Construction and Design

This section will briefly guide through electronic-associated subjects such as surface mounted devices and printed circuit boards.

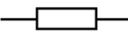
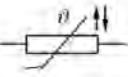
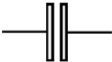


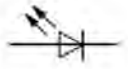
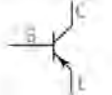

### 1.6.1 Electronic Components

Electronic Components are the electronic parts which have to fulfill their related tasks. They come in many different shapes and sizes, operating their functions depending upon their purpose of application. This is usually achieved by mounting them onto a PCB, which is manufactured to the favor of its field of operation. A PCB therefore acts as the connecting base plate.

There are two categories of parts, the passive and the active components. While a passive device does not contribute power (is not amplifying) to a circuit or system, active components are capable of controlling voltages or amplifying currents or signals. They additionally can act as switches within the circuit. Prominent passive devices are resistors, capacitors and inductors. Active SMDs are usually semiconductor devices such as transistors or operational amplifiers (describes cascades of transistors).<sup>[22]</sup>

Beyond their properties in function and contribution a categorical separation into discrete and integrated circuits takes place. A component packed with one or two functional elements is known as a discrete component, e.g. a resistor limiting the current passing through. An integrated circuit is a combination of several interconnected discrete components packaged in a single case to perform multiple functions, e.g. a microprocessor. Additionally, a further notable classification exists. The lead configuration separates through-hole components and surface mounted devices (SMDs). As the name suggests, the priorly mentioned ones have their leads mounted through the holes of a PCB, while SMDs are mounted on the surface, i.e. a processor it is a SMD. To not put this section to an extent, this subsection will be concluded by showing the most important components.<sup>[18, 22]</sup>

Table 1.6: Basic electronic components mounted on PCBs. Note that this is just an abstract of the most common components.

Wiring Symbol <sup>[6]</sup>	El. Component	Functionality
	Resistors	allow to vary voltage/current concerning ohmic law
	Thermistors	temperature (positive or negative) dependent resistors
	Capacitors	stores electrical charge
	Inductors	coils which establish electrical energy due to an magnetic field
	Diodes	two electrodes in which one current flow direction is preferred
	LEDs	light emitting diodes, basically a pn junction that emits light when forward biased
	Transistors	allow to control voltage and current gain in an electronic circuit
	Thyristors	advanced transistors, switchable and amplifiable, allow to maintain holding current without gate current

### 1.6.2 Printed Circuit Boards

A printed circuit board (PCB) or printed wiring board (PWB, more often used term in the USA) is an insulating material onto which an electronic circuit has been printed or etched. It consists of one or more sheets (multi-layer PCBs) of an insulated material (e.g. R1566WN or R1570, PANASONIC). The PCB provides both the physical structure for mounting and holding electronic components as well as the electrical interconnection and insulation between components. The first patent application filed was at the US Patent Office in 1925, submitted by Mr. Charles Ducas, who proposed to mount electrical metal deposits in the shape of conductors directly onto the insulation material to simplify common electrical constructions. Why PCBs have good reasons for their purpose of use<sup>[9, 18, 22]</sup>:

1. The size of component assembly is reduced, it provides a convenient structural

platform for the components

2. Quantity production can be achieved at lower unit cost.
3. Component wiring and assembly can be mechanized.
4. Circuit characteristics can be maintained without introducing variation in inter-circuit capacitance.
5. They ensure a high level of repeatability and offer uniformity of electrical characteristics from assembly to assembly.
6. The location of parts is fixed, which simplifies identification and maintenance of electronic equipment and systems.
7. Inspection time is reduced because printed circuitry eliminates the probability of error.
8. Printed wiring personnel require minimal technical skills and training. Chances of miswiring or short-circuited wiring are minimized.

The components of a PCB are the base material (or core material, which is under exploration in this thesis), which is a thin board of insulating material, rigid or flexible, which supports all conductors and components, and the conductors, high purity copper in tiny structures of appropriate shapes firmly attached to the base matter. The base provides the mechanical support to all the copper areas including all components attached to them. It is of major concern, that the electrical properties are controlled towards high dielectric properties. In contrast the conductors provide the electrical connections between the components and provide solderable attachment points for the passive or active electrical components.<sup>[9, 18, 22]</sup>

The board can be designed as a single-sided board (Wiring available only on one side of the insulating substrate), as a double-sided board (both sides allow wiring, see Fig. 1.5) and multi-layer boards.

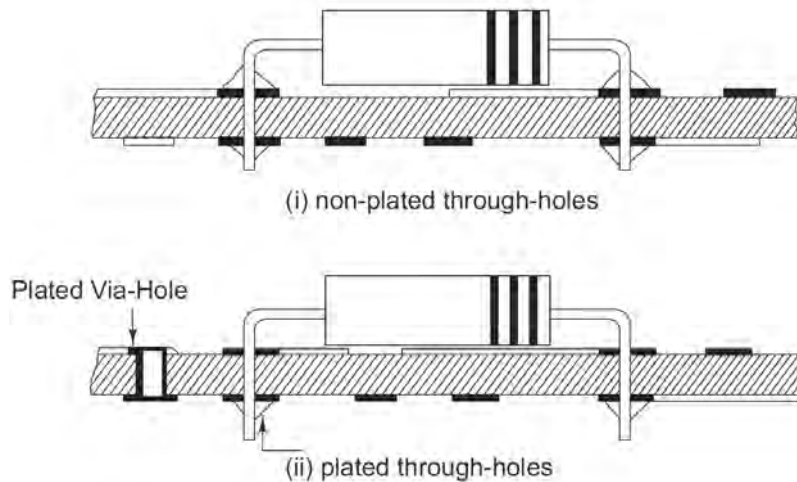


Fig. 1.5: Constructional details of double-sided boards with plated through-hole connection (PTH) and without plated through-hole connection (non-PTH).<sup>[22]</sup>

Depicted in the following picture are multi-layer boards. The B-stage material it is often called prepreg and denotes a core (or base) material which is impregnated with a certain resin.

In prior chapters, the base material was already mentioned as "glass reinforced epoxy resin composite membrane" (GREC). This term will be mainly held on in chapters within this thesis. For the manufacture of conventional rigid multi-layer boards three basic sets of raw materials are used

1. A resins system (commonly epoxides, conventional or modified, exhibiting flame-resistance and high dielectric properties, as well as polyimides)
2. A reinforcing fabric (woven glass cloth, exhibiting good resistance to water, fair resistance to alkali and poor resistance to acid but high dimensional stability.)
3. An electric conductor (commonly copper, exhibiting improved elongation properties at elevated temperatures and special bonding treatments for adhering resins)

In order to illustrate the process<sup>[22]</sup>, a four-layer board construction, superposed by a descriptive step-by-step bottom to top outline is shown below.

- (a) Thermal insulation material to control rate of temperature rise
- (b) Bottom laminate fixture or caul plate
- (c) Sheet of release material such as Teflon glass cloth

- (d) Bottom circuit panel
- (e) Prepreg
- (f) Inner circuit Panel
- (g) Prepreg
- (h) Top circuit panel
- (i),(j) Sheet of release material
- (k) Top lamination fixture
- (l) Thermal insulation material

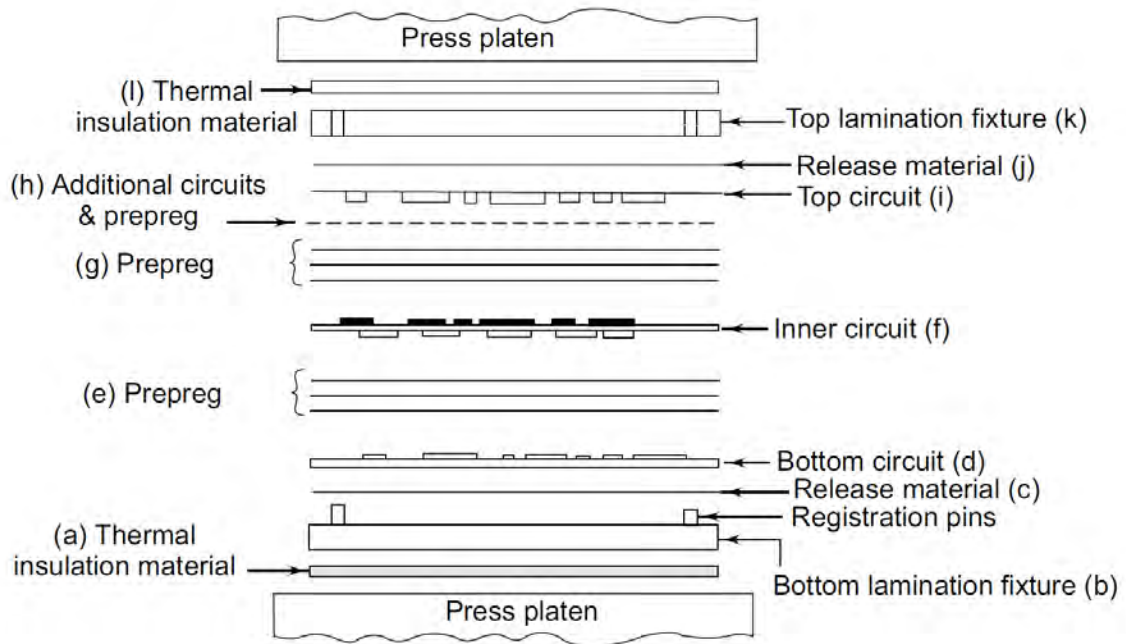


Fig. 1.6: Multi-layer board (MLB) lamination process lay-up.<sup>[22]</sup>

Before closing this subsection and leading over to the next one, a flow chart will give an idea of the major steps in the fabrication of a single-sided printed circuit board.

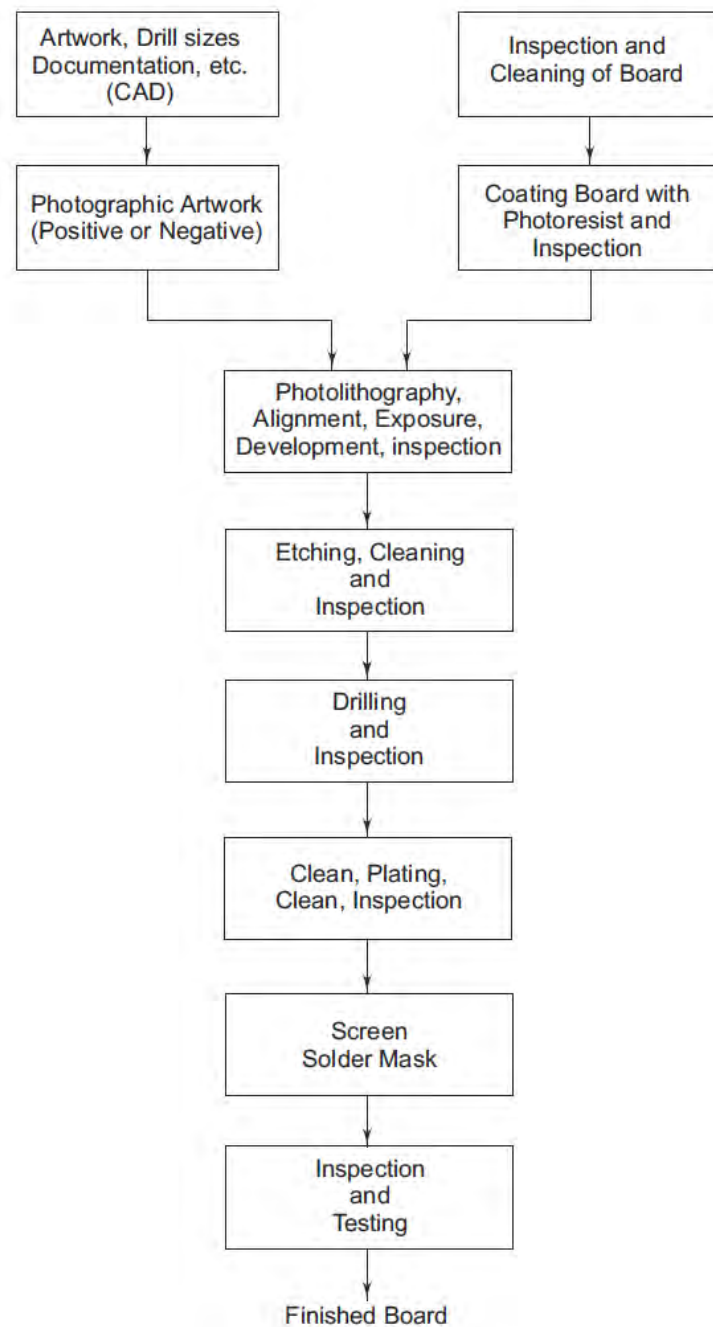


Fig. 1.7: Major steps in the fabrication of a single-sided PCB.<sup>[22]</sup>

Since the photolithography is major step not only in the fabrication, it is either associated to many issues that may cause CAF and it therefore worth to being mentioned.

"Both sides of the board are covered with a thin layer of a photoresist, which may be solid or a liquid, and either positive or negative. A solid negative working resist is mostly used. The image transfer process occurs with the resist removed from the area where the tracks are to be kept. This

is the reverse of the print and etch process. The copper areas, which will remain on the finished PCB and the hole walls, are unprotected. All other areas are covered by the hardened photoresist. Developing of both sides is usually done in an automatic spray machine."<sup>[22]</sup>

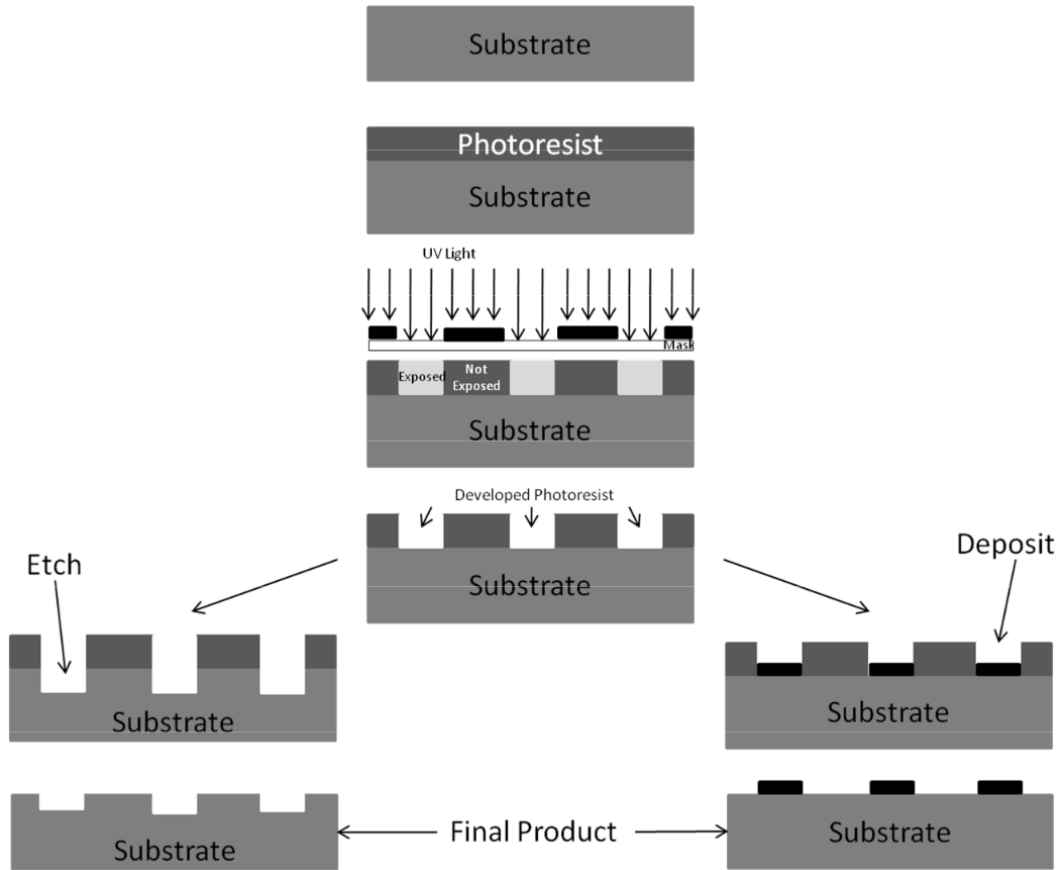


Fig. 1.8: Basic steps of photolithography.<sup>[4]</sup>

In this procedure chemicals with respect to those that will show up in section "2.4.2" are used. It is assumed that they contribute to CAF formations.



## 1.7 Conductive Anodic Filament

The conductive anodic filament describes a failure mode, which latently develops in printed circuit boards due to the presence of moisture and high voltage gradients, and appears as fatal, irreversible failure in PCBs. Firstly reported in 1976, 51 years after patenting the first PCB, today's wiring density of electronics is increasing rapidly. To prevent CAF formation of causing drop-outs, which sometimes appear to be dangerous not only in losing anticipated function by affecting electronic assemblies, its nature has to be understood. Equipment relying on these packaged circuitries have their field of operation frequently in outside areas, where conditions might be very harsh and environment can not be controlled. Coherently, the E-mobility sector draws attention to high DC voltage boards which are permanently exposed to elevated potential differences in strong alternating environments. The huge temperature differences such devices are sometimes exposed to, involves condensation effects that arise when underrun dew points. Even hermetically insulated systems, molecules may get absorbed as a result of diffusion. It is therefore of great interest to drive investigation towards reliability by simultaneously keeping device's performance. Researchers at Bell Labs discovered this new failure mode, termed CAF in 1976, which is characterized by an abrupt and unpredictable loss of insulation resistance between conductors that are held at a potential difference. Prior to this, Der-Marderosian had noted a failure they termed "punch-thru" which is similar to CAF, except the filament grows between circuit layers rather than along a E-glass fiber. In both, punch-thru and CAF, a filament penetrates either, the layers or through the channel along a glass fiber from anode to cathode. Thus, when conditions and deposited material are reaching an ideal threshold, an internal short or a loss of current supply cause severe failures and discard the associated device. In most cases it is not possible to allocate the CAF that defected a device, since the amount of external and internal structures is tremendously high and CAF may bridge conductors with a distance of 1 mil (1 mil = 1  $\mu$ in or 25.4  $\mu$ m) or less. For the investigation of CAF, established test methods can be found at the IPC. Via observing coupons, i.e. prepregs containing comb structures of different conductor distances after treating in a highly accelerated stress test (HAST), surface insulation resistance measurements and optical observation methods like SEM provide an opportunity to focus on a CAF that has developed within a small volume of matter. <sup>[33, 41]</sup>

"IPC has instituted a CAF test procedure at the end of 2003 but OEMs in the industry use their own test vehicles along with their own test conditions. To date, there is no standard for CAF testing."<sup>[10]</sup>

It is of importance, that CAF should not be confused with dendrite growth. While dendritic growth is a simple electrochemical process, where at the anode metal ions go into solution and redeposit on the cathode, exhibiting needle- or treelike shapes, CAF growth either emanates from the anode, but differs in its electrochemical mechanism. CAF contains copper and a halide ion (typically chloride) rather than pure metal (typically copper) as in the case of dendritic growth. Furthermore they differ in their pathway allocation. CAF formation appears to be a subsurface phenomenon, while dendritic growth occurs as a surface phenomenon.

For CAF to occur within the laminate it is well known in industry, that certain conditions need to be active. The parameters which can trigger CAF include high environmental humidity, high voltage (DC) under test, high moisture content, surface and resin ionic impurities, glass to resin bond weakness enhanced by thermal excursion that goes simultaneously by the exposure to high assembly temperatures (e.g. soldering, lead free applications).<sup>[10]</sup>

Factor	Acceleration Condition
Materials	<i>Fast</i>   Ag > Cu > Pb > SnPb Solder > Sn > Au   <i>Slow</i>
Temperature	High
Humidity	High
Voltage	High
pH	Acidic
Ionic impurities	Halides
PCB material	<i>Fast</i>   Paper phenol > Glass epoxy > Polyimide > Ceramic   <i>Slow</i>

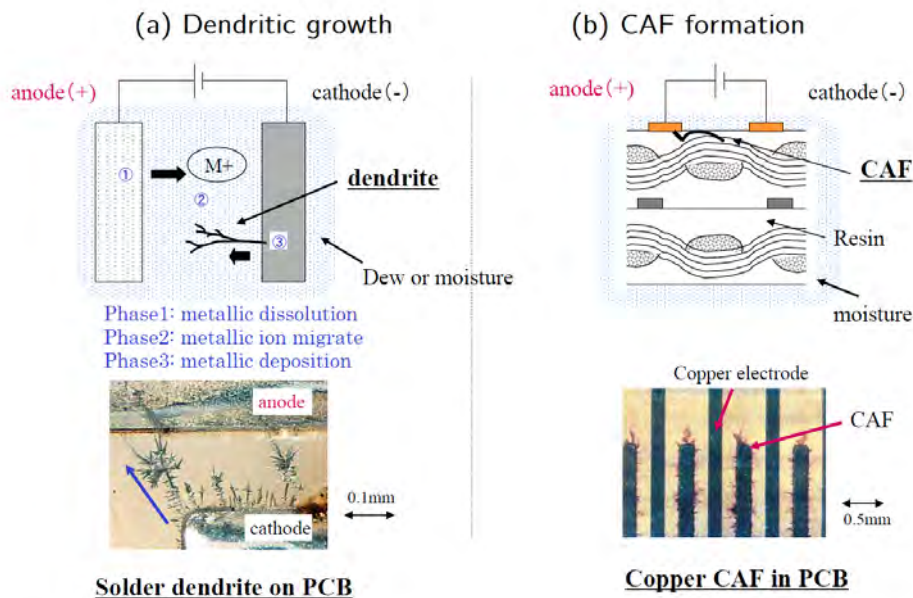


Fig. 1.9: ECM acceleration conditions and mechanisms, (a) dendritic growth, (b) CAF formation.<sup>[13]</sup>

The following reaction scheme shows the reaction equation of a CAF within a PCB. It only indicates the attendance of three major components, copper, water and oxygen. Due to the driving forces of the bias applied, these electrochemical oxidation and reduction reactions are triggered. The potentials<sup>[19]</sup> shown below are with respect to the standard hydrogen electrode (SHE), having said that this is the very basic scheme that excludes possible side reactions (organic complexing or chelating agents) and the very counterions within the system.

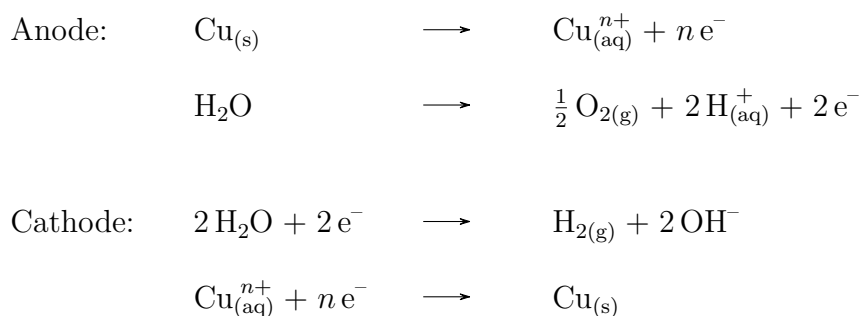


Table 1.9: An abstract of electrochemical series with respect to copper and associated counter ions.<sup>[19, 27]</sup>

$\text{Cu}^{+} + e^{-} \rightleftharpoons \text{Cu}$	-0.521 V vs SHE
$\text{Cu}^{2+} + e^{-} \rightleftharpoons \text{Cu}^{+}$	-0.153 V vs SHE
$\text{Cu}^{2+} + 2 e^{-} \rightleftharpoons \text{Cu}$	-0.342 V vs SHE
$\text{Cu}^{3+} + e^{-} \rightleftharpoons \text{Cu}_2^{+}$	-0.240 V vs SHE
$\text{Cu}_2\text{O}_3 + 6 \text{H}^{+} + 2 e^{-} \rightleftharpoons 2 \text{Cu}^{2+} + 3 \text{H}_2\text{O}$	-2.000 V vs SHE
$\text{Cu}^{2+} + 2 \text{CN}^{-} + e^{-} \rightleftharpoons [\text{Cu}(\text{CN})_2]^{-}$	-1.103 V vs SHE
$\text{Cu}^{2+} + \text{Cl}^{-} \rightleftharpoons \text{CuCl}$	-0.538 V vs SHE
$\text{CuI}_2^{-} + e^{-} \rightleftharpoons \text{Cu} + 2 \text{I}^{-}$	0.000 V vs SHE
$\text{Cu}_2\text{O} + \text{H}_2\text{O} + 2 e^{-} \rightleftharpoons 2 \text{Cu} + 2 \text{OH}^{-}$	-0.360 V vs SHE
$\text{Cu}(\text{OH})_2 + 2 e^{-} \rightleftharpoons \text{Cu} + 2 \text{OH}^{-}$	-0.222 V vs SHE
$2 \text{Cu}(\text{OH})_2 + 2 e^{-} \rightleftharpoons \text{Cu}_2\text{O} + 2 \text{OH}^{-} + \text{H}_2\text{O}$	-0.080 V vs SHE
$2 \text{H}_2\text{O} \rightleftharpoons \text{O}_2 + 4 \text{H}^{+} + 4 e^{-}$	-1.229 V vs SHE
$2 \text{H}_2\text{O} + 2 e^{-} \rightleftharpoons \text{H}_2 + 2 \text{OH}^{-}$	-0.828 V vs SHE

Both, the bias and the spacings of the structures assume a voltage gradient [V/m], which in detail is huge. Inherently associated is the pH gradient which simultaneously evolves. On the anode, the hydrolysis reaction accumulates hydronium ions, thus generating an acidic environment which forces solid copper to dissolve. Vice versa on the cathode hydroxide ions are formed in statu nascendi, providing an alkaline environment. The copper ions will try and travel through any weak point in the laminate, which is certainly the epoxy/fiber interface, from the anode attracted to the cathode, driven by the pH gradient.<sup>[10]</sup> At a pH above 5 (potential > 0.2 V), the solubility of copper ions declines rapidly and they becoming nearly insoluble at a pH around 8.6, indicated in Fig. 1.10, showing a simple Pourbaix diagram of copper.<sup>[41]</sup>

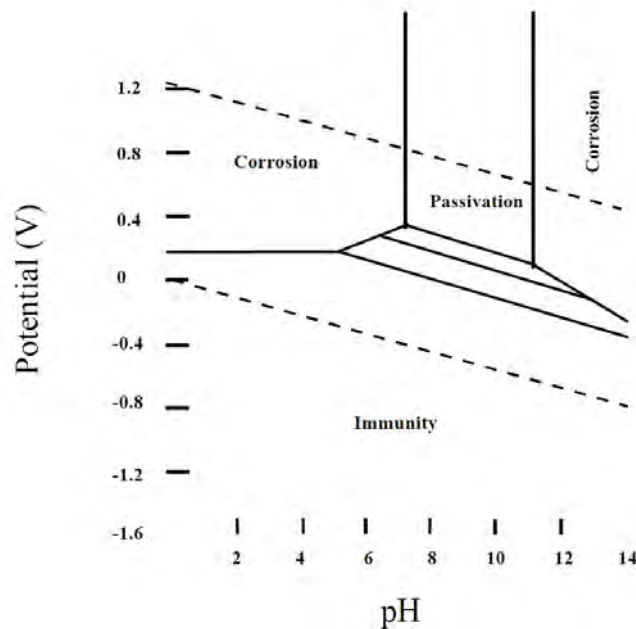


Fig. 1.10: Simplified Pourbaix diagram for the system copper.<sup>[41]</sup>

As a consequence, the copper ions deposit preferably near the glass interface, which is assumed to provide an environment that is more alkaline versus that offered by the channel moisture solution. With elapsing time, more copper accumulates as a copper salt that is growing along the epoxy/fiber interface, forming a conductive filament emanating from the anode, which is called CAF. The presence of a solution containing salt and moisture at a certain point provides an interconnect between the electrodes, thus when a bridge has established, an electrical failure occurs. However, the reaction scheme shows, that water molecules and oxygen in the laminate are major contributors to the formation of a CAF. Since a total exclusion of that precursors can not be achieved, knowledge can at least be gathered by ascertaining materials related

properties. In order to avoid diffusion and sorption processes, manufacturers can measure, control and change fabrication processes and materials' composition, respectively.

On the following pages, schemes (including exaggerated scales and distances) that will illustrate the filament growth in presence of water and the pH gradient that is inherently related to the applied voltage gradient. The figures' descriptions will reveal further information to the reader.

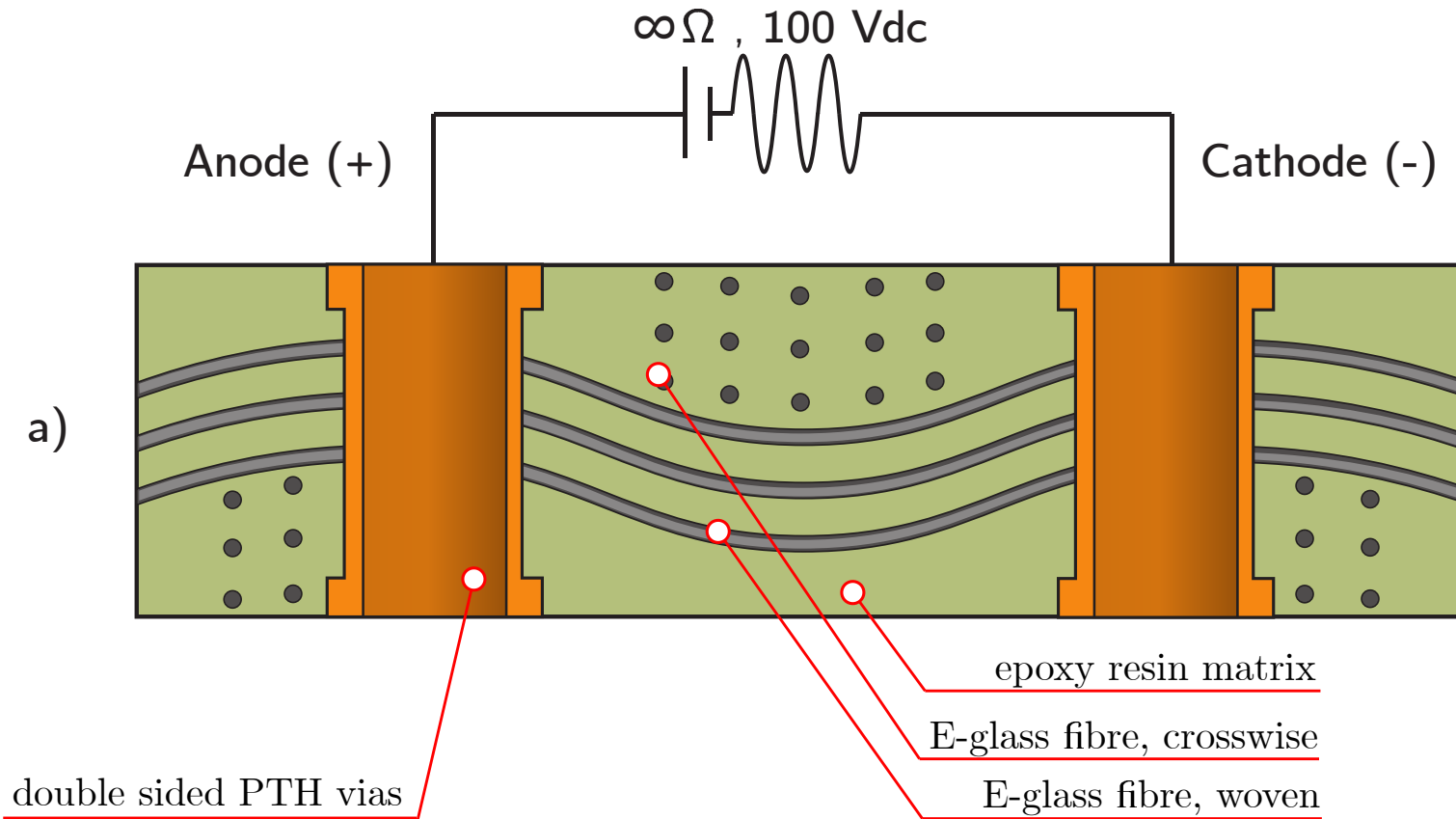


Fig. 1.11: A cross section of an ideal printed circuit board containing two PTHs. The illustration assumes infinite resistance at applied voltage as well as a perfectly interconnected epoxy/glass composite without any defects or absorbed molecules foreign to the matrix. The conductor assembly exhibits a hole-to-hole configuration what is considered to be worst for CAF formation.

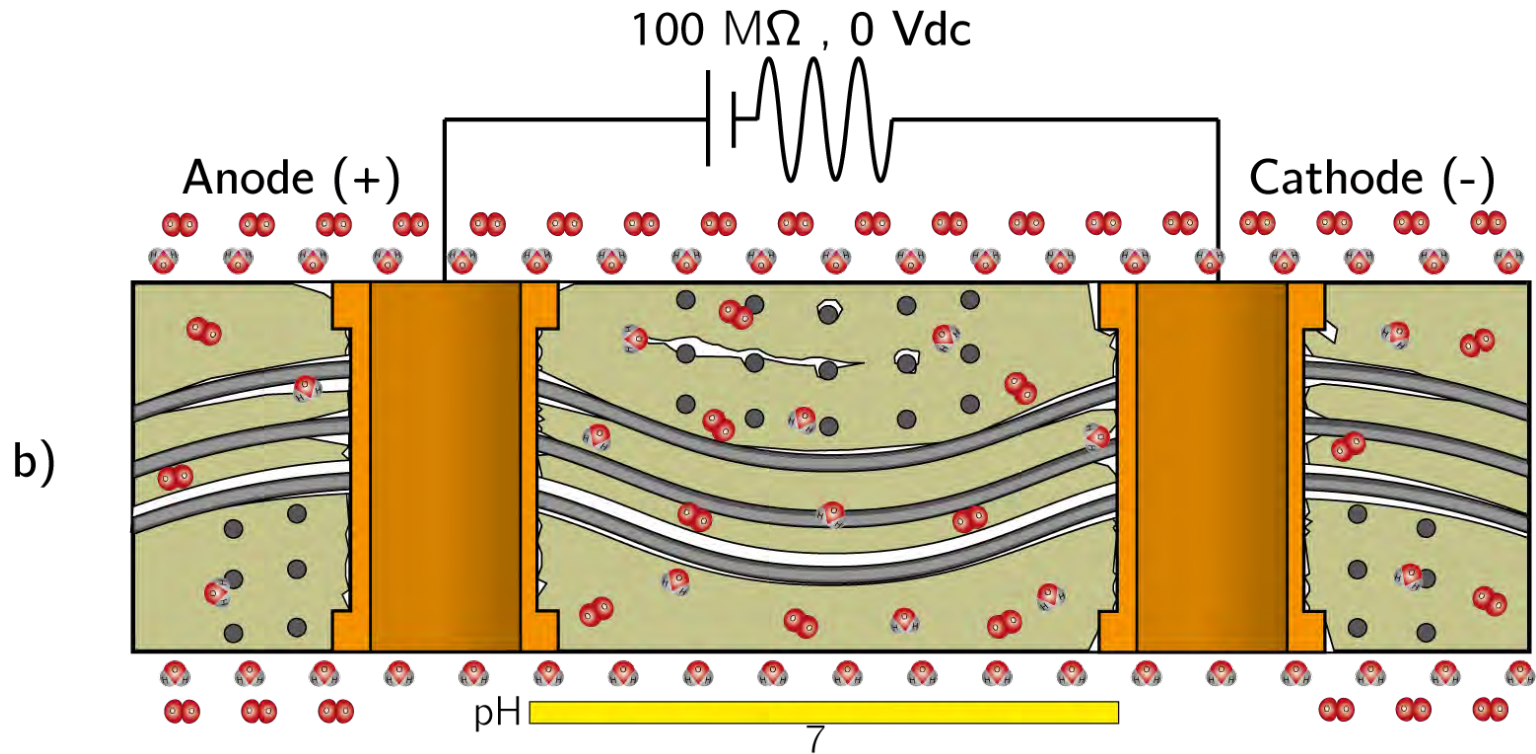


Fig. 1.12: This illustration is referred to a more realistic case, visualizing cracks, blisters, measles and absorbed molecules like water and oxygen. Due to soldering and drilling steps during the fabrication of the, delamination and substrate-to-PTH void interstitials have been developed. "Non-biased" this dielectric device assumes a resistance of 100 M $\Omega$ . The internal environment's acidity is neutral being at a pH value around 7. Additionally, a surface condensed water film is shown.

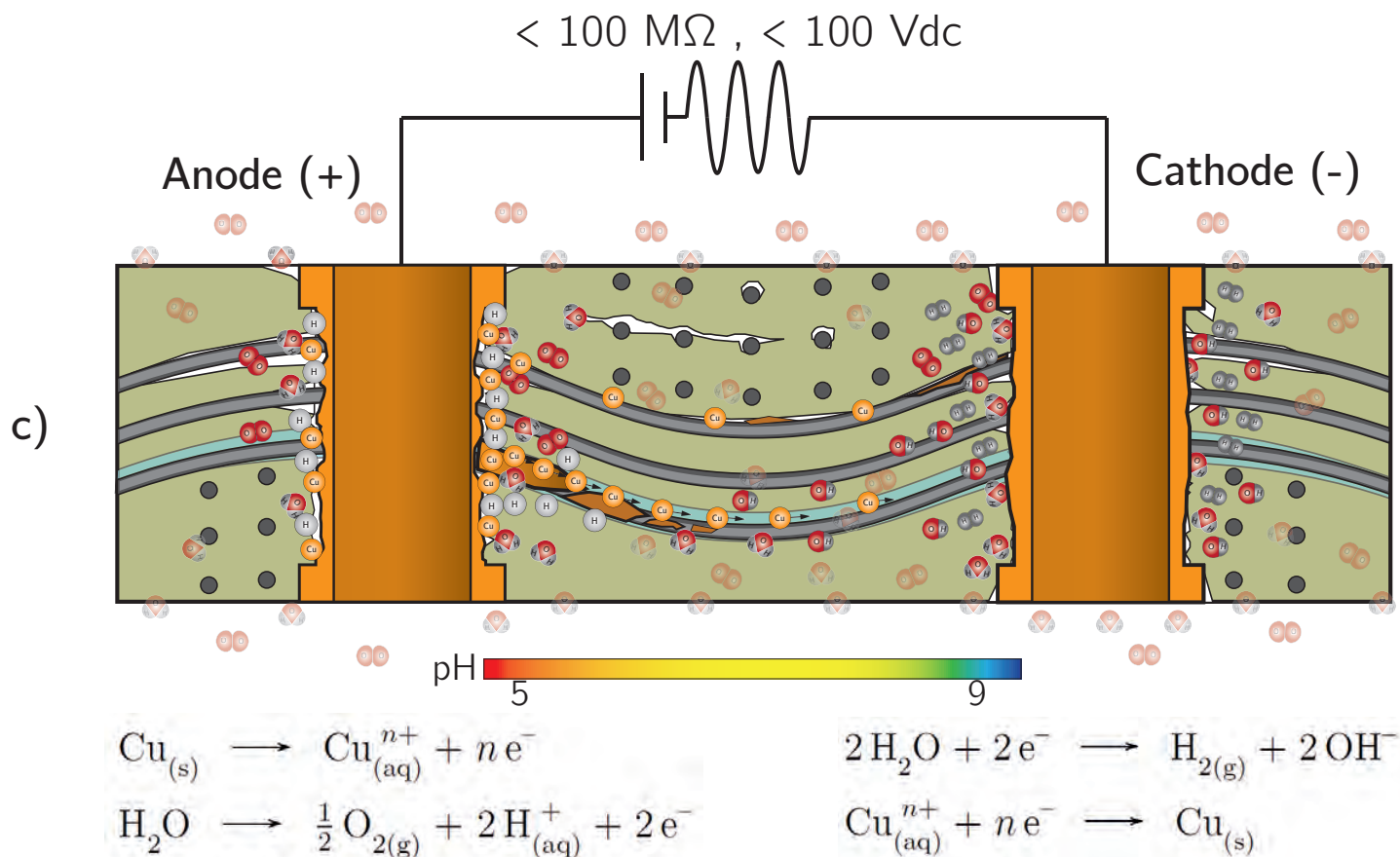


Fig. 1.13: By exposing the PCB to a bias of 100 V, a voltage gradient arises. After a certain period of time, the hydrolysis created an pH drop at the anode forcing the Cu corrosion products to become soluble. These ions, positively charged then try to travel through weak channels, attracted by the negatively polarized cathode. At a pH of approx. 5, the ions get more and more insoluble and full precipitation occurs at a pH of around 8.6. The glass fibers are mostly treated with basic surface functional groups to stabilize the epoxy/glass interface, so that Cu ions preferably deposit on the fiber's surface. While the anode depletes in copper, the cathode try to accumulate and reduce available copper. The pH gradient between the electrodes now looks like a polynomial of third order.



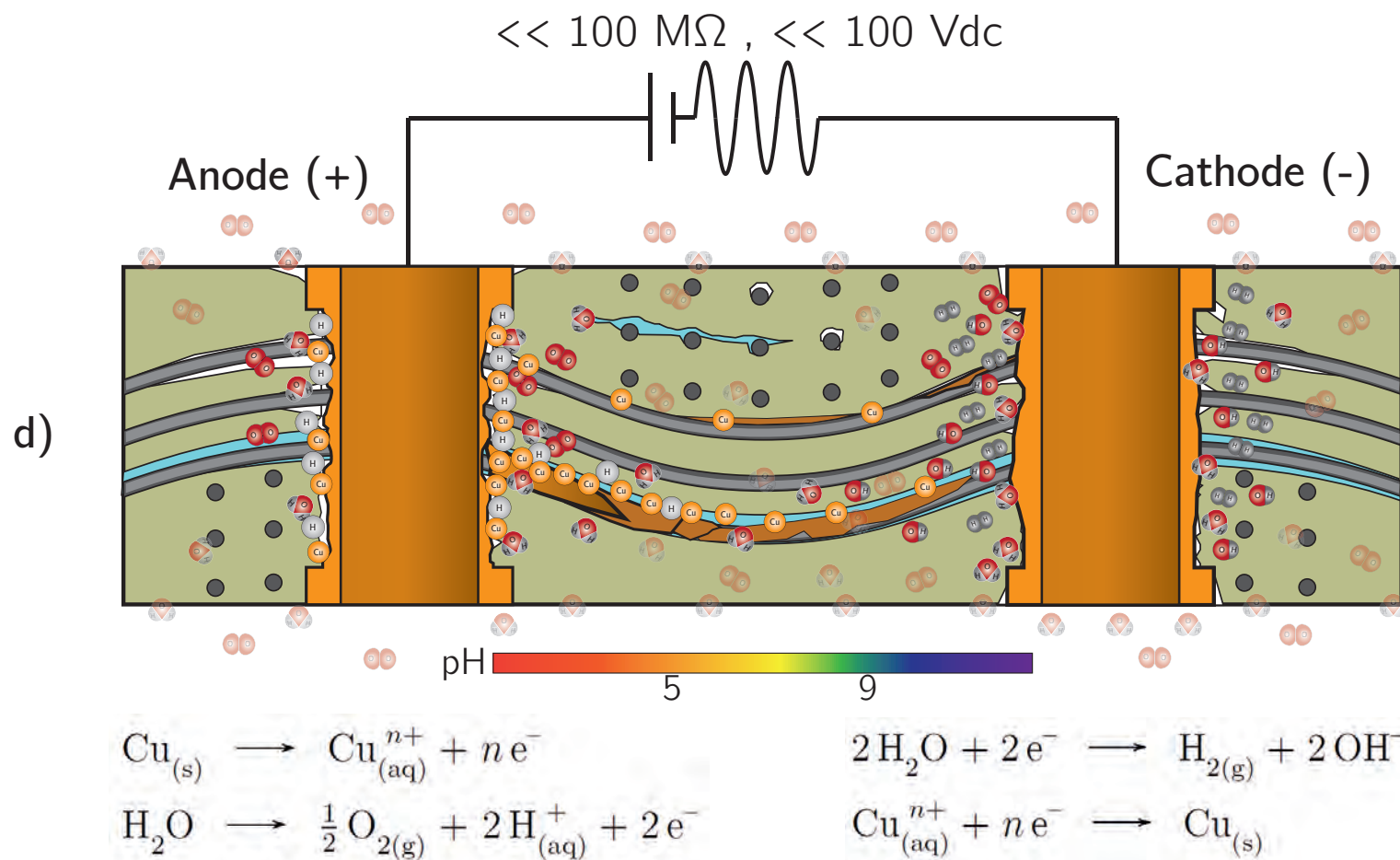


Fig. 1.14: Within progression of time, the filament grows further and further, emanating from the anode to the cathode. The filament itself provide locations for hydrolysis to occur. The higher gradient in pH depletes the anode steadily. Voltage and Resistance are decreased as a result of filament growth and the conductive salt solution.

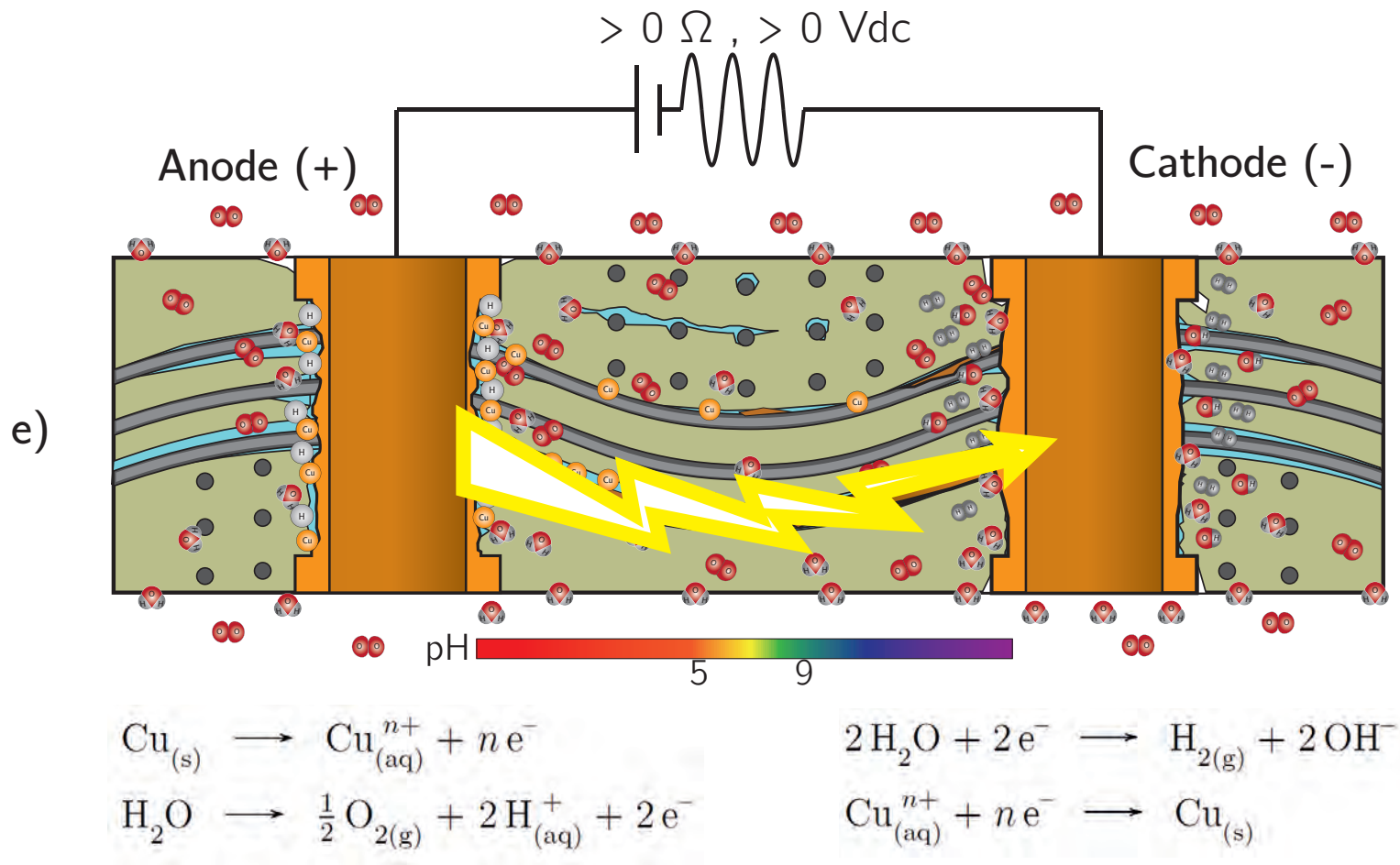


Fig. 1.15: The filament has critically grown in length, the channel got saturated by conductive ions and salts. Resistance and voltage are distinguishable from the priorly measured stats. After exceeding a threshold, a short is created between the electrodes as a consequence of CAF. The PCB is irreversibly damaged.

Depicted in Fig. 1.16 the process of anodic filament formation is shown in detail. When applying a bias to the PCB at the anode water electrolysis (1) yields hydronium ions and oxygen molecules. The hydronium ions accumulate on the anode and oxidation (2) of metallic copper is facilitated. The released copper ions are now attracted (3) to the cathode to achieve a charge equalization within the pH gradient. At certain conditions (pH 5-8), the ions become insoluble, reaching total insolubility (4) at a pH around 8.6.<sup>[41]</sup> Since the glass fibers are treated with surface functional groups like  $\gamma$ -aminopropyltriethoxysilane (AMEO) to increase epoxy/glass adhesion, the glass surface provide an periphery that is more alkaline than that of the general environment being acidic. A considerable amount of copper ions and derivatives is subsequentially adsorbed (5) to the glass surface. With elapsing time, more and more copper and copper-associated salts are deposited, forming a filament (6) conductive to wattless currents. The precipitation proceeds (7) until a concentration threshold is reached, causing a short (8), indicated by the loss in resistivity, between anode and cathode. The PCB is irreversibly damaged.

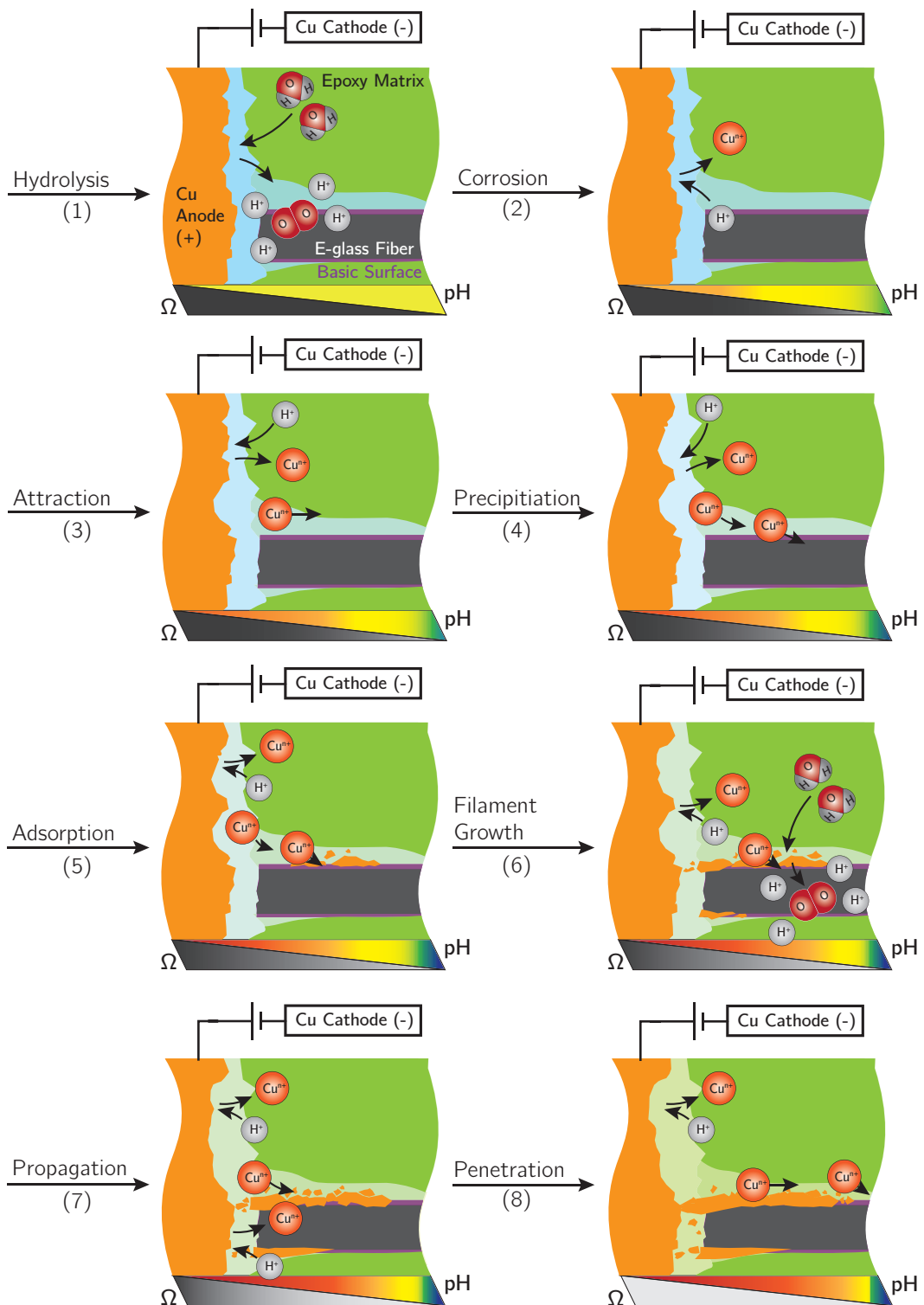


Fig. 1.16: Process of conductive anodic filament formation in detail, showing resistivity and pH gradient. Further indicated is the ion-saturation of the aqueous solution.

Turbini and Ready<sup>[41]</sup> categorized factors which affect CAF formation into two types, internal variables and external influences.

Internal variables are intrinsic to the design of the board and include choices such as substrate material, component and circuit layout. External influences are related to assembly and production control and may be easy changeable factors, involving ambient conditions in the manufacturing plant, chemical compositions of solder fluxes or HASL fluids.

### (1) Internal Variables

- Substrate Material Choice

Rudra<sup>[21]</sup>, Ready<sup>[32]</sup> performed extensive experimental comparison towards CAF susceptibility among substrates applied in circuitry packaging industry in 1994.

"Of all materials tested by these investigators, the BT material proved to be most resistant to CAF formation (due to its low moisture absorption characteristics). Conversely, the MC-2 substrate proved to have the least resistance to CAF formation. The susceptibility of the materials follows the trend below and also depends on factors such as conductor configuration, conductor spacing, the presence of a conformal coating, etc.:

MC-2 » Epoxy/Kevlar > FR-4 » PI > G-10 > CEM-3 > CE > BT.

The substrates are polyphenolic epoxy resins that fulfill the requirements to IPC standards for printed circuit boards' materials. For more information to the abbreviations refer to p.IX. To insure immunity to CAF, the laminate of preference is BT. However, there is a cost penalty to consider."<sup>[41]</sup>

- Conductor Configuration

Depending on the conductor configuration, the CAF may either bridging two surface tracks, two PTHs, or a PTH and a surface track, considering anode/cathode allocation. Lando et al<sup>[24]</sup> showed that the hole-to-hole configuration is the most attractive for CAF to occur, due to the direct contact of a PTH barrel with the glass fibers, enforced by threads that are caused by drilling steps. The

track-to-track configuration, they derived, was the least susceptible to filament growth. A situation, in which the hole is the anode is worse than the reverse configuration, where the hole is the cathode. However, the susceptibility is preferred in descending order  $a > b > c > d$ , as likely illustrated in Fig. 1.17.<sup>[33, 41]</sup>

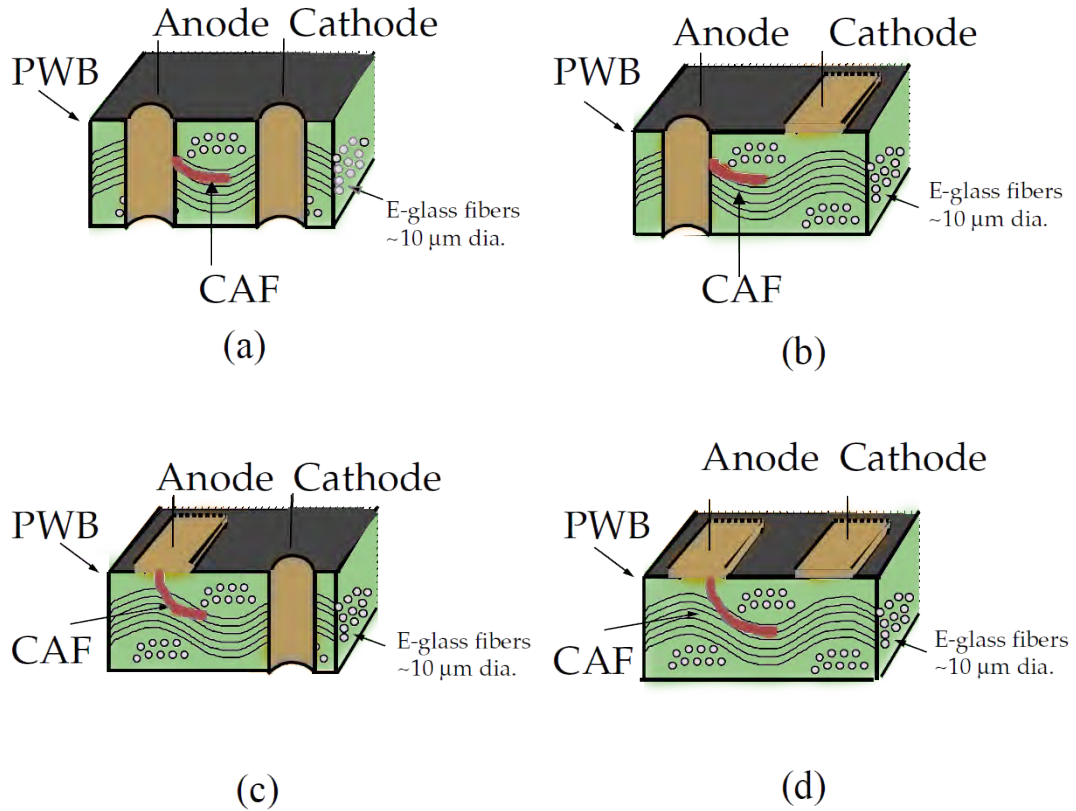


Fig. 1.17: Schematic representation of CAF pathways (dimensions exaggerated for clarity): (a) PTH to PTH, (b) PTH to track, (c) track to PTH, and (d) track to track.<sup>[33, 41]</sup>

- Voltage Gradient Effects

The voltage gradient subsequently builds a pH gradient and an associated scheme is shown at p. 28. It is a critical factor, since an assembly containing a +20 V power plane with an adjacent via biased at +60 V has a potential difference between plane and via of 40 V, which is not considered to be a high potential difference in electronic assemblies. Assuming a distance of 5 mils between power plane and the via results in a voltage gradient of 8 V/mil, which synergized by other parameters is enough to trigger CAF, though.

## (2) External Influences

- Solder Flux / HASL Fluid Composition

Polyglycols diffuse into the epoxy during soldering and degrade the insulation resistance. When a PCB is exposed to temperatures above its glass transition temperature  $T_g$ , the elevated temperatures enhance the structure's accessibility for contaminants to intrude. An absorption of Polyglycols to the substrate has been shown to reduce performance by increasing moisture uptake, thus the propensity for CAF formation is increased. Brous<sup>[8]</sup> stated that the diffusion of polyglycols occurs during elevated temperatures of soldering operations and confirmed that lower molecular weight polyglycols are more likely to penetrate into the substrate. He could further show, that SIR measurements at 35 °C / 90 % RH initially were in the range of  $10^8$  to  $10^9 \Omega$  resulting in one order of magnitude higher SIR values when polyglycols diffuse out of the epoxy. For polyethylene glycol (PEG) this behavior could not be observed. He believed that PEG is trapped within the polymeric backbone, preventing a release of the PEG. He further found that the laminate became hygroscopic when polyglycols absorb polyglycols.

- Thermal Excursions

As already discussed above, the diffusion of polyglycols into the PCB substrate occurs during soldering. As shown in section "1.1" on p. 1, the diffusion process follows Arrhenius behavior and therefore, exposure to elevated temperatures above  $T_g$  will strongly affect the electrical properties. It is shown<sup>[20]</sup>, that higher thermal treatments exhibited SIR levels orders of magnitudes lower than lower those processed under less aggressive thermal conditions, having said that the mismatch in coefficients of thermal expansions (CTE) will weaken the bond between substrate and glass fibers. Thus, the higher the amount of thermal excursions, the higher the propensity for polyglycol diffusion to occur, the higher the moisture uptake and the higher the epoxy-fiber separation. The channels (surface defects like crazing, delamination, blistering or measles) developed provide higher volumes for moisture to settle down, forcing filaments to grow in presence of a voltage gradient.

- Cleaning

Several solvent combinations for removing polyglycols from epoxy-glass were studied, concluding that soaking the board in acetonitrile for 24 hours provides the best removal efficiencies.

- PCB Storage: Ambient Humidity Effects

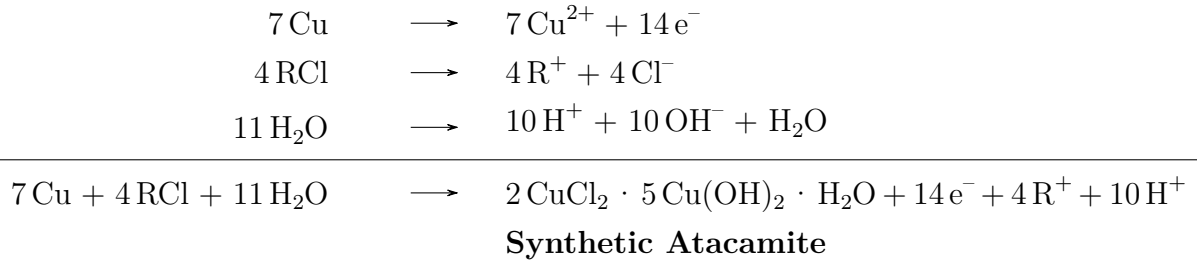
- There is a humidity threshold below which CAF formation will not occur, depending on operating voltage and temperature.

- For 50 V applied @ 25 °C the critical RH for CAF formation is ~80 %
- Moisture absorption can even happen during assembly, transportation or storage
- An 1 wt% water absorption leads to an 8 °C decrease in  $T_g$
- FR-4 has greatest affinity for moisture uptake.
- Moisture in substrate: internal shorts, metal migration, delamination, poor electronic and mechanical performance and a change in dimensional stability
- Diffusion is the rate-limiting process for SIR loss<sup>[40]</sup>
- Primary conduction path is along interfaces between glass fiber material and epoxy matrix
- Minimum time for catastrophic SIR loss is approx. 50 hours, which relates to the time required for water to penetrate the glass fiber channels.
  
- Takahashi et al<sup>[40]</sup> expanded the concept of moisture causing a breakdown of the interface:

"They noted that an abrupt loss of adhesion at the epoxy/glass interface occurred when the epoxy is equilibrated in air whose relative humidity is in excess of a critical value. This critical relative humidity is defined as the point at which there is a surge in moisture pickup. They determined that an irreversible loss of adhesion occurs and that the polymer chain was permanently altered when this critical relative humidity was exceeded."<sup>[41]</sup>

Until now there has been no request for the role of the counter ions that form the copper salts. The schemes discussed in this section excluded them to intendendly keep mechanisms simple. The work of Ready et al<sup>[33]</sup> involved investigations using SEM/TEM EDS, for optical, structural and compositional observations, respectively. They could clearly show that CAF is copper and chlorine containing. The electron diffraction results provided evidence for the CAF being synthetic atacamite. Results obtained by X-ray powder diffraction also identified green atacamite as common corrosion product on PCBs. They state that the formation of atacamite in moist air can be completed in a few hours. That shows that CAF formation as a result of electrochemical corrosion can be quite rapid. To reveal the stoichiometric chemical equations for synthetic atacamite refer to the equations below.<sup>[33]</sup>





To conclude this section:

- Processing steps in PCB manufacturing like drilling or soldering provide origins for conductive anodic filaments to grow
- Thermal excursions, i.e. soldering stresses the epoxy/glass interface and weaken this area, above  $T_g$  polyglycol uptake is increased
- Polyglycols increase moisture absorption by the substrate, hence CAF formation
- The presence of moisture is required for a CAF to develop
- High voltage gradients, resulting in pH gradients exacerbate CAF formation
- Polyglycols coupled with elevated hydrobromic acid concentrations increase CAF formation
- Acetonitrile soaks are a proper choice for the removal of polyglycols from substrates
- The higher electronegativity and its smaller ionic radius makes chloride more favorable for CAF than bromide
- A critical RH threshold exists for all PCB substrates
- The susceptibility towards CAF varies between different substrate materials
- Conductor configuration plays an important role, hole-to-hole (via-via) is worst, track-to-track best to prevent CAF formation
- CAF mainly consists of copper and chlorine, resulting in a stoichiometry of synthetic atacamite

## 1.8 Mean-Time-To-Failure Formula (MTTF)

The mean-time-to-failure (MTTF) describes the expected time to failure a system which is irreversibly damaged and therefore non-repairable. Sony was the first to raise a MTTF formula related to PCB related materials in the 90s. Welsher et al<sup>[43]</sup> stated that the MTTF obeys an Arrhenius relationship in the range 50-100 °C and concerning time to failure ( $t_f$ , Eq. 1.10 and 1.11) results the relative humidity seemed to have an strong dependence to the material. With their data they could confirm that CAF in PWBs, particularly in those with closely spaced PTHs, is a potentially serious reliability problem.<sup>[33]</sup>

$$t_f = a(H)^{-b} \quad (1.10)$$

$$t_f = c + \left(\frac{d}{V}\right) \quad (1.11)$$

where

$H$  : Relative humidity (RH)

$V$  : Applied voltage

$a, b, c, d$  : Positive material dependent constants

They derived the MTTF formula (Eq. 1.12) by combining time to failure formulas ( $t_f$ ), Eq. 1.10 and Eq. 1.11.

$$MTTF = a(H)^{-b} \exp\left(\frac{E_a}{k_b T}\right) + d \left(\frac{L^2}{V}\right) \quad (1.12)$$

where

$H$  : Relative humidity (RH)

$E_a$  : Activation energy

$k_b$  : Boltzman's constant ( $8.62 \cdot 10^{-5}$  eV/K)

$T$  : Temperature [K]

$L$  : Spacing between conductors [mil]

$V$  : Applied voltage

$a, b$  : material dependent constants

$d$  : Temperature and humidity dependence

Ready et al<sup>[33]</sup> quantified the inter-relation between voltage und conductor distance for PTH test patterns to be a  $L^4/V^2$  relationship. However, the MTTF formula should provide a tool to presume materials average lifetime. By the means of computer numeric simulations Georg Reiss from the MCL could solve the conductor associated term. For the determination of the humidity related factors, further investigations, i.e. ascertaining activation energy, have to be done.

## 1.9 Cooperative Studies

Andreas Tschepp and Markus Postl from Joanneum Research Materials performed the determination of the oxygen transmission rate and measurements on the electric properties of PCBs, especially impedance spectroscopy accompanying the phase angle  $\phi$ .

### 1.9.1 Oxygen Transmission Rate - Joanneum Research

Briefly explained, the OTR measurements (Fig. 1.18) showed a penetration rate of  $1.3 \text{ cm}^3 \cdot \text{m}^{-2} \cdot 24 \text{ h}^{-1} \cdot \text{bar}^{-1}$  and approximately  $3.3 \text{ cm}^3 \cdot \text{m}^{-2} \cdot 24 \text{ h}^{-1} \cdot \text{bar}^{-1}$  for both, the bare core R1566WN /  $100 \mu\text{m}$  and the bare core R1570 /  $100 \mu\text{m}$ , respectively.

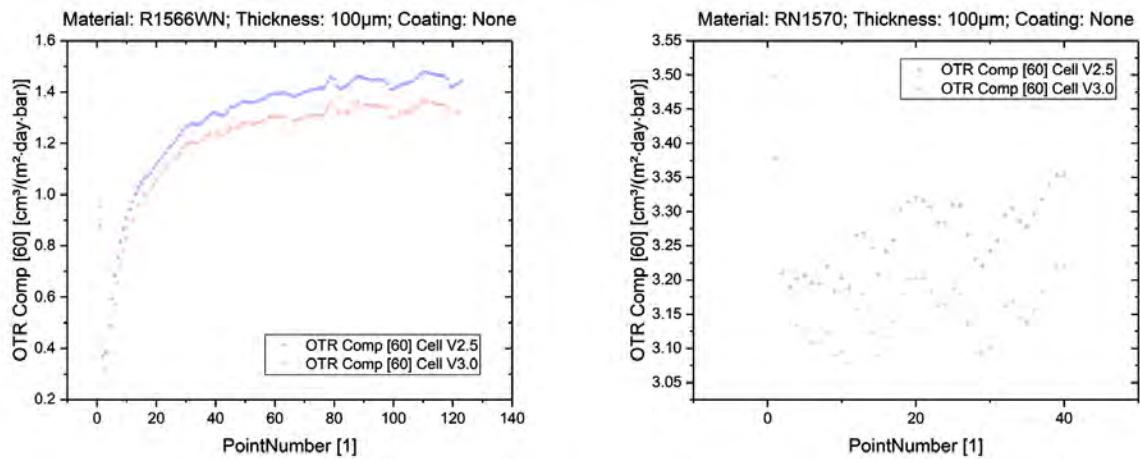


Fig. 1.18: OTR measurements on both, uncoated R1566WN and RN1570.

Even if the data points associated with R1570 are varying significantly, their range and the trend provide an identification to the OTR. The values obtained allow furthermore to distinguish between both materials and suggest that R1570 core material is twice as prone to the permeation of  $\text{O}_2$ .

## 1.9.2 Surface Insulation Resistance Measurements - Joanneum Research

CAF testing via impedance spectroscopy was performed to determine if a material is prone to grow a conductive path between adjacent conductors.<sup>[34]</sup> It comprises the influence of moisture on the phase angle and the frequency-resistance behavior during the "accelerated life test" (ALT). In Fig. 1.19, the comb structures of the tested PCB coupons are illustrated.

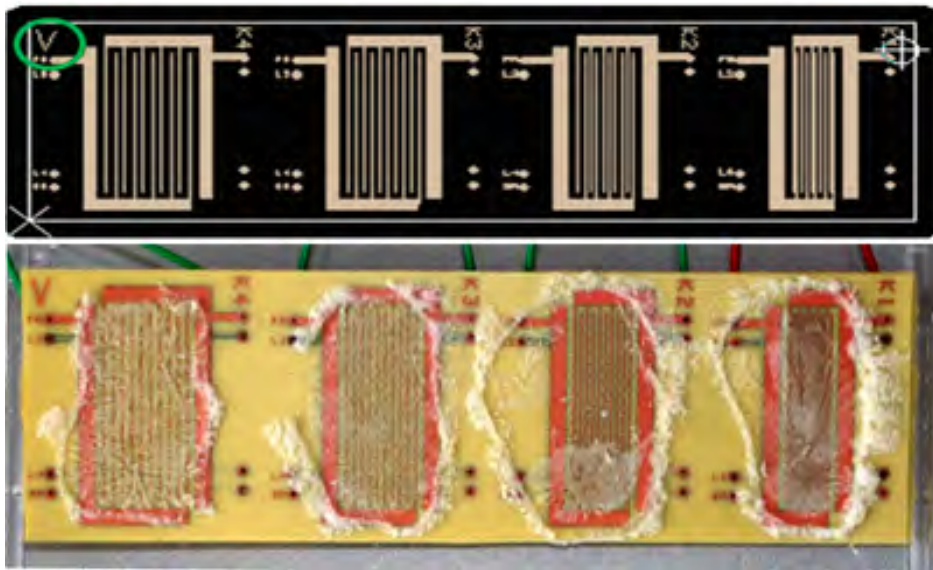


Fig. 1.19: PCB coupons, engineering concept and real platine superposed by NaCl.

By facilitating a humidity chamber, see Fig. 1.20, the coupons under discussion were covered by different salts (see Fig. 1.19) and the tests were carried out under different measurement routines, allowing final threshold conditions of  $85^{\circ}\text{C} / 85\% \text{RH}$  at 40 VDC. The former treatment at  $25^{\circ}\text{C} / 40\% \text{RH}$  was arbitrarily chosen to provide an initial control.

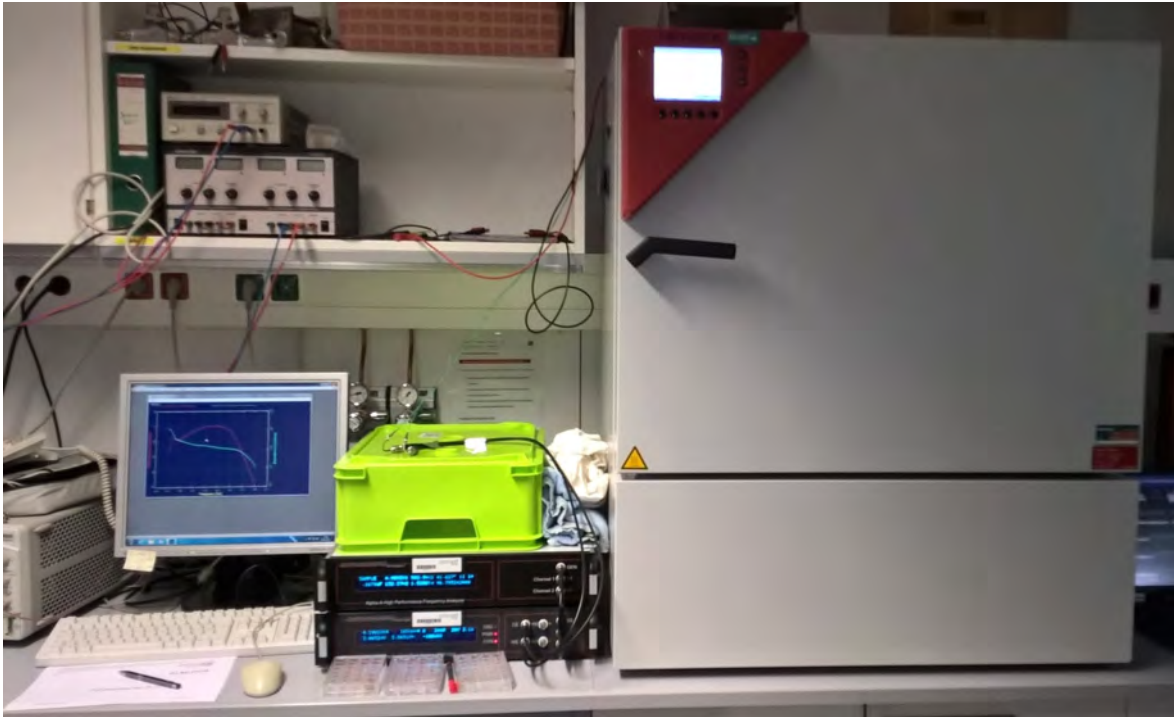


Fig. 1.20: Measurement setup showing the humidity chamber.

Comparison of the tests on S4-K3 (NaCl) in Fig. 1.21, non-stressed vs. stressed at 25 °C/40 % RH, respectively, does not reveal any impacts of salt/humidity on the impedancy measurements. While "Z", the impedancy provides information towards surface insulation resistance (SIR), a phase shift of  $\phi$  indicates a rise in capacitance, which vice versa assumes the presence of CAF within the prepreg.

# Stress Test CAF 0101H S4-K3 (NaCl)

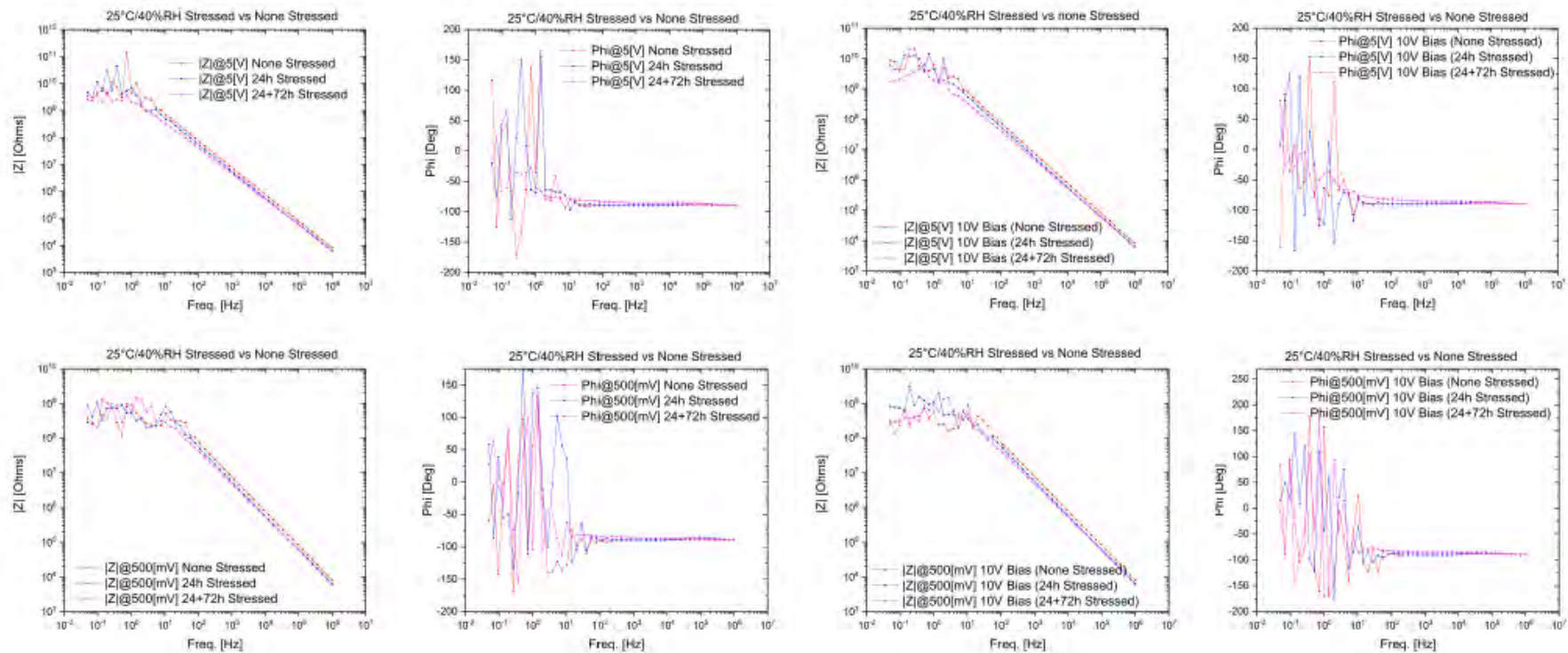


Fig. 1.21: Overview of impedancy measurements on S4-K3 containing surface-side NaCl.

Measurements on S4-K4 (NaCl) showed alteration of insulation resistance in the environment 85 °C /85 % RH specified by an IPC TM-650. The impedancy decreased approximately two orders of magnitude at aforementioned conditions, confirming the propensity of moisture influencing the material. The measurement at 20 °C / 40 % RH exhibited a resistance, re-ascended to data ascertained priorly.

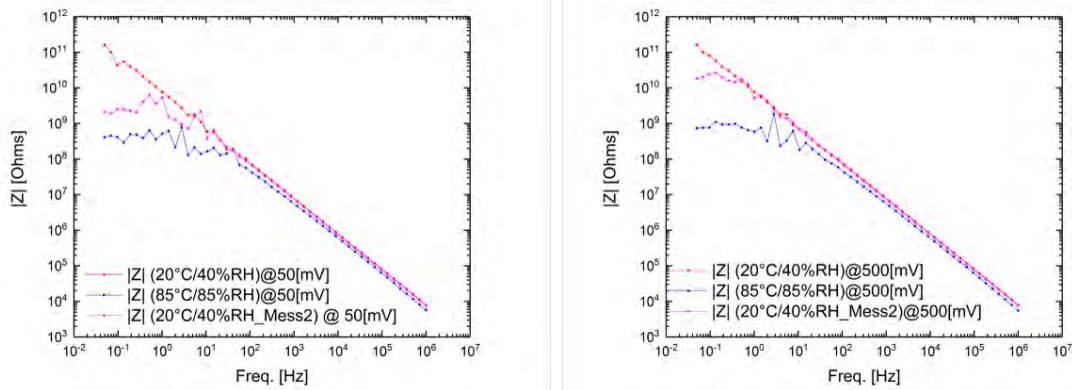


Fig. 1.22: Diagrams visualizing the indicated measurement routine.

Stressing the coupons at various exposure times at 5 V indicates an ohmic drop, six to seven orders of magnitude lower in contrast to the 20 °C / 40 % RH treatment. Either the phase angle exhibits critical shifts.

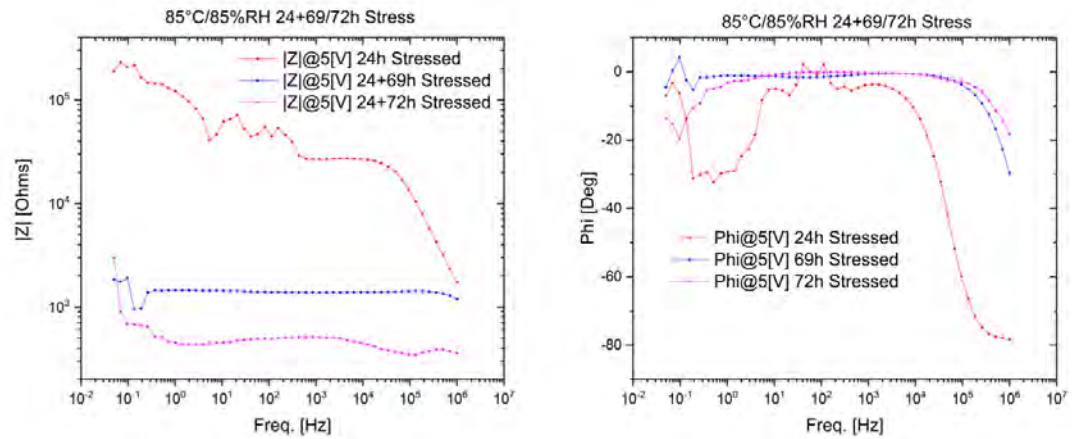


Fig. 1.23: Diagrams visualizing the impact of 85 °C / 85 % RH on the impedancy and the phase angle at 0.5 V

As a result of lowering the applied voltage stressing the comb structures for 120 h, the data points reveal the tremendous impact the parameters moisture, temperature and voltage have on the material.



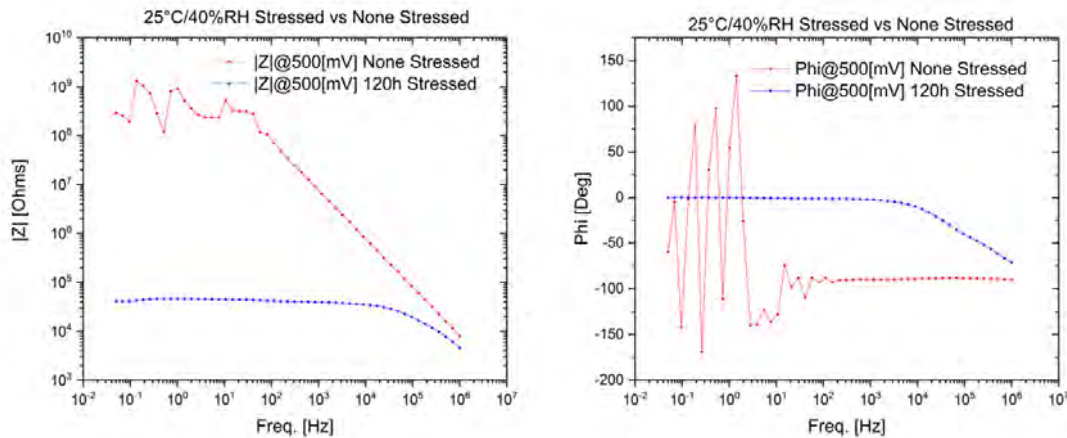


Fig. 1.24: Diagrams visualizing the impact of 85 °C / 85 % RH on the impedancy and the phase angle at 0.5 V

To conclude, the measurements performed by JR showed critical influences of temperature, moisture and voltage towards the alteration of electric properties of the materials.

### 1.9.3 Simulation of Influencing Parameters on the Electric Field - Materials Center Leoben

Computer numerical simulations, executed by Georg Reiss (research associate at the MCL, manuscript in preparation) revealed, that the parameters roughness, potential configuration, inhomogeneous permittivity, permittivity and copper trace slopes are preferred in descending order, respectively, influencing the electric field within a printed circuit board.

If assuming an ideal and homogeneous prepreg, the permittivity does not influence the potential distribution and the electric field, but the influence increases with the difference in the permittivity between the pure epoxy ( $\epsilon_{epoxy} = 3.6$ ) and the GREC (glass fiber,  $\epsilon_{glassfiber} = 6.3$ ) itself. An increase of a prepreg's permittivity to a value of 10 increases the max. peak of the electric field by 60 %, he states. The roughness is strongly affecting the electric field, especially when roughness peaks are facing each other tip to tip. Vice versa, a decrease of the electrical field in case of two valley points in-line may be assumed.

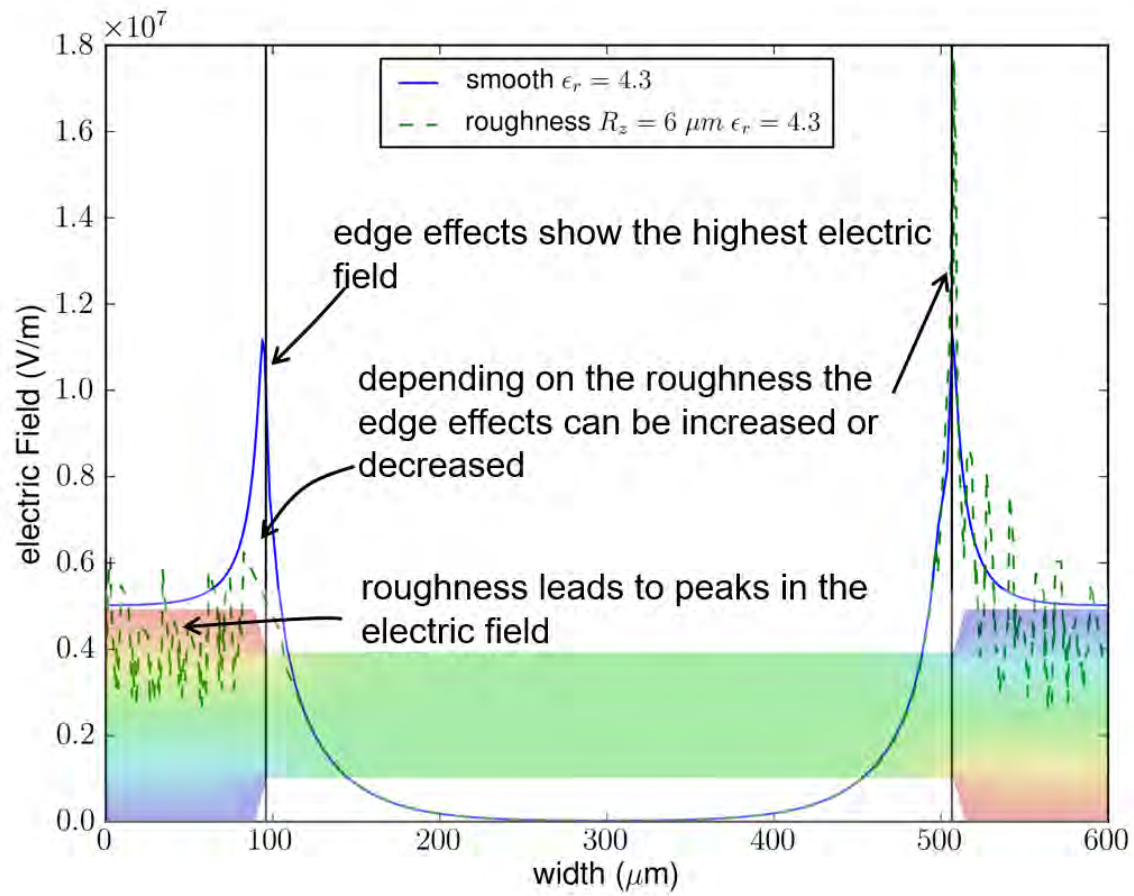


Fig. 1.25: Sensitivity analysis (simulation) of the electric field dependent on the local roughness.

Georg Reiss was further able to ascertain a part of the aforementioned MTTF formula, revealing numerical constituents and coefficients, having said again that this is one of the major tasks within the whole research.

## 2 Experimental Section

### 2.1 Introduction - Research Focus

As already reviewed in chapter "Theoretical Aspects" in the section "Conductive Anodic Filament" on p.21, CAF is a not very well understood error occurring in PCB's. It appears between the electrodes within the layers, preferentially migrating along the glass fibers, latently damaging the device. To find out which parameters exhibit the strongest influences related to the ionic acceleration factors including applied voltage, materials used, exposed temperature and humidity, a project, funded by FFG-COMET was set up. Within the research facilities, JR, MCL, TUG and ESI were consulted to cooperate with the industrial partners AT&S and PANASONIC to ascertain a MTTF formula. This formula should provide an evaluation method for the endurance of a PCB to take place under certain conditions, yielding a strong tool either for lifetime indication as well as an information carrier in the quality control segment.

The task for the Institute for Inorganic Chemistry on the Graz University of Technology (TUG) lies in a permeability study to evaluate diffusion of aqueous species inside solid industrial dielectric materials. A closer look to the materials will be taken in section "2.1.1 Matter of Interest" on p.48. The MCL coordinates the project properly and brings in an expertise in electronic knowledge.

While ESI focuses on imaging already treated materials by using imaging methods like SEM et cetera, JR carries out electrochemical impedance spectroscopy in a conditioning cabinet. PANASONIC and AT&S officiate as competence facilities, providing fabrication, assembly, and materials to investigate.

The following chapter will inform about the materials to be investigated as well as experiments and studies being held within the project.

### 2.1.1 Matter of Interest

Glass reinforced epoxy resin composites are a material of choice for the fabrication of a non-conducting basement to SMD's. They layers consist of glass reinforced polymers and are treated by several fabrication steps and are further on adhered layer by layer using some kind of resin. The former fabrication steps already include customer requests concerning etching connections. After "baking" of the printed circuit boards in a corresponding oven, the production is more or less completed. The former fabrication steps therefor already include customer requested connections.

The materials to be examined in the experimental time of the diploma thesis envisage only so called core matter. Core material is the single layer of a PCB, consisting only of the dielectric polymer and the stabilizing glass fiber scaffold including a distinct mass fraction. CAF is known to be primarily emerging at the fiber-polymer interlayer, synergized by channels caused by delamination, demasking and further.

By the reason of being a corporate secret, only a few information of the GREC cores were revealed. The materials investigated are R1570 and R1566WN and pending further disclosures no further clues will be available by industrial partners.

In order to measure diffusion or potentials, AT&S provided uncoated and two side copper coated sheets of R1570 and R1566WN. On the following pages, more information to the membrane material will be revealed.

## 2.2 Development of an Evaluation Environment

In order to achieve reliable measurement data, an environment to evaluate the diffusion of water in the matter of interest had to be created. To exclude influence by the surrounding atmosphere and hence value corruption due to external humidity, test vehicles were designed and manufactured.

The conditions the test vehicle had to fulfill were the following:

- A lockable cell which allows ...
- The implementation of an analyte, preferentially a sheet of matter to be investigated to the diffusion of substances ...
- Avoiding trespassing streams, thus ...
- Being reliable and assuring value repeatability ...
- Exhibiting durability resistance against aggressive and persistent chemicals ...
- Allowing users to modify measurement parameters by ...
- Providing insight into the analyte's space due to cells transparency, ...
- Possessing a long life span and being ...
- Economically designed to ...
- Avoid high cost by simultaneously ...
- Providing low maintenance and service attention ...
- Safe and simple in its application ...

Drawing attention to this constraints the cell was designed using SolidWorks 2015. Due to supply difficulties as well as not holding production costs in a first instance, the five cells were scaled down in length and diameter, though.

### 2.2.1 Diffusion Cell

The aforementioned test vehicle therefore describes a custom-built cell, which consists of two main parts, offering many measuring methods to execute. Due to the unexpected time consumed in the main data acquisition, no further experiments than those are written down in this thesis were performed, though. However, the diffusion cell is built of one half cell referred as an analyte part, which is separated by the analyte membrane from the second one half cell, providing an intruding substance to be examined in the analyte part.

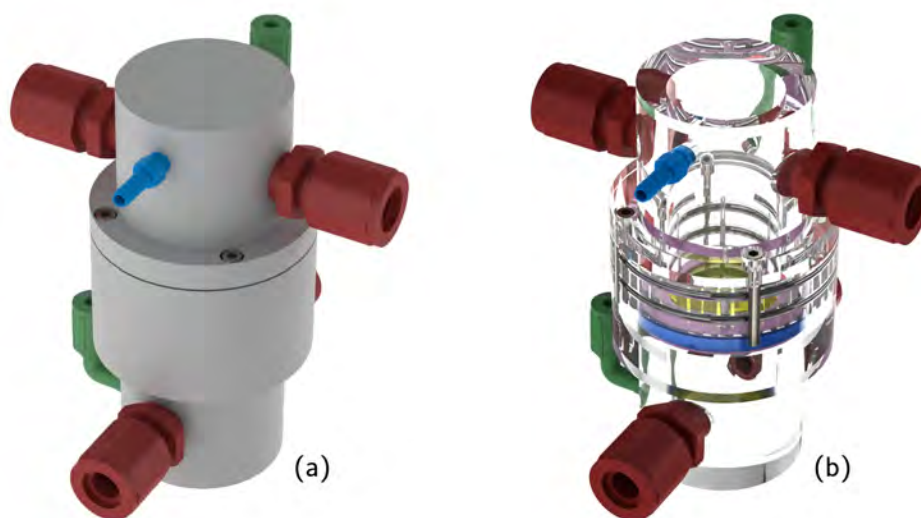


Fig. 2.1: Visualisation of the diffusion cell for (a) light sensitive tracing methods; (b) standard intention using transparent PMMA.

An additional content including images of the diffusion cell(s) are provided in the "Appendix".

During measurement data acquisition, the analyte cell is hermetically insulated against environment gases and a corresponding measurement device (e.g. pH or conductivity electrode) collects a substantial change over time, respectively. A membrane, literally the primary analyte, separates the two half cells from each other and is exposed to diffusion of the superposed substance due to a concentration gradient. As mentioned, several connections allow a change of measurement parameters to the favor of the responsible person in charge.

In 2.2 a part-labeled diffusion cell is depicted.

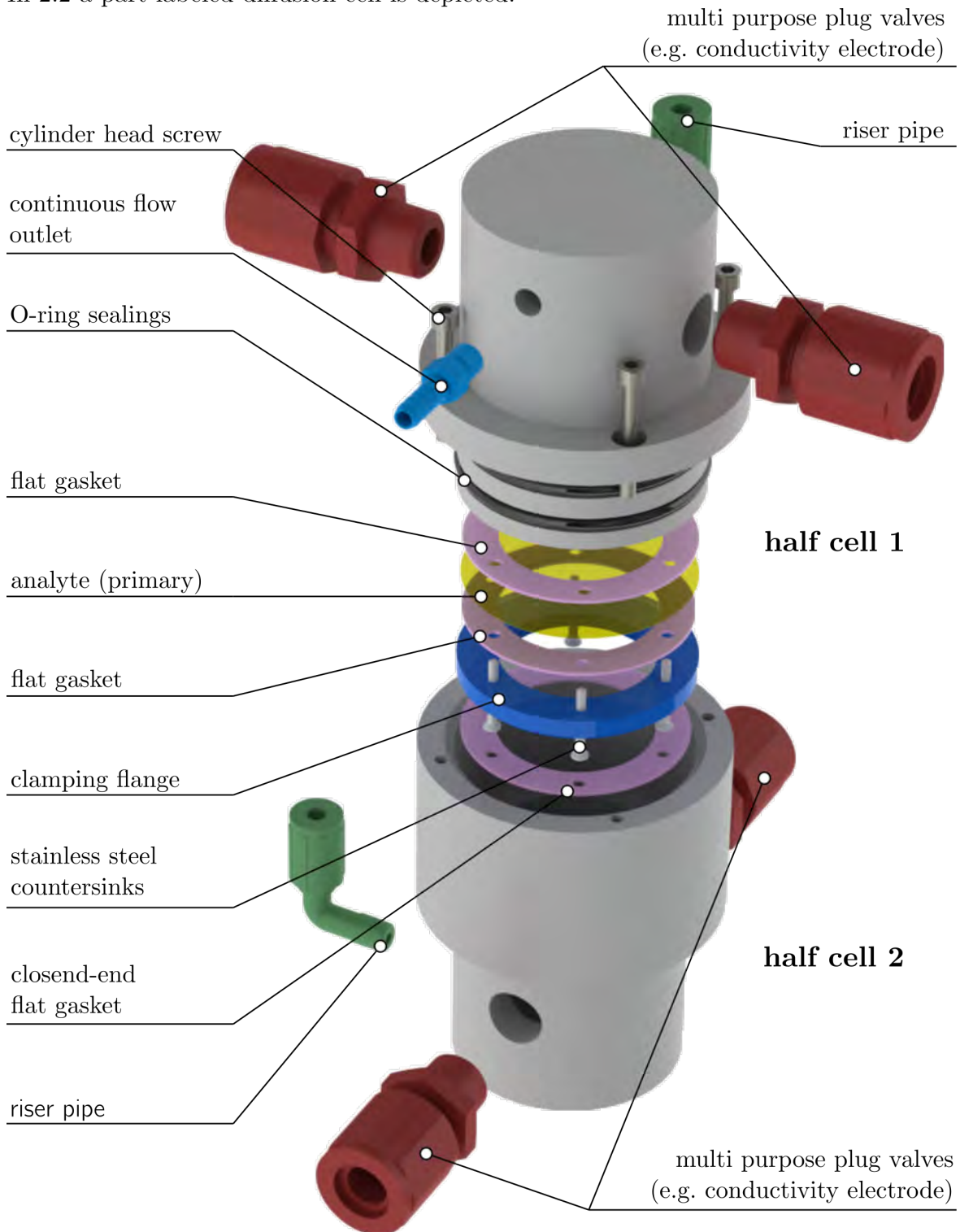


Fig. 2.2: Visualisation of the planned IR-Diffusion Cell in assembled state and dismantled.

A pathway to apply a gravimetric measurement is shown in section "5.3.1", p. 131.

### 2.2.2 IR-Diffusion Cell

In an early stage of the project declaration where work packages for the corresponding research facilities had to be stated, an idea for a second cell to evaluate water diffusion was under discussion. This test vehicle, combined with an IR analysis device should be able to ascertain the permeability of aqueous species having dipol interactions. The budget was to the favor of the standard diffusion cell, since it is more comprehensive and allows proof of concept in a first instance. Nevertheless a few images of the intended construction are depicted in the following. The corresponding engineering drawings can be found on p. 151.



Fig. 2.3: Visualisation of the planned "IR-Diffusion Cell" in assembled state.

The concept of this cell is to insert a membrane, superposed by a flat gasket and the reservoir stamp, which provides a force to seal the membrane against leaking. At the entry and exit of the Swagelok<sup>®</sup> adapters, sealed and windowed caps were intended to insulate the cell interior. By supplying the riser cap with a aqueous substance, an IR sepctrum is expected within a period of time due to permeation, respectively. Perpendicular to the Swagelok<sup>®</sup> two holes are positioned to allow rinsing of the adsorption chamber by inserting the certain valves. For the conditions the cell has to hold, only simple use and low production cost at paramount reliability are matter of interest. Additionally, the dimensions were properly chosen to mount the test vehicle into a conventional IR-device.



In Fig. 2.4 the setup, neither front-end caps and rinse valves shown, is depicted. To provide an idea of the function, the IR-beam is exaggeratedly displayed.

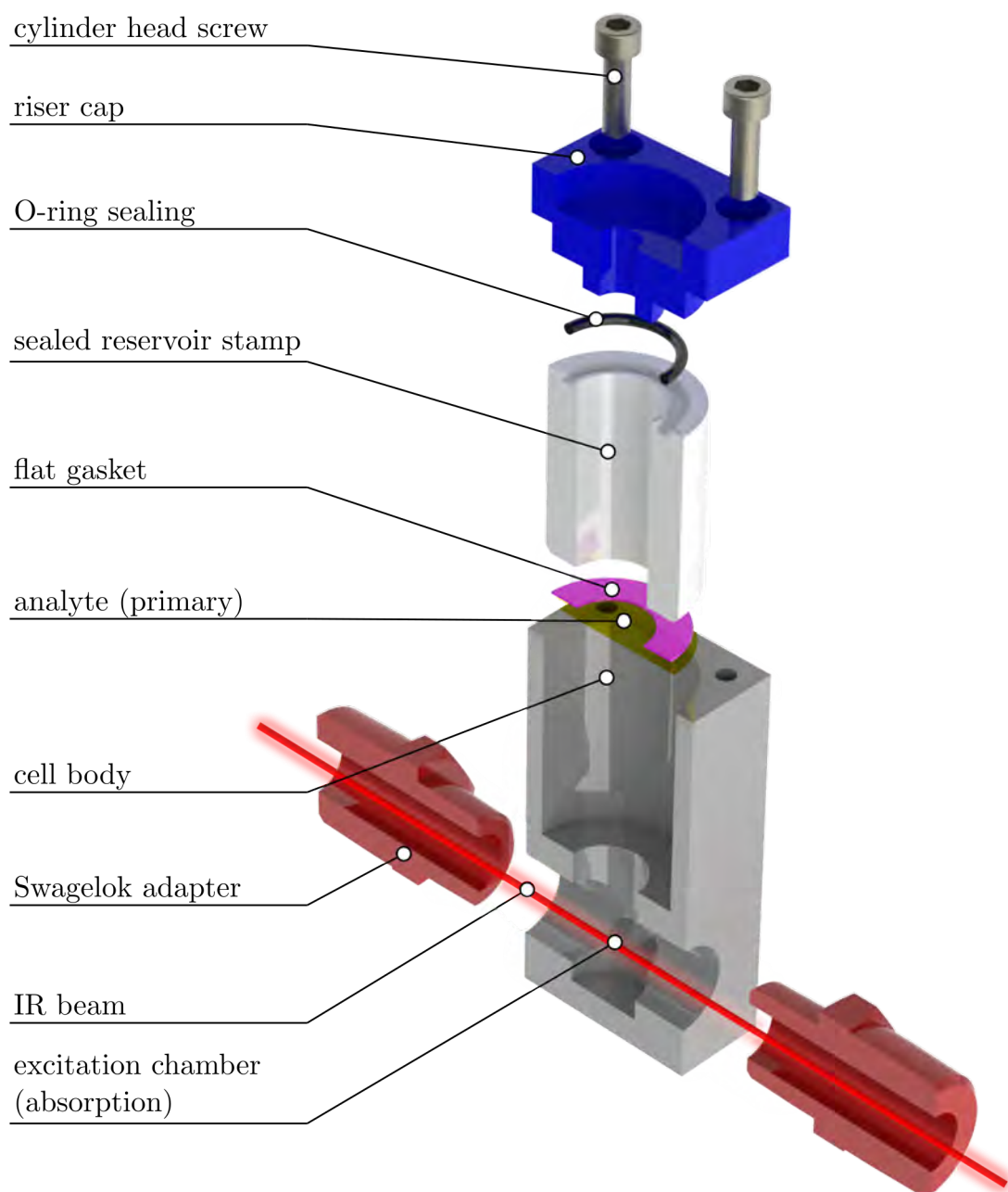


Fig. 2.4: Explosion drawing of the IR-diffusion cell excluding front-end caps and rinse valves.

For the corresponding engineering drawings consider a look to p. 151.

### 2.2.3 Fabrication of Rapid Analysis Cells

Since the comparison of a reference to the matter of interest is an essential and conventionally adopted method when doing analytical investigation, two different materials in various application cells were carried out. While the implementation of the reference membrane is paramount in order to state equality procedure, the use of a dialysis tube (Roth® ZelluTrans, Art Nr: E679.1, Nominal MWCO: 12,000-14,000, flat width: 45 mm, length: 30 mm, wall thickness: 20  $\mu\text{m}$ ), mounted in simple modified 20 ml PP vials served as a flash test. The fabrication of these test vehicles and the subsequent permeability check appeared to be very rapid and cheap. In addition, the measurements exhibited unexpected reliability.



Fig. 2.5: "Rapid Analysis Cells" as predecessors for gravimetric reference analysis. Dialysis tubes are clamped in into PP vials to build a barrier for the determination of diffusion to occur. The bottle is an empty storage vessel for metallic lithium, filled with drying agent.

Despite the fact that the dialysis tube was not preconditioned with water, the membrane kept tight and did not separate in action. The measurement setup was designed in that manner, that five water-filled test vehicles including the membrane to be investigated were introduced into a lockable glass vessel loaded with a tremendous amount of molecular sieve. However, the measurement was carried out in a total time of 96 h deriving from 24 h increments. As a method of measurement, once more gravimetric analysis was used to determine the water uptake in the drying agent. Fortunately, by taking advantage of the lightweight vials an additional parameter could increase relia-

bility by evaluating the loss of mass in each water reservoir by reason of permeability. For the corresponding measurement data refer to p.100.

## 2.3 Analyte's Preparation

In this thesis, the term analyte is sometimes diffuse, since it is used either for the GREC membrane as well as for the drying agent. While the latter has deserved this expression for being in direct correspondence with the gravimetric value, the really matter of interest, the GREC is named primary analyte.

### 2.3.1 Primary Analyte - GREC's

The glass reinforced epoxy resin compound membrane (GREC) as the name suggests is a polymer, reinforced by a glass scaffold spun in a defined mass fraction including intended mesh size. The term epoxy may not obligatory be related to an oxirane monomer unit, though. Details about the materials R1570 and R1566 are not disclosed to the cooperative research facilities. Visually the R1566 is more yellowish and may conservatively estimated as more rigid than R1570. The investigations required on the materials were specified by the industrial partners.

#### 2.3.1.1 1566/1570 Core Preparation

The diffusion cell has requirements towards the membrane geometry to operate properly. The matter to be examined has to provide an outer diameter of approximately 54 mm including 6 x 60° equidistant stamp holes of Ø 5.5 mm. Restricting the permeability to dense materials, the thickness of the specimen can theoretically be adopted as infinite. In preliminary experiments, the material to be examined was hand cut using scissors and a paper punch. Unfortunately the core material is a compound consisting of a polymer adhering on a crosswise arranged glass fiber scaffold. When cutting with orthodox tailoring tools the edges are inevitably frazzling out. Thus the sample geometries, either those copper-coated, were processed via a laser-cutting CNC-machine at AT&S in Leoben, Styria.

#### 2.3.1.2 Pre-Drying the GREC Cores

Although the core material should be in a dried stage after fabrication steps, humidity residues could cause significant deviations when carrying out gravimetric analysis. Furthermore, as shown in section "3.5 Measurement Series" on p.77, potentially wet matter was supposed to be a trigger to yield initially high mass adsorptions within the

first 24 h. Hence, a pre-drying of the membranes to being measured were carried out, furthermore a dry and sterile storage of indoors material should be maintained. In a first attempt, the membranes were stored on a PE-coated steel wire, gaped one by one using hexagonal nuts in an desiccator. This method turned out to be awkward since the abstraction of the membranes was very difficult to execute. To store them dry and sterile, a membrane tower (see section "5.1 Development of Supply Tools" on p. 127 was designed and 3D-printed. It provides possibility to store membranes of distinct materials, enables quick and ease extraction of the sheets and latter can be labeled. As shown in section "3.3 Pre-Drying Cores" on p. 74, no significant drying of the GREC's could be observed. The procedure of dry storage of the membranes was hold until the end of the research study.

### **2.3.1.3 Blank Preparation**

In every analytical measurement method, inevitable background signals can be observed. Those values, merging from either internal sources such as signals from electronic measurement devices and/or external origins, which for example involves associated species, channel streams et cetera cannot be avoided and have to be considered when gathering results. In the diffusion cell, we have deviation values due to channel streams, adhesion of water on the membrane and cell walls itself and internal cell volume humidity as relevant factors, not to forget effects concerning condensing/evaporating of aqueous species into or out of matter by virtue of significant temperature differences. Thus the blank of the cells was determined in 24 h increments, yielding an overall blank value in action for 96 h at 60 °C . To realize the blank value evaluation, five impermeable diffusion barriers, using aluminum, 0.5 mm in depth, were prepared. The diameter was produced by scissor tailoring, the screw holes by stamping with a commercially paper punch.

### **2.3.2 Secondary Analyte - Drying Agents**

The theoretical aspects of drying agents have already been discussed in the first chapter. The following paragraph already implies and enlists the finally chosen desiccant as well as the initially used drying agents. This section can already be seen as a foreclose to section "3.5", exactly on p. 79, where the reasons for the selections are described in context.

### 2.3.2.1 Desiccant Selection

This section will give a brief conclusion to the finally used drying agent to determine water adsorption. Initially, phosphorous pentoxide was deployed as absorbant. Additionally, it's application provided a fast statement for the presence of water, channeling through the matter of investivation, by indicating a quick change in color by an introduced tracer sensitive to water. In an advanced stage of reliable data evaluation, unfortunately  $P_4O_{10}$  misfitted for further experiments, since its capability of drawing aqueous species was too excessive to collect reasonable values to distinct. Not only that it seemed to leech humidity through the weak points of the system, it additionally drew out substances of the sealings, yielding dark-colored liquid content of polyphosphorous species. Corresponding measurements concerning mass adsorption revealed either high amounts of mass expected, or no match of internal blank to core material. In a further experiment using magnesium sulfate as a drying agent, a very strong contrast to the beforehand chosen  $P_4O_{10}$  could be observed. It proved the difference expected between an internal blank and the GREC's, but failed in providing reasonable values regarding LOD. Furthermore, the drying agent trickled out of the desiccant boxes due to an electrostatic charge rose by the wall friction when opening the cells. The next drying agent deployed, molecular sieve 4 Å showed excellent performance in respect to drying efficiency, drying capacity and ease of use. It provides superior hygroscopic properties (0.2 g  $H_2O$  per gramm of desiccant) and is available as small granules of  $D > 1$  mm, hence if a pellet gets lost it can easily put back into the measurement vessel. To conclude, molecular sieve 4 Å yields perfect LODs over a reasonable period of time and is easy to handle in action. Additionally it can be dried and regenerated over vacuum at 200 °C.



Fig. 2.6:  $P_4O_{10}$  after absorption of water shows a polyphosphorous liquid containing black residues.

## 2.4 Process of Data Evaluation

### 2.4.1 Execution of Gravimetric Analysis

The main acquisition of data in this thesis was done by the gravimetric analysis. By utilizing the diffusion cell, the membranes to be investigated are observed towards their permeability to aqueous solutions. The GREC membranes therefore are insulated and separating both cell halves hermetically. The upper part is filled with the desired diffusive species, the lower part is equipped with a drying agent. This desiccant acts as a secondary analyte, is weighed on an analytical balance to ascertain the mass adsorbed to it within defined periods of time. Thus, setting up different measurement series made it possible to accumulate the certain information to provide material specific diffusion data. To get an idea of the practical implementation and the use of the diffusion cell to yield gravimetric data, refer to section "5.3.1" on p. 131.

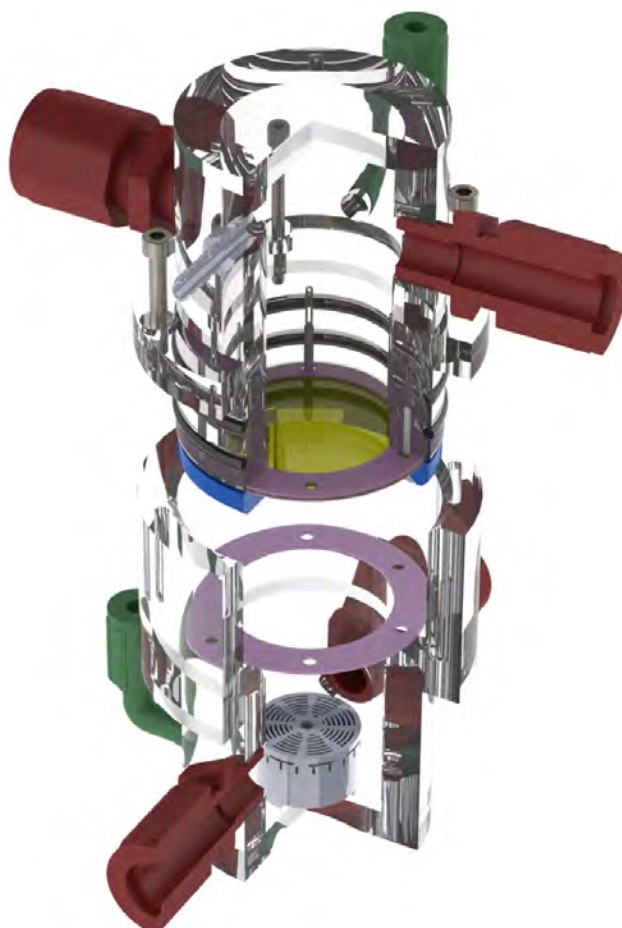


Fig. 2.7: Explosion illustration of the diffusion cell containing a drying agent filled "Gravi-box". A picture including part-labels is found on p. 131 in section "5.3.1".

Dependence on the certain measurement series, the process of assembling the cells is slightly different. Therefore a description only for the final setup is represented in detail. The prior evaluation series were mainly recorded to gain information of influencing parameters to maintain a steady repetition of measurement values. Since the final setup includes the amount of the maximal parts involved, the beforehand taken series of measurement are part of the bottom-up process.

I. Cell Assembly:

a) Sealings

To provide a hermetically sealed measurement environment, the cells are equipped with O-ring-sealings in the designated channels.

b) Attachments

As shown in Fig. 5.6 on p. 134 the Cells are mounted with purpose-built attachments. The threads have to be wrapped with Teflon to protect the connection against destruction on the one hand and leak-tightness on the other hand side.



Fig. 2.8: Diffusion cell, utilized with a conductivity electrode to detect ions passed through the membrane.

Both cell halves are now fully assembled and a measurement setup can be defined and mounted.

## II. Analysis Preparation

### c) Membrane Insertion

A custom-built membrane matter can now being inserted into the cell using the PMMA-flange. To simplify the mounting process it is advisable to arrange the stainless steel countersinks and the flange face to face with the base plate (e.g. table plate) and add the flat-sealings and the membrane step-by-step, see p.5.5 fitting to the bolts. As soon as the assembly includes connecting elements and the sealings/membrane in the order screws-flange-sealing-membrane-sealing, this unit can be (handle with care, loss of screws) deployed onto the Cell. By initially fastening the joining elements carefully to the cell by using a slotted screwdriver, the applied final force should be maintained by using the first pitch of the lever drill of a cordless drilling machine. Since the assembly is mounted outside of an inert atmosphere, the adherence of moisture can not be avoided. It is advised to store the cells in a hot and dry atmosphere while configure the desiccant vessels.

### d) Desiccant Preparation

In order to setting up the desiccant boxes, one should aware of not mixing any parts between the boxes. This includes the screws. Before filling in the beforehand vacuum dried mole sieve, the tare weight should be assigned to each box-assembly using an analytical balance. To fill in the mole sieve into the weight-characterized drying agent boxes it is advised, to deploy the screw inside the holes to avoid drawing in of desiccant beads. The connection of the grid cover to the vessel and tightening the screws should be followed by the weighing of the filled boxes using the analytical balance. Note that the drying agent should not be exposed to the surrounding environment/humidity over a period of time.

## III. Finalizing the Cells

### e) Lubrication

Before placing the desiccant boxes into the cell bottom by using tweezers, lubrication of the O-ring sealings is a well recommendation. Remove the smaller PA6.6 screw from the drying agent cell to avoid compressing air



between the cells when fitting in the membrane cell.

f) Deploying of the Drying Agent

The beforehand filled desiccant boxes now have to be deployed into the cell-bottom.

g) Insertation of the closed-end Sealing.

As a last step before closing the unit, the closed-end PE-foam sealings have to be deployed. Subsequently the cell halves can be fitted together. After closing the drying agent side with the ventilation screw, the compression screws have to be tightened to fastening both cells together and pack the closed-end PE-foam. Prior to deploying the cells into a drying cabinet, the membrane cells may be filled with a desired aqueous solution. For low volatile solutions, the cap nuts may be hand-tightened. Note that volatilization may cause high pressures, leading to membrane expansion and therefore elevated and corrupted values in gravimetric evaluation. In most cases the measurement intervals were 24 h, stacking up to 96 h full evaluation procedure. To yield reference values, water adsorption of cell 0 and cell 4 was only determined at the end of the series. For practical ease of execution it is recommended to use the Guide "Gravimetric Analysis" at p. 131.

### 2.4.2 Execution of Electrokinetic Potential Analysis

The electrokinetic potential analysis ( $\zeta$ -potential) was performed to get an idea of the influence of chemicals used in fabrication processes. The behind intention considers an enforcement of ionic migration due to generated surface charges raised priorly by the purpose of manufacture. Thus, small sheets of R1570 and R1566 were cut out and placed into vials filled with chemical solutions applied in industry. The conditioning at RT took at least three days until the  $\zeta$ -potential analysis was subsequently performed. The chemicals are solutions of substances and are labeled "Chemisch Kupfer", "Galvanisch Kupfer" and "Ätzer". The ingredients of these solutions as part of the sub-processes called "Kupferprozess" and "Photoprozess" are shown in the following, respectively.

Table 2.1: Overview of reviewed industrial chemicals in electrokinetic potential analysis.

Chemisch Kupfer	Galvanisch Kupfer	Ätzer
NaOH (30 %)	$\text{Cu}^{2+}$	$\text{CuCl}_2$
Cu-Lösung Printoganth P	$\text{Fe}^{2+}$	HCl
Basislösung Printoganth P	$\text{Fe}^{3+}$	$\text{H}_2\text{O}_{\text{deion.}}$
Stabilisator Printoganth P+	$\text{H}_2\text{SO}_4$ (50 %)	
Cu-Reduktionslösung	$\text{FeSO}_4$ (50 %)	
	$\text{Cl}^-$ (50 %)	
	Glanzzusatz Impulse	
	Grundeinebner H6	

In order to gain reference observations, the GREC membranes were either immersed into standard chemicals, which may play a partial role in fabrication process. The chemical agents used were  $\text{H}_2\text{SO}_4$  (95%),  $\text{H}_2\text{O}_2$  (50%) and NaOH (5M).

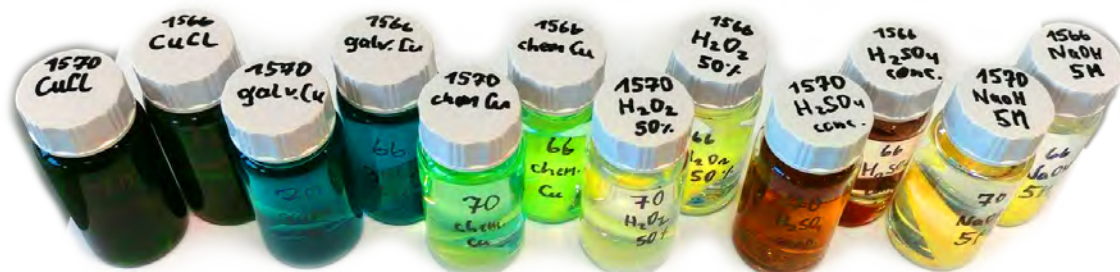


Fig. 2.9: R1570 and R1566, preconditioned in standard chemicals for  $\zeta$ -potential analysis.



Fig. 2.10: Coloring of  $\text{H}_2\text{SO}_4$  in presence of R1570 (dark red) and R1566 (light red). Both GREC membranes develop a reddish surface when getting immersed into concentrated sulphuric acid.

By the means of an ATIR device, the R1570 and R1566WN were investigated due to their IR-behavior. In the course of measuring IR bands (see section "3.7"), all the treated membranes have undergone the same procedure to find a correlation towards zeta potentials.

For the determination of the isoelectric point, which describes a state of charge equalisation of the ions on the solid surface, an electrokinetic measurement device called SurPASS™ 3, Anton Paar, was used. The following pages will provide a brief introduction in how to perform a measurement. The corresponding values (IEP) obtained by this method are listed in the section "Electrokinetic Potential Analysis" on p. 101. For a guide to handle a zeta potential analysis refer to p. 135.

For economic reasons it is strongly recommended to have the certain solutions in stock. The solutions includes calibration standards on the one hand and measurement solutions on the other hand side. Prior to the measurement, one have to calibrate the device towards conductivity, which may be achieved by either a conductivity standard, shown in Fig. 5.7 or by manually preparing a concentration of KCl as suggested from Anton Paar, see Fig. 2.11. Additionally it is obligatory to adjust the pH-electrode using the buffer solutions depicted in Fig. 5.7.

Before operating the device, the same has to be activated and simultaneously the N<sub>2</sub>-valve should be opened, which conserves conditions within the measurement cell. On p. 144, Fig. 5.16 indicates the device's parts.



Fig. 2.11: Solutions (KCl 1 mM, HCl 50 mM, Milli-Q) to be prepared for rinsing and measuring on the SurPASS™ 3.

## 2.5 Alternative Experiments and Studies for Permeability Detection

In the course of a simultaneously investigative work towards permeability and adsorption of water an alternative route to assess the quantity passed by was introduced. While the majorly applied measurement methods intentionally includes gravimetric analysis, conductivity determination as well as other ion detection methods, the idea was to check the adsorption ratio by the difference of metals relating to the electrochemical series. By opposing two metals of different potentials vs. SHE in humidified environment, separated by a solid electrolyte and a separator itself, a comparison of results should be obtained. However, a substance to stand for the solid electrolyte had to be found, which is suitable in terms of fabrication, providing superior hydrophilic properties. By setting up solubility series including derivatives of celluloses, ethyl cellulose was chosen to give it a try in an experiment. Due to the fact, that the metals in a first instance were aluminum and copper, only an appropriate amount of current could be observed. The reason lies within the passivation of aluminum, which instantly builds passivation layers (industrially applied in anodic coating) in the presence of oxygen. Nevertheless a current could be proved, though. However, by replacing aluminum with zinc, higher direct currents were achieved. The anode was a simple commercially available hot-dip galvanized steel tape, which was similarly to the cathode, dip-coated with ethyl cellulose and conducting salt, dissolved in tetrahydrofuran (THF). A cellulose hydrate foil (cellophan) acted as a rigid separator between the electrodes, either coated with the solid electrolyte. The first prototype was a wooden board, where the cathode (Cu) was adhered using a two-component adhesive, superposed by custom-cut frame of R1570 to avoid channel and leakage currents. A large-area piece of cellophan was stretched across the topically insulated cathode metal to provide intended-only currents. By using a multimeter, a current could be observed when contacting the zinc- and EC coated steel tape to the cathodic contact area by the premise of humidity presence (water droplets).

To enhance quality of the experiment, hence improving reliability a second prototype was invented. The new assembly has the opportunity to switch either the anodic or cathodic part, providing possibilities to generate measurement series of different metals as well as different solid electrolytes (SEs). Furthermore, the demand for a pure anodic zinc metal prompted an inhouse galvanisation of a copper substrate. By the means of a potentiostat and a custom-built electrochemical cell, zinc was deposited on the copper substrate. As a depletion substrate, commercially available zinc granules

were drilled and chained one by one on a stripped copper cable. Despite using native zinc, strong dendrite growth could be observed at the burrs as a fact of grinding and polishing the metal. To avoid the unfavored deposition at electric field tips, literature found additives were introduced to the cell.<sup>[28]</sup> By inserting polyethylenglycole (PEG) and tetrabutyl ammonium iodide (TBAI), a strong alteration to the favor of surface smoothness could be observed. At least, a mixture of 1 M ZnCl, containing 21 mg PEG and 41 mg TBAI, was chosen. By the utilization of a SEM the topical differences of brightener-introduced methods are depicted in section "3.8" on p. 117.

## 3 Results and Discussion

Beginning with the experimental data of this chapter providing the important information about permeability rates, the measurement series will be represented in detail to get access to the attempts which finally yield the appropriate measurement series 11 to 16. Additionally, the  $\zeta$ -potential analysis will be discussed.

### 3.1 Results' Abstract

This section will comprise the certain data of interest, which includes permeability rates in a SI-conformer demonstration as well as hard facts derived by the electrokinetic analysis.

#### 3.1.1 Gravimetric Analysis

Besides the spreadsheets for the determination of the line diagrams which assume cumulative and incremental slopes of the diffusion rates within the corresponding time segments, tables of important values will expose the data of interest. In order to execute the gravimetric analysis, an analytical balance KERN ALS 220-4 was used. The molecular sieve 4 Å deployed in cells and facilitated in measurements was received from VWR Chemicals (1 kg, CAS: 70955-01-0).

The following table will reveal the final permeability rates in grams per square meter per day [ $\text{g} \cdot \text{m}^{-2} \cdot 24 \text{h}^{-1}$ ]. For the sake of comprising reliable values only, the table contains only the data ascertained in the measurement series 11 to 18. Series 10 reflects the blank\* value that has already been subtracted from the former measurement values in series 11 to 18. It is advised to keep in mind that the references differ in membrane width. The PET reference is 250 microns in width and is known to provide a diffusion rate of  $2.4 \text{g} \cdot \text{m}^{-2} \cdot 24 \text{h}^{-1}$  at 25 °C, the determined value derived at 60 °C. The MCE dialyses membranes (40 microns width) were treated in rapid analysis cells at 22 °C which exhibited a smaller diameter for diffusion to occur. The increased SDs in the GRECS are assumed to arise from the higher surficial roughness.

Table 3.1: Final mean values of the max. adsorption levels including standard deviations. The values are derived by normalizing 96 h measurement data to 24 h.

Series #	GREC	Temp. [°C]	pH	Permeability Mean $\pm$ SD [g · m <sup>-2</sup> · 24 h <sup>-1</sup> ]
10	Al*	60	7.00	15.9 $\pm$ 1.3
11	R1570	60	7.00	9.2 $\pm$ 4.3
12	R1566	60	7.00	4.1 $\pm$ 3.0
13	R1570	60	4.01	9.8 $\pm$ 2.5
14	R1566	60	4.01	10.5 $\pm$ 3.4
15	R1570	60	9.00	11.8 $\pm$ 3.5
16	R1566	60	9.00	8.6 $\pm$ 2.3
17	PET	60	7.00	11.4 $\pm$ 1.1
18	MCE	22	7.00	980 $\pm$ 135

Summarizing the data shown above, considering a pH range of 4 to 9 at approx. 60°C, one can conclude an overall materials' permeability rate of 9.0 g · m<sup>-2</sup> · 24 h<sup>-1</sup>, which is similar to the diffusion rate of the PET reference of 250 μm in width.

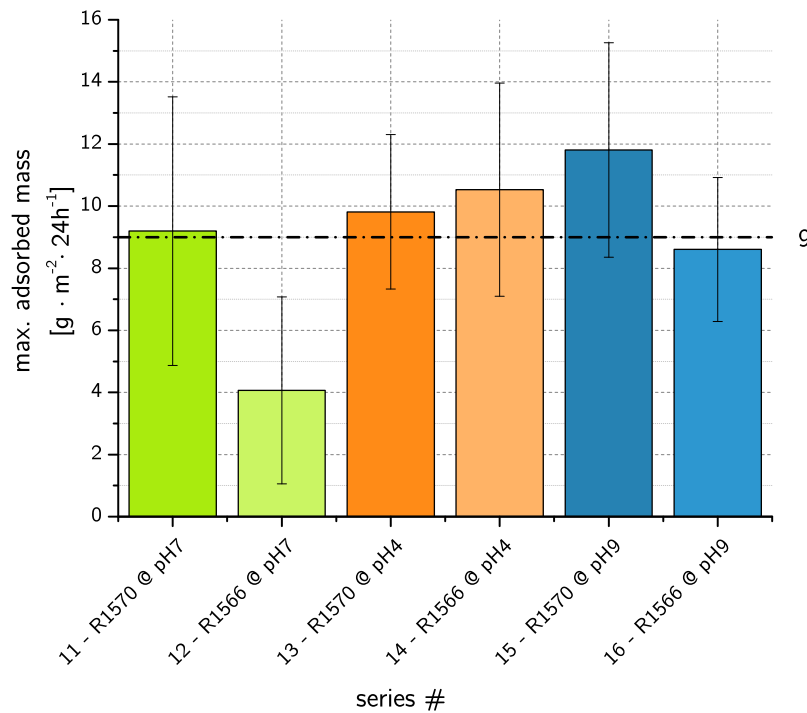


Fig. 3.1: Final permeability values including average of the means and row standard deviations.



In order to address the pH dependent permeation rates to the resins themselves, the following diagrams depicted show the means of both the resins R1566 and R1570.

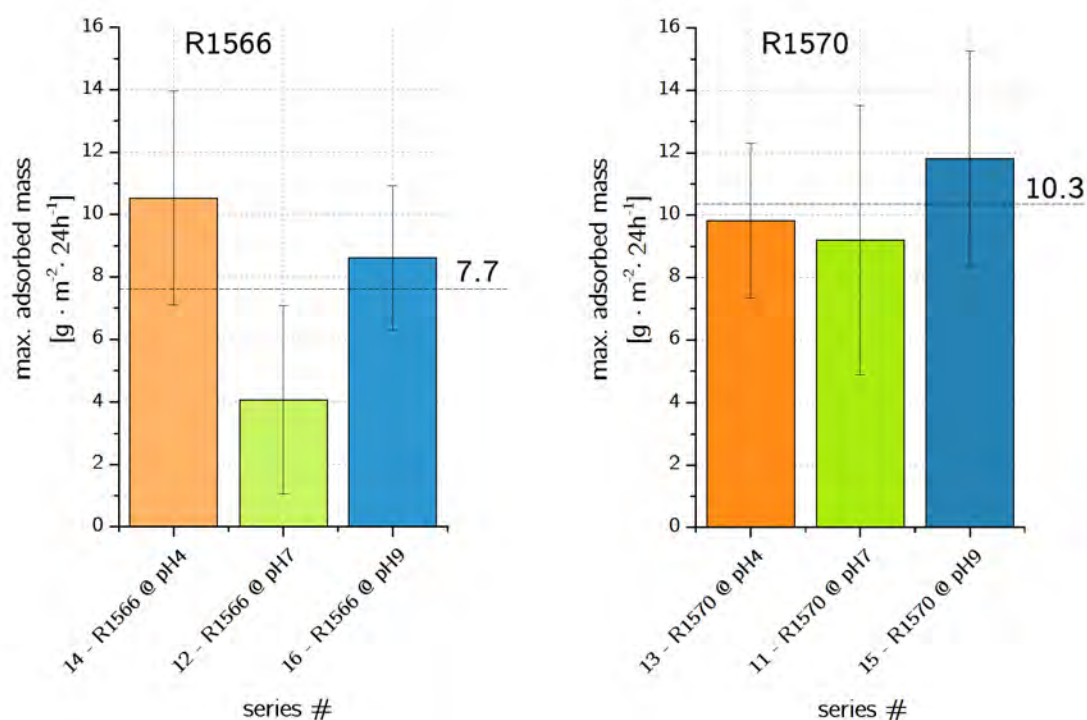


Fig. 3.2: Final permeability values including average of R1566 (left) versus R1570 (right).

Despite the columns reveal strong standard deviations, the means allow to distinguish between the diffusion rates of the cores. R1566 claims an mean permeability rate of  $7.7 \text{ g} \cdot \text{m}^{-2} \cdot 24 \text{ h}^{-1}$  while R1570 shows  $10.3 \text{ g} \cdot \text{m}^{-2} \cdot 24 \text{ h}^{-1}$  in average. With a difference of  $2.6 \text{ g} \cdot \text{m}^{-2} \cdot 24 \text{ h}^{-1}$  from R1566 to R1570, the latter resin seems to be more prone to the diffusion of aqueous penetrants, the former core though, assumes to be more susceptible to the buffer solutions. Comparing these results to the OTR measurements on p. 40 one might recognize a trend. In contrast to R1566, R1570 is twice as susceptible to the penetration of oxygen and exhibits an approx. 25% higher diffusion rate and that core material should be, putting it mildly, more prone to the formation of a CAF.

As depicted in Fig. 3.3 the final data are derived by deducting the mean value of the blank series from the mean values of the GREC membrane series, taking into account the error propagation<sup>[5]</sup>.

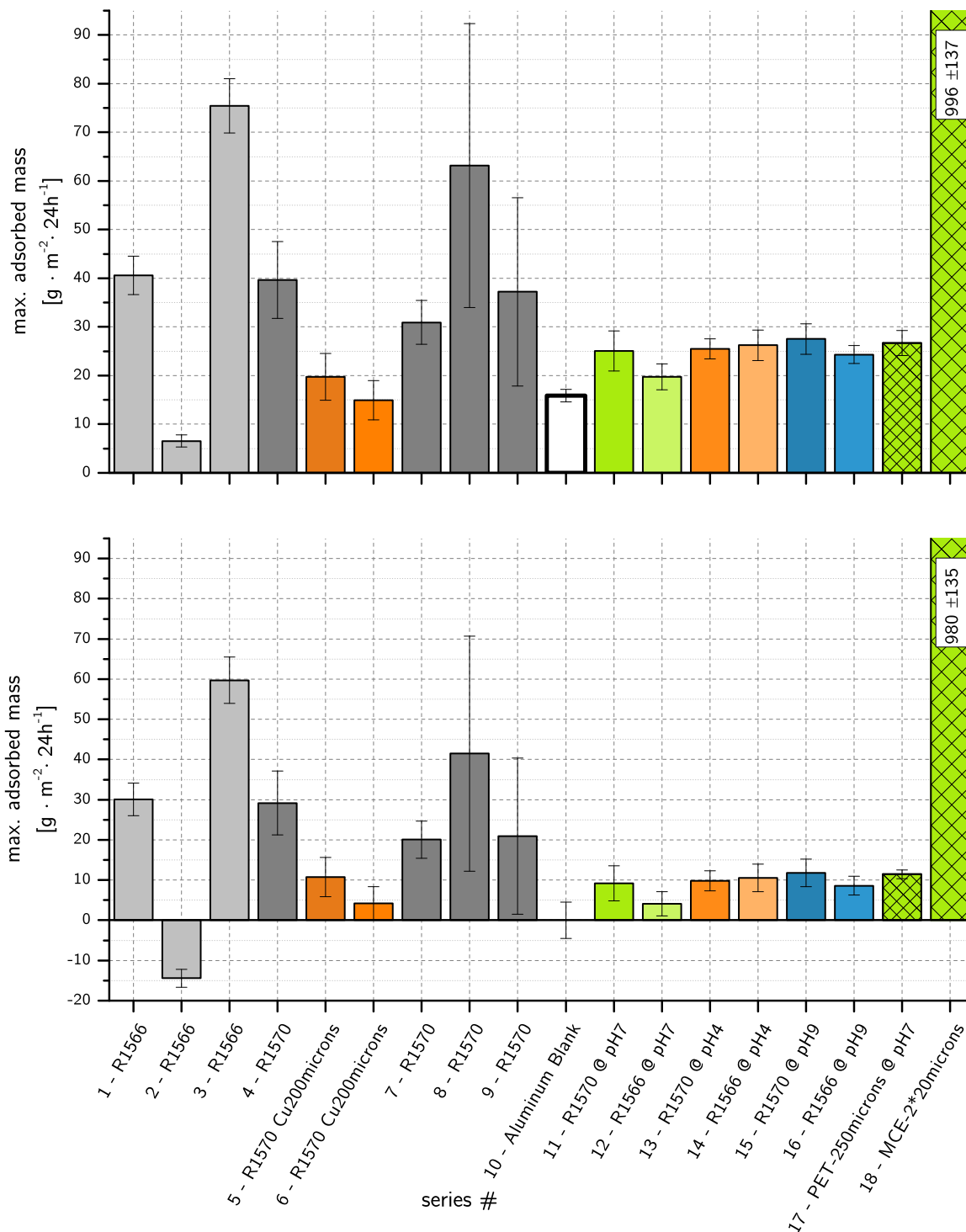


Fig. 3.3: All the measurement series showing max. raw data evaluated above and blank-corrected values below.

The figure not only takes out how to proceed with the raw data, it gives information about the process of achieving diffusion cells' reliability. The values of the first attempts reaching series 10 are indistinguishable from the following series 10 to 17. Additionally, observing series 5, 6 and 10 reveals parity of diffusion barriers.

By being an order of magnitude larger than the highest GREC membrane series, the last series is noteworthy, manifesting superior properties in terms of water admission. Take into account, that the membranes used here are  $2 \cdot 20 = 40$  microns in thickness. The temperature, which exponentially influences the diffusion coefficient, is kept at  $22^\circ\text{C}$ , though. This property makes this membrane matter, a mixed cellulose ether, a paramount material for the application as a fluid exchange membrane, primarily known as dialysis tubes in medicine.

As the temperature dependance of the diffusion coefficient was recently mentioned, a closer look to the gravimetric analysis of the PET reference offers confirmation of discussion. At  $60^\circ\text{C}$  the material exhibits a permeability of  $11.4 \text{ g} \cdot \text{m}^{-2} \cdot 24 \text{ h}^{-1}$  in contrast to the industrially ascertained value of  $2.4 \text{ g} \cdot \text{m}^{-2} \cdot 24 \text{ h}^{-1}$  at RT. In what extent this could be ruled as law is a matter of enhanced investigative work, specifically by deploying the diffusion cells to action. It is assumed that the cells approximates a real value rather well, unless the terminal value is not confirmed yet by a calibration office by the means of references. Coming back to the PET material, a value, foreign from linear ascend is reached, which states and refers back again to the aforesaid cells' real value approximation. Taking into account the abundance of influences, the last measurement series are prominent in terms of reliability at the cost of the former measurement series 1 to 9. If the originally intended parts were provided from the beginning on, seriously carried out measurements could presumably be taken from the closest beginning, though. Fortunately, a step-by-step improvement could be developed by continuously approximating to the intended construction. It is therefore of relevance to show the affords being taken in the preliminary phase, which is found on p. 79.

### 3.1.2 Electrokinetic Potential Analysis

The electrokinetic potential analysis or zeta potential analysis revealed that there are significant differences between both materials R1570 and R1566.

Table 3.3: Summary of facts of the zeta potential analysis, containing conditioning agents, acidity and IEP values.

Treatment	R1566	R1570	swelling
untreated	acidic, IEP @ pH 3.7	acidic, IEP @ pH 3.3	-
chemCu	inert, IEP @ pH 3.9	acidic, IEP @ pH 3.7	-
galvCu	inert, IEP @ pH 3.8	acidic, IEP @ pH 4.1	-
CuCl <sub>2</sub>	acidic, IEP @ pH 4.4	acidic, IEP @ pH 4.3	-
H <sub>2</sub> O <sub>2</sub>	acidic, IEP @ pH 3.3	acidic, IEP @ pH 3.2	1570
H <sub>2</sub> SO <sub>4</sub>	acidic, IEP @ pH 2.7	acidic, IEP @ pH N/A	1566/1570
NaOH	acidic, IEP @ pH 3.2	acidic, IEP @ pH 3.5	-

Table 3.3 indicates, that all the membranes, even the untreated GRECs exhibit acidic behavior. In some cases swelling is observable, but this revokes any interest in the present objective. Concerning ionic migration, especially for the formation of CAF, an acidic environment enforces the transition of metallic copper to copper ions, which in solution provide electronic conductivity. When the copper ions reach neutral or basic surroundings, they are reduced to metallic copper again, forming CAF and this subsequently damages the insulation and therefor the PCB. Whether the material is known nor further experiments are admitted. It is consequently a tough business to state if this possible acidic surface functionalities are seriously a threat to be aware of. All the measurements using the zeta potential analysis for evaluating surface related information indicated an acidic behavior.

## 3.2 Indication Methods

Due to the fact that the GREC membranes are very dense in respect to permeability, only gravimetric analysis could be executed in the scheduled period of time to evaluate diffusion parameters. Beyond this investigation method, a  $\zeta$ -potential analysis was carried out with stripe shaped R1570 and R1566, pretreated in various chemicals, as already discussed in chapter "2.4.2" on p. 62. Additionally, the influence of the already mentioned chemicals to the material was checked by infrared analysis.

### 3.3 Pre-Drying Cores

Exiting the production line the membranes should be in a dry stage, unless the fabricant indicates an aqueous residue content of 2% per fraction of mass. By pre-drying the membranes in vacuum over molecular sieve, conditions enforced to the cell interior are simulated to yield information about water encapsuled. The membranes are sorted due to their composition and discarded in the labeled racks of the drying tower.

Table 3.5: Difference in mass after drying of membranes over MS 4 Å/ CaCl<sub>2</sub> in vacuum for 24 h.

Rack #	GREC	05.11.2017 [mg]	06.11.2017 [mg]	Difference [mg]
A	R1566	423.6	423.6	0.0
B	R1566	422.5	423.4	-0.9
C	R1566	423.1	423.9	-0.8
D	R1566	422.1	423.0	-0.9
E	R1566	422.6	423.2	-0.6
F	R1566	422.5	423.2	-0.7
G	R1566	422.7	423.2	-0.5
H	R1566	422.7	423.1	-0.4
I	R1566	422.4	422.5	-0.1
J	R1566	424.2	424.7	-0.5
K	R1570	426.7	426.9	-0.2
L	R1570	425.9	425.9	-0.1
M	R1570	421.6	421.7	-0.5
N	R1570	426.6	427.1	-0.4
O	R1570	425.1	425.5	-0.4
P	R1570	423.8	424.3	-0.5
Q	R1570	424.4	425.0	-0.6
R	R1570	424.7	425.0	-0.3
S	R1570	421.9	422.2	-0.3
T	R1570	422.2	422.0	0.2

As illustrated in table 3.5 there hardly is a change in mass after 24 h. The negative value is out of any significant evidence. After a several days of storage, a more notable change in mass (Table 3.7) seems to occur, though.

Table 3.7: Difference in mass after drying of membranes over MS4Å/CaCl<sub>2</sub> in vacuum for several days.

Rack #	GREC	06.11.2017 [mg]	13.11.2017 [mg]	20.11.2017 [mg]	Difference [mg]
A	R1566	423.6	423.0	-	0.6
B	R1566	423.4	422.9	-	0.5
C	R1566	423.9	422.9	-	1.0
D	R1566	423.0	421.4	-	1.6
E	R1566	423.2	422.0	-	1.2
F	R1566	423.2	-	421.5	1.7
G	R1566	423.2	-	420.3	2.5
H	R1566	423.1	-	421.5	1.6
I	R1566	422.5	-	421.5	1.0
J	R1566	424.7	-	423.1	1.6

The longer period of time within the desiccator shows lower mass fractions of humidity in the composites. The descending level of humidity within such a long period of time should not effect the diffusion measurement.

### 3.4 Adsorption Test

In order to determine if drying agent effects causes enhanced adsorption rates within the first 24 h, a measurement series composed of four diffusion cells was set up. While two of them are measured in the standard procedure, the opposite ones get each a new desiccant charge after every intervall of data acquisition. The membranes were superposed by water.

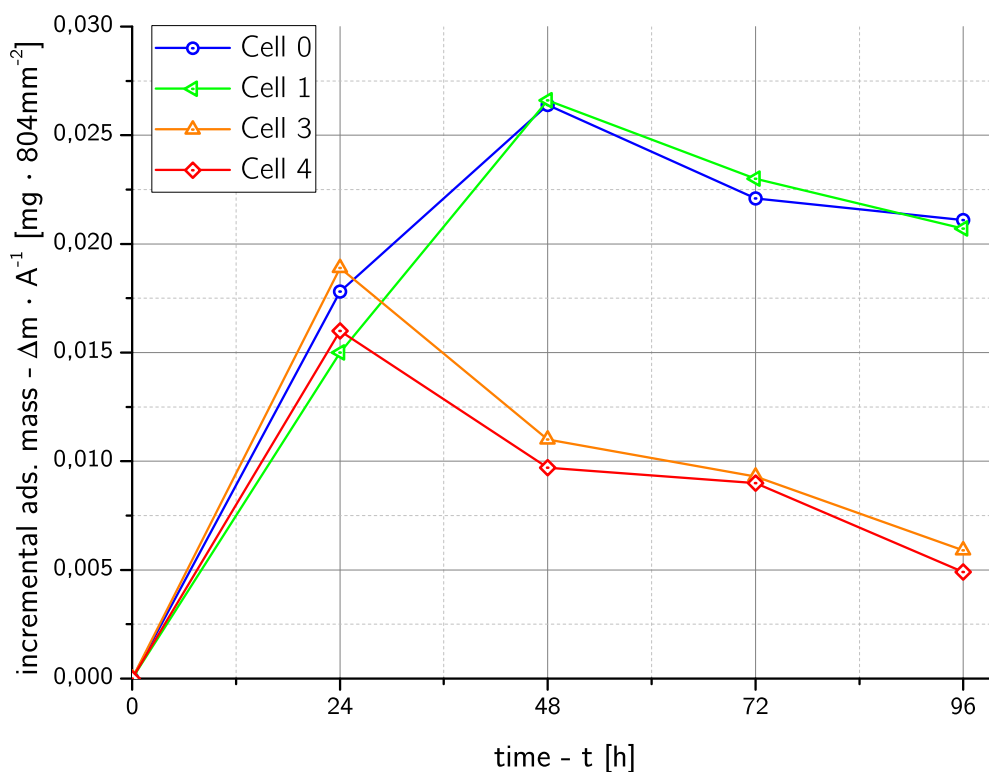


Fig. 3.4: Visualisation of an adsorption test keeping one drying agent (Cell0 and Cell1) for the whole process of data acquisition and recharging new desiccant, vice versa (Cell3 and Cell4).

Given the diagram above, adsorption-isotherm related behaviors drop out of discussion. It is assumed that within the initial 24 h a redrying of the closest surfaces and gas space occurs. Despite the cells are pre-dried in order to setting up a measurement, a long period of time elapses. Consequently water may adsorb in significant amounts, which is captured within the first intervall of data acquisition. During a short period of measurement, the cells are even warm, a re-adsorption of aqueous species should not take place.



### 3.5 Measurement Series

This section provides information of every diffusion cell experiment taken. In order to achieve a standardized series of measurements, the chapter is divided into a preliminary phase and a final phase, where the path to accomplish comparable data series is stated. This in fact is the reason of illustrating all the data acquisition approaches to satisfy the step-by-step improvement.

In every measurement series, the five diffusion cells distinguish from each other. For example, one cell provides information being an internal standard by having aluminum as a diffusion barrier built-in or it may not be opened for data acquisition until the last point of measurement to gain knowledge about the influence of humidity concerning humidity-contamination while being exposed to the environment. Others will include a sealing or other enhancing parts. This might make the understanding of either the intention of the operator of a measurement series as well as the difference to other series difficult. Hence, it is important to have a legend of symbols ready when sliding through the results.

The characterization methods which are illustrated on the following pages are all about gravimetric analysis. After every interval of time (i.e. 24 h), the cells are opened, the box containing drying agent is removed and the mass is recorded.

The blank values (mainly determined in measurement series 10) are not subtracted in the series raw data illustration. Furthermore, keep in mind that many factors are protruding errors, strongly distorting the diagrams between target value and real value. Additionally, statistical declarations are tough to state, since five cells yield poor spreadsheets.

Additionally, the scales of axis may differ, especially in the preliminary phase there will be huge differences due to the different capacities of deployed drying agents. In the final phase the axis will be fully aligned to a fixated scale.

### 3.5.1 Description of Abbreviations

As aforesaid it is essential to know the arguments within a measurement series' paragraph. The illustration provides all the necessary information to follow the subsequently following paragraphs, it is essential in terms of reading assigned measurement parameters.

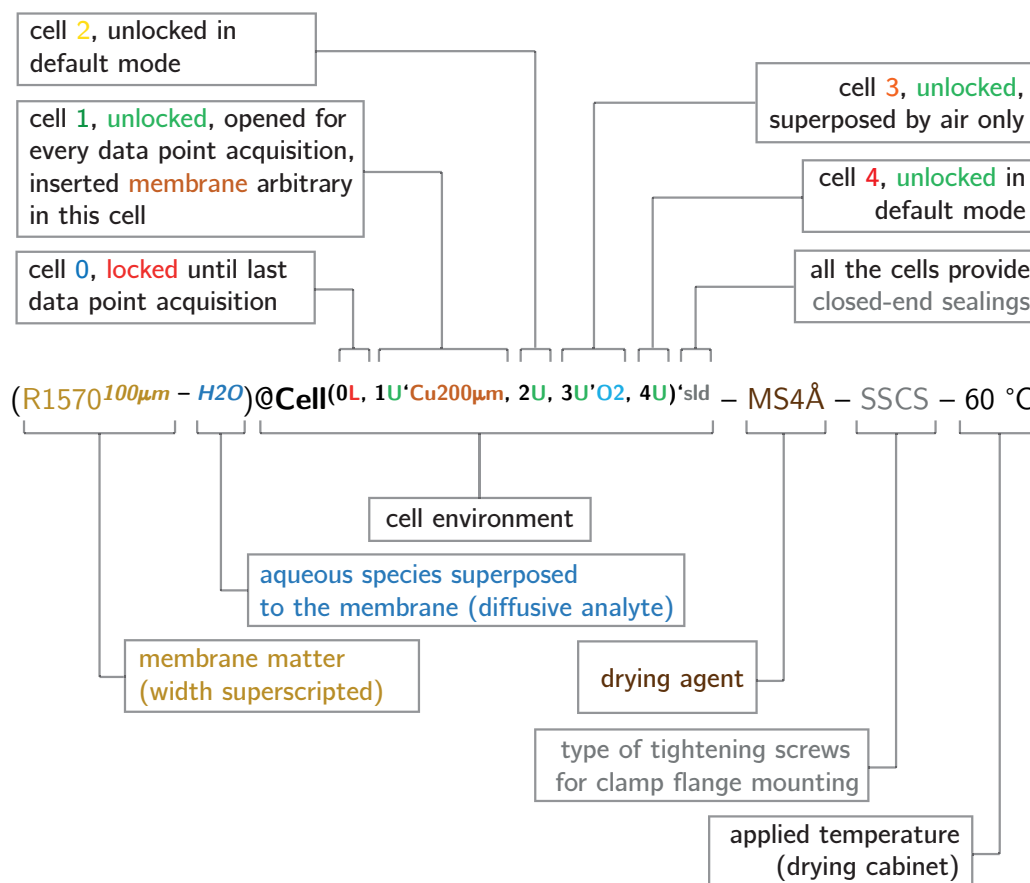


Fig. 3.5: This is an illustration of an fictional measurement series to provide an idea of the abbreviation approach.

### 3.5.2 Preliminary Phase I - Drying Agent Improvement

The preliminary phase was necessary to achieve a modus operandi by the virtue of reliability and repeatability. The measurement series within this phase show data, collected step-by-step to reach a final phase of data acquisition, where a standard procedure of operating the cells is approved. It concludes with the choice of drying agent and insulation improvements. In this section the improvement of the drying agent choice is depicted in three series.

#### 3.5.2.1 (R1566<sup>100 μm</sup> - H<sub>2</sub>O)@Cell<sup>(0L, 1U'O<sub>2</sub>, 2U, 3U, 4U)</sup> - P<sub>4</sub>O<sub>10</sub> - PA 6.6 - 60 °C

In the first of the measurement series, P<sub>4</sub>O<sub>10</sub> was chosen to determine the permeability of water through a 100 microns membrane of R1566WN. To check if there is a difference between a aqueous species and a gas superposed the the primary analyte, cell 1 acted as a gas cell, where the upper part was exposed to environmental air/humidity.

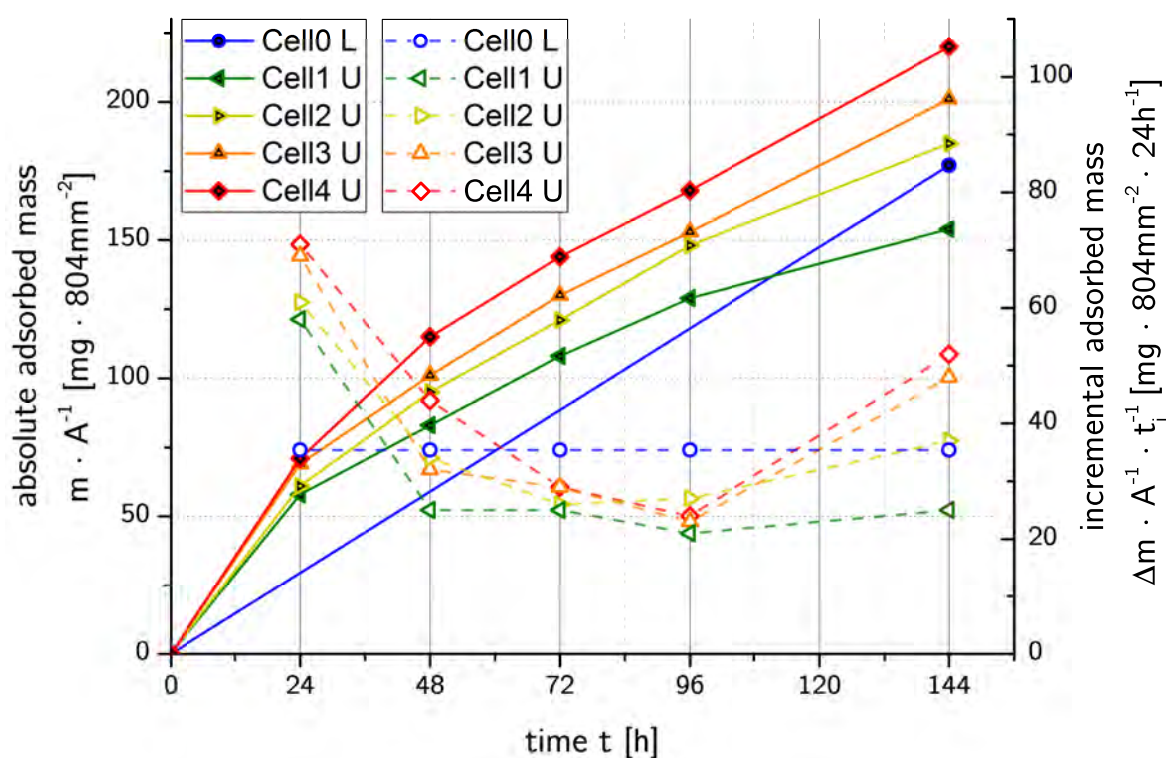


Fig. 3.6: Measurement series 01 - First attempt collecting information about P<sub>4</sub>O<sub>10</sub> as a desiccant. Cell0 was locked until the end of the experiment, while cell 1 acted as a gaseous blank to check aggressivity of the drying agent.

The diagram shows the cumulative mass of water to adsorb in the drying agent to the left and the daily uptake to the right ordinate. As expected the absolute values form a linear behavior. Possible reasons for the increased values within the first

24 h are discussed in section "3.4" on p. 76. Since the lines between the measurement points only serve as connectors they may irritate readers eye in terms of tremendously looking value ascensions.

To determine if air humidity is strongly influencing the drying agent when opening the cells for measurement intervalls, cell0 was kept closed for the whole period of measurement series until the last point of data acquisition. As depicted in the diagram, the values of the opened cells spread homogenously around the data point of cell0. An inkind of critical error due to environment exposure intervalls can be omitted.

As already mentioned in chapters before, phosphorous pentoxide is a highly efficient drying agent, a significant difference between the GREC membrane cells and cell1 (aluminum sheet), which was exposed to environmental air only, was not observable. Additionally, a blackening of the developed polyphosphorous liquid could be observed. A reaction of the  $P_4O_{10}$  with the initially used vial caps as a vessel was excluded. It is supposed, that the dessicant could draw various volatile substances out of the sealings. Subsequently, another drying agent should come in service.

### **3.5.2.2 (R1566<sup>100 μm</sup> - H<sub>2</sub>O)@Cell(0L, 1U<sup>O<sub>2</sub></sup>, 2U, 3U, 4U) - MgSO<sub>4</sub> - PA 6.6 - 60 °C**

Changing the drying agent was an important step due to the strong affinity of  $P_4O_{10}$  to aqueous substances. In this measurement series, a neutral and non-hazardous salt was introduced instead of phosphorous pentoxide. Magnesium sulfat is a hygroscopic salt with its origin in sulphuric acid, forming several hydrates in the presence of water. In contrast to the former desiccant it stays in a powdery form.

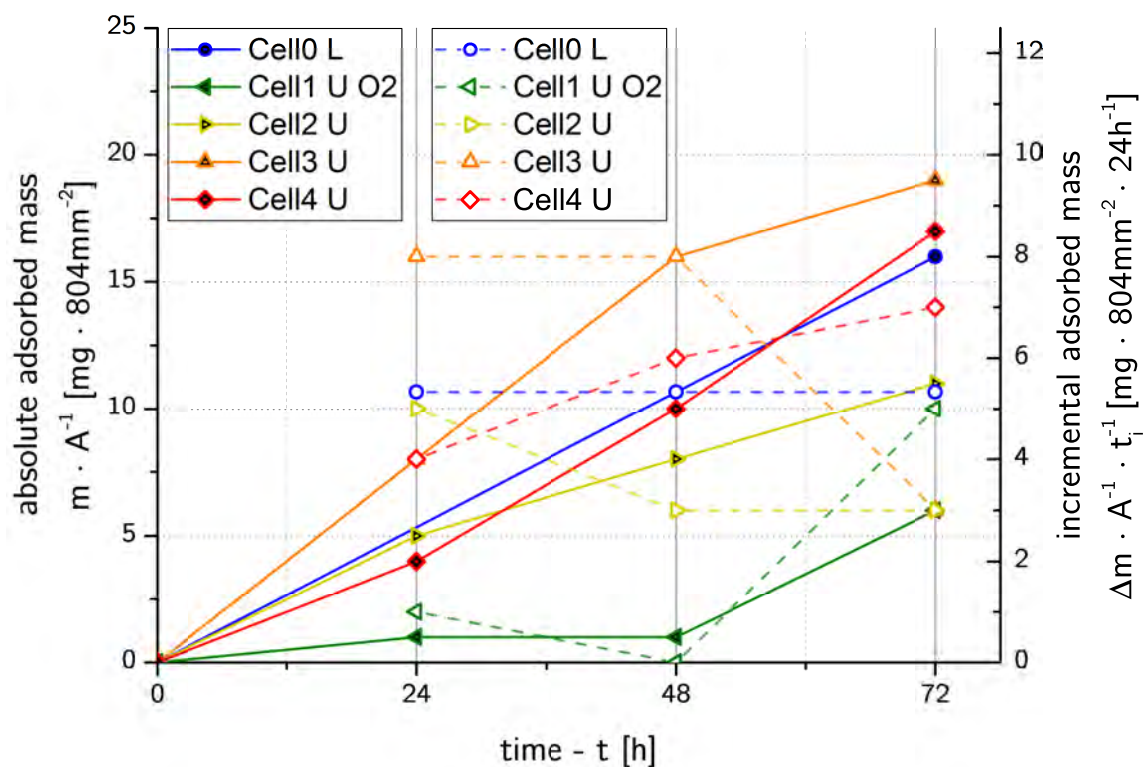


Fig. 3.7: Measurement series 02 - Deploying  $\text{MgSO}_4$  as a drying agent shows strong deviations in adsorption rates. This is due to the weak affinity to water in gaseous phases. Hence the mass arguments are out of the available devices's LOD.

Depicted in Fig. 3.7, a broad distribution of values within a range of 5 to 20 mg per 72h can be observed. Unfortunately,  $\text{MgSO}_4$  it is not sufficient in its drying efficiency. Hence, a reasonable statement can not be proved with these values scraping on a device's LOD border. A further negative aspect of this powder is the "out-trickling" when a electric charge forms due to the wall-to-wall friction when opening the cells. A strong error raises when loosing mass in gravimetrical analysis.

The impact of environment exposure time (water inkind) appears to be absent, though. Furthermore, this series is capable of showing a difference between the air and water, superposed to the membranes in cell 1 to the others, respectively.

3.5.2.3 (R1566<sup>100 μm</sup> - H<sub>2</sub>O)@Cell<sup>(0L, 1U'Al, 2U, 3U, 4U)</sup> - MS 4 Å - PA 6.6 - 60 °C

By excluding some negative factors of the priorly executed measurement series, which involves hazardousness, hydrophilicity and shape of the drying agent, the choice fell to the favor of molecular sieve of 4 Å in mesh size. It provides appropriate capability for water uptake, does neither harm the operator or the device and its around 1.7 mm spheric globes are easy to handle.

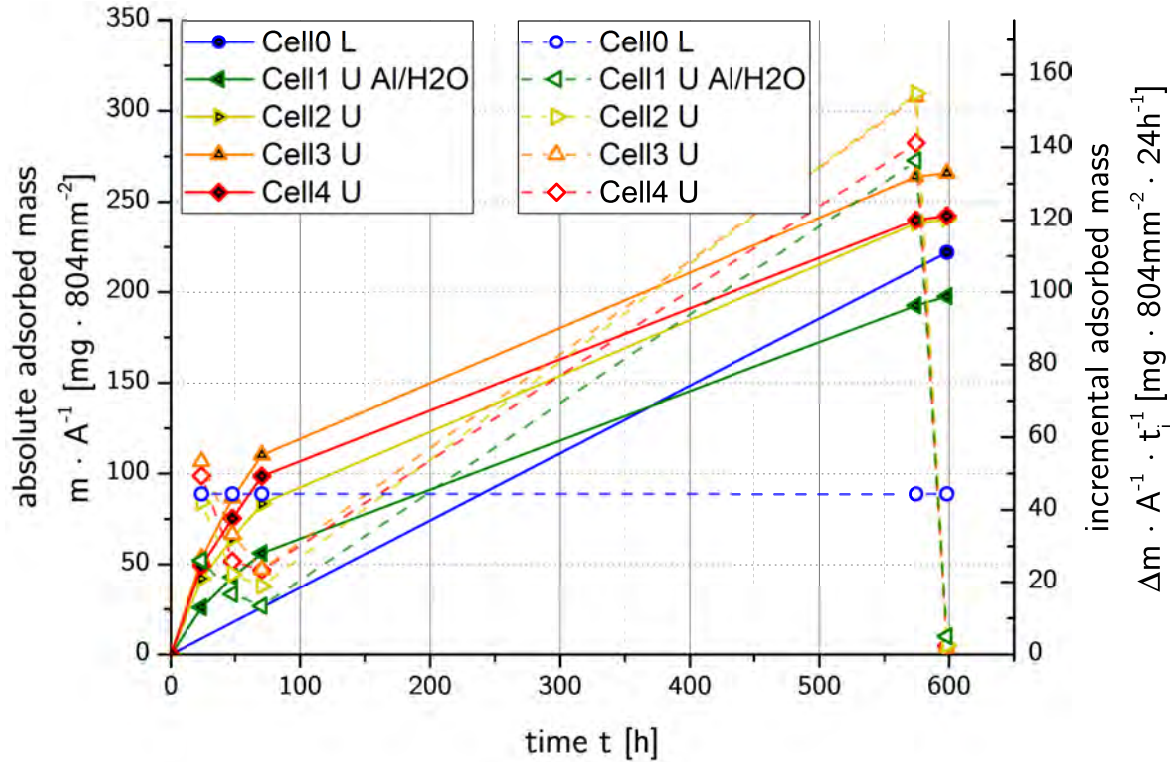


Fig. 3.8: Measurement series 03 - Visualization of the data points within the first 96 h of measurement. The molecular sieve exhibits acceptable values within an applicable time of investigation.

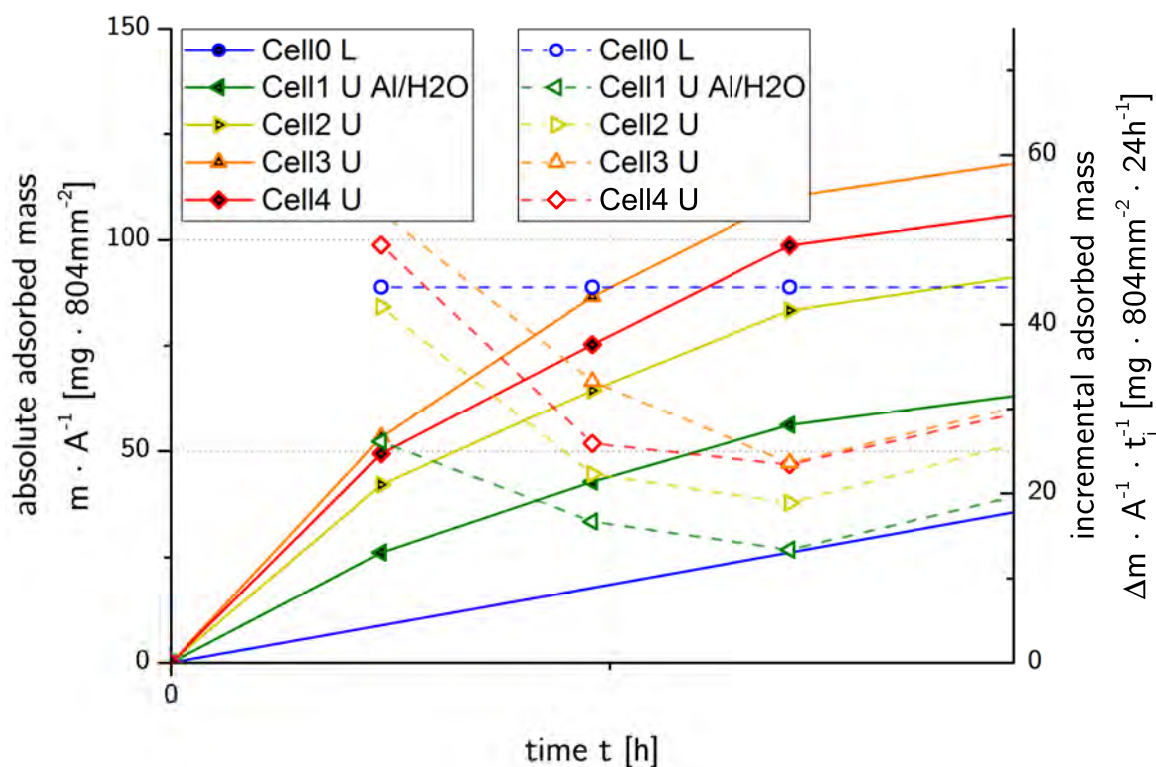


Fig. 3.9: Measurement series 03 - Visualization of the data points within the complete time of measurement. The molecular sieve exhibits acceptable values within an applicable time of investigation.

Although the ascending lines spread widely exhibiting strong variations in slope, the molecular sieve values move within an appropriable measurement range. In comparison to series 1, it proves the difference between the aluminum barrier used in cell 1 and the other cells. It seems that cell 0 is lower in adsorption rate before reaching an exposure time of 300 h, but this is deflected by the reason of a linearly extrapolated line between  $t = 0$  h and  $t = 599$  h. Even after this period of time, the drying capacity has not been exceeded. With setting seal on this drying agent, the first stage of the preliminary phase is closed.

### 3.5.3 Preliminary Phase II - Insulation Enhancement

The MS 4 Å turned out to be a proper choice in aforesaid properties. In the following series, a final "modus operandi" for repeatable and reliable, especially comparable measurement series should be determined. It is of essential interest to lack out dilatation and insulation issues, which might be caused by thermal expansion. Six measurement series are represented on the following pages to yield the final stage of data point acquisition.

3.5.3.1 (R1570<sup>100 μm</sup> - H<sub>2</sub>O)@Cell<sup>(0L, 1o'Cu200μm, 2U, 3U, 4U)</sup> - MS 4 Å - PA 6.6 - 60 °C

By repeating the series3 with an exchange of aluminum to a copper-coated 200 microns GREC membrane, a similar behavior of adsorption is expected.

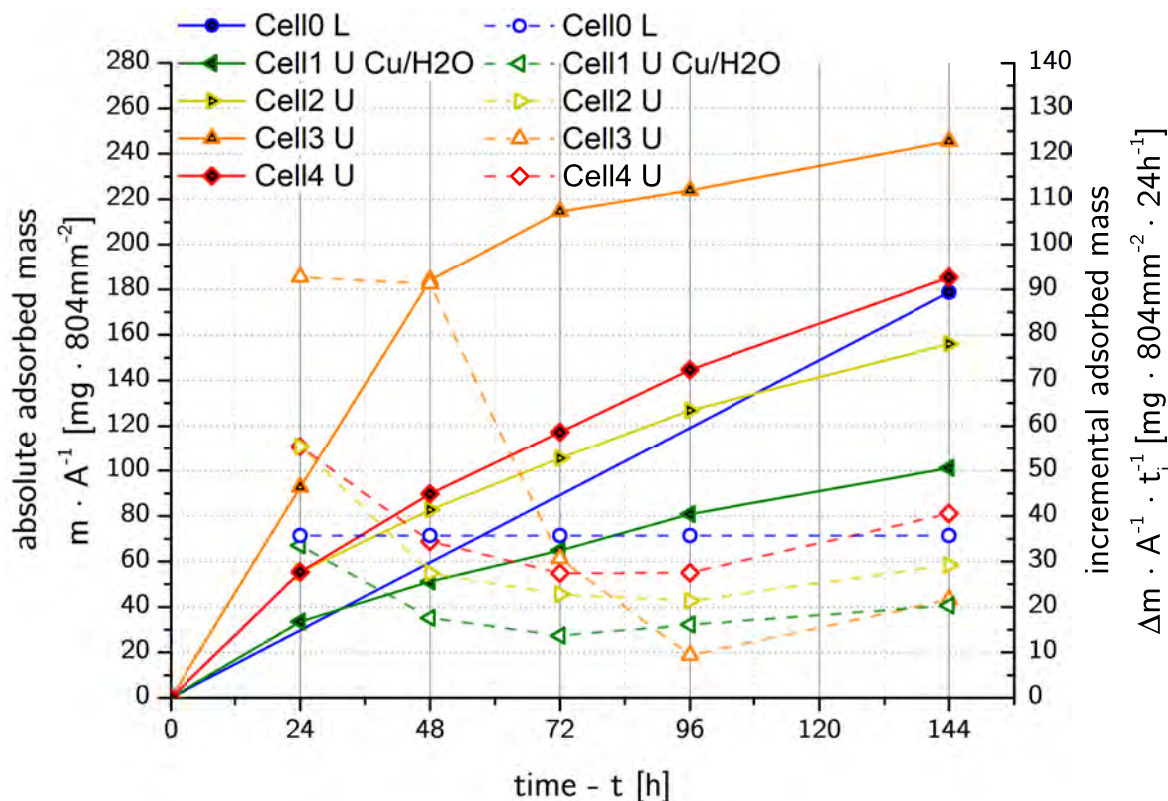


Fig. 3.10: Measurement series 04 - Strong spread of values. The green line shows the "internal standard", which is compared to former diffusion barriers. The adsorption rate behaves as expected being lower as verified before.

The expectance was stated by a lower adsorption rate for cell 1 including a diffusion barrier. While aluminum had an increase of mass of approx.  $42 \text{ mg} \cdot 804 \text{ mm}^{-2} \cdot 48 \text{ h}^{-1}$ , copper showed  $51 \text{ mg} \cdot 804 \text{ mm}^{-2} \cdot 48 \text{ h}^{-1}$ , moving surely within an acceptable deviation range. When disassembling the cells, damaged membranes could be observed. It is assumed that the cracks formed due to condensation effects in the upper cell part, forming a vacuum, straining the membrane to a critical point, finally cracking in a path aligned to the screw-holes. In the diagram this should have been observable, if it has been within data point acquisition.



3.5.3.2 ( $R1570^{Cu200\ \mu m - H_2O}$ )@Cell<sup>(0L'sld, 1U'sld, 2U'sld, 3U, 4U)</sup> - MS 4 Å - PA 6.6 - 60 °C

Originally, a closed-end sealing was intended to built an elastic counterpart between both cell halves, avoiding channel streams through the screw holes. To find an alternative, a PE-foam (commercially available for insulating windows et cetera) was custom-cut and introduced. By deploying them to distinct cells only, in a further series vice versa could be checked out if there is a counter-various decrease in diffusion.

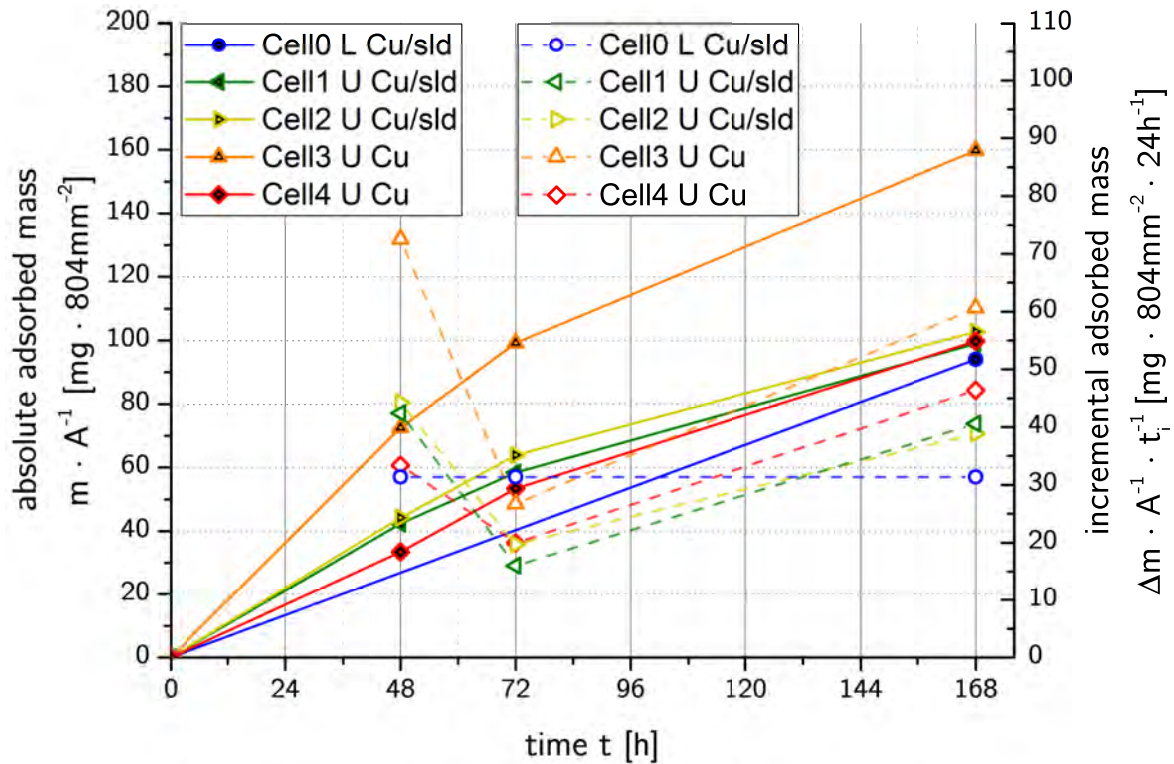


Fig. 3.11: Measurement series 05 - The first three cells includes PE-foam sealings at the closed-end of contacting faces. Cell3 has tremendously increased data points, which nullifies the experiment in its intention.

Unfortunately the diagram shows a much higher rate in a non-insulated cell3, but this is not true for cell4, though. A valuable declaration can not be stated.

3.5.3.3 (R1570<sup>Cu200 μm - H<sub>2</sub>O</sup>)@Cell<sup>(0L, 1U, 2U, 3U'sld, 4U'sld)</sup> - MS 4 Å - PA 6.6 - 60 °C

This series should be executed to yield a vice versa measurement to series 5, deploying the closed end sealings to cell 3 and cell 4.

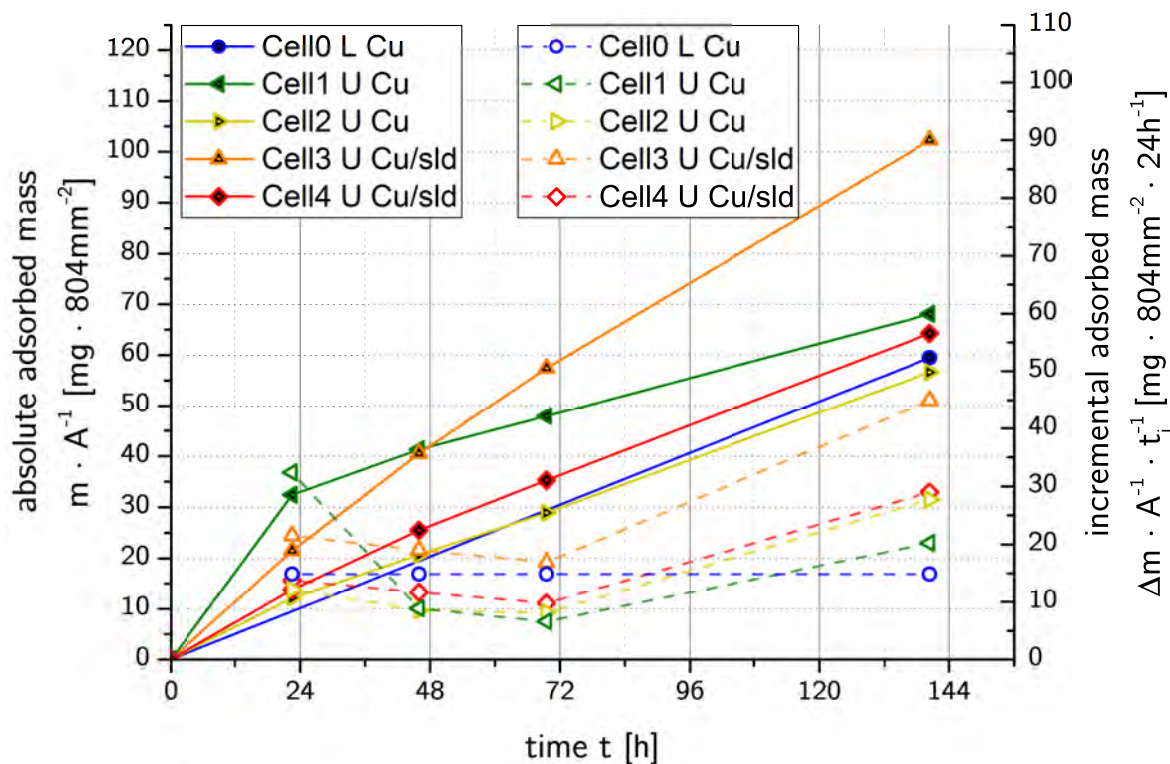


Fig. 3.12: Measurement series 06 - Being the contrary measurement series to series 5 (Fig. 3.11), cell 3 and cell 4 should state lower adsorption rates by being supported by the PE-foam closed-end sealing. Cell 3 is still critically increased, which either makes the experiment futile.

The issue which has appeared in series 5 found repetition. The cells 3 and 4 should exhibit lower permeability rates than cell 0, cell 1 and cell 2, but it is quite the very reverse, though. It is assumed that on the one hand the flat gasket sealings are not properly fitting and/or on the other hand a thermal expansion of the mixed material system is the clue. In the further experiments, information will be revealed.

**3.5.3.4 (R1570<sup>100 μm</sup> - H<sub>2</sub>O)@Cell<sup>(0L, 1U<sup>Cu</sup>200μm, 2U, 3U, 4U)</sup>slid - MS 4 Å -  
PA 6.6 - 60 °C**

This measurement series contains closed-end sealings in the whole row of cells. Additionally, the flat gaskets were renewed and the screws were tightened by a distinct force. Cell 1 again were mounted with a copper-coated 200 microns GREC membrane.

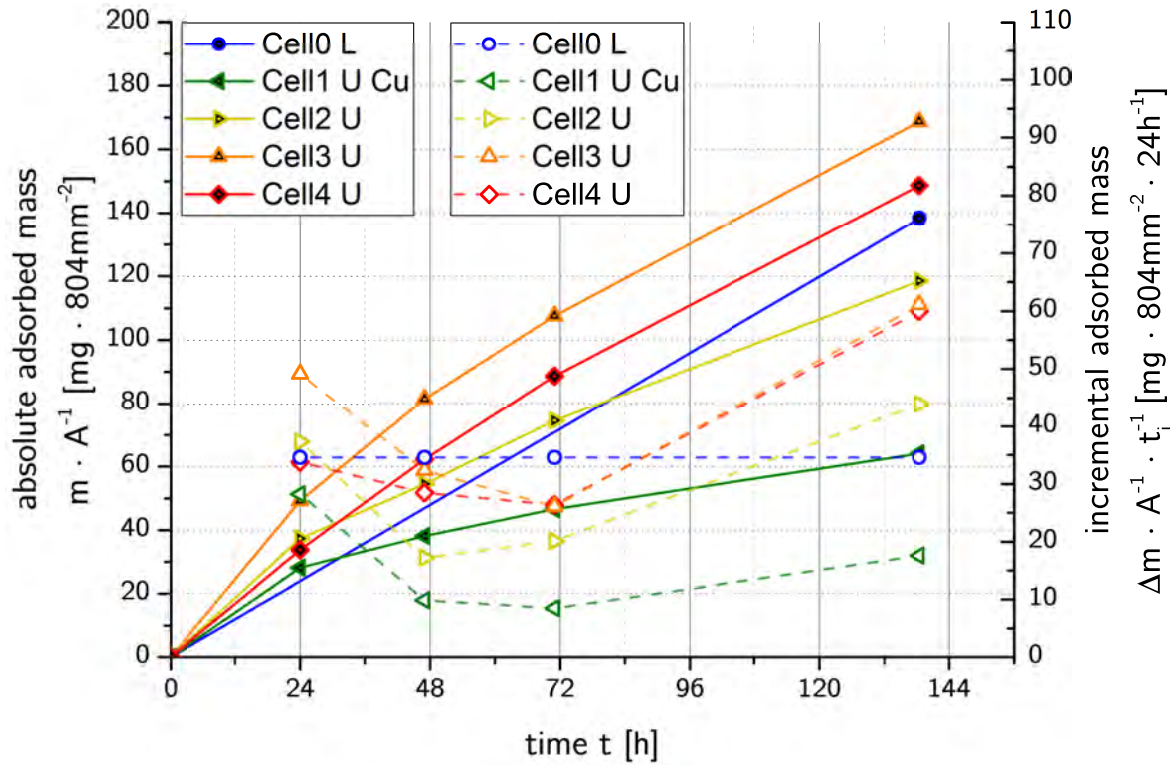


Fig. 3.13: Measurement series 07 - Inserting closed-end sealings draw expectations to lower permeability rates. Unfortunately this does not hold, another issue must corrupt the measurements.

Illustrated in Fig. 3.13, the reference cell 1 yields a lower increase of mass, while the rest exhibit a rather low distribution in respective to the former series 5 and 6. Despite this homogeneity, a contrary fact is observed. This series shows generally higher adsorption rates than prior ones. This reveals, that one has to assess the influence of the thermal expansion of the different materials. Since there is hardly a chance to change the modular and insulating parts of the cell, the only replaceable parts are the countersink screws.

3.5.3.5 (R1570<sup>100 μm</sup> - H<sub>2</sub>O)@Cell<sup>(0L, 1U'Cu200 μm, 2U, 3U, 4U)</sup>'slid - MS 4 Å - SSCs - 60 °C

By providing stainless steel countersinks to the cells, more reliable values are expected to be ascertained. Every cell is mounted with an closed end sealing, cell 1 is again equipped with a copper-coated membrane.

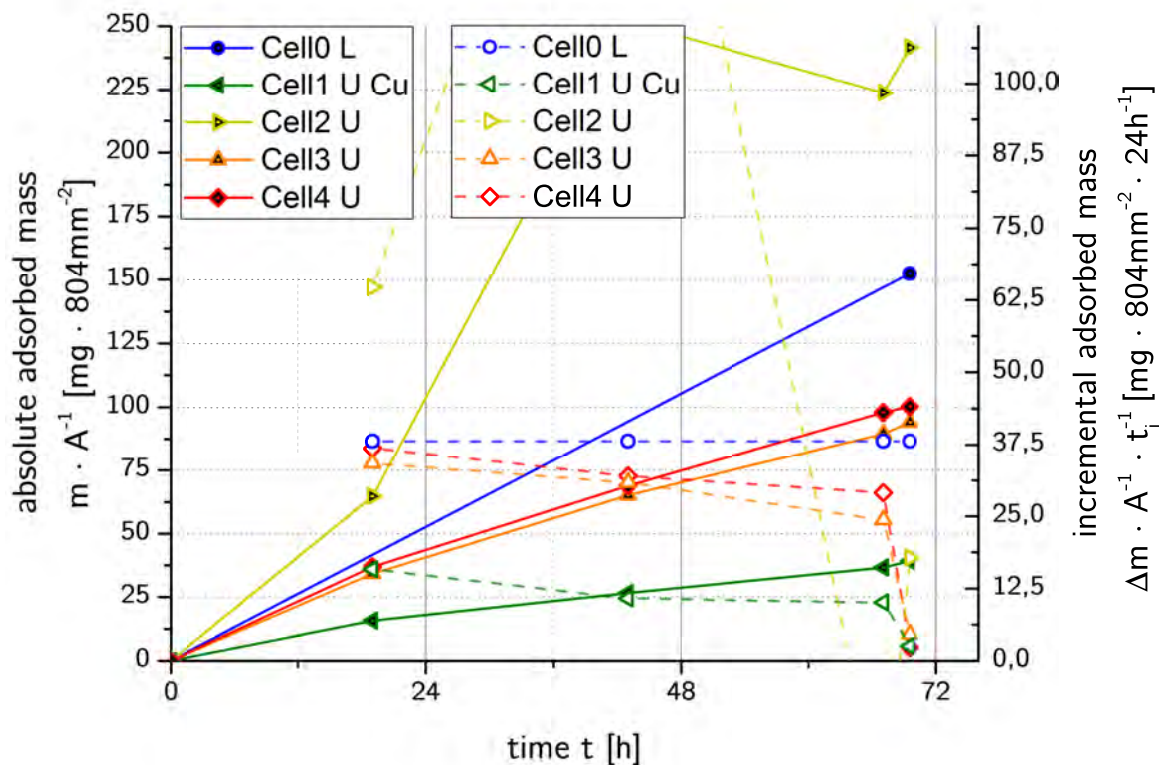


Fig. 3.14: Measurement series 08 - An exchange of the clamp flange screws should provide a distinct force to the mounting unit. Additionally the force can be enhanced without forcing cracking due thermal expansion issues.

The damage which occurred in cell 2 is clearly visible and it was therefore discarded for further calculations within this series. The difference of the diffusion barrier cell to the membrane cells is declared to be constitutional. Despite cell 3 and 4 are close to each other, cell 0 is intensely higher in adsorption.

3.5.3.6 (R1570<sup>100 μm</sup> - H<sub>2</sub>O)@Cell(0U'd, 1U'O<sub>2</sub>'d, 2U'h, 3U'Cu200 μm'h, 4U'h)'sld - MS 4 Å - SSCs - 60 °C

In this series, a check towards the impact of pre-dried membranes, exposed to either water and air should be executed.

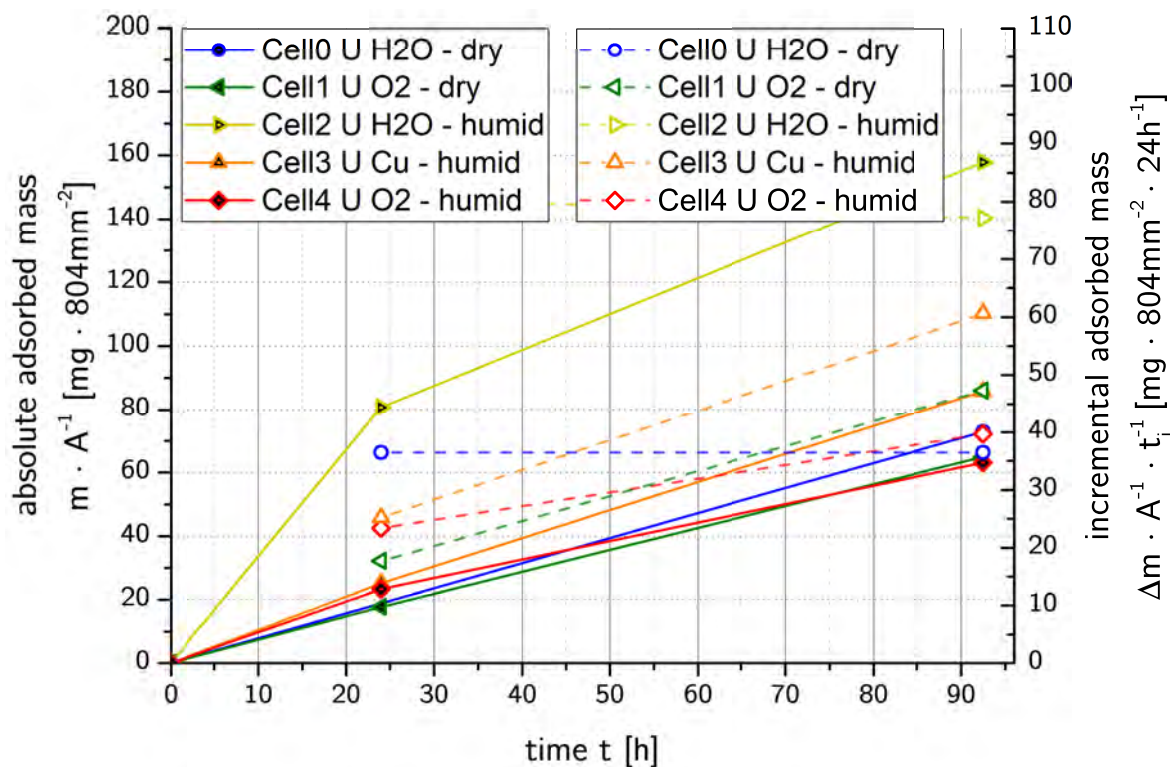


Fig. 3.15: Measurement series 09 - This series should show differences of untreated material and pre-dried membranes. Due to No significant declarations can be stated though. The yellow points reveal a damaged membrane.

When comparing cell0 (pre-dried) with the cell2 (untreated), the measurement seems to be legit in terms of influence but when taking a closer look to cell1 (pre-dried) to cell4 (untreated), which are superpsed by O<sub>2</sub> only, a meaningful statement does not hold. As illustrated on p.74 before, the effect of pre-drying the membranes is marginally.

### 3.5.4 Blank Evaluation

#### 3.5.4.1 (Aluminum<sup>H<sub>2</sub>O</sup>)@Cell<sup>(0L, 1U, 2U, 3U, 4L)</sup>slid - MS 4 Å - SSCs - 60 °C

In the following measurements, the series show the standardized execution of the measurement experiments, where every series were treated the same. This includes that cell0 and cell4 always act as locked cells to provide at least two unaffected absolute values. The diagrams in the following sections are themselves normalized to fixated axis scales to allow a direct comparison between the series.

Series 10 describes a measurement important to evaluate a blank value of the cells. Since there are factors like channel streams, different visible analyte diameters due to elastic deformation of the touching flat gaskets and further, it is necessary to determine this value. By inserting aluminum sheets of 0.5 mm in width, diffusion barriers are generated to yield only information about by- and trespassing moisture.

Series 10 should provide a blank evaluation. By forwarding present series in a same way in terms of either the procedure of mounting as well as ingredients/chemicals, a reliable bond between series should be evolved. By using the first level of the torque wheel of a rechargeable drill, conservation of force should be maintained

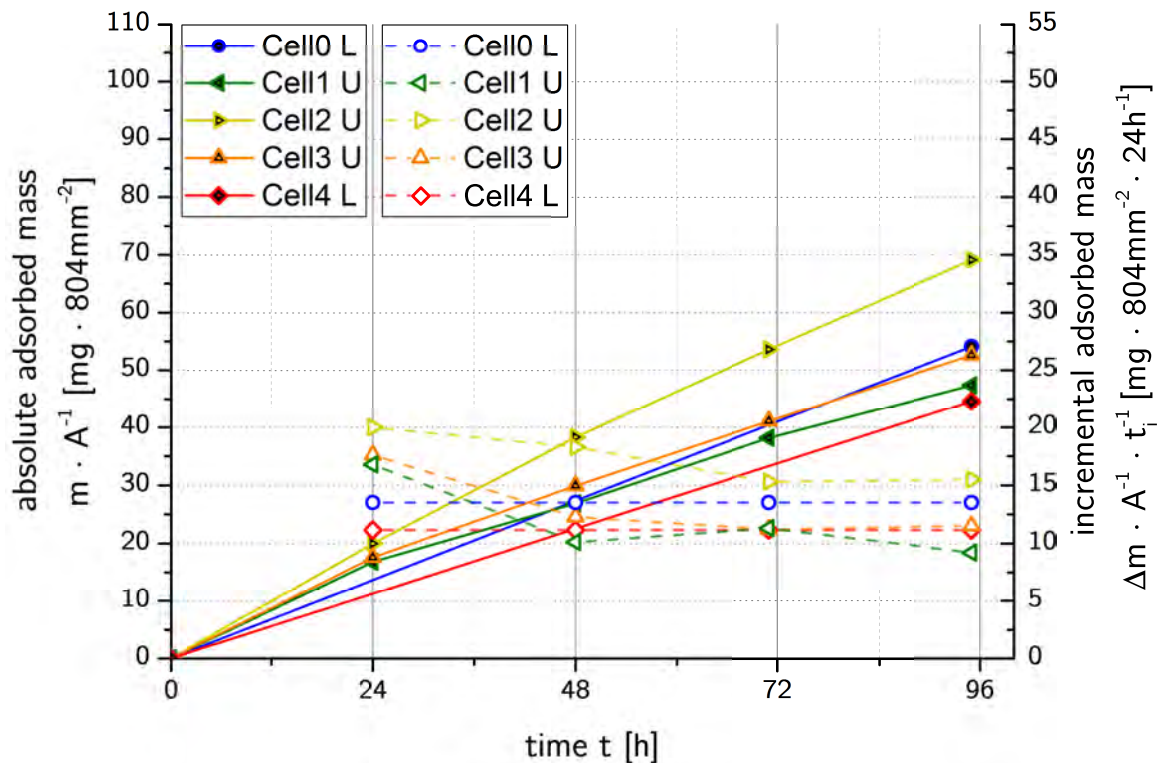


Fig. 3.16: Measurement series 10 - Blank value evaluation for the calculation of the absolute diffusion rates of the GREC membranes. The average value including it's SD will be subtracted from each's final phase series mean value.

In contrast to former visualized permeability measurements, a closer spread of data points is observable. The clamping flange from this series on was tightened by the first level of an electrical drill and pressed forward in all the measurement series to gain a mounting force being quite equal in all the cells.

### 3.5.5 Final Phase - Adsorption Data Evaluation

As the name suggests the final phase involves the evaluation of the values of interest. The series' numbers are not chronological sorted like they do in corresponding datasets, they are renamed to the favor of "material to pH dependency" visualization, comprising the same information, though. Within the final phase, aqueous solutions of different pH values are used. For an acidic environment, potassium hydrogen phthalate ( $C_8H_5KO_4$ ) and for basic conditions, a mixture of boric acid, potassium chloride and sodium hydroxide ( $Na_2B_4O_7 + NaOH + KCl$ ) is deployed, respectively. Cell 0 and cell 4 are locked in the following experiments, the lines in the diagrams are subsequently extrapolated linearly!



Fig. 3.17: Buffer solutions for pH-dependent investigation on GREC membrane permeability.



3.5.5.1 (R1570<sup>100 μm</sup> - pH 7.15)@Cell<sup>(0L, 1U, 2U, 3U, 4L)</sup>'sld - MS 4 Å - SSCs - 60 °C

This series stands in relationship to the setup of the series 3.5.5.2 at pH 7 (water), varying in just the GREC membrane matter.

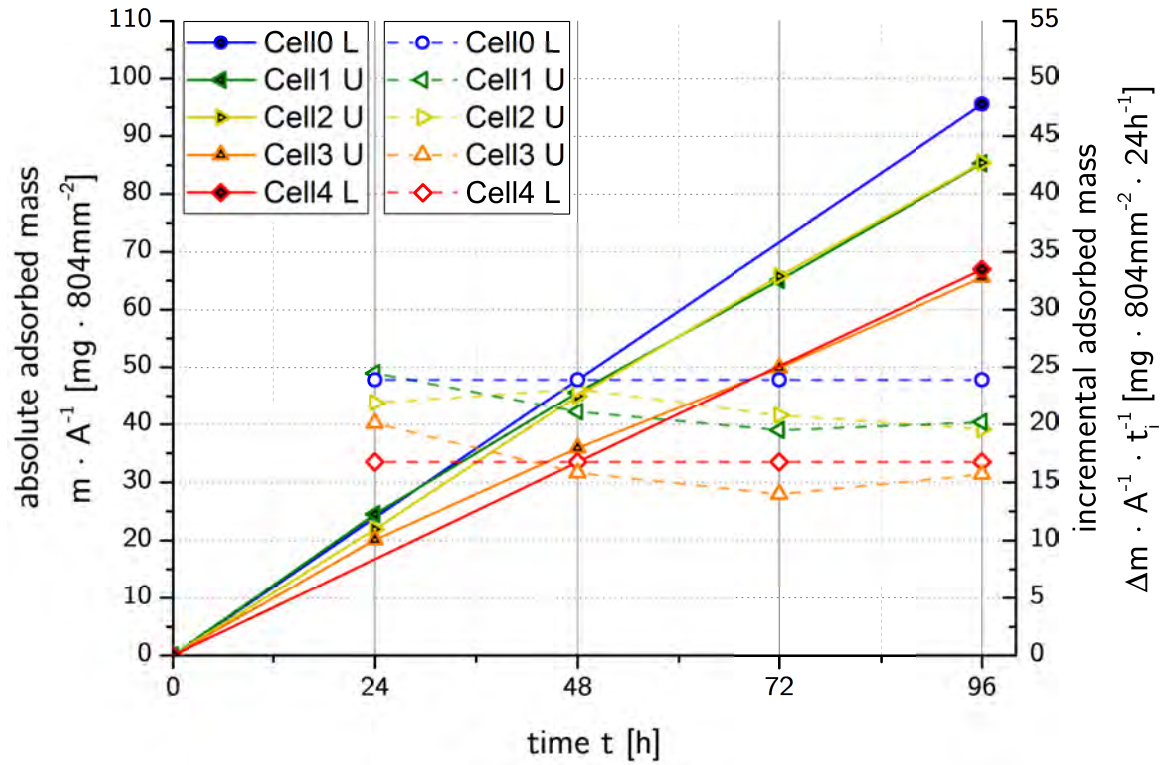


Fig. 3.18: Measurement series 11 - First attempt to seriously ascertain significant permeability rates.

The cells 3 and 4 as well as cells 1 and 2 are quite sharing the same amount of adsorption rate, while cell 0 is a little beyond.

3.5.5.2 (R1566<sup>100 μm - pH 7.15</sup>)@Cell<sup>(0L, 1U, 2U, 3U, 4L)</sup>'slid - MS 4 Å - SSCs - 60 °C

This series stands in relationship to the setup of the series 3.5.5.1 at pH 7 (water), varying in just the GREC membrane matter.

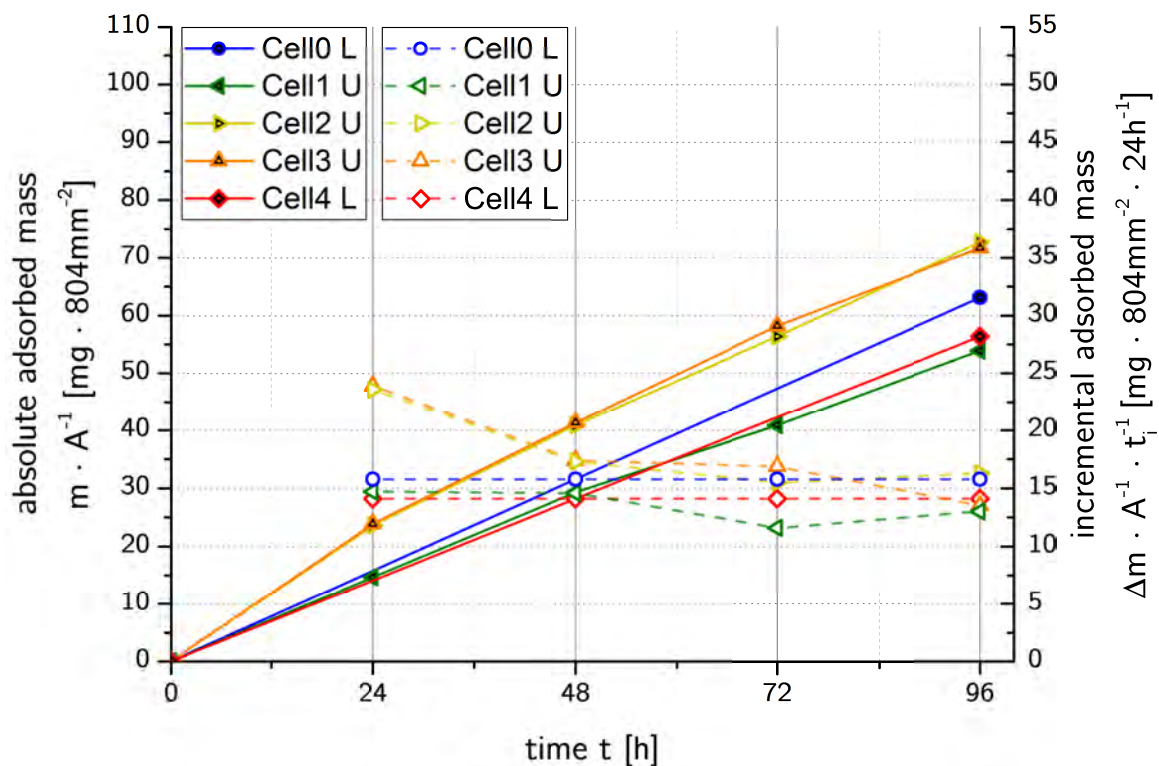


Fig. 3.19: Measurement series 12 - Second experiment similar to the priorly showed measurement series, including R1566 as an analyte instead.

Being lower in adsorption rates this R1566 matter shows internal correlation of the cells 3 and 2, a small deviation of cells 1 and 4 with a cell 0 centering in between the data points.

**3.5.5.3 (R1570<sup>100 μm</sup> - C<sub>8</sub>H<sub>5</sub>KO<sub>4</sub> @ pH 4.01)@Cell<sup>(0L, 1U, 2U, 3U, 4L)</sup>'slid - MS 4 Å - SSCs - 60 °C**

This series stands in relationship to the setup of the series 3.5.5.4 at pH 4.01 (potassium hydrogen phthalate, C<sub>8</sub>H<sub>5</sub>KO<sub>4</sub>), varying in just the GREC membrane matter.

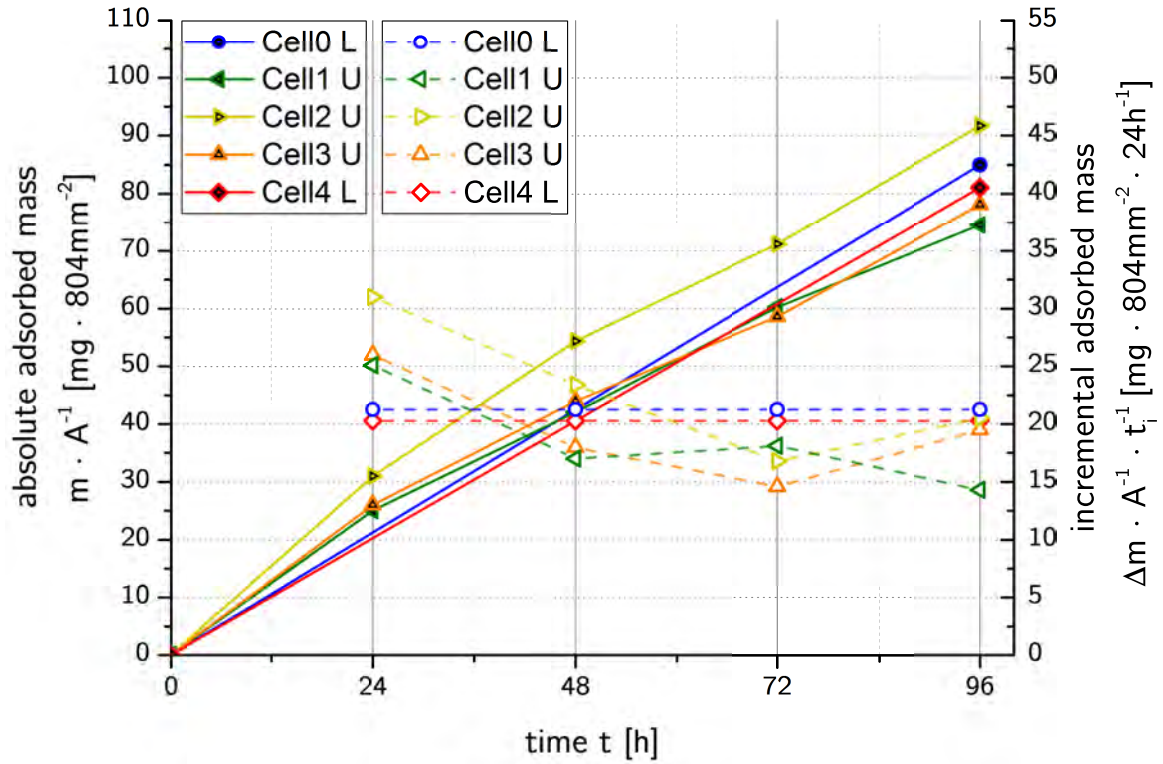


Fig. 3.20: Measurement series 13 - Exchange of the diffusive species for the first time using a potassium hydrogen phthalate buffer with pH 4.01.

The R1570 series superposed by a pH acidic solution achieve rather well cell adsorption correlations. Contrary to former series very low deviations are observed.

### 3.5.5.4 (R1566<sup>100 μm</sup> - C<sub>8</sub>H<sub>5</sub>KO<sub>4</sub> @ pH4.01)@Cell<sup>(0L, 1U, 2U, 3U, 4L)</sup>'slid - MS 4 Å - SSCs - 60 °C

This series stands in relationship to the setup of the series 3.5.5.3 at pH 4.01 (potassium hydrogen phthalate, C<sub>8</sub>H<sub>5</sub>KO<sub>4</sub>), varying in just the GREC membrane matter.

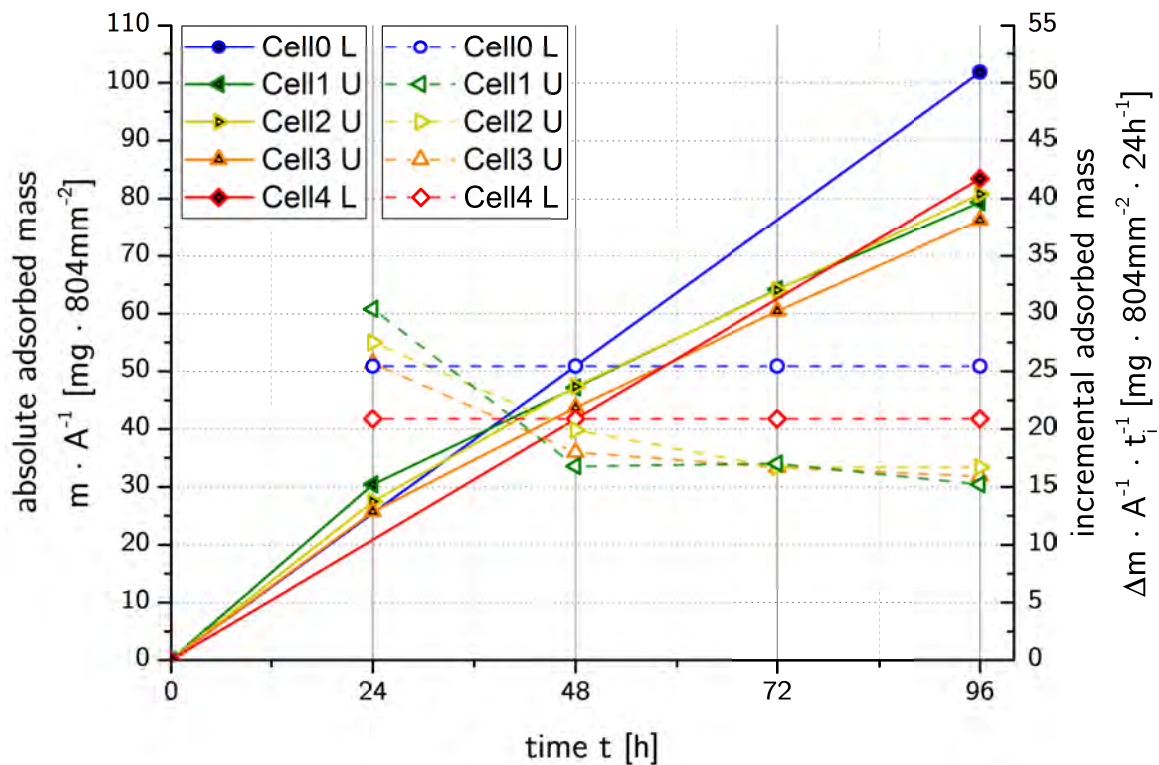


Fig. 3.21: Measurement series 14 - Analyte specific pendant to the pH-acidic R1570 measurement series.

The gravimetrical analysis visualization in the diagram reveals quite equal adsorption kinetics than shown before in the R1570 GREC. Unfortunately cell 0 is corrupting the average since it is much higher than the correlating rest.

**3.5.5.5 (R1570<sup>100 μm</sup> - Na<sub>2</sub>B<sub>4</sub>O<sub>7</sub>+NaOH @ pH9.00)@Cell<sup>(0L, 1U, 2U, 3U, 4L)</sup>slid - MS 4 Å - SSCs - 60 °C**

This series stands in relationship to the setup of the series 3.5.5.6 at pH 9.00 (mixture of boric acid, sodium hydroxide and potassium chloride, Na<sub>2</sub>B<sub>4</sub>O<sub>7</sub> + NaOH + KCl), varying in just the GREC membrane matter.

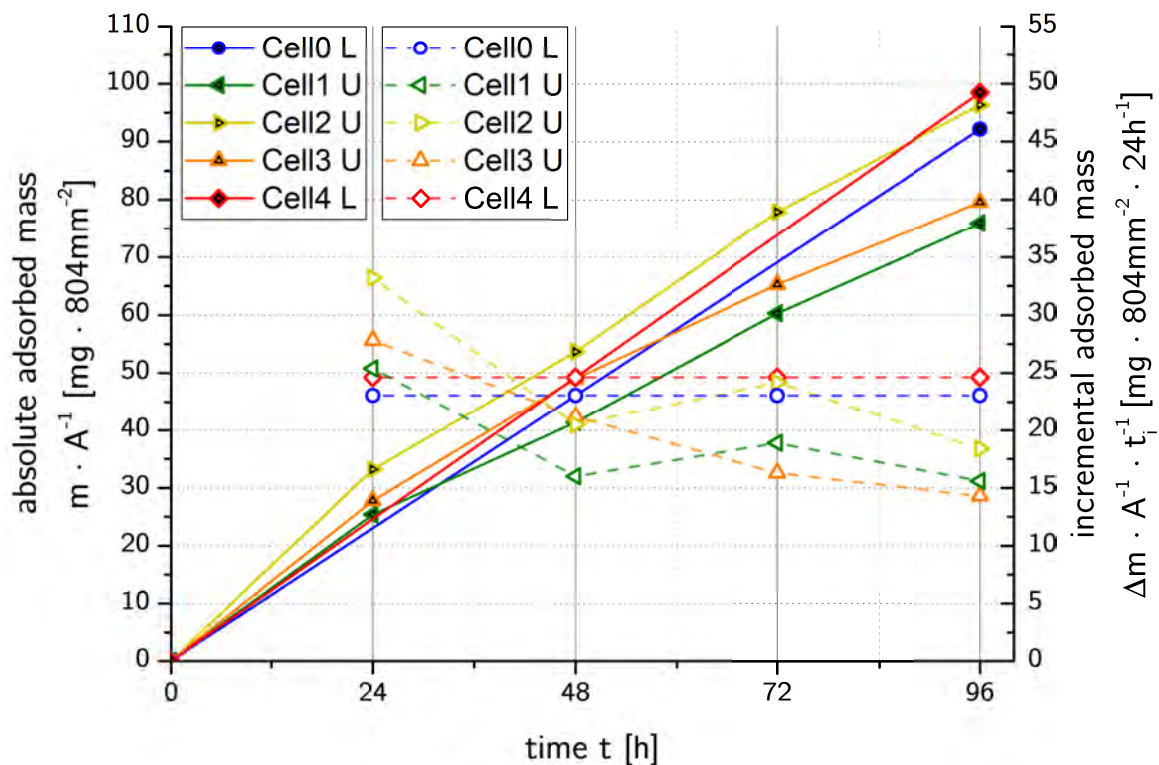


Fig. 3.22: Measurement series 15 - Adding a pH9.00 buffer to the upper cell to get an idea of the influence to the R1570 membrane.

Spreading around an average value of  $89 \text{ mg} \cdot 804 \text{ mm}^{-2} \cdot 96 \text{ h}^{-1}$ , excluding standard deviation, this experiment reveals the highest adsorption rates of all the series.

**3.5.5.6 (R1566<sup>100 μm</sup> - Na<sub>2</sub>B<sub>4</sub>O<sub>7</sub>+NaOH @ pH9.00)@Cell<sup>(0L, 1U, 2U, 3U, 4L)</sup>slid - MS 4 Å - SSCs - 60 °C**

This series stands in relationship to the setup of the series 3.5.5.5 at pH 9.00 (mixture of boric acid, sodium hydroxide and potassium chloride, Na<sub>2</sub>B<sub>4</sub>O<sub>7</sub> + NaOH + KCl), varying in just the GREC membrane matter.

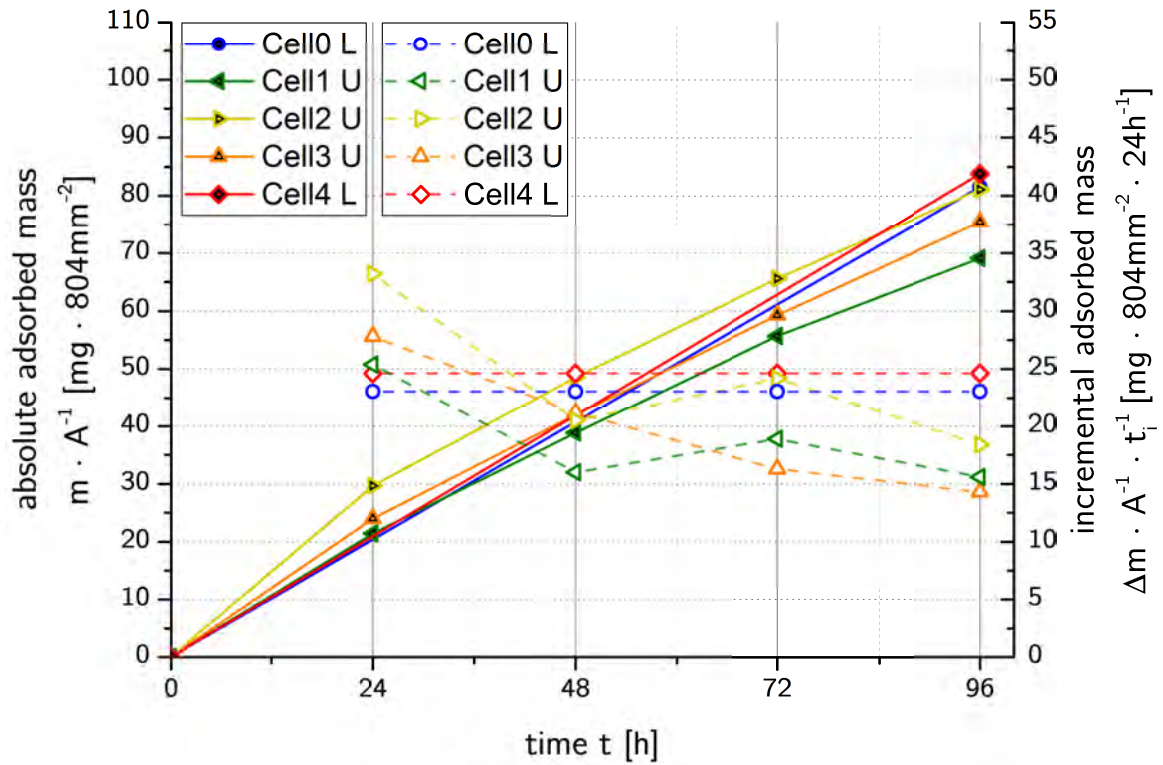


Fig. 3.23: Measurement series 16 - Visualization of the data points of R1566 exposed to a mixture of boric acid, sodium hydroxide and potassium chloride (pH 9.00 buffer)

In contrast to the related R1570 data acquisition, the average of 78 mg · 804 mm<sup>-2</sup> · 96 h<sup>-1</sup> is slightly lower.

### 3.5.6 Reference Matter Evaluation

#### 3.5.6.1 (PET<sup>250 μm</sup> - H<sub>2</sub>O)@Cell(0L, 1U, 2U, 3U, 4L)'slid - MS 4 Å - SSCs - 60 °C

The last series of the diffusion cell measurements was executed to get an idea of a reference material of well-known permeability. For the PET material, which find its application in solar panels, the diffusion is characterized to be at  $2.4 \text{ g} \cdot \text{m}^{-2} \cdot 24 \text{ h}^{-1}$  at RT.

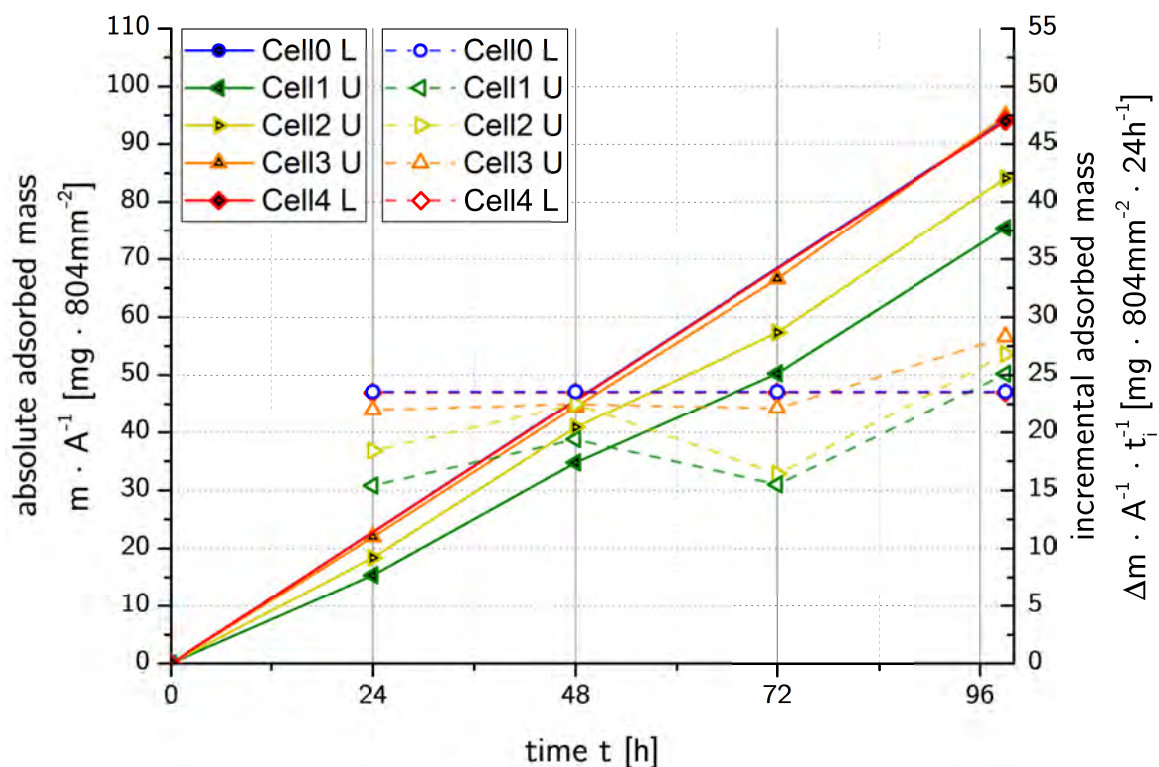


Fig. 3.24: Measurement series 17 - Illustration of the reference material (PET), used in solar panel fabrication.

As depicted in Fig. 3.24 the permeability of the reference polymer seems to lie within a range of the investigated materials. Note that the membrane used here is 250 microns in width, though, and the max. time of measurement is 99h instead of 96h. By reducing the time to 96h, an average value of  $89 \text{ mg} \cdot 804 \text{ mm}^{-2} \cdot 96 \text{ h}^{-1}$  is ascertained, which equals approximately  $27 \text{ g} \cdot \text{m}^{-2} \cdot 24 \text{ h}^{-1}$  at  $60 \text{ }^\circ\text{C}$ , being 250 microns in width.

3.5.6.2 (MCE-DT<sup>40 μm</sup> - H<sub>2</sub>O)@RACell<sup>(0U, 1U, 2U, 3U, 4U)</sup> - MS 4 Å - SCGC - 22 °C

In this series, the rapid analysis cell were used to utilize MCE for data evaluation.

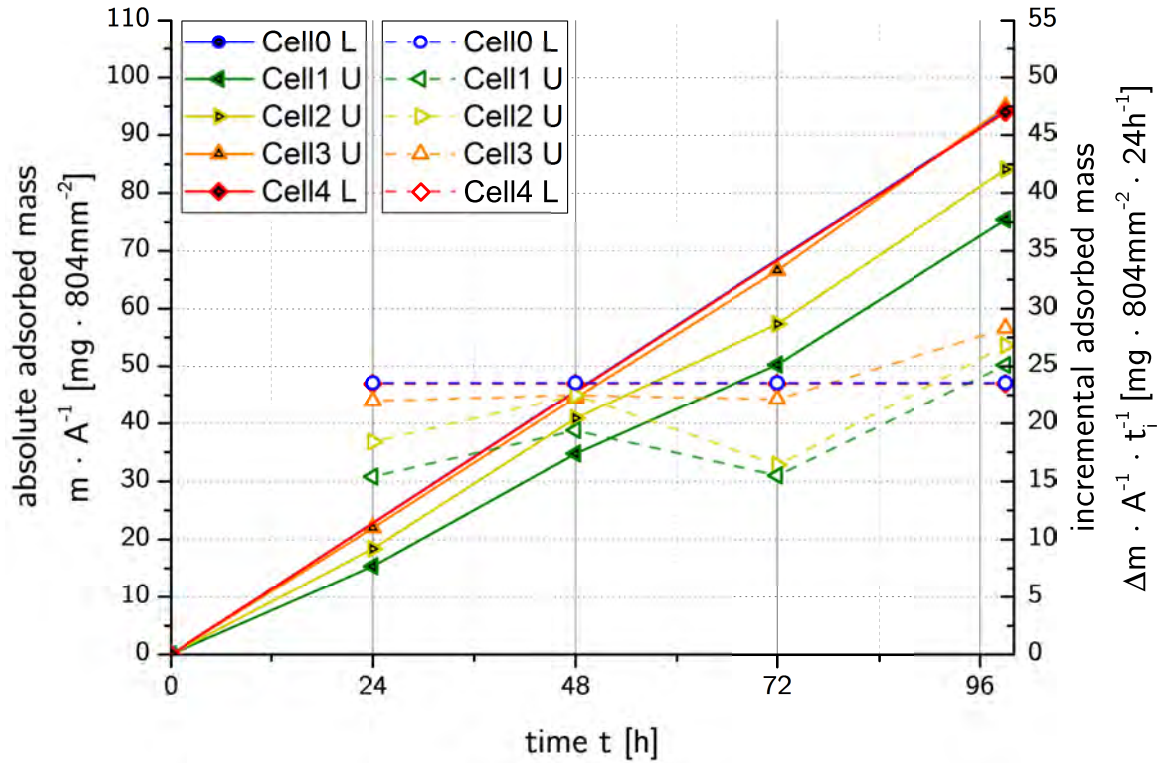


Fig. 3.25: Visualization of the adsorption rates measured via rapid cells at RT.

Although this experiment was expected to fail in terms of mounting issues, the diagram exhibits fairly well slopes. The 24 h trend does again hold for this series and the absolute values exceed GREC membrane measurements in approx. two orders of magnitude, at RT vs. 60 °C, respectively.



### 3.6 Electrokinetic Potential Analysis

The electrokinetic potential analysis ( $\zeta$ -potential) was performed to get an idea of the influence of chemicals used in fabrication processes. The behind intention considers an enforcement of ionic migration due to generated surface charges raised priorly by the purpose of manufacture. Thus, small sheets of R1570 and R1566 were cut out and placed into vials filled with chemical solutions applied in industry. The conditioning at RT took at least three days until the  $\zeta$ -potential analysis was subsequently performed. To ensure the absence of a second IEP at higher pH, two attempts were taken by titrating into a basic direction using a NaOH (0.05 M). As expected, the data points kept a zero-slope on the lower plateau between -30 and -60 mV.

### 3.6.1 R1566WN/R1570 - Blank Evaluation

As depicted in Fig. 3.26, the zeta potential analysis of the untreated GREC membranes shows the expected starting potentials in the range -40 mV to -20 mV relating to polymeric materials of mostly inert behavior. It is commonly known for polymers to exhibit an IEP at pH 4, lacking functional surface groups. What the diagram assumes is that R1566 seems to be slightly acidic, being lower in acidity than R1570 does. If this is due to unlikely occurring oxidization effects from environmental oxygen, this could cause severe problems within PCB's in action. As discussed in "1.18", oxygen permeability is observed in a significant amount in the GRECs. Certainly, if acidic surface functional groups raised by either the presence of oxygen or are simply attendant on R1570 like the diagram suggests, this could protrude tremendous issues, especially enforcing CAF due to a higher concentration gradient of  $H_3O^+$ -ions, which are inevitably present on the positive electrode (anode) see, p. 21. For the gap height, no significant change is observable, swelling can be excluded.

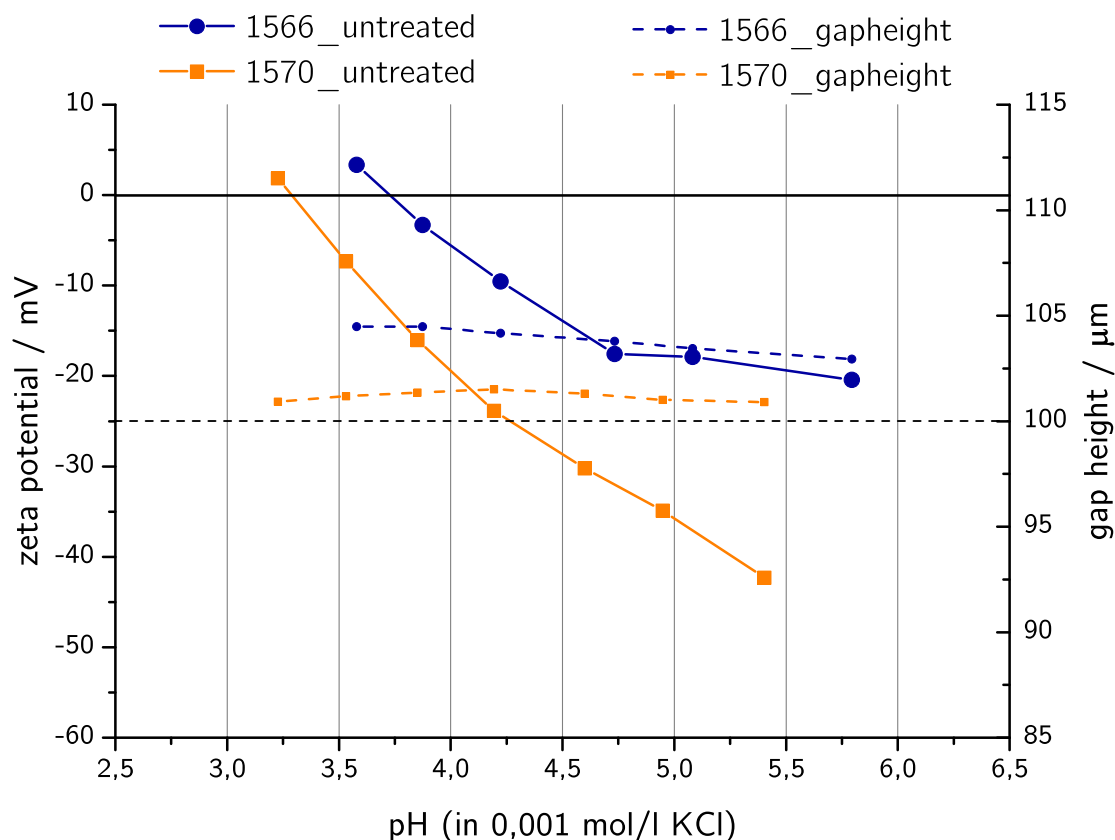


Fig. 3.26: Zeta-potential analysis of the untreated laminates.

### 3.6.2 Industrial Chemicals Treatment

#### 3.6.2.1 Chemisch Kupfer - Kupferprozess (chemCu)

Complementary to the untreated samples of R1570 and R1566, the conditioning of the material with industrial chemicals show slight differences. Illustrated in the figure, the slopes are steady linear. The GREC R1570 exhibits again a more acidic behavior than R1566, though it's IEP increased from pH 3.3 to 3.7, suggesting the included NaOH (30%) may possibly have reduced  $H^+$ -species attendand on the surface. The R1566 visualizes a perfectly linear slope to an IEP of pH4, which concludes inert behavior of the surface. Both materials are shifted to the right in quite equal pH intervals. The gap height is slightly decreasing for both the materials, which may be explained by a re-substitution of  $H_2O/H_3O^+$  to the certain species adhered on the surface.

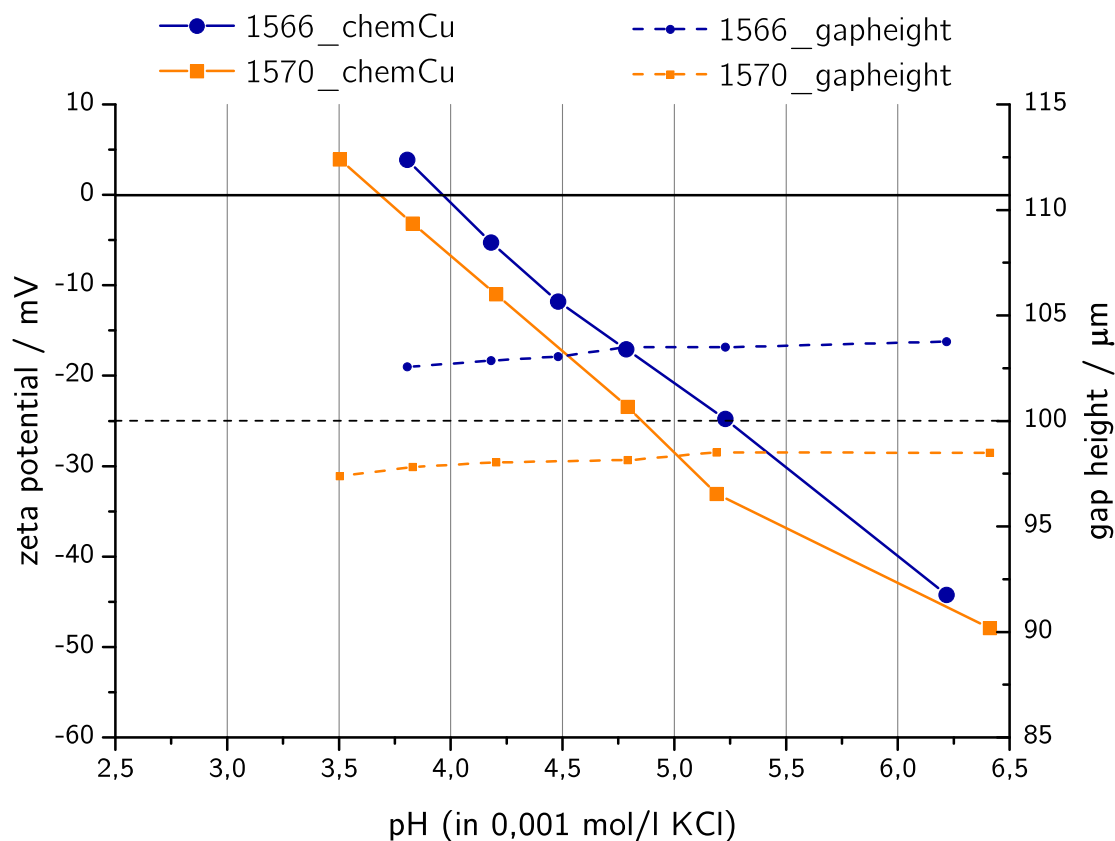


Fig. 3.27: Zeta-potential analysis of the chemCu treated laminates.

#### 3.6.2.2 Galvanisch Kupfer - Kupferprozess (galvCu)

The inert behavior of R1566 is confirmed once more. The gap height keeps an almost steady slope. The R1570 raised in IEP from the untreated measurement of pH 3.3 to

pH 4.1, illustrating a slightly acidic slope.

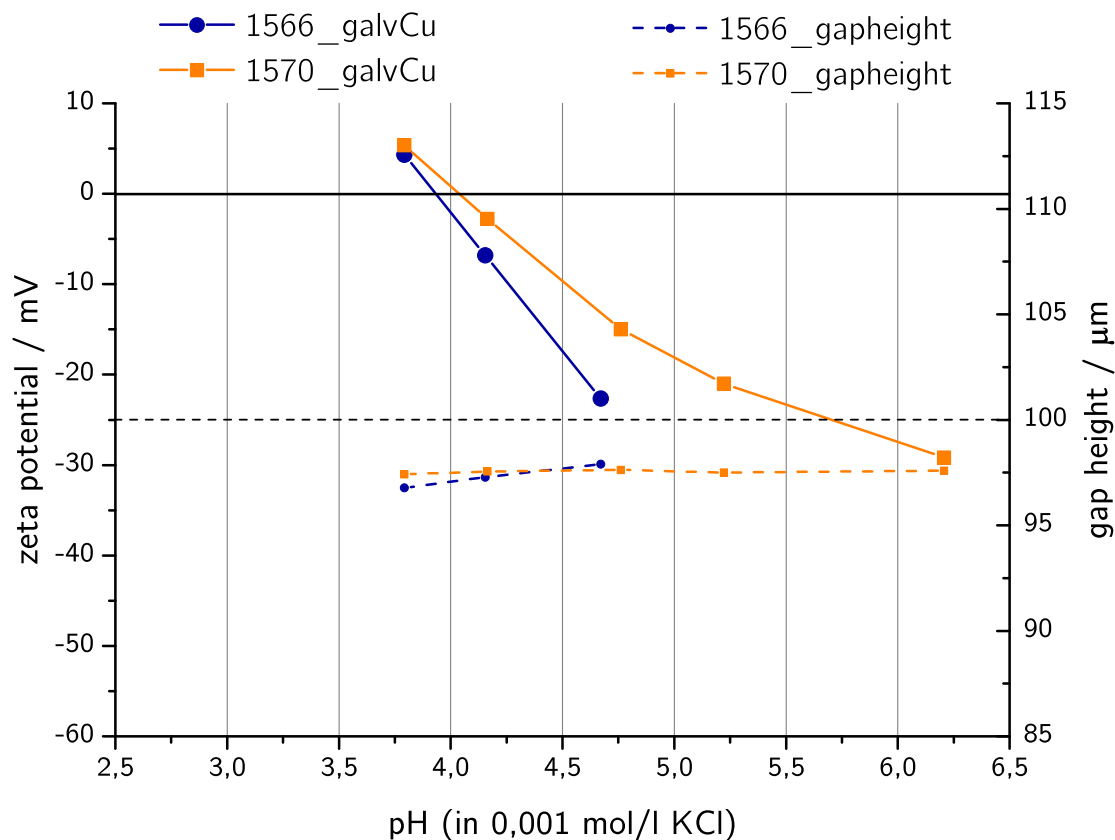


Fig. 3.28: Zeta-potential analysis of the galvCu treated laminates.

### 3.6.2.3 Etch Bath - Photo Process ( $\text{CuCl}_2$ )

The influence of the copper(II) chloride solutions seems to cause a shift to both the potentials of the membranes, especially affecting the normally inert GREC R1566, forcing it to a higher IEP and a more acidic appearance. The system of the etch bath, containing a mixture of  $\text{CuCl}_2$  and  $\text{HCl}$  dissociated in  $\text{H}_2\text{O}_{\text{deion}}$  might corruptify the surfaces of the membranes in a way, that cations adsorb to the surface, though, increasing to aforesaid higher IEPs. If taking into account the high amount of  $\text{Cl}^-$ -ions and  $\text{Cu}^{2+}$  present in the etch bath solution, could possibly catalyse any mechanistic rearrangements at the EDL, consisting of both the inner Helmholtz plane (IHP) and the outer Helmholtz plane (OHP).

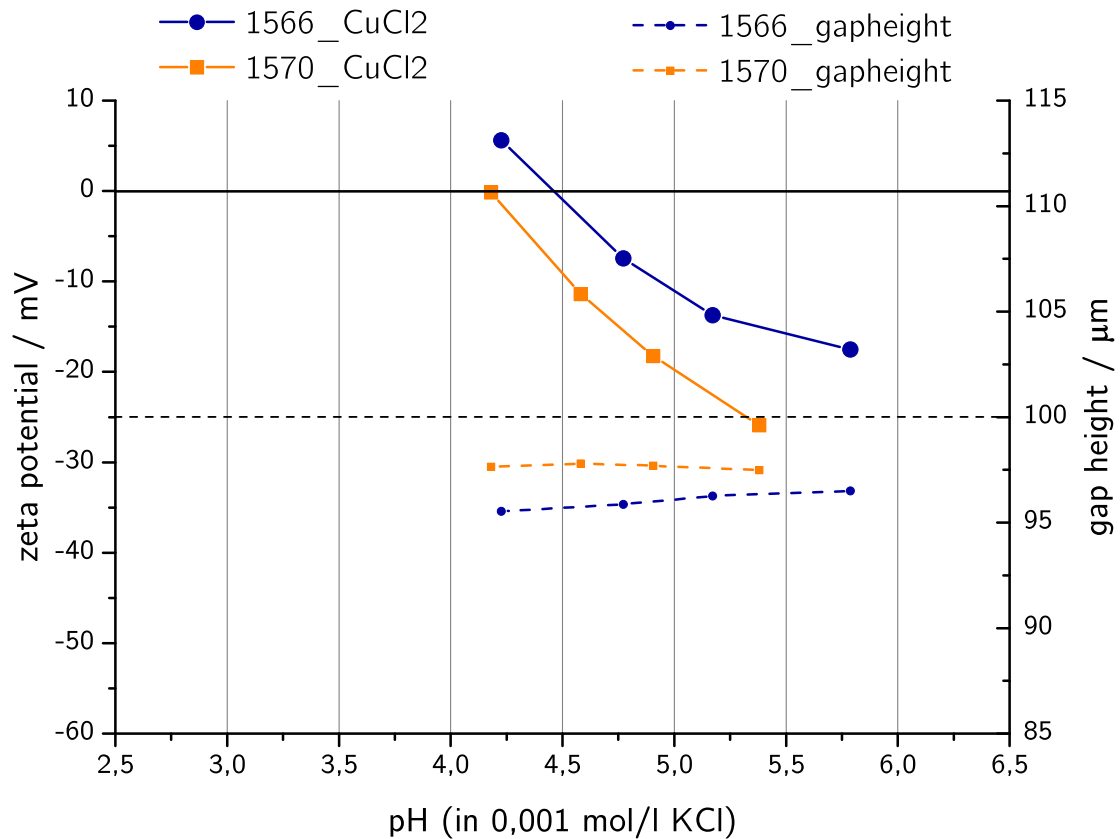


Fig. 3.29: Zeta-potential analysis of the CuCl<sub>2</sub> treated laminates.

### 3.6.3 Standard Chemicals Treatment

#### 3.6.3.1 Hydrogen Peroxide (H<sub>2</sub>O<sub>2</sub>)

In contrast to the untreated samples, hydrogen peroxide draws the IEP's to lower pH values. The R1566 seems to be stronger affected to the favor of higher hydrophilicity, while the GREC R1570 is keeping the usual slope in the zeta potential, although it's gap height is tremendously decreasing. This reduction of 12 μm in channel width suggests a swelling of the material, which might be activated by the treatment with the peroxide.

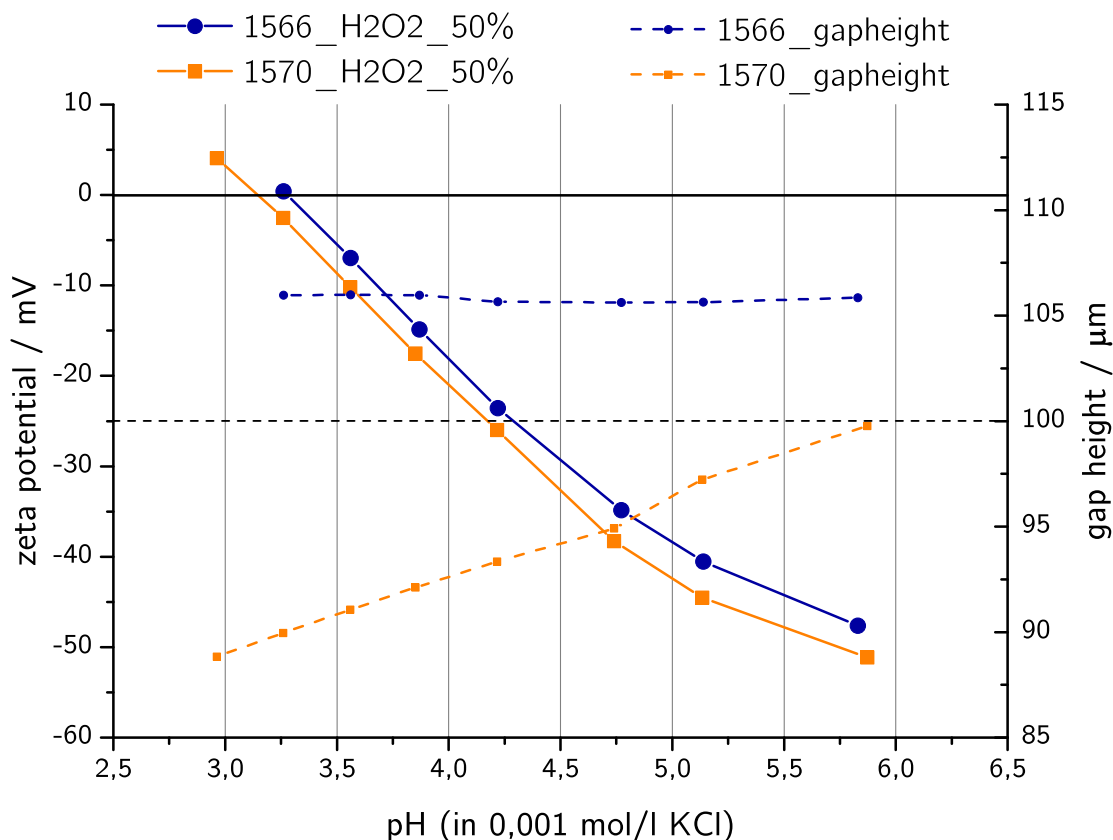


Fig. 3.30: Zeta-potential analysis of the H<sub>2</sub>O<sub>2</sub> treated laminates.

### 3.6.3.2 Sulphuric Acid (H<sub>2</sub>SO<sub>4</sub>)

As already discussed in section "2.9", the conditioning of the membranes in concentrated H<sub>2</sub>SO<sub>4</sub> showed a remarkable reddening of the membranes. Depicted in Fig. 3.31, the allocation and the slopes of the zeta potentials inherently link the treatment of the membranes to the visual changes of its surfaces. Both exhibit very acidic behavior, resulting in increased hydrophilic properties, which may be somehow comprised by the swelling of the material. Starting at -3 mV, both EDLs seem to exhibit charge equalisation. It is assumed that sulfonate acid groups are linking to the available spots while conditioning in the certain solution, either those provided by the polymeric compounds as well as those possibly offered by uncovered and exposed glass sites. In contact with the aqueous salt solution of the measurement setup, the titration solution provides H<sup>+</sup>-ions for the reformation of the sulfate groups back again to sulphuric acid, indicating a permanently descending pH. This unfortunately would vice versa not explain a swelling, which is assumed to raise due to the exchange of surface functional groups of different ion-radii.

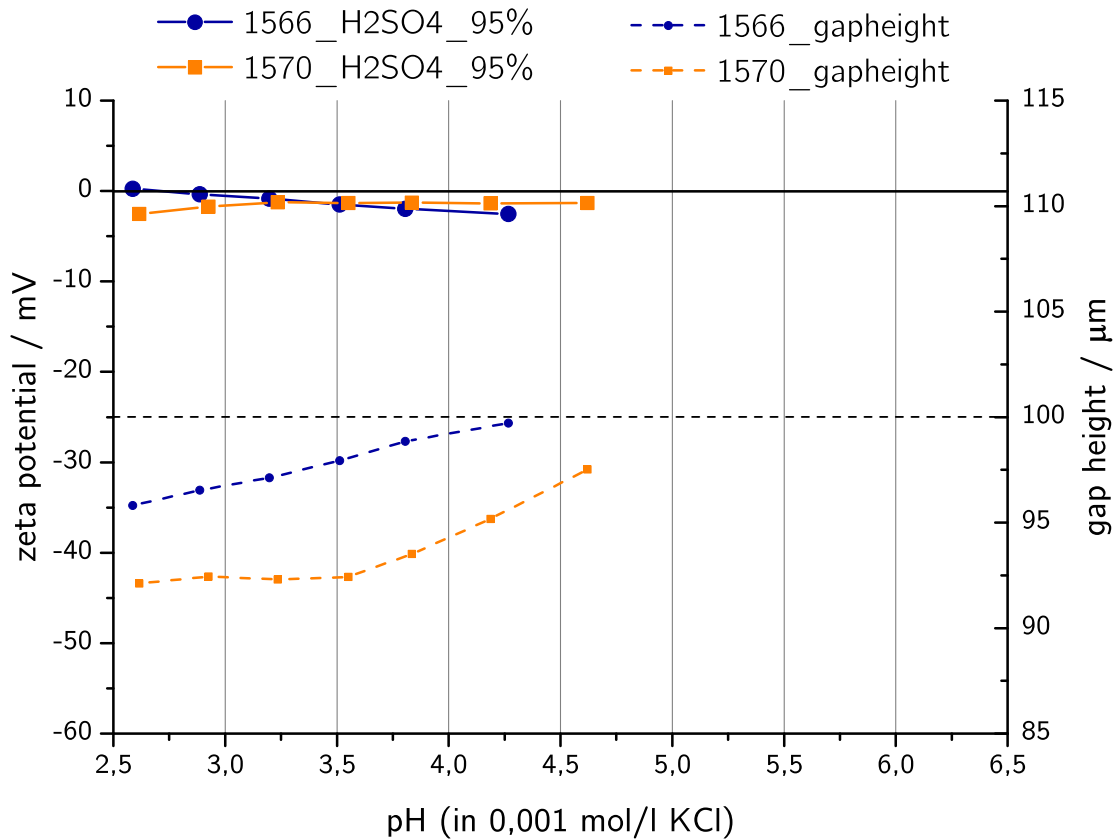


Fig. 3.31: Zeta-potential analysis of the  $\text{H}_2\text{SO}_4$  treated laminates.

### 3.6.3.3 Sodium Hydroxide (NaOH)

The sodium hydroxide treatment seems to be strange in its appearance. The IEP of the GREC 1566 is strongly drawn to a lower pH value, although it shows quite the same slope than the untreated sample. The very negative starting potential may be explained by the following:

"Due to preferable adsorption of hydroxide ions, hydrophobic surfaces exhibit a negative zeta potential when they come in contact with an aqueous solution."<sup>[26]</sup>

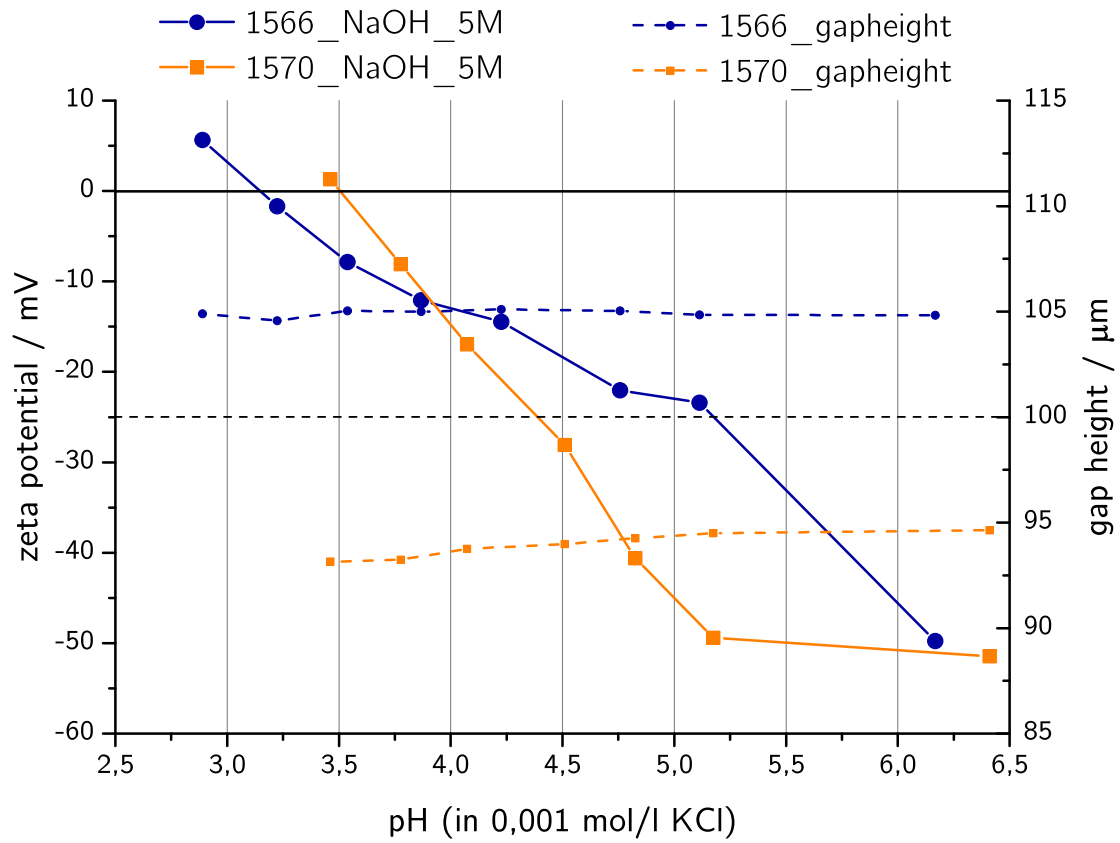


Fig. 3.32: Zeta-potential analysis of the NaOH treated laminates.



### 3.7 ATIR Spectra Analysis

The infrared spectra were taken after performing the zeta potential measurements. It has been already discussed that the resin composition is unknown to the accompanying research facilities. Therefore it is necessary to note that all the absorption bands revealed are just assumptions to the certain substances that might be incorporated in the membranes. Furthermore, to check if there are compositional deviations apparent versus those results gained by the zeta potential measurements, the chemicals-treated membranes were investigated by ATIR either. Sanapala et al<sup>[36]</sup> collected absorption bands from many resin-related sources to state their investigations. Those bands were utilized to allocate and define absorption peaks in the spectra of R1566 and R1570. A Bruker Alpha FTIR spectrometer was used for the analysis.

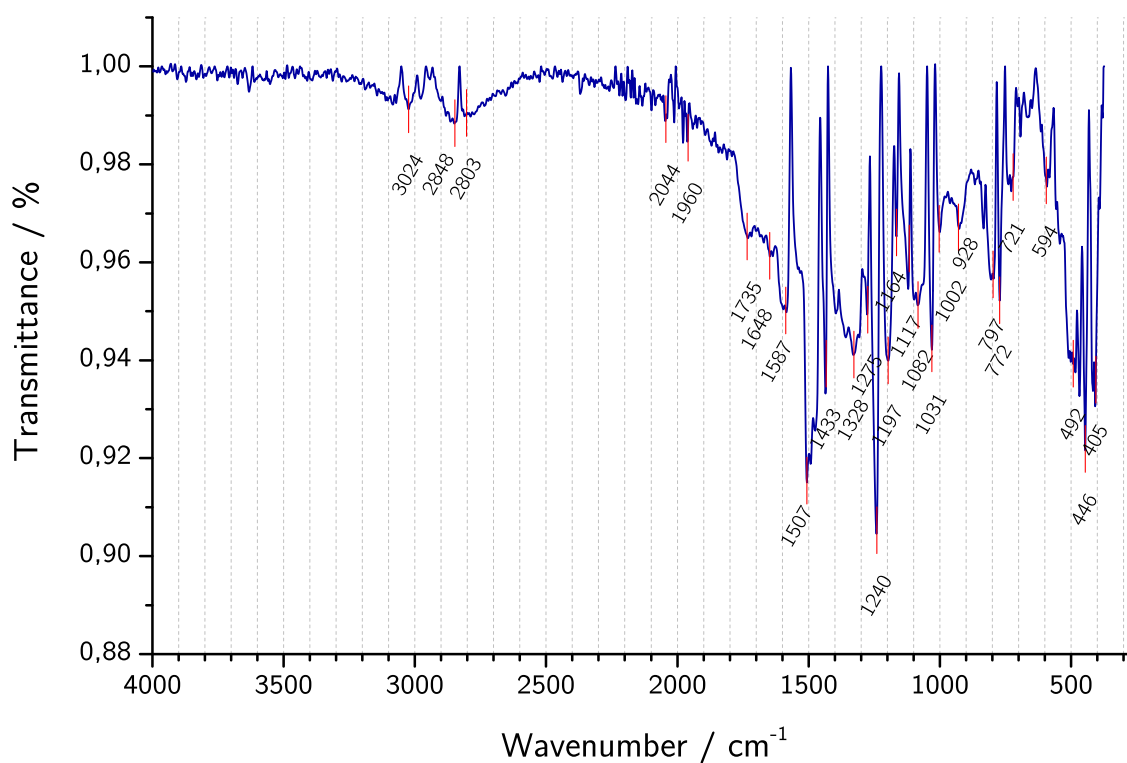


Fig. 3.33: IR spectrum of the GREC R1566.

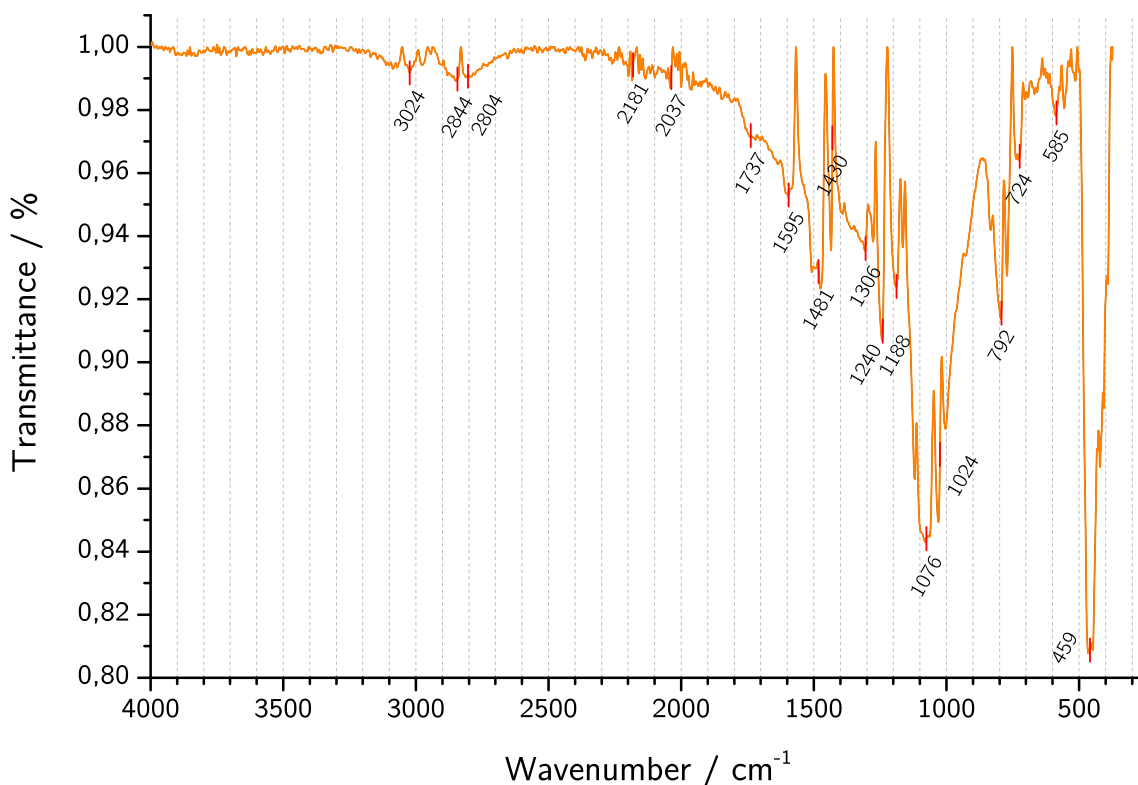



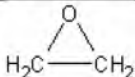
Fig. 3.34: IR spectrum of the GREC R1570.

Table 3.9: Functional groups and wave numbers that might be present in the GRECs.<sup>[36]</sup>

Wave number [cm <sup>-1</sup> ]	Functional groups	Origin
2848, 2844	-CH	From WSR-HPPE (epoxy resin with phosphorus flame retardant)
2181	-C≡N (Nitrile)	From DICY-cured epoxy
1737, 1735	-C=O (Carbonyl)	From DICY-cured epoxy
1650	-C≡N	From DICY-cured epoxy
1595	Aromatic C-C	From DDS curing agent
1587	phenyl-P	From DHPDOPO (phosphorous based flame retardant)
1507	Aromatic C-C	From epoxy resin
1481	Aromatic C-C	From BHPPO (phosphorus containing flame retardant)

1460 - 1306	phenyl-P	From BGPPO (phenyl phosphine) resin with DDS curing agent
1240	-C-O-C-	From epoxy resin
1197	P=O	From DHPDOPO flame retardant
1184	P=O	From DGEBA with DHPDOPO and BPA(phosphorus containing epoxy system)
1164 - 1117	phenyl-P-O-C	From organo phosphate esters (phosphorus containing copoly esters (PET-co-PEPPs))
1082, 1076	phenyl-Br	From DGEBTBA (brominated epoxy)
1031	P-O-C	From WSR-HPPE(phosphorus based flame retardant epoxy system)
1002	phenyl-O-C	From DGEBTBA (brominated epoxy)
928, 772	phenyl-O-P	From DHPDOPO flame retardant

The spectra give clues towards the presence of DICY and phenolic (bisphenolic pattern) curing agents as well as DGEBA. The following tables show the typical absorptions of the associated functional groups.

1. Resin (DGEBA)		2. Curing agent			
Functional groups	Absorption (cm <sup>-1</sup> )	DICY curing agent		Phenolic curing agent	
		Functional groups	Absorption (cm <sup>-1</sup> )	Functional groups	Absorption (cm <sup>-1</sup> )
-C-OH	3500-3400	-NH-	3350-3200	Functional groups listed in 1 (Resin) also exist in phenolic curing agent	
-C-H	3000-2850	-C=N-	1650		
	1600-1450				
phenyl-O-C	1040-1000				
	915-905				

3. Flame retardant (FR)			
Bromine based FR		Phosphorus based FR	
Functional groups	Absorption (cm <sup>-1</sup> )	Functional groups	Absorption (cm <sup>-1</sup> )
phenyl-Br	1066	phenyl-P	1590, 1460, 1350
		P=O	1300-1180

Fig. 3.35: Typical functional groups present in the epoxy laminate systems.<sup>[36]</sup>

### 3.7.1 IR - Industrial Chemicals

Preconditioning the GREC in the certain chemicals obtained by AT&S at RT for several days does barely show any deviations in transmittance. Only  $\text{CuCl}_2$  seems to affect the absorption at  $1000\text{ cm}^{-1}$ . However, an impact of conditioning periods at elevated temperatures, i.e.  $60^\circ\text{C}$  may cause shifts in the IR spectra.

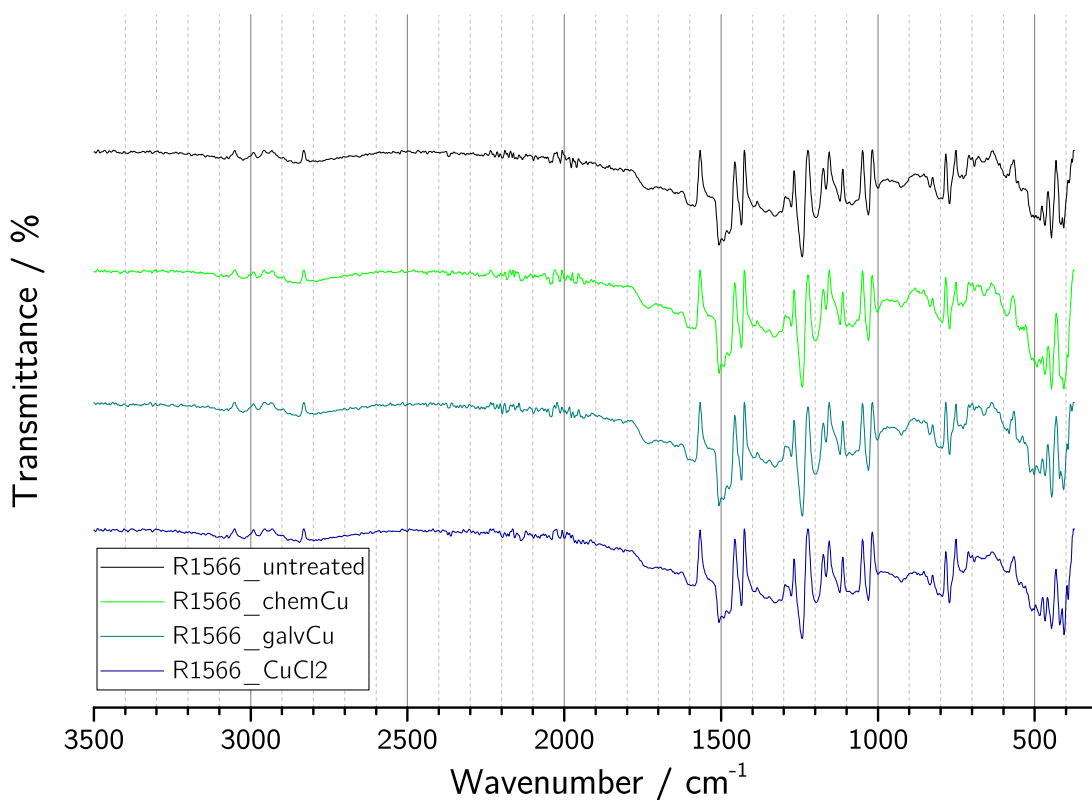


Fig. 3.36: IR spectra of R1566 laminate treated with industrial chemicals.

In contrast to R1566 there neither is an impact on the GREC R1570 by the industrial chemicals. Further investigation on elevated temperatures would yield a better comparability to the fabrication steps, though.

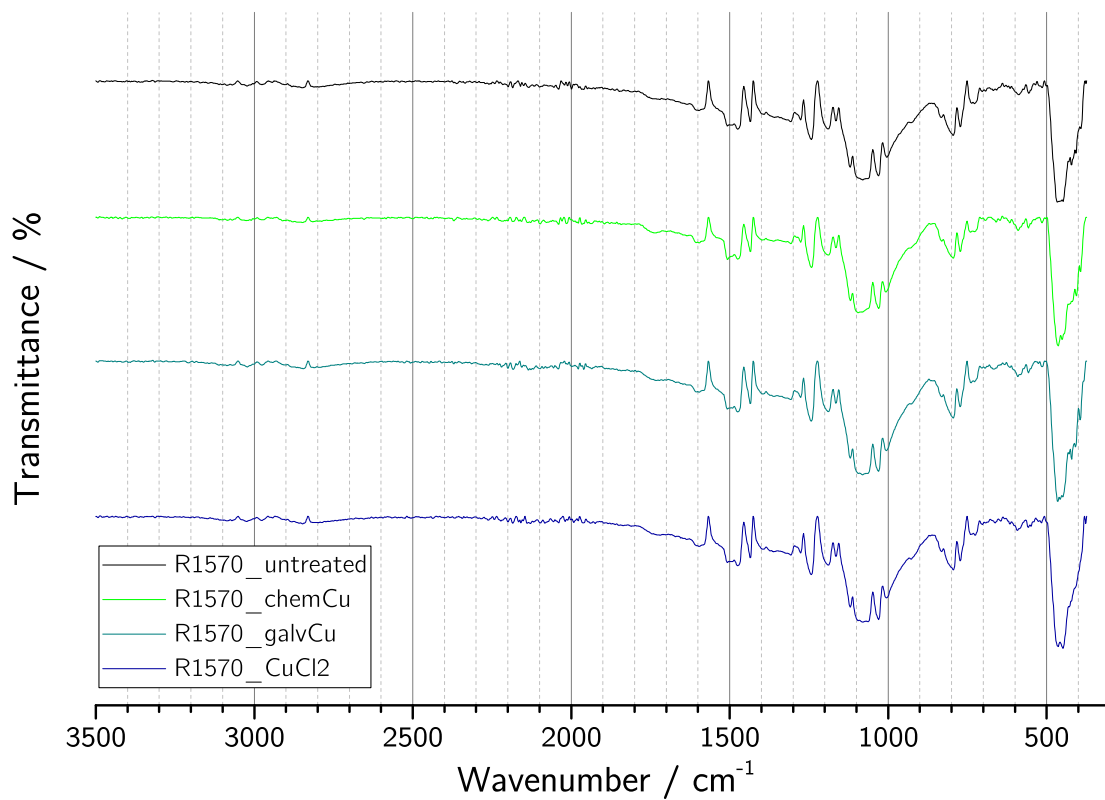


Fig. 3.37: IR spectra of R1570 laminate treated with industrial chemicals.

### 3.7.2 IR - Standard Chemicals

Whether sodium hydroxide nor hydrogen peroxide seems to have an critical impact to the membranes. Treating the epoxy resin composite in a concentrated sulphuric acid shows strong changes in the range of  $800\text{ cm}^{-1}$  to  $1200\text{ cm}^{-1}$ . In the fingerprint area there is also an alteration of the transmittance to higher wave numbers observable.

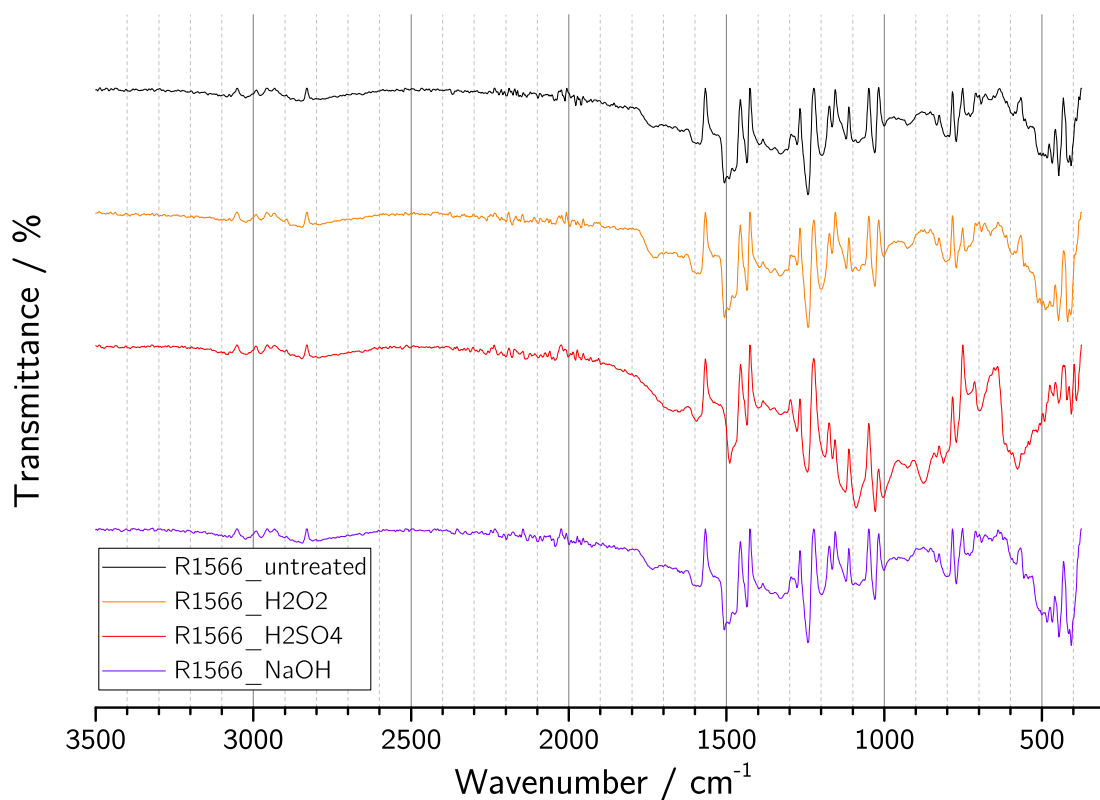


Fig. 3.38: IR spectra of R1566 laminate treated with standard chemicals.

All the standard chemicals affect the GREC R1570. While the peroxide only acts in the fingerprint area, the sodium hydroxide depresses the transmittance bands in the range  $900\text{ cm}^{-1}$  to  $1200\text{ cm}^{-1}$  and in the fingerprint area. Vice versa, the acidic environment provided by the sulphuric acid yields higher bands in those areas. Even at  $600\text{ cm}^{-1}$  a transmittance band is arising due to the presence of acid.

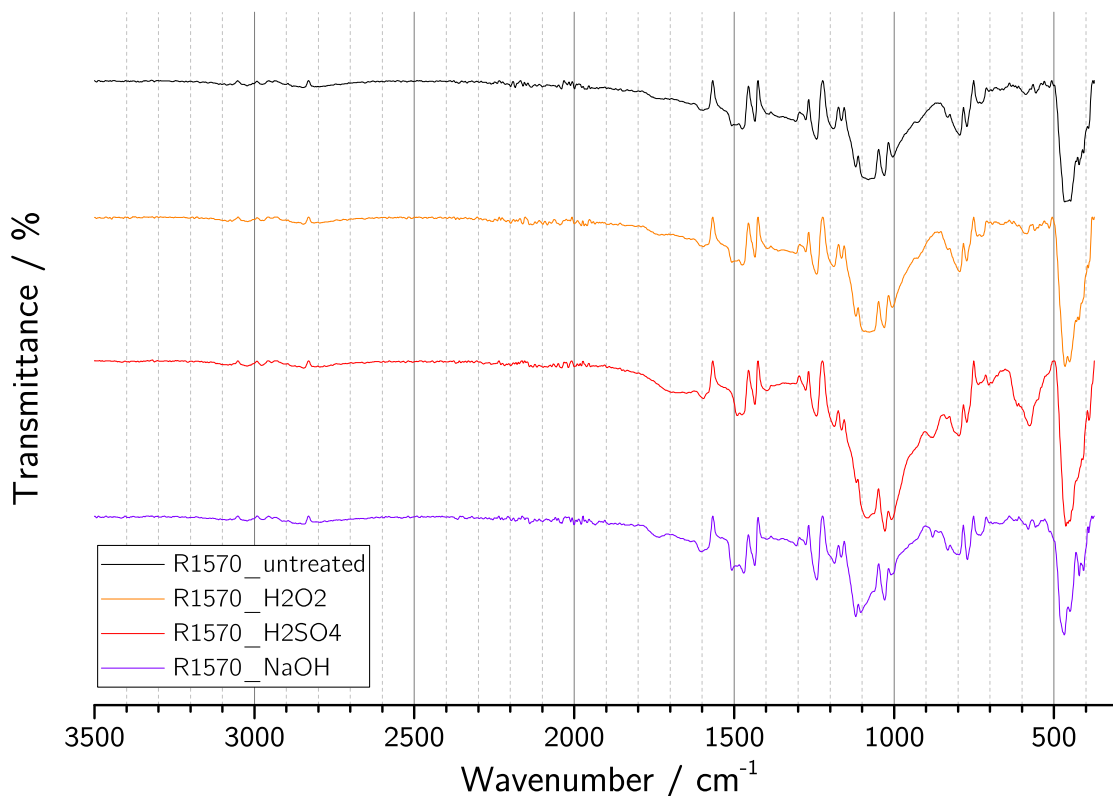


Fig. 3.39: IR spectra of R1570 laminate treated with standard chemicals.

### 3.7.3 IR - Conclusion

While the membranes conditioned in the industrial chemicals seem not to strongly interfere with the untreated materials, the standard chemicals, especially the concentrated  $\text{H}_2\text{SO}_4$ , alter the resins tremendously. Mentioned in prior sections, the sulphuric acid reddened the membranes and the glass weave appeared to stick out. This incidentally not only reveals the certain sizing agents, the acid does either affect the chemistry of resin. Comparing both the sodium hydroxide and the sulphuric acid, they apparently seem to visualize the mechanistic differences of the treating agents to the chemistry of the oxirane structures. With the work of Sanapala et al<sup>[36]</sup>, some of the peaks could be, carefully said, "specified". Wang et al<sup>[42]</sup> and Cholake et al<sup>[12]</sup> recently published journals that proves coherency of IR observations on such epoxy systems. The following picture shows constituents which were detected in the laminate

investigated in Sanapala's work.

Constituent	Major function(s)	Example material(s)
Reinforcement	Provides mechanical strength and electrical properties	Woven glass (E-grade) fiber
Coupling agent	Bonds inorganic glass with organic resin and transfers stresses across the matrix	Organosilanes
Resin	Acts as a binder and load transferring agent	Epoxy (DGEBA)
Curing agent	Enhances linear/cross polymerization in the resin	Dicyandiamide (DICY), Phenol novolac (phenolic)
Flame retardant	Reduces flammability of the material	Halogenated (TBBPA) or Halogen-free (Phosphorous compounds)
Fillers	Reduces thermal expansion	Silica
Accelerators	Increases reaction rate, reduces curing temperature, controls cross-link density	Imidazole, Organophosphine

Fig. 3.40: Typical constituents of FR-4 laminates.<sup>[36]</sup>

Constituents that are primarily found in GRECs are illustrated in the following figures.

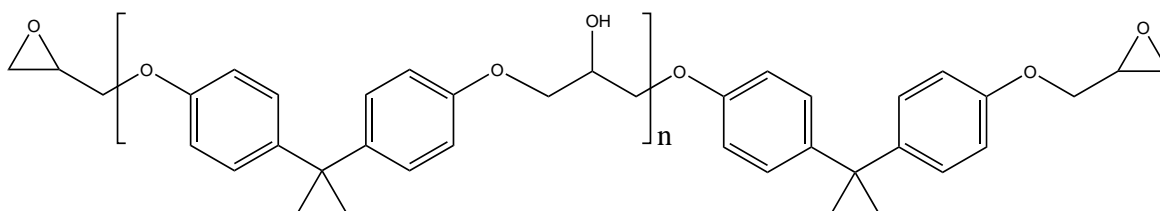


Fig. 3.41: Diglycidyl ether bisphenol A (DGEBA).

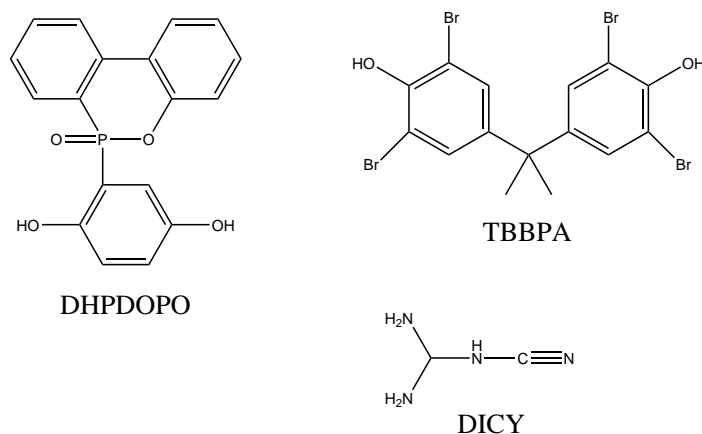


Fig. 3.42: 10-dihydro-9-oxa-10-phosphaphenanthrene-10-oxide (DHPDOPO), tetrabromobisphenol A (TBBPA) and dicyandiamide (DICY).<sup>[1, 31, 42]</sup>



## 3.8 Permeability Detection by an electrochemical Method

The electrodes were coated in a custom-built electrolysis cell. The first depositions yielded electrodes bearing huge dendrites at the circumference. To prevent dendritic growth, polyethylene glycole (PEG) and tetrabutyl ammonium iodide (TBAI) were introduced to the ZnCl-solution.<sup>[28]</sup>

### 3.8.1 SEM/EDX Images

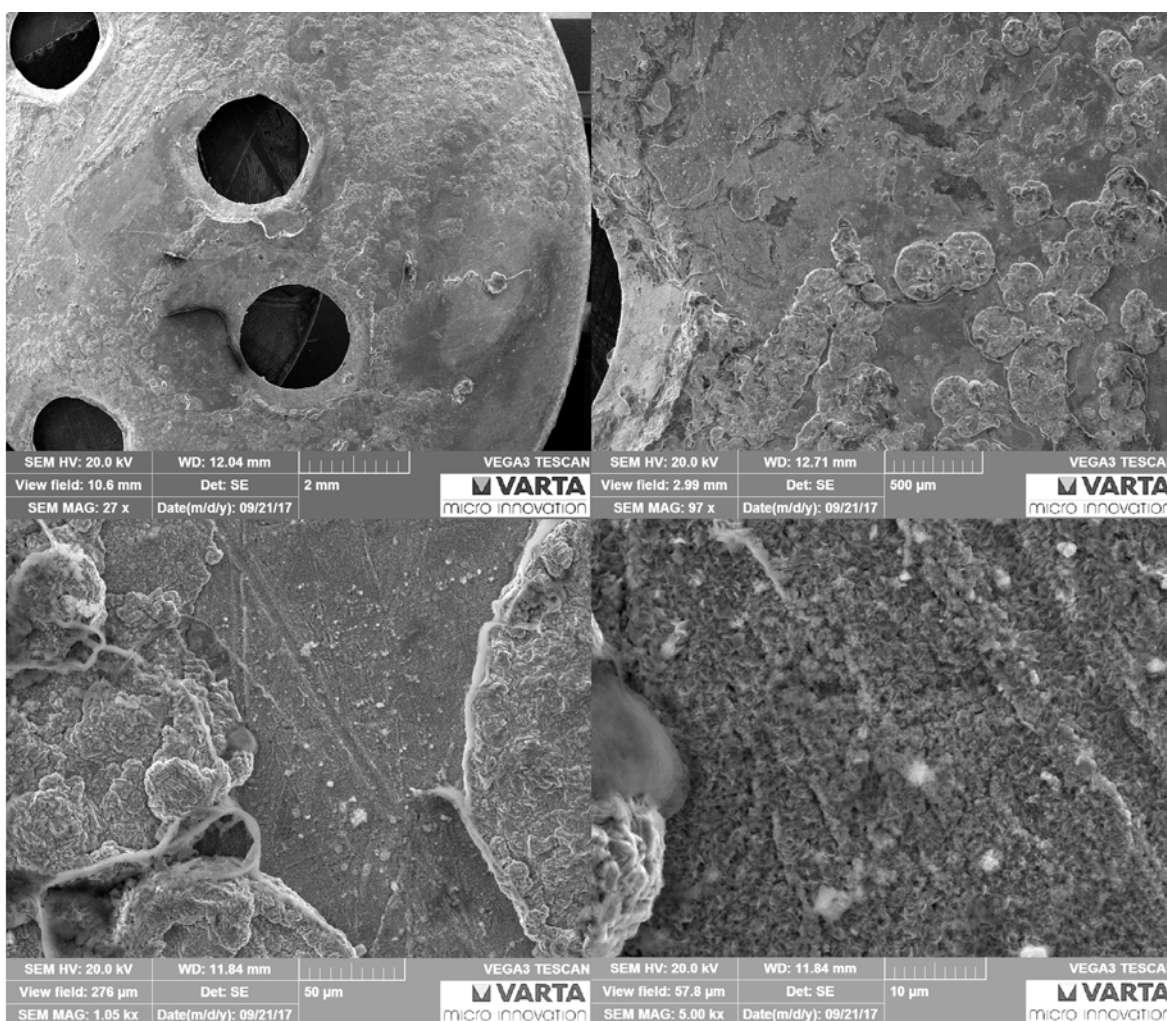


Fig. 3.43: SEM image (P11) of a copper substrate, zinc-coated in a 1 M ZnCl-solution, containing 26 mg PEG and 45 mg TBAI. The time for deposition was 120 min at 0.7 V and 30 mA. The overall surface is appropriate with except of some preferably deposited volumes between the drillings. In a 1000x magnification, inhomogeneous depositions and polishing rills are observable.

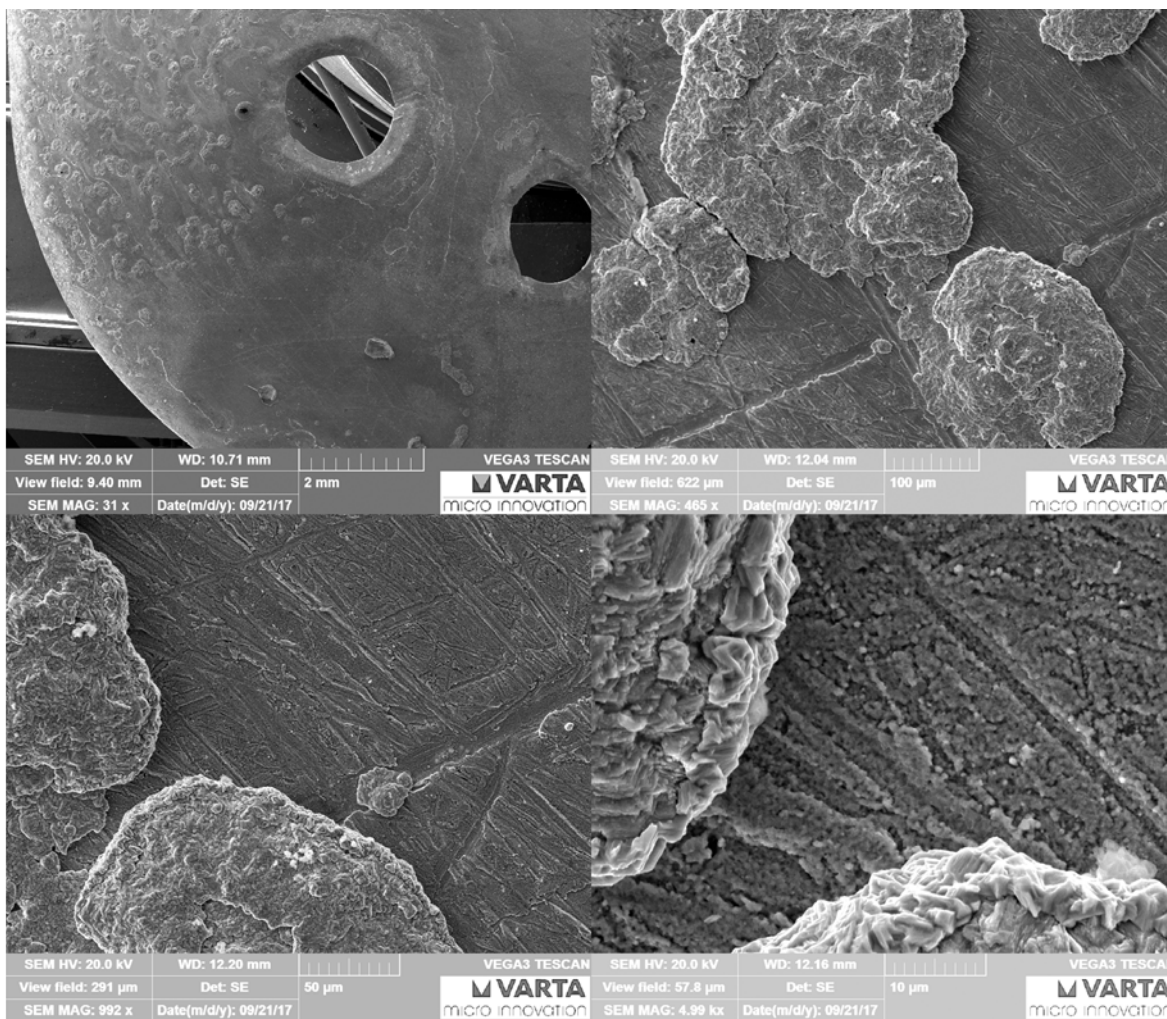


Fig. 3.44: SEM image (P12) of a copper substrate, zinc-coated in a 1 M ZnCl<sub>2</sub>-solution, containing 20 mg PEG and 41 mg TBAI. The time for deposition was 120 min at 0.7 V and 11 mA. The overall surface is appropriate with partially very smooth areas. A closer look at a magnification of 1000x reveals clusters and polishing rills.

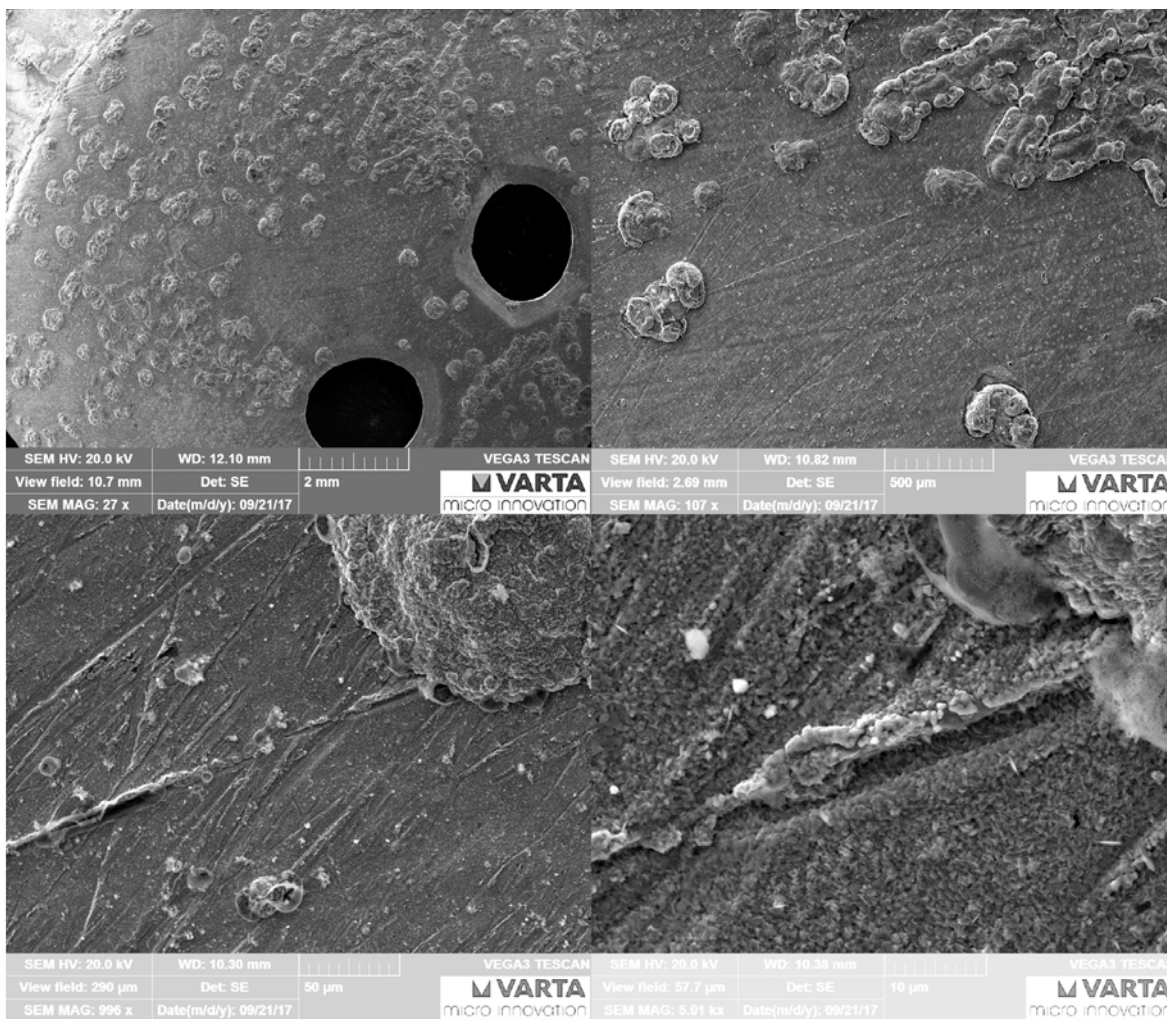


Fig. 3.45: SEM image (P13) of a copper substrate, zinc-coated in a 1 M ZnCl<sub>2</sub>-solution, containing 17 mg PEG and 36 mg TBAI. The time for deposition was 120 min at 0.7 V and 11 mA. The surface is pockmarked and denotes, that a lower amount of brightener is enforcing the roughness. At higher magnifications, again striations as a result of fabrication are observable.

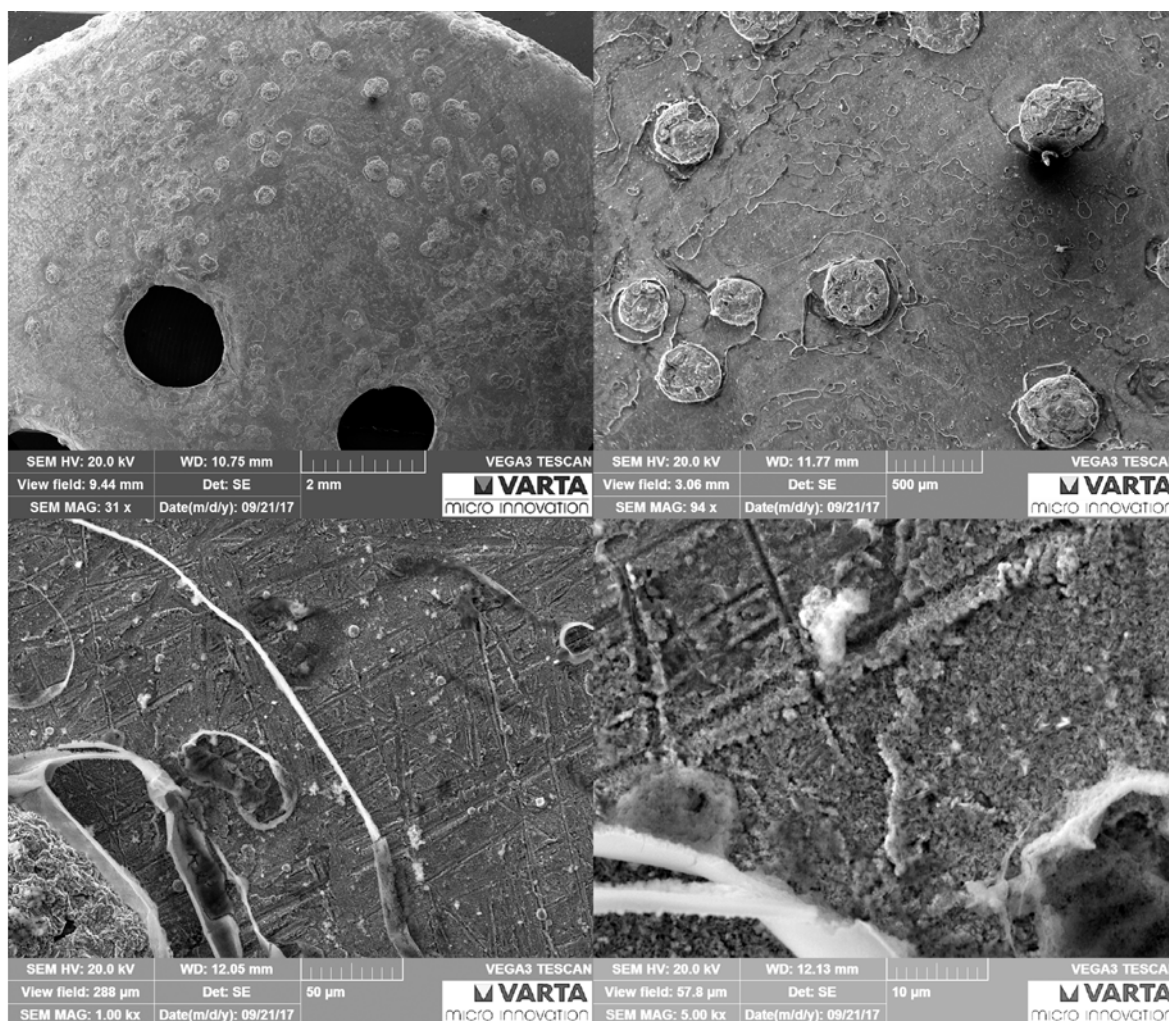


Fig. 3.46: SEM image (P14) of a copper substrate, zinc-coated in a 1 M ZnCl<sub>2</sub>-solution, containing 21 mg PEG and 41 mg TBAI. Additionally, 7 ml dimethylketone (acetone) were added. The time for deposition was 119 min at 0.7 V and 16 mA. Despite the presence of a few clusters the surface exhibits superior smoothness. An mag. 100x reveals the zinc pustules sticking out the surface.

There is an indistinguishable contrast between the electrode coated without and electrodes coated with brighteners. The slight differences in PEG/TBAI amounts do not show critical alterations. However, those containing > 20 mg PEG and > 40 mg TBAI, P11, P12 and P14 respectively, exhibiting somehow smoother surfaces than P13 which contained 17 mg PEG and 36 mg TBAI.

EDX was used in order to check the chemical composition of the surface. The following illustration shows the mass fractions covering the copper electrode. Residues from TBAI are visible and in P14, carbon and oxygen have higher presence on the surface. This might come from the acetone which was introduced in this method.

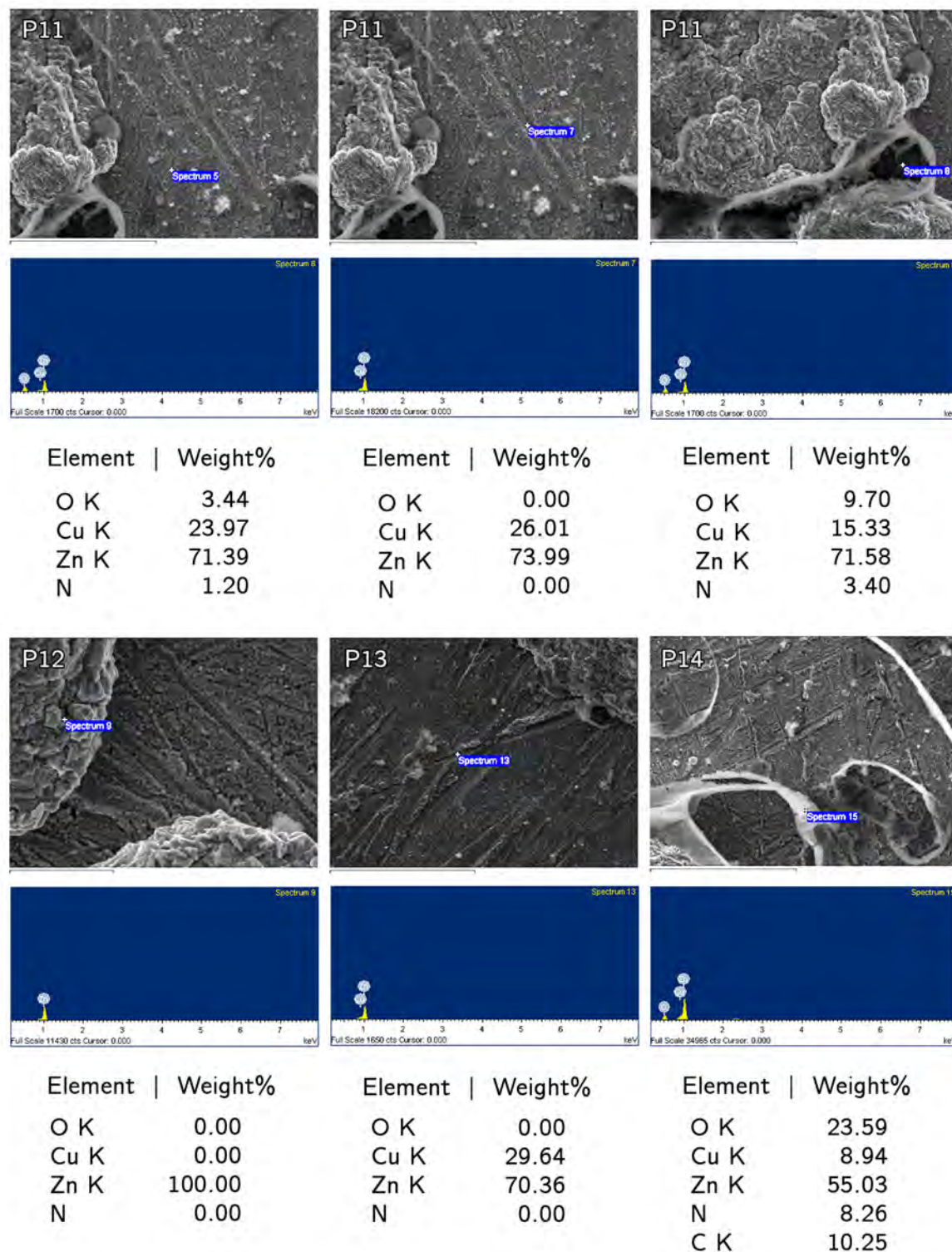


Fig. 3.47: EDX spectra showing chemical composition and mass fractions at chosen locations.

### 3.8.2 Voltage/Current Specification

By the means of a multimeter, voltage and current were recorded before and after deploying droplets of water onto the electrode-membrane assembly. The dry initial resistance was measured to be infinite to the measurement device. After a less than one minutes exposure time, a current established and a few data points were recorded. As expected for the system Cu/Zn the electric power is lower in yield than the system Au/Zn.

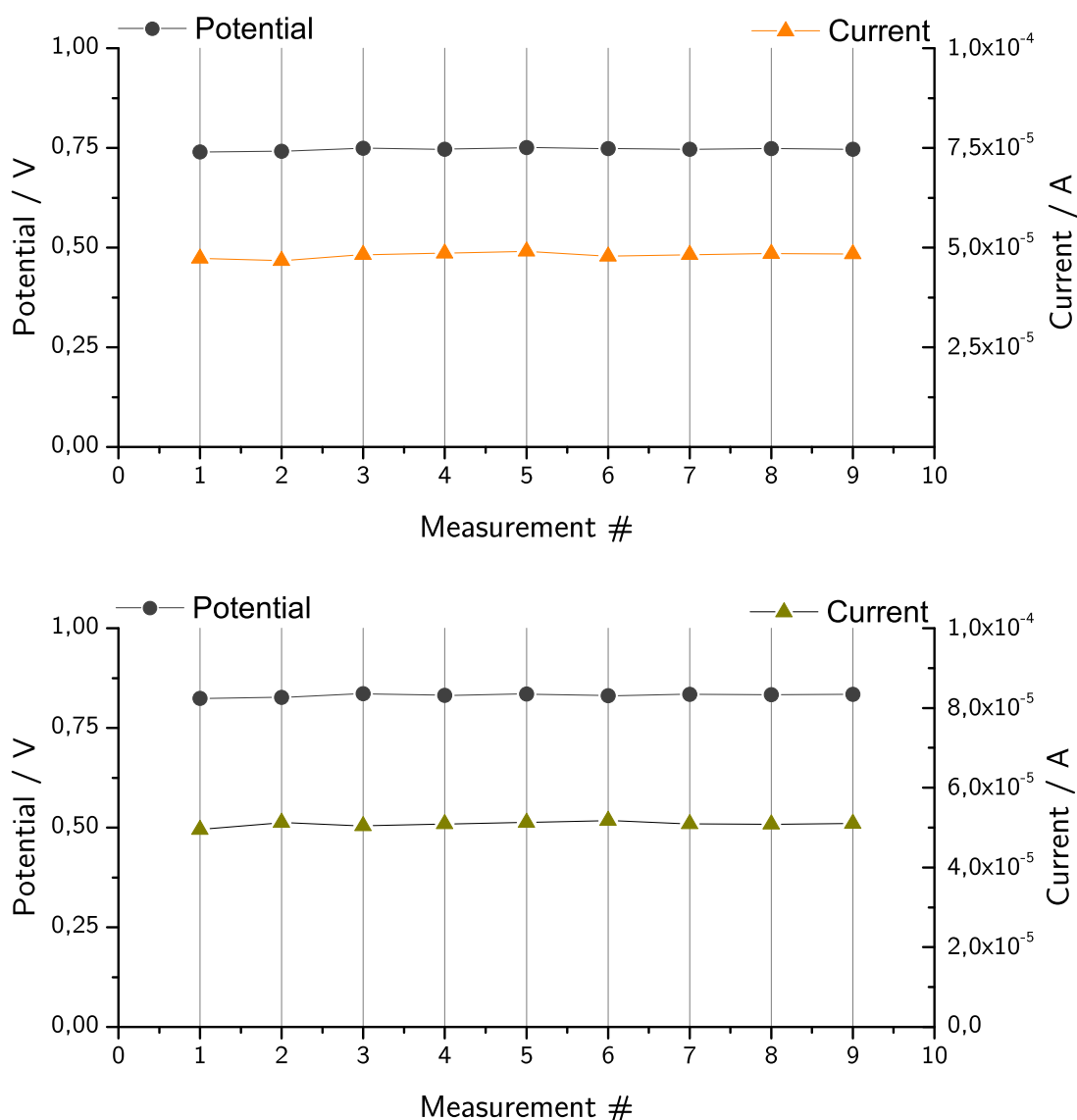


Fig. 3.48: Curves for the measurement of voltage and current. The top diagram illustrates the system Cu/Zn and the bottom diagram the system Au/Zn, respectively.

The data points does not stand in relation to each other due to the fact, that only

one multimeter device was provided. Ascertaining the corresponding values was done within five minutes, though. Not visible in the diagrams is the very slight increase in slope, which may be stated by the fact that swelling and permeation effects are raising. By utilizing the averages of voltage and current, the electrical output is in the range of  $36 \cdot 10^{-6}$  W and  $42 \cdot 10^{-6}$  W for Cu/Zn and Au/Zn, respectively. In order to get more reliable values comprising certain material and environmental properties further investigations will be performed in future.

This study has shown that membranes that exhibit a rigid and dense appearance are capable to transfer aqueous species in high amounts. In the presence of conductive species, even high voltages and currents, especially membrane thickness related voltage gradients may be achieved. An intended investigation, which would utilize the diffusions cell to determine the water flux trespassing these materials could not be executed. This is on the plan, simultaneously to the exact recording of the voltage/current curves.

## 4 Conclusion and Outlook

In chapter "1.7" on p.21 the mechanisms that are suspected to trigger CAF formation has been shown. Related to literature, humidity is a key element for a CAF to evolve in PCBs.<sup>[41]</sup> The purpose of this research was to investigate the behavior of PCB core laminates towards their tendency to absorb and transfer moisture at certain conditions. By providing associated data ascertained, the research facilities should gather more information about critical factors that might enhance CAF formation. To study the materials affinity to the adherence and permeation of water, the diffusion rates were determined gravimetrically. An electrokinetic potential analysis of pre-treated materials should provide more information to the presence of surface functional groups that are capable of synergizing moisture uptake and ionic migration. For the determination of permeability rates, custom-built diffusion cells were designed and manufactured. An Anton Paar SurPASS<sup>TM</sup> 3 was utilized to identify surficial environment of the pre-treated core laminates R1566WN and R1570. Via ATIR detection, the alteration of the epoxy resins after conditioning in certain chemicals was observed. For the diffusion flux, an overall rate was determined and compared to a permeability barrier material (PET) that is used in solar panel packaging. The materials turned out to be equal in terms of their overall moisture penetration rates  $9.0 \text{ g} \cdot \text{m}^{-2} \cdot 24 \text{ h}^{-1}$  versus  $11.4 \pm 1.1 \text{ g} \cdot \text{m}^{-2} \cdot 24 \text{ h}^{-1}$ , GREC versus PET, respectively. In detail R1566, exhibits an average diffusion rate of  $7.7 \text{ g} \cdot \text{m}^{-2} \cdot 24 \text{ h}^{-1}$  and R1570 shows an mean value of  $10.3 \text{ g} \cdot \text{m}^{-2} \cdot 24 \text{ h}^{-1}$ . Comparing both the materials, R1570 seems to be more prone to aqueous penetrants than GREC R1566 does, although it assumes to be more susceptible to pH-dependent solutions. The zeta potential analysis revealed, that chemicals, industrially applied and standard chemicals, affect the surface towards hydrophilicity. The infrared spectra of the pre-treated membranes did not show notable impacts to the material, except for concentrated sulphuric acid. The research partners could show, that SIR measurements are strongly affected by humidity and temperature, yielding strong deviations in resistance and phase angle, both are indication factors for the formation of CAF. With the OTR measurements, values that show twice the oxygen penetration rate for R1566 versus R1570,  $1.3 \text{ cm}^3 \cdot \text{m}^{-2} \cdot 24 \text{ h}^{-1} \cdot \text{bar}^{-1}$  and approximately  $3.3 \text{ cm}^3 \cdot \text{m}^{-2} \cdot 24 \text{ h}^{-1} \cdot \text{bar}^{-1}$ , respectively,



could be collected. Oxygen is assumed to have a strong impact towards moisture and gas equilibrium in the formation of pH gradients when applying a bias. The conversion of  $\text{CuCl}_x$  to (par-)atacamite ( $\text{CuCl}_2 \cdot 3 \text{Cu}(\text{OH})_2 \cdot \text{H}_2\text{O}$ ) is addressed to not only rely on relative humidity and temperature. Factors that are important are partial pressure and oxygen concentration.  $\text{CuCl}_x$  exists only in the absence of oxygen at low pH values while (par-)atacamite needs  $\text{O}_2$  in order to exist.<sup>[30]</sup> At the MCL Georg Reiss achieved to solve a term of the MTTF formula, which is a great success. Megan Cordill from the ESI visualized CAF in specimen by the means of imaging/tomographical methods, i.e. SEM. In an alternative study it has been shown that water may suddenly trigger a current conduction in a former insulating system. Literature has stated that in their investigations CAF consistently was containing copper and chlorine. Performed electron diffractions by Ready et al<sup>[33]</sup> revealed that CAF was hydrous copper chloride, synthetic atacamite (empirical formula  $\text{Cu}_2\text{Cl}(\text{OH})_3$  or  $2 \text{CuCl}_2 \cdot 5 \text{Cu}(\text{OH})_2 \cdot \text{H}_2\text{O}$ ). To conclude, beyond thermal excursions that cause delamination and PEG penetration which enhances water uptake, the presence of high voltage, moisture and oxygen is a major requirement for CAF formation.<sup>[7, 8, 33]</sup>

Although ascertained diffusion rates take part on establishing a MTTF formula, more investigative work applying the diffusion cells has to be done. An observation of the water penetration through the membranes as well as the reference at RT will yield important information to establish diffusion rates and a corresponding diffusion coefficient. In addition, measuring the conductivity by attaching the conductivity electrode to the diffusion cell will provide further parameters that reflect the material dependent characters in the MTTF formula. For the zeta potential, more reliable statements can be obtained by conditioning the laminates in the same chemicals at fabrication-related temperatures. Combining infrared and gravimetric analysis, selected measurements of pre-dried, semi dried and wet membranes are enlisted to compare residual water content (absorption) to that given by literature<sup>[11, 17]</sup>. Furthermore, obtaining more diffusion related series, the diffusion coefficient<sup>[14, 25, 29]</sup> could be derived for the materials. Without the information about the resin composition it is tough to reveal properly specified results, though.

## **5 Appendix**

## 5.1 Development of Supply Tools

Besides setting up a measurement device which complies with the operation purpose it is a crucial point to arrange the research environment to the favor of comfortability. To simplify the measurements, relief equipment makes R&D much more convenient in terms of reliability and economy of time.

In preliminary studies the measurement conditions were tough since the drying agent on the one hand was powdery and on the other hand the desiccant boxes were vial caps and subsequently open and bare, prone to discharges out of the measurement box. The diffusion cell had always to keep in balance during the mounting and measurement process. In addition the GREC membranes are drawing water in an underestimated amount. Consequently they had to be stored in a contactless manner in dry environment.

To eliminate this circumstances and make the data evaluation a progress of ease, a 3D printer provided remedy. Adjacent to changing the powdery desiccant to more handsome molecular sieve granules, the vial caps were replaced by a 3D printed box including a barrier grid to avoid spilling out of the drying agent spheres.



Fig. 5.1: Gravibox, a vessel for drying agent, having a removable slitted cap to provide access to humidity to pass by.

Initially the membranes were hang up onto a steel wire and stored in an desiccator. Not only keeping distance beneath the epoxy sheets were generating troubles, either the withdrawal did. Consequently a multipurpose membrane drying tower was developed to ease the drying in the desiccator and the subsequent extraction steps.



Fig. 5.2: A drying tower, providing the possibility to label and sort membranes of certain materials. In the lower part, different drying agents can be deployed. The removal of a membrane of interest is a process of ease by just unlocking and rotating the corresponding tray.

## 5.2 Troubleshooting - Drawbacks and Opportunities

This section provides a brief information about the problems occurred in the experiments and how they were eliminated. Since the construction of the diffusion cell was an early-stage task the diploma thesis, the provided information did only fulfill principal points, hence some issues showed up when receiving the fabricated diffusion cells. Besides the fact that the measurements of the cells were scaled to the favor of economics, the intended sealings did either. At this time, O-ring sealings were introduced to seal the GREC to the cells. But those initially used radial sealings were untrustworthy in terms of strength of shape, tremendously when using them at increased temperature experiments, very strong deformations were observed.



Fig. 5.3: Deformed O-rings as a result of thermal treatment in a drying cabinet.

However, those O-rings were replaced by the originally intended flat gaskets, which demanded a huge drawback concerning time schedule. Fortunately, the flat gaskets provided hermetically tightness and the execution of the measurement experiments could take place in a secure behavior.

As already discussed in section "2.3.2.1 Desiccant Selection" on p. 57, the initially used powdery drying agents were either too aggressive or too prone against electric charging, leading to a loss of the desiccant and hence gravimetical values corrupted. This problem was solved using MS 4 Å as a drying agent.

Providing the 3D printed containers ("Gravibox", see above), the desiccant could be stucked in position.

Due to the tightening of the flange-clamp it may not be simply removable from the cell itself due to adhering on spot. It needs some afford to dismount the flange by

using a plastic hammer or a screwdriver to level it out. This can be bypassed by just removing the screws and retreat the cell including the flange in the drying cabinet. After an one hours time it may easily be removed.

After one experiment one flange was destroyed by trying to remove it. Utilizing a 3D printer, a spare flange could be printed and inserted, yielding proper values.

In former experiments (series 1-6), the chosen lubricant seems to be an appropriate choice at RT, but after thermal treatment it behaved sticky, made the process of dismantling the cells halves difficult. By replacing the originally used to a "KORASILON-Paste 35 g, Kurt Obermeier GmbH & Co. KG", simplified the measurements significantly.



Fig. 5.4: To mount or separate both cell halves, a lubricant simplifies the process. The finally chosen lubricant is visualized.

For the proper storage of the custom-built GREC membranes, the drying tower, shown above, was introduced to the experiments.

The cells are exposed to strong varying conditions relating to chemical, thermal and mechanical stress. There is hardly a way to avoid the fatigue and wear effects. The only thing one can do is to keep the cells clean and dry and avoid dismounting attachments frequently.

## 5.3 Guides

### 5.3.1 Gravimetical Analysis

#### A - Mounting the Membranes

The custom-cut GREC membranes of the materials R1566WN and R1570 have to be deployed to the cells by suiting the 6 x 60° equidistant stamp holes of  $\text{Ø} 5.5 \text{ mm}$  to the screws planted in the clamping flange.

1. plant the flange in a way that its sinkings face to a flat surface
2. insert the screws perpendicular from the bottom through the drillings of the flange, the screw heads should either face to the bottom surface
3. deploy the first flat gasket to the screw columns to come in touch with the flange
4. carefully superpose the membrane in a same way
5. repeat with the second flat gasket

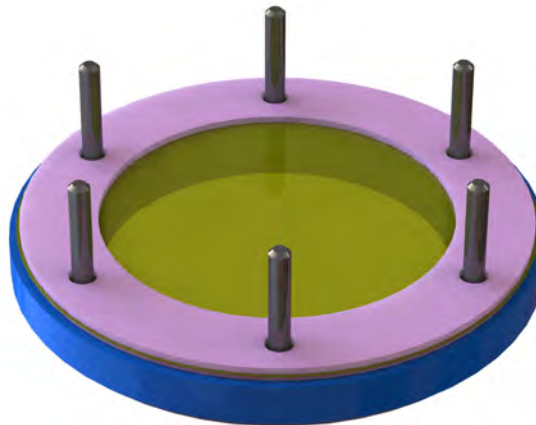


Fig. 5.5: Flange (face-to-bottom) to mount gaskets and membranes layer by layer.

6. carefully rotate that arrangement around the x or y axis for 180° to discover the faces of the flange and the screw heads, be aware of not to lose the screws!
7. deploy the layered composition to the half cell 1 by entrapping the screws to the corresponding thread holes.
8. carefully tight the screws cater-corned by using a screwdriver or a rechargeable drill

9. use the first level of drill's torque to fasten the screws properly

## **B - Preparation of the Gravibox**

To keep the drying agent in position for data acquisition, the Gravibox was invented. It provides a slotted cap which is detachable for refilling desiccant. It is recommended to pre-dry the drying agent over vacuum by using a heatgun. The desiccant should subsequently be stored in N<sub>2</sub> atmosphere and dispensed to the Gravibox providing N<sub>2</sub> crossflow.

10. label the desiccant containers to be in relation with a cell
11. by using an analytical balance the masses of the graviboxes tara should be recorded
12. prepare the opened Graviboxes to deploy them in a right order to the cells
13. fill in the MS 4 Å into the containers by providing a crossflow of inert gas stream
14. try to equalize level of desiccant in the boxes
15. mount the related caps
16. determine the masses gravimetrically and note them down

## **C - Completion of the Cell Assembly**

The following steps presume the half cells to be set up like described in prior chapters. Additionally all the cells should be pre-dried and cleaned before resuming with the assembling steps.

17. remove one of the half cells valves to avoid gas compression when marrying the cell parts
18. insert a closed end PE-foam to insulate screw channels
19. be sure to lubricate the O-ring sealings with a proper lubricant (KORASILON-Paste 35 g, Kurt Obermeier GmbH & Co. KG)
20. insert half cell 1 into half cell 2 (see Fig. 5.6)
21. plug in the priorly removed valve again (be sure teflon tape is applied on the thread)



22. screw the cell halves together
23. fill half cell 1 with a substance of demand and close valve if possible

#### **D - Adsorption Data Acquisition**

Depending on the material to be investigated, it may be necessary to enforce diffusion velocities by temperature. Whether or not, the cell should not be opened for a long period of time. The adsorption of monolayers of humidity can not be avoided without handling the setup in a glovebox, tough.

24. remove the cells from the drying cabinet, if optionally chosen
25. remove the screws
26. detach a valve of the secondary analyte cell (2)
27. separate the cell halves
28. move with the desiccant cell to an analytical balance
29. use tweezers to move and positionate the Graviboxes to the balance
30. record the masses of each container
31. after data acquisition, close the cells vice versa to the separation process
32. proceed in the same way for the time intervalls of favor

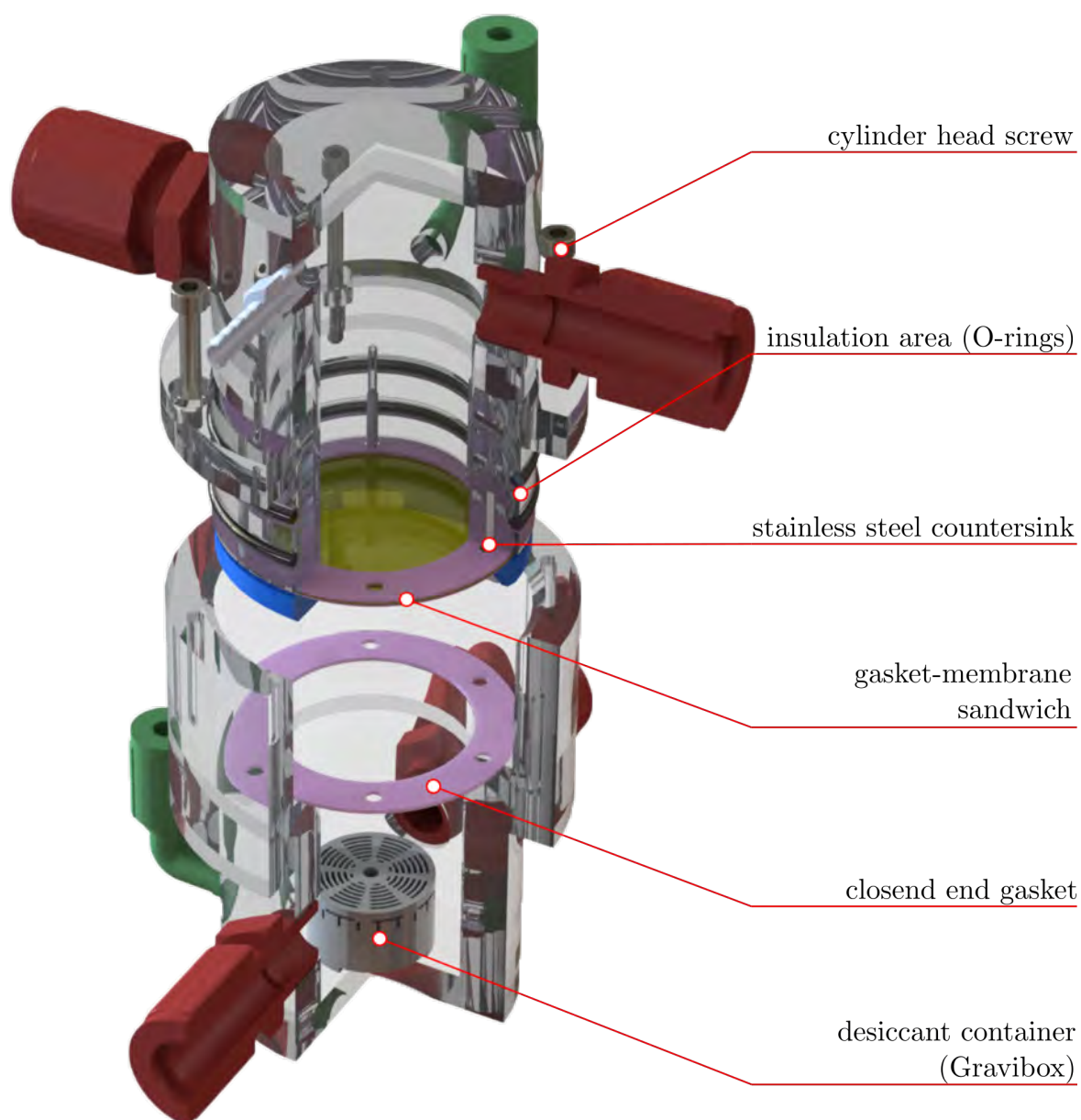


Fig. 5.6: Half-section of the diffusion cell showing fully assembled cells and the Gravibox encapsulating drying agent.

### 5.3.2 Elektrokinetic Analysis

#### A - Launching the Device(s)

Before operating the device, the same has to be activated and simultaneously the  $N_2$ -valve should be opened, which conserves conditions within the measurement cell.

1. activate the device using the switch on the rear side of the SurPASS™ 3
2. switch on the corresponding computer including SurPASS™ 3 software
3. open the  $N_2$  valve to provide a slight gas stream to the gassing tube
4. insert the gas tube into the electrode holder
5. enable external pressure unit, indicated in Fig. 5.13

#### B - Calibration of the Electrodes

By launching the corresponding SurPASS™ 3 software, the information of how to proceed should be given. If the device was out of service for about 30 days, one has to calibrate both the pH electrode and the conductivity electrode. Therefore the buffer solutions of pH 4.01/7.01/10.01 and the conductivity standard allow remediation.

6. prepare the following solutions to the periphery: buffer solutions pH 4.01/7.01/10.01 and conductivity standard



Fig. 5.7: Calibration solutions used in  $\zeta$ -potential analysis.

7. prepare a waste beaker and a spray bottle filled with  $H_2O_{\text{deion}}$  to rinse the electrodes

8. click on maintenance and choose "pH Calibration", subsequently "Begin calibration"
9. rinse the pH electrode and insert it into the buffer solution vial specified by the software
10. start the calibration and proceed with the same way for the raising pH values and with the conductivity electrode
11. by clicking "Adjust" the calibration data acquisition is finished
12. insert the electrodes into the corresponding holes of the electrode holder

### **C - Preparing the Measuring Environmet**

Setting up the measurement provides solutions of KCl (1 mM), HCl (50 mM) and Milli-Q.

13. take the rinse cell and mount it to the device, the arrow on the cell indicates the top of the cell, use force to fully align the cell to the SurPASS<sup>TM</sup> 3
14. tight the cell using the fastening-lever
15. provide a beaker (200 ml, tall shape) filled with 200 ml of Milli-Q
16. by lifting the electrode holder, the beaker can be easy deployed into the device
17. at the titration unit, exchange the SCHOTT bottle (100 ml) to the one filled with HCl 0.05 M (red dispense line)
18. take out the titration hose and insert it contactless into a waste beaker
19. in the section "Clean" (see Fig. 5.8, p. 137) on the bottom software side, click "Fill the titration units", the dispense lines will provide a stream of HCl to the outlet; when finished, check if their neither are bubbles inside the red tube, repeat "Fill the titration units" if necessary

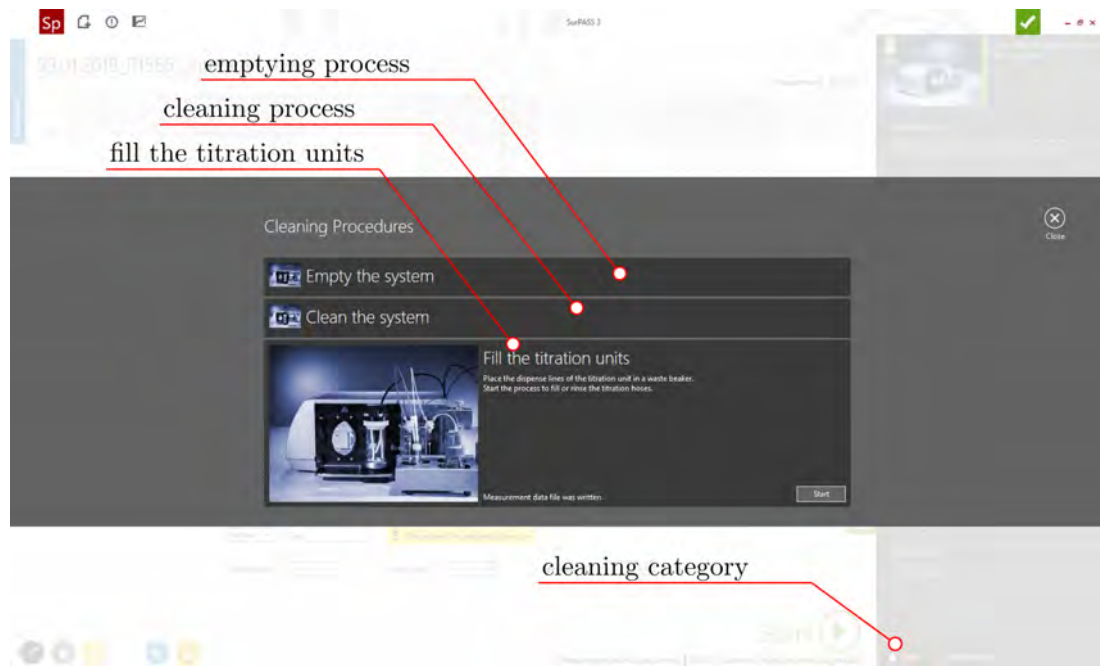


Fig. 5.8: Cleaning procedures within the SurPASS<sup>TM</sup> 3 software.

20. put the titration tube into the last possible hole of the electrode holder.
21. check if the white waste tube is properly placed on the white cap of the device's waste beaker
22. descend the electrode holder in a way, that the white measurement beaker cap is well aligned between the holder and the beaker itself, check if the transparent suction hose is not squeezed between the holder and the cap
23. at this moment, pH electrode, conductivity electrode, N<sub>2</sub> bubbler, titration dispense outlet and suction hose should be deployed and a bubbling of N<sub>2</sub> should be observable, additionally the rinse cell should be mounted properly
24. in the software, switch from "Fill the titration units" to "Clean the system" - it will immediately fill the device cleaning the interior of the SurPASS<sup>TM</sup> 3.
25. after cleaning the system, switch to empty the system to unload the solution.

## D - Specimen Preparation

The sample to be investigated always has to be scaled towards the size of the sample holders. By using a special tesa<sup>®</sup> adhesive tape the matter is adhered and furthermore trimmed by using a scalpel. It is strongly recommended to use powderless sterile gloves to avoid contamination of the surfaces to be examined.

26. use gloves in this process
27. place the matter of interest on a clean cutting board
28. use the sample holders and stick them to the specified red tesa® adhesive tape, be meticulous in economically consuming tape (expensive)



Fig. 5.9: Adhesive tape to adhere sample membranes.

29. by using a cutter knife or a scalpel, the tape can be trimmed down to perfectly match to the sample holder measurements (20 x 10 mm)
30. remove the safety film and place the sticky side carefully onto the material to be investigated
31. trim down again to match with the sample holder measurements

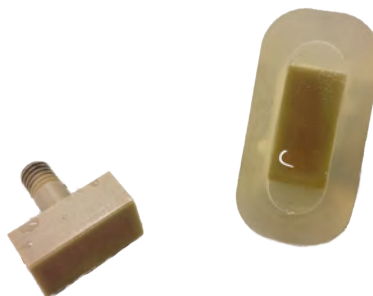


Fig. 5.10: Sample brackets with adhered analyte material.

32. place the sampleholder into the correspondiv channel sealings (small to small, tall to tall)

33. the small holder has to be mounted to the micrometer screw excluded part, whereas the tall one has to be inserted into the variable part
34. the membrane on the small holder should be aligned coplanar to the cell face
35. use the torque key (0.5 Nm, Torx) to fastening the small holder to the cell half
36. try to insert the big holder in a way that the material to be investigated is approx. 100 microns below cell face level
37. using the torque key again, tight the holder (keep the micrometer screw locked in position)
38. mount together the cell halves using the tension screws and the torque key

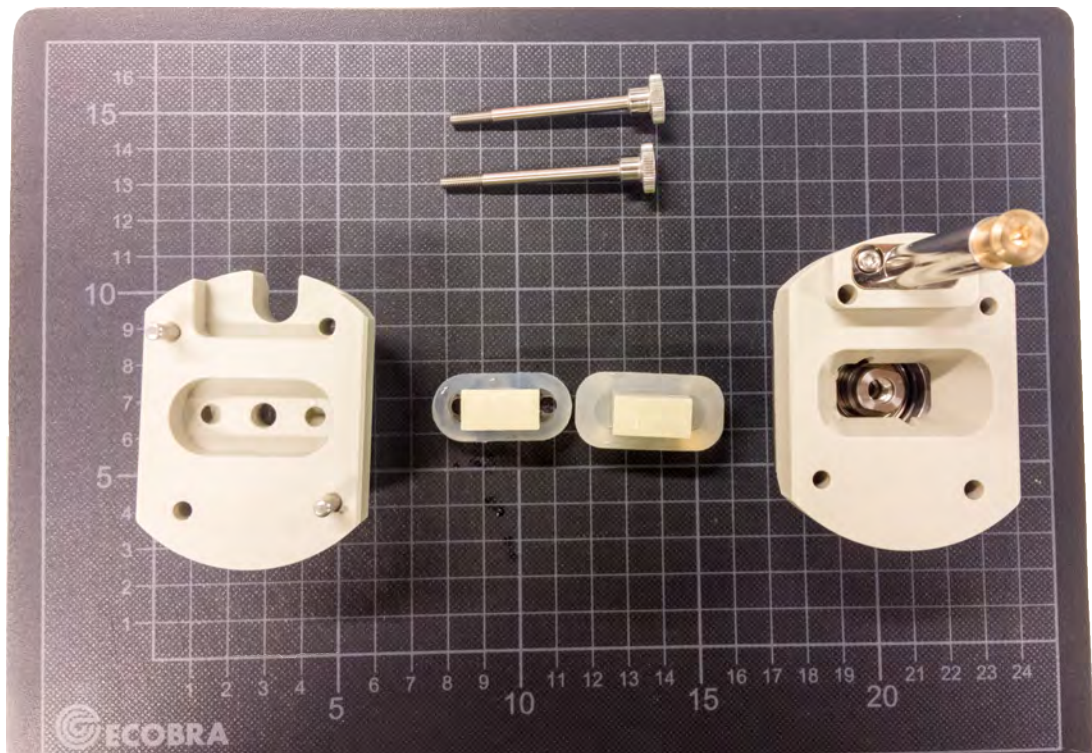


Fig. 5.11: Measuring cell parts including GREC membranes, adhered on sample brackets in the corresponding sealings. The background shows the cutting board for trimming adhesive tape and membranes.

39. remove the rinse cell and place the measurement cell
40. remove the beaker (200 ml, tall shape) and replace it with the same shape including 1 mM KCl solution, deploy a magnetic stirr bar
41. place the waste hose into the white beaker cap hole to establish circulation of the fluid

## E - Performing a Measurement

The execution of a electrokinetic potential analysis demands either rinse cycles with Milli-Q as well with the measuring solution to set the measurement conditions. The gap height for instance should be at around  $100\ \mu\text{m}$ . Further values indicating everything is fine like a conductivity of 12 to 16 mS/m are depicted in Fig. 5.13.



Fig. 5.12: Micrometer - 0.5 mm thread. One graduation line therefore equals  $25\ \mu\text{m}$ .

42. in the upper left corner, start a "New experiment" and fill in sample name and path of execution
43. click on "Rinse" in the left bottom corner using the settings of demand
44. start the rinse cycle, the measurement curve is indicated in Fig. 5.13, as a result should be achieved a gap height of approx.  $100\ \mu\text{m}$  , repeat rinse cycle to achieve 100 microns gap height



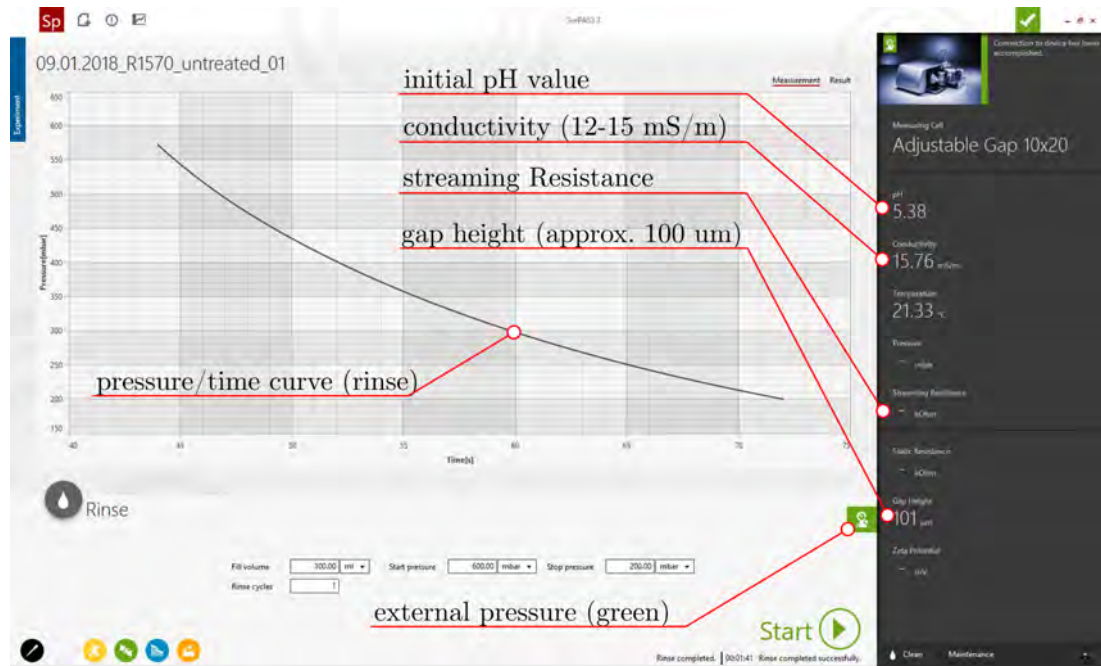


Fig. 5.13: Screenshot of the software indicating how values/curve should look like.

45. switch to the method of favor in the left bottom corner (here IEP)
46. vary the settings to your need
47. start the measurement procedure
48. after finishing the measurement (see Fig. 5.14), switch the waste hose to the waster beaker cap



Fig. 5.14: Finished acquisition of the isoelectric point at pH 3.28.

49. replace the measurement solution by a 200 mL solution of Milli-Q
50. launch "Clean the system" again and empty it afterwards
51. replace the measurement cell with the rinse cell and repeat cleaning and emptying
52. disassemble the measurement cell and proceed with further experiments
53. for closing the measurements, remove the electrodes and rinse them, put the pH electrode back into the 3 M KCl solution vial
54. replace the dispense line from the electrode holder into a waste beaker and change the titration solution bottle to the former SCHOTT bottle

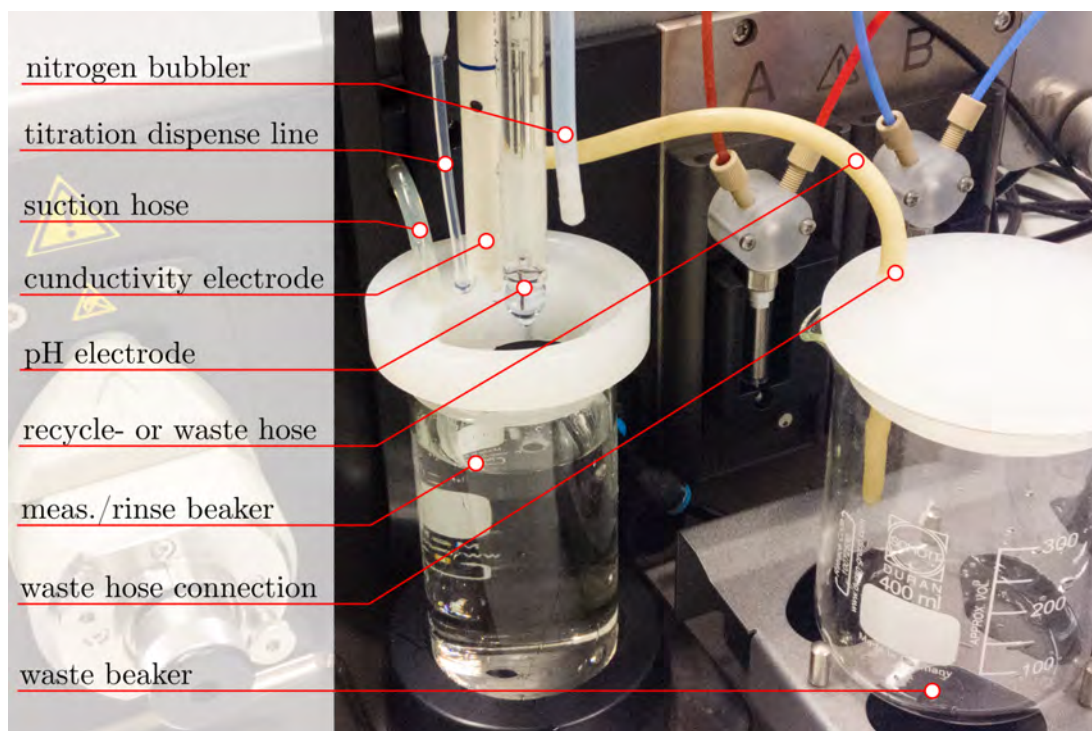


Fig. 5.15: Measuring periphery showing electrodes and hoses. The waste hose is depicted in fluid disposal function.

55. click on "Fill the titration units" to discharge liquid
56. clean and empty the system using the rinse cell
57. remove the rinse cell when done
58. shut the  $N_2$  switch
59. switch of the device
60. close the software
61. done

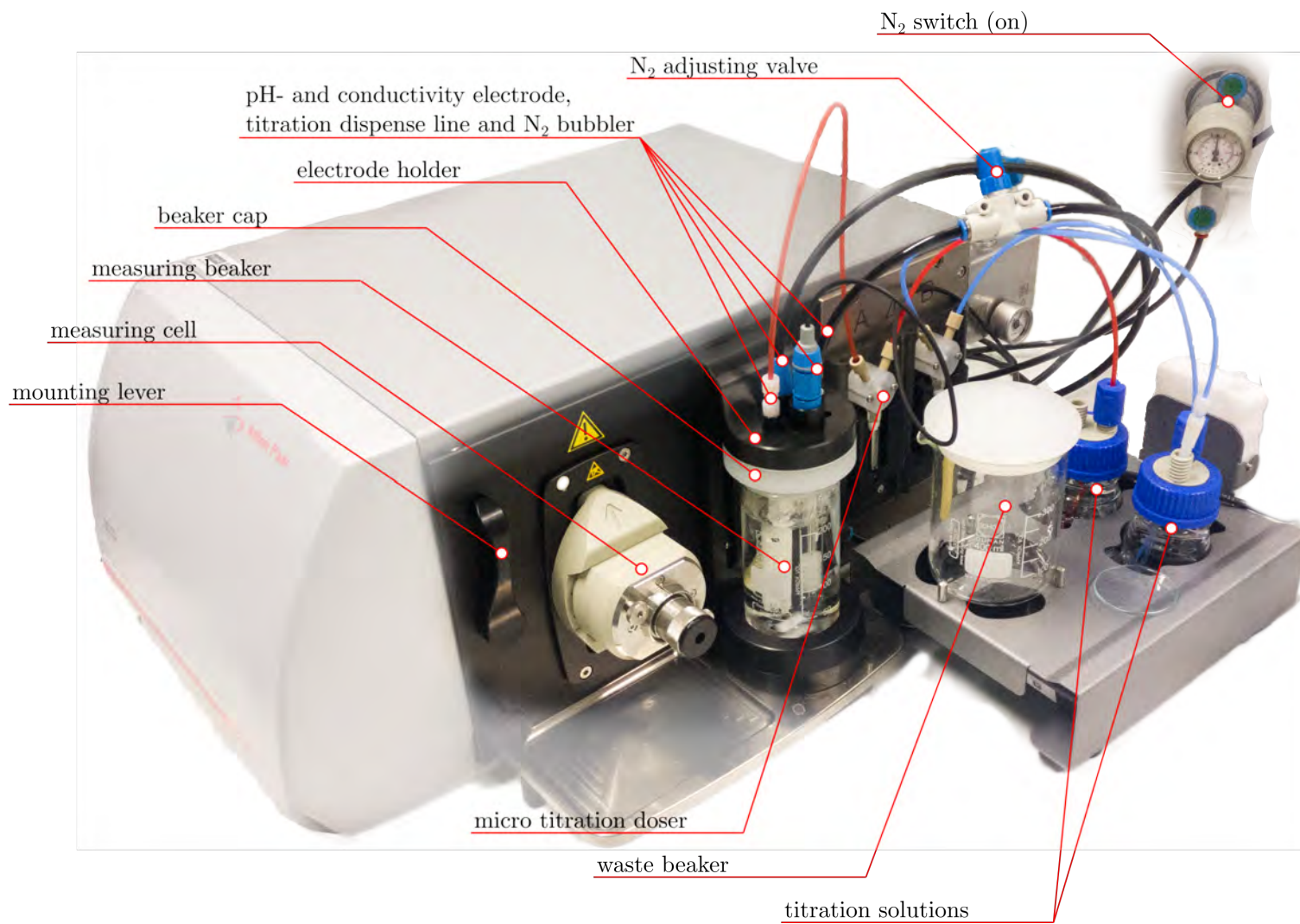


Fig. 5.16: SurPASS™ 3.

## 5.4 Data and Tables

### 5.4.1 Drying Agents

Drying Agent	Suitable for Drying	NOT Suitable for Drying	Residual Water mg H <sub>2</sub> O/L Dried Air	g H <sub>2</sub> O/g Desiccant	Regeneration	Reaction Mechanism
Aluminum Oxide	Hydrocarbons, air, ammonia, argon, helium, nitrogen, oxygen, Freon, H <sub>2</sub> O, CO <sub>2</sub> , SO <sub>2</sub>		0.003	0.2	175°C	Chemisorption Adsorption
ANHYDRONE® (Magnesium Perchlorate anhydrous)	Inert gas, air	Most Organics (May form explosive compound when exposed to organic vapors.)	0.001	0.2	250°C with Vacuum	Hydration
Barium Oxide	Organic bases, alcohols, aldehydes, amines	Acidic Compounds, CO <sub>2</sub>	0.00065	0.1	Not Recommended	Absorption and Adsorption
Boric Anhydride	Formic Acid			0.8	450°C	
Calcium Chloride (<20 Mesh)	Alkyl and Aryl Halides, most esters, saturated and aromatic hydrocarbons, ethers	Alcohols, amines, phenols, aldehydes, amides, amino acids, some esters, ketones	0.14-0.25	0.2 (1H <sub>2</sub> O)	250°C	Hydration
				0.3 (2H <sub>2</sub> O)		
Calcium Oxide	Alcohols, amines and ammonia gas	Acidic compounds, esters	0.007	0.3	1000°C	Chemisorption
Calcium Sulfate	Most organic compounds		0.005	0.066	235°C	Absorption
Cupric Sulfate	Esters, alcohols (excellent for benzene and toluene)		01. Apr	0.6	200°C	
Lithium Aluminum Hydride	Aldehydes, ketones, esters, carboxylic acids, peroxides, acid anhydrides, acid chlorides, ethers	Acid and its derivatives, aromatic nitro compounds				
Magnesium Oxide	Hydrocarbons, aldehydes, alcohols, basic gases, amines	Acidic compounds	0.008	0.5	800°C	Hydration
Magnesium Sulfate	Most compounds, incl. Acids, ketones, aldehydes, esters, nitriles	Acid sensitive compounds	1.0	0.2 - 0.8	200°C and red heat	Hydration
Molecular Sieve Activated Type 3A	Molecules of diameter >3 angstroms	Molecules of diameter <3 angstroms		0.18	117-260°C	Adsorption
Molecular Sieve Activated Type 4A	Molecules of diameter >4 angstroms	Molecules of diameter <4 angstroms, Ethanol, H <sub>2</sub> S, CO <sub>2</sub> , SO <sub>2</sub> , C <sub>2</sub> H <sub>4</sub> , C <sub>3</sub> H <sub>4</sub> , and strong acids	0.001	0.18	250°C	Adsorption
Molecular Sieve Activated Type 5A	Molecules of diameter > 5 angstroms, e.g., branched chain compounds and those having 4 carbon or larger rings	Molecules of diameter <5 angstroms, e.g., butanol, n-C <sub>4</sub> H <sub>10</sub> to n-C <sub>22</sub> H <sub>48</sub>	0.003	0.18	250°C	Adsorption
Phosphoric Acid			0.003		Not recommended	Absorption and Solution
Phosphorous Pentoxide	Saturated hydrocarbons, aromatic hydrocarbons, ethers, alkyl halides, aryl halides, nitriles, anhydrides, nitrites, esters	Alcohols, acids, amines, ketones, HF and HCl vapors	3x10 <sup>-8</sup>	0.5	No	Chemisorption leading to H <sub>3</sub> PO <sub>4</sub>
Potassium Carbonate	Alcohols, nitriles, ketones, esters, amines	Acids, phenols		0.2	300° C	Hydrate Formation
Potassium Hydroxide	Amines, organic bases	Acids, phenols, esters, amides, acidic gases, aldehydes	0.3	Indeterminate	No	Hydration and Solution Formation
Silica Gel 6-16 Mesh	Most organics	HF vapors	0.03	0.2	200-350°C	Adsorption
Sodium	Saturated and aromatic hydrocarbons, ethers	Acids, alcohols, aldehydes, ketones, amines, esters, organic halides, and any substance with high water content			Not Recommended	Leads to  NaOH + H <sub>2</sub>
Sodium Hydroxide Pellets	Amines	Acids, phenols, esters, amides	0.16	Indefinite	Not Recommended	Absorption and Solution Formation
Sodium Sulfate Anhydrous	Alkyl halides, aryl halides, aldehydes, ketones, acids		12	01. Feb	150°C	Hydration
Sulfuric Acid	Inert gases, HCl, Cl <sub>2</sub> , CO, SO <sub>2</sub> , air used in desiccators	Too reactive to actually contact organic materials	0.003	Indefinite	No	Hydration
Zinc Chloride	Hydrocarbons	Ammonia, amines, alcohol	0.9	0.2	110°C	Hydration

Fig. 5.17: List of drying agents including several properties.<sup>[15]</sup>



## 5.5 Pictures/Images

### 5.5.1 CAF

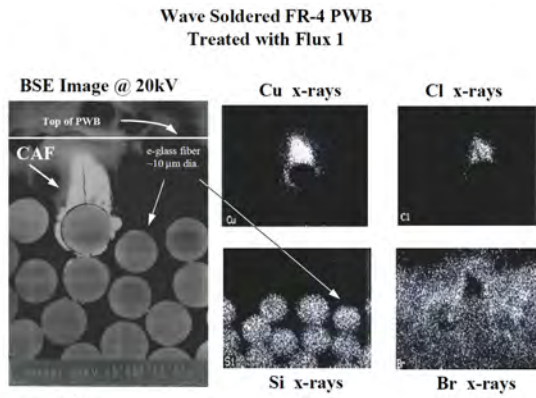


Figure 22.

CAF from left of Figure 21 is revealed in SEM micrograph (above left) as traveling along the separated fiber / epoxy interface. EDS elemental map (above right) of CAF show that it is copper and chlorine containing.

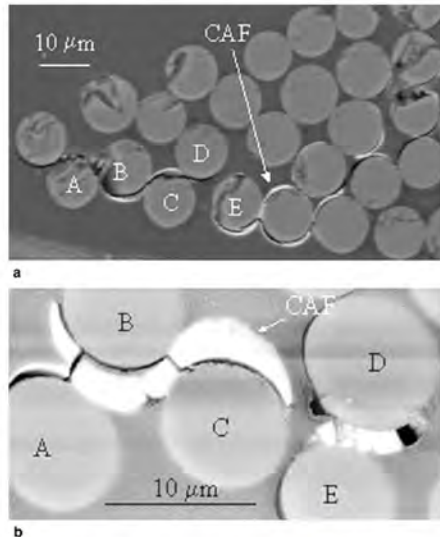


Fig. 9. SEM image of two sequential cross sections of CAF on control PWB. (a) approximately 100  $\mu\text{m}$  from the anodic PTH. (b) approximately 50  $\mu\text{m}$  from the anodic PTH. The individual E-glass fibers are labeled to aid in visualization.

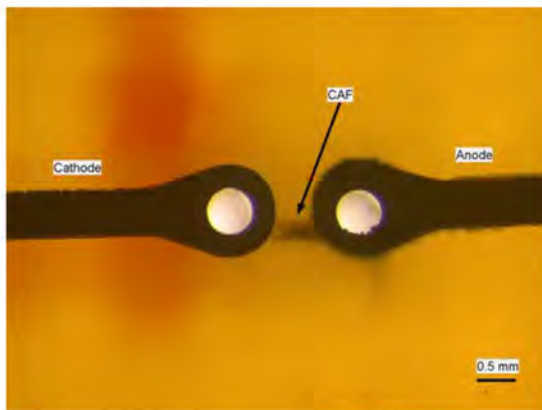


Fig. 4. Typical backlighting image illustrating CAF.

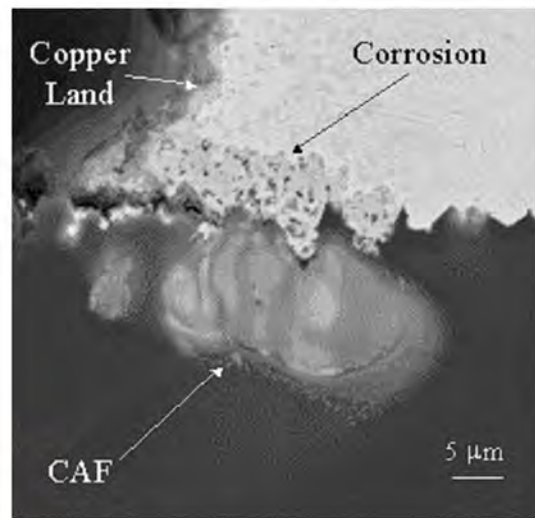
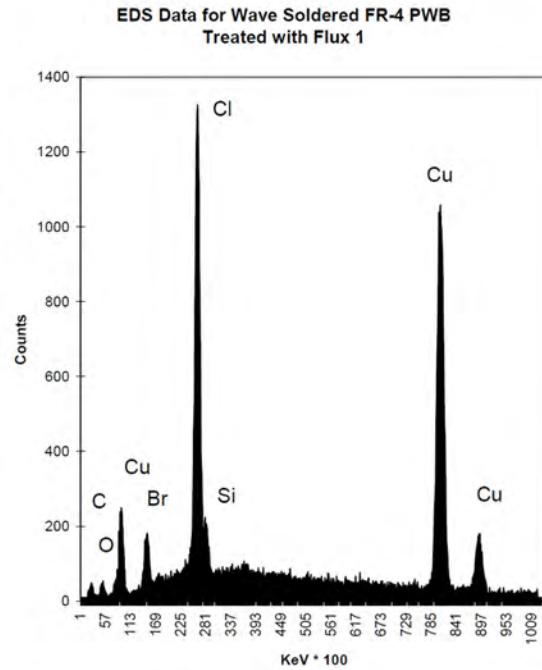


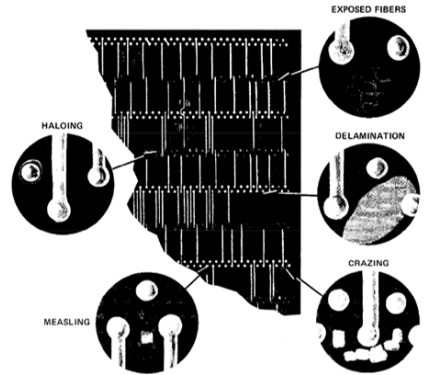
Fig. 13. SEM image (top) and EDS elemental map (bottom) of CAF initiation point at PTH on PWB processed with PG3-4. The portion labeled copper land is actually the PTH "Nailhead" on PWB surface.

Fig. 5.18: Selected images of CAF, abstracted from literature<sup>[10, 32, 33]</sup>.

### Identification of Measles and Other Surface Defects

Studies have proven that it is difficult to identify measled boards. This is true because, as you can see in the illustration below, in a given printed circuit board you may find measles as well as indications of other surface conditions.

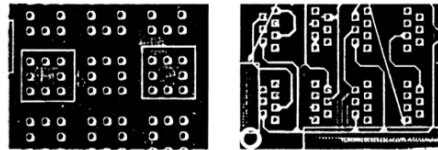
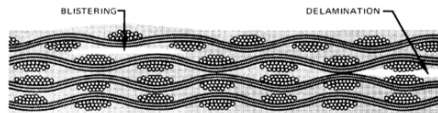
We invite you to carefully study the illustration below, as well as to study the drawings and photographs that appear on the next five pages.



### Identification of BLISTERING

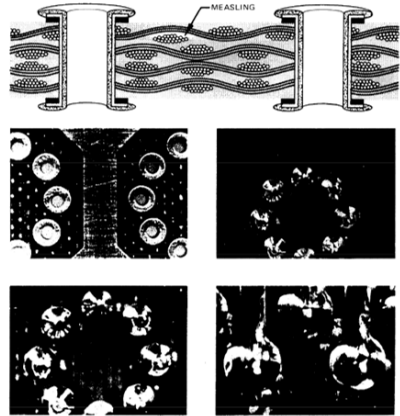
**BLISTERING** - A localized swelling and separation between any of the layers of the base laminate and/or between the laminate and the metal cladding.

**DELAMINATION** - A separation between any of the layers of the base laminate and/or between the laminate and the metal cladding.



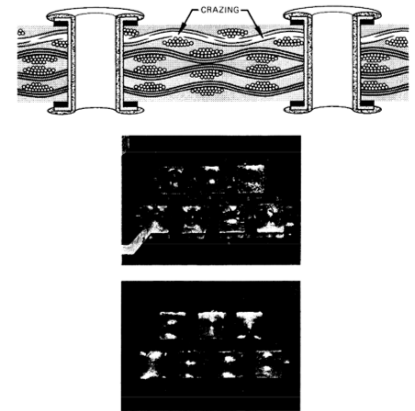
### Identification of MEASLES

**MEASLING** - A condition existing in the base laminate in the form of discrete white spots or "crosses" below the surface of the base laminate, reflecting a separation of fibers in the glass cloth at the weave intersection.



### Identification of CRAZING

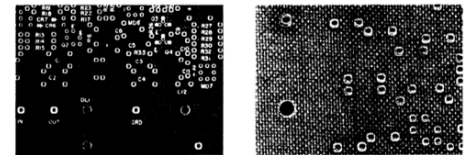
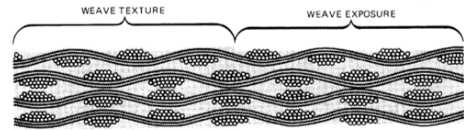
**CRAZING** - A condition existing in the base laminate in the form of connected white spots or "crosses" on or below the surface of the base laminate, reflecting the separation of fibers in the glass cloth and connecting weave intersections.



### Identification of WEAVE TEXTURE AND WEAVE EXPOSURE

**WEAVE TEXTURE** - A surface condition in which the unbroken fibres are completely covered with resin but yet exhibits the definite weave pattern of the glass cloth.

**WEAVE EXPOSURE** - A surface condition in which the unbroken woven glass cloth is not uniformly covered by resin.



### Identification of HALOING

**HALOING** - A condition existing in the base laminate in the form of a light area around holes and/or other machined areas on or below the surface of the base laminate.

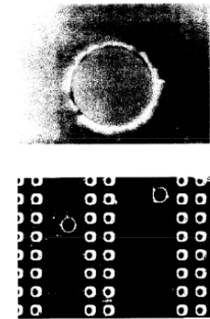


Fig. 5.19: Failures associated with the epoxy/glass interface.<sup>[16]</sup>



### 5.5.2 Diffusion Cell



Fig. 5.20: Selected pictures of the diffusion cells.

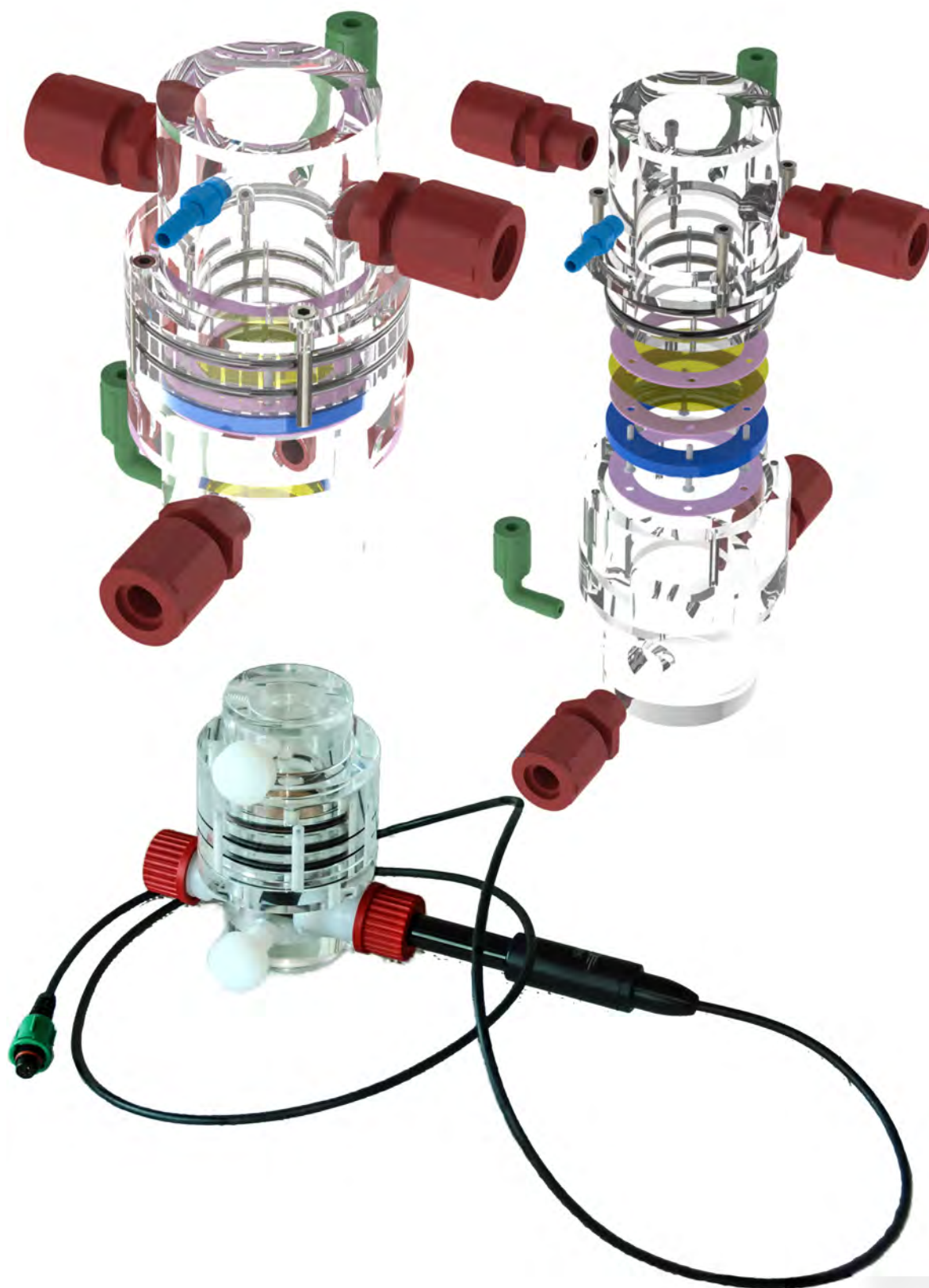
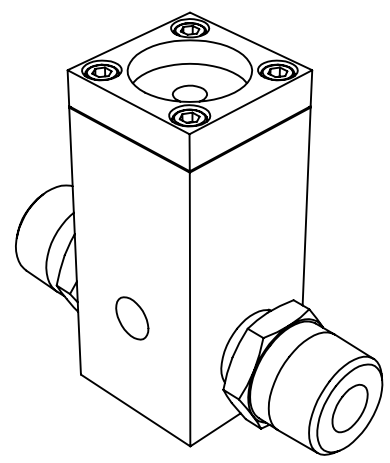
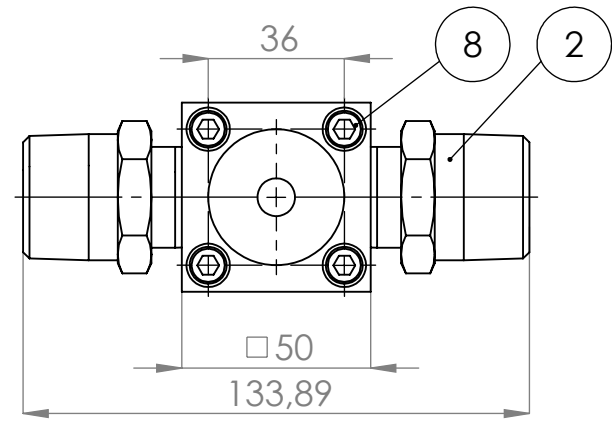
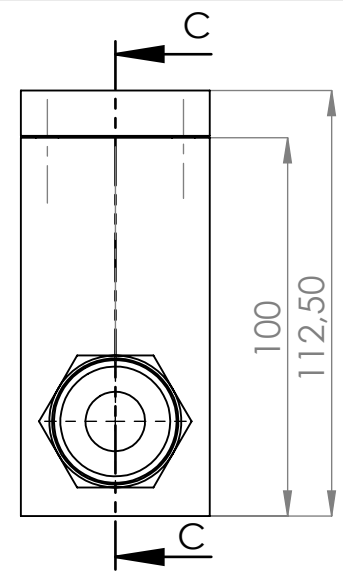
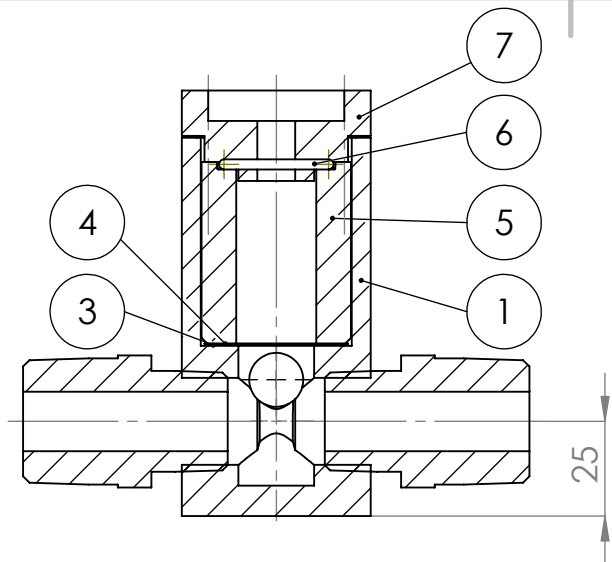


Fig. 5.21: Images of the diffusion cell.

## 5.6 Engineering Drawings



POS-NR.	BENENNUNG	NORM	MENGE
1	Gehaeuse		1
2	SS_16_HRN_12_21120		2
3	Flachdichtung		1
4	Epoxid_Folie		1
5	Analytzelle		1
6	O-Ring	DIN 3771	1
7	Verschlussdeckel		1
8	wasi_edelstahl_a2_din_912_m6x20	DIN 912 M6x20	4

WENN NICHT ANDERS DEFINIERT:  
 BEMASSUNGEN SIND IN MILLIMETER  
 OBERFLÄCHENBESCHAFFENHEIT:  
 TOLERANZEN:  
 LINEAR:  
 WINKEL:

OBERFLÄCHENGÜTE:  
 ENTGRATEN  
 UND SCHARFE  
 KANTEN  
 BRECHEN

ZEICHNUNG NICHT SKALIEREN

ÄNDERUNG

NAME	SIGNATUR	DATUM
GEZEICHNET Lauterbach		
GEPRÜFT		
GENEHMIGT		
PRODUKTION		
QUALITÄT		

BENENNUNG:  
**IR-Diffusionszelle**

ZEICHNUNGSNR.  
**IR-Diffusionszelle**

MASSSTAB:1:2

BLATT 1 VON 1

4 3 2 1

F

F

E

E

D

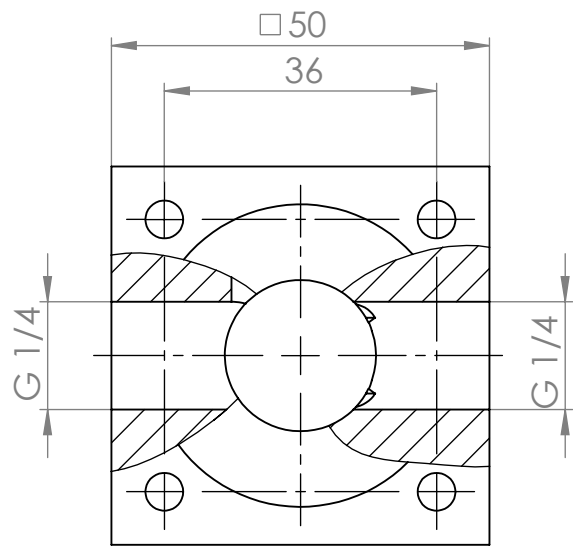
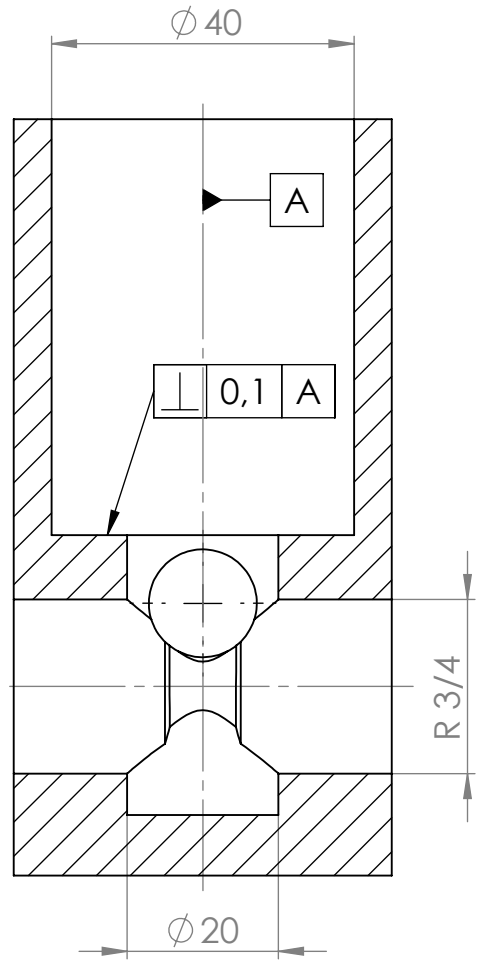
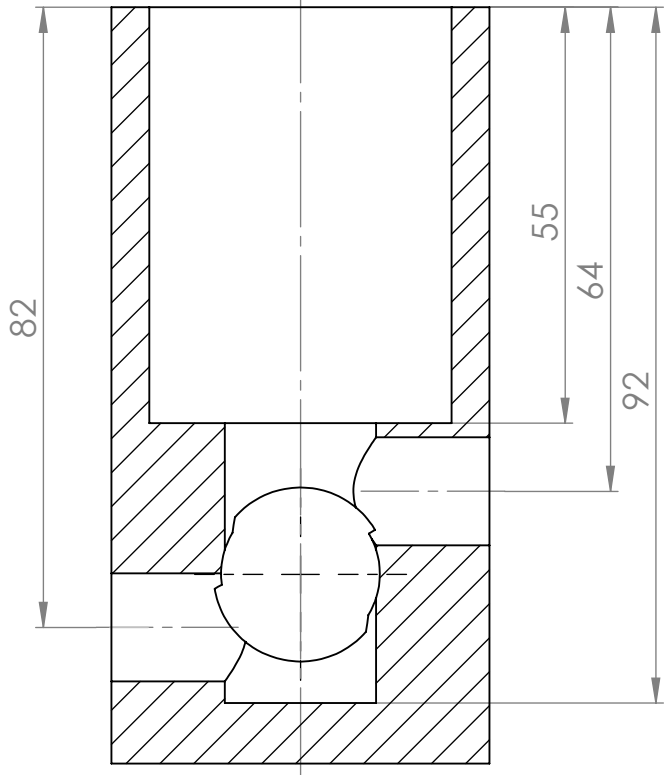
D

C

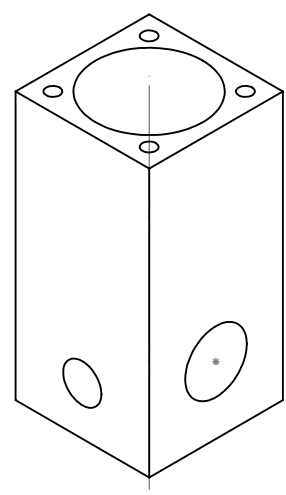
C

B

B



Ra 3,2



WENN NICHT ANDERS DEFINIERT:  
BEMASSUNGEN SIND IN MILLIMETER  
OBERFLÄCHENBESCHAFFENHEIT:  
TOLERANZEN:  
LINEAR:  
WINKEL:

OBERFLÄCHENGÜTE:  
ENTGRATEN  
UND SCHARFE  
KANTEN  
BRECHEN

ZEICHNUNG NICHT SKALIEREN

ÄNDERUNG

NAME	SIGNATUR	DATUM	WERKSTOFF:
GEZEICHNET			
GEPRÜFT			
GENEHMIGT			
PRODUKTION			
QUALITÄT			

BENENNUNG:  
ZEICHNUNGSNR.  
**Gehaeuse**  
A4  
MASSSTAB: 1:1  
BLATT 1 VON 1

4 3 2 1

4

3

2

1

F

F

E

E

D

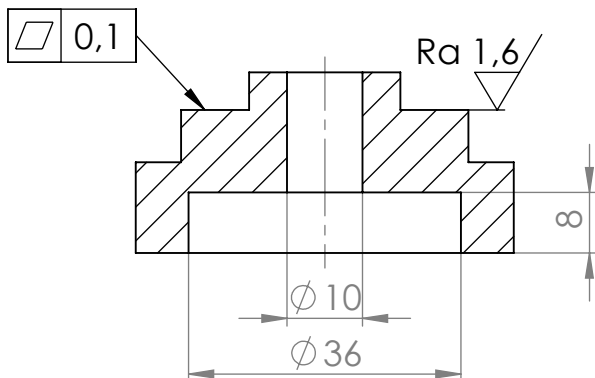
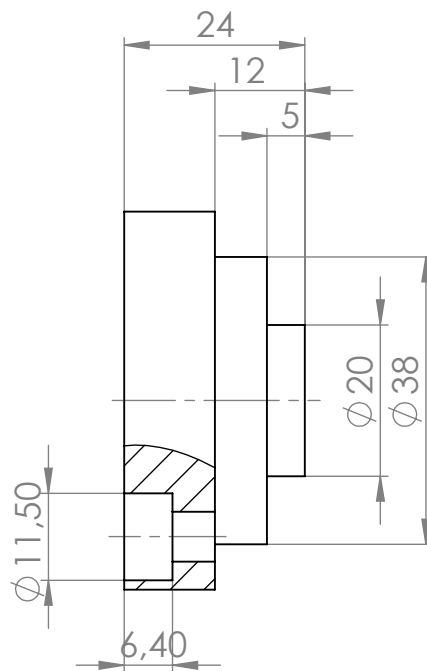
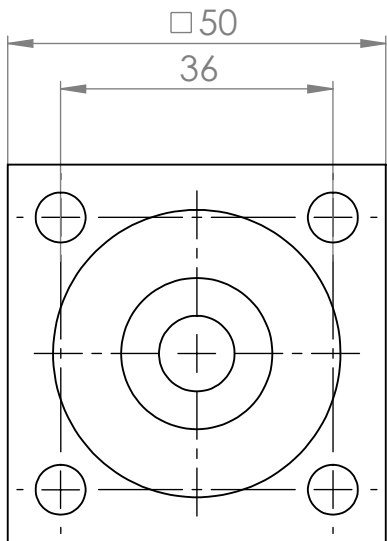
D

C

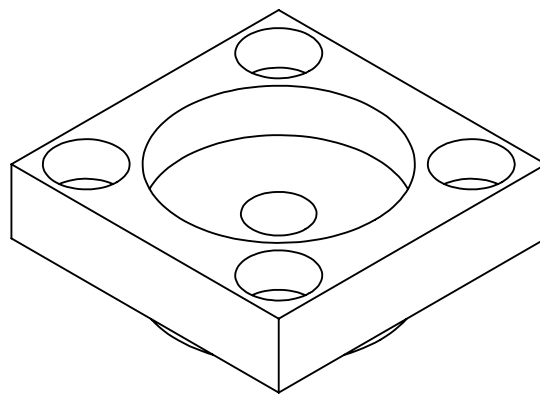
C

B

B



Ra 3,6



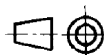
WENN NICHT ANDERS DEFINIERT:  
BEMASSUNGEN SIND IN MILLIMETER  
OBERFLÄCHENBESCHAFFENHEIT:  
TOLERANZEN:  
LINEAR:  
WINKEL:

OBERFLÄCHENGÜTE:

ENTGRATEN  
UND SCHARFE  
KANTEN  
BRECHEN

ZEICHNUNG NICHT SKALIEREN

ÄNDERUNG



	NAME	SIGNATUR	DATUM	
GEZEICHNET				
GEPRÜFT				
GENEHMIGT				
PRODUKTION				
QUALITÄT				
				WERKSTOFF:
				GEWICHT:

BENENNUNG:

ZEICHNUNGSNR.

Deckel01

A4

MASSSTAB:1:1

BLATT 1 VON 1

4

3

2

1

A

A

# Bibliography

- [1] W Ashcroft. “Curing Agents For Epoxy Resins”. In: *Three Bond Technical News* 32 (1990).
- [2] Donald R. Askeland. *The Science and Engineering of Materials*. 6th ed. Global Engineering, 2010.
- [3] P Atkins. *Physical Chemistry*. 9th ed. W. H. Freeman, 2010.
- [4] Robert Balma, Kevin Petsch, and Tolga Kaya. “Development of Thin Film Photolithography Process: Patterning Printed Circuit Boards (PCBs) and Copper Electroplating”. In: *ASEE NC & IL/IN Section Conference* (2011), pp. 1–9.
- [5] H J Bartsch. *Taschenbuch Mathematischer Formeln für Ingenieur und Naturwissenschaftler*. 22nd ed. HANSER, 2011.
- [6] K Beuth. *Bauelemente - Elektronik 2*. 19th ed. Vogel Buchverlag, 2010.
- [7] Mira R Bisengalieva et al. “The molar heat capacity of hydrous copper chloride : atacamite  $\text{Cu}_2\text{Cl}(\text{OH})_3$ ”. In: (1997), pp. 345–352.
- [8] J Brous. “Water Soluble Flux and its Effect on PC Board Insulation Resistance.” In: *Electronic Packaging and Production*, 21.7 (1981).
- [9] W D Callister. *Materials Science and Engineering - An Introduction*. 7th ed. Wiley VCH, 2007.
- [10] Antonio Caputo. “Conductive Anodic Filament ( CAF )”. In: (2010).
- [11] Edward K.L. Chan and Matthew M.F. Yuen. “Study of interfacial moisture diffusion at epoxy/Cu interface”. In: *Journal of Adhesion Science and Technology* 23.9 (2009), pp. 1253–1269.
- [12] S Cholake. “Quantitative Analysis of Curing Mechanisms of Epoxy Resin by mid-and near-fourier transform infra red spectroscopy”. In: *Defence Science Journal* 64.3 (2014).
- [13] Espec Corp. *Ionic Migration on Printed-Circuit Boards*.
- [14] Ss Dutta. “Water absorption and dielectric properties of Epoxy insulation”. PhD thesis. 2008, pp. 1–51.

- [15] Erowid.org. *Drying Agent Selection Guide*.
- [16] R Facey. *Measles in Printed Wiring Boards*. Tech. rep. Institute of Printed Circuits, 1973.
- [17] X J Fan. *Moisture Sensitivity of Plastic Packages of IC Devices*. Springer, 2010.
- [18] M P Groover. *Fundamentals of Modern Manufacturing - Materials, Processes, and Systems*. 5th ed. Wiley VCH, 2013.
- [19] W M Haynes. *CRC Handbook of Chemistry and Physics*. 96th ed. 2016.
- [20] Jenny A. Jachim, Garth B. Freeman, and Laura J. Turbini. “Use of surface insulation resistance and contact angle measurements to characterize the interactions of three water soluble fluxes with FR-4 substrates”. In: *IEEE Transactions on Components Packaging and Manufacturing Technology Part B* 20.4 (1997), pp. 443–450.
- [21] David Jennings and Michael Pecht. “Assessing Time-To-Failure Due To Conductive Filament Formation In Multilayer Organic Laminates”. In: *IEEE Transactions on Components Packaging and Manufacturing Technology Part B* 17.3 (1994), pp. 269–276.
- [22] R S Khandpur. *Printed Circuit Boards - Design, Fabrication, and Assembly*. 1st ed. McGraw-Hill, 2006.
- [23] M Kochsiek. *Handbuch des Wägens*. 2nd ed. Springer Fachmedien Wiesbaden GmbH, 1989.
- [24] D. J. Lando, J. P. Mitchell, and T. L. Welsher. “Conductive Anodic Filaments in Reinforced Polymeric Dielectrics: Formation and Prevention”. In: *17th International Reliability Physics Symposium* (1979), pp. 51–63.
- [25] Liang Li et al. “Water transportation in epoxy resin”. In: *Chemistry of Materials* 17.4 (2005), pp. 839–845.
- [26] T Luxbacher. *The Zeta Guide*. 1st ed. ANTON PAAR GmbH, 2014.
- [27] G Milazzo. *Elektrochemie I - Grundlagen und Anwendungen*. Springer Basel AG, 1980.
- [28] L. E. Morón et al. “Electrodeposition and corrosion behavior of Zn coatings formed using as brighteners arene additives of different structure”. In: *Surface and Coatings Technology* 205.21-22 (2011), pp. 4985–4992.
- [29] P Neogi. *Diffusion in Polymers*. Marcel Dekker, Inc.
- [30] M Pourbaix. *Corrosion and Metal Artifacts - A Dialogue Between Conservators and Archaeologists and Corrosion Scientists*. 1977.



- [31] Rapra. “Polymers in Electronics 2007”. In: ().
- [32] W J Ready. “Factors Which Enhance Conductive Anodic Filament (CAF) Formation”. PhD thesis. 1997.
- [33] W J Ready and L J Turbini. “The effect of flux chemistry, applied voltage, conductor spacing, and temperature on conductive anodic filament formation”. In: *Journal of electronic materials* 31.11 (2002), pp. 1208–1224.
- [34] P Reid. “Dielectric Material Damage vs. Conductive Anodic Filament Formation”. In: *SMTA Proceedings* ().
- [35] H Römpp. *Chemie Lexikon*. 6th ed. Franckh’sche Verlagshandlung Stuttgart, 1966.
- [36] R Sanapala. “Characterisation of FR-4 printed circuit boards laminates before and after exposure to lead-free soldering conditions”. In: *Faculty of the Graduate School of the University of Maryland, College Park* 1 (2008).
- [37] Bob Sandor. *A Brief History of Analytical Balances*. 2011.
- [38] P Schuller. *Schätzen - Vergleichen - Wiegen*. GRIN Verlag, 2011.
- [39] J F Shackelford. *Introduction to Materials Science for Engineers*. 8th ed. Pearson, 2015.
- [40] Ken M Takahashi. “Conduction Paths and Mechanisms in FR-4 Epoxy/Glass Composite Printed Wiring Boards”. In: *Journal of The Electrochemical Society* 138.6 (1991), pp. 1587–1593.
- [41] Lj Turbini and Wj Ready. “Conductive anodic filament failure: a materials perspective”. In: ... *Conference on Advanced Materials and ...* (1998).
- [42] X Wang. “Synthesis, characterization, and cure properties of phosphorus-containing epoxy resins for flame retardance”. In: *European Polymer Journal* 40.2 (2004).
- [43] T. L. Welsher, J. P. Mitchell, and D. J. Lando. “CAF in Composite Printed-Circuit Substrates: Characterization, Modeling and a Resistant Material”. In: *18th International Reliability Physics Symposium* (1980), pp. 235–237.

# Figures

Fig.1.1	Properties of polymers used for package encapsulation. <sup>[9]</sup> . . . . .	4
Fig.1.2	The scheme of a beam balance showing the levers bearing their masses, being in equilibrium around the pivot. . . . .	10
Fig.1.3	A model of the electrochemical double layer showing the solid-liquid interface and the corresponding potentials. . . . .	11
Fig.1.4	Visualization of hypothetical slopes for acidic (IEP @ pH 2), inert (IEP @ pH 4), amphoteric (IEP @ pH 7) and basic (IEP @ pH 9) surface behaviors. . . . .	13
Fig.1.5	Constructional details of double-sided boards with plated through-hole connection (PTH) and without plated through-hole connection (non-PTH). . . . .	17
Fig.1.6	Multi-layer board (MLB) lamination process lay-up. . . . .	18
Fig.1.7	Major steps in the fabrication of a single-sided PCB. . . . .	19
Fig.1.8	Basic steps of photolithography. <sup>[4]</sup> . . . . .	20
Fig.1.9	ECM acceleration conditions and mechanisms, (a) dendritic growth, (b) CAF formation. <sup>[13]</sup> . . . . .	22
Fig.1.10	Simplified Pourbaix diagram for the system copper. <sup>[41]</sup> . . . . .	24
Fig.1.11	A cross section of an ideal printed circuit board containing two PTHs. The illustration assumes infinite resistance at applied voltage as well as a perfectly interconnected epoxy/glass composite without any defects. The conductor assembly exhibits a hole-to-hole configuration what is considered to be worst for CAF formation. 26	
Fig.1.12	This illustration is referred to a more realistic case, visualizing cracks, blisters, measles and absorbed molecules like water and oxygen. Due to soldering and drilling steps during the fabrication of the, delamination and substrate-to-PTH void interstitials have been developed. "Non-biased" this dielectric device assumes a resistance of 100 MΩ. The internal environment's acidity is neutral being at a pH value around 7. Additionally, a surface condensed water film is shown. . . . .	27

---

Fig.1.13	By exposing the PCB to a bias of 100 V, a voltage gradient arises. After a certain period of time, the hydrolysis created an pH drop at the anode forcing the Cu corrosion products to become soluble. These ions, positively charged then try to travel through weak channels, attracted by the negatively polarized cathode. At a pH of approx. 5, the ions get more and more insoluble and full precipitation occurs at a pH of around 8.6. The glass fibers are mostly treated with basic surface functional groups to stabilize the epoxy/glass interface, so that Cu ions preferrably deposit on the fiber's surface. While the anode deplets in copper, the cathode try to accumulate and reduce available copper. The pH gradient between the electrodes now looks like a polynomial of third order.	28
Fig.1.14	Within progression of time, the filament grows further and further, emanating from the anode to the cathode. The filament itself provide locations for hydrolysis to occur. The higher gradient in pH deplets the anode steadily. Voltage and Resistance are decreased as a result of filament growth and the conductive salt solution. . .	29
Fig.1.15	The filament has critically grown in length, the channel got saturated by conductive ions and salts. Resistance and voltage are distinguishable from the priorly measured stats. After exceeding a threshold, a short is created between the electrodes as a consequence of CAF. The PCB is irreversibly damaged. . . . .	30
Fig.1.16	Process of conductive anodic filament formation in detail, showing resistivity and pH gradient. Further indicated is the ion-saturation of the aqueous solution. . . . .	32
Fig.1.17	Schematic representation of CAF pathways (dimensions exaggerated for clarity): (a) PTH to PTH, (b) PTH to track, (c) track to PTH, and (d) track to track. . . . .	34
Fig.1.18	OTR measurements on both, uncoated R1566WN and RN1570. .	40
Fig.1.19	PCB coupons, engineering concept and real platine superposed by NaCl. . . . .	41
Fig.1.20	Measurement setup showing the humidity chamber. . . . .	42
Fig.1.21	Overview of impedancy measurements on S4-K3 containing surface-side NaCl. . . . .	43
Fig.1.22	Diagrams visualizing the indicated measurement routine. . . . .	44
Fig.1.23	Diagrams visualizing the impact of 85 °C / 85 % RH on the impedancy and the phase angle at 5 V . . . . .	44

---

---

Fig.1.24	Diagrams visualizing the impact of 85 °C / 85 % RH on the impedancy and the phase angle at 0.5 V . . . . .	45
Fig.1.25	Sensitivity analysis (simulation) of the electric field dependend on the local roughness. . . . .	46
Fig.2.1	Visualisation of the diffusion cell for (a) light sensitive tracing methods; (b) standard intention using transparent PMMA. . . . .	50
Fig.2.2	An explosion drawing of a fully assembled diffusion cell, showing exterior and interior. . . . .	51
Fig.2.3	Visualisation of the planned "IR-Diffusion Cell" in assembled state and dismantled. . . . .	52
Fig.2.4	Explosion drawing of the "IR-Diffusion Cell" excluding front-end caps and rinse valves. . . . .	53
Fig.2.5	"Rapid Analysis Cells" as predecessors for gravimetrical reference analysis. Dialysis tubes are clamped in into PP vials to build a barrier for the determination of diffusion to occur. The bottle is an empty storage vessel for metallic lithium, filled with drying agent. . . . .	54
Fig.2.6	P <sub>4</sub> O <sub>10</sub> after absorption of water shows a polyphosphorous liquid containing black residues. . . . .	57
Fig.2.7	Explosion illustration of the diffusion cell containing a drying agent filled "Gravibox". A picture including part-labels is found on p. 131 in section "5.3.1". . . . .	58
Fig.2.8	Diffusion cell, utilized with a conductivity electrode to detect ions passed trough the membrane. . . . .	59
Fig.2.9	R1570 and R1566, preconditioned in industrial- and standard chemicals for ζ-potential analysis. . . . .	62
Fig.2.10	Coloring of H <sub>2</sub> SO <sub>4</sub> in presence of R1570 (dark red) and R1566 (light red). Both GREC membranes develop a reddish surface when getting immersed into concentrated sulphuric acid. . . . .	63
Fig.2.11	Solutions (KCl 1 mM, HCl 50 mM, Milli-Q) to be prepared for rinsing and measuring on the SurPASS™ 3. . . . .	64
Fig.3.1	Final permeability values including average of the means and row standard deviations. . . . .	68
Fig.3.2	Final permeability values including average of R1566 (left) versus R1570 (right). . . . .	69
Fig.3.3	All the measurement series showing max. raw data evaluated above and blank-corrected values below. . . . .	70

---

---

Fig.3.4	Visualisation of an adsorption test keeping one drying agent (Cell 0 and Cell 1) for the whole process of data acquisition and recharging new desiccant, vice versa (Cell 3 and Cell 4). . . . .	76
Fig.3.5	This is an illustration of an fictional measurement series to provide an idea of the abbreviation approach. . . . .	78
Fig.3.6	Measurement series 01 - First attempt collecting information about $P_4O_{10}$ as a desiccant. Cell 0 was locked until the end of the experiment, while cell 1 acted as a gaseous blank to check aggressivity of the drying agent. . . . .	79
Fig.3.7	Measurement series 02 - Deploying $MgSO_4$ as a drying agent shows strong deviations in adsorption rates. This is due to the weak affinity to water in gaseous phases. Hence the mass arguments are out of the available devices's LOD. . . . .	81
Fig.3.8	Measurement series 03 - Visualization of the data points within the first 96 h of measurement. The molecular sieve exhibits acceptable values within an applicable time of investigation. . . . .	82
Fig.3.9	Measurement series 03 - Visualization of the data points within the complete time of measurement. The molecular sieve exhibits acceptable values within an applicable time of investigation. . . .	83
Fig.3.10	Measurement series 04 - Strong spread of values. The green line shows the "internal standard", which is compared to former diffusion barriers. The adsorption rate behaves as expected being lower as verified before. . . . .	84
Fig.3.11	Measurement series 05 - The first three cells includes PE-foam sealings at the closed-end of contacting faces. Cell 3 has tremendously increased data points, which nullifies the experiment in its intention. . . . .	85
Fig.3.12	Measurement series 06 - Being the contrary measurement series to series 5 (Fig. 3.11), cell 3 and cell 4 should state lower adsorption rates by being supported by the PE-foam closed-end sealing. Cell 3 is still critically increased, which either makes the experiment futile. . . . .	86
Fig.3.13	Measurement series 07 - Inserting closed-end sealings draw expectations to lower permeability rates. Unfortunately this does not hold, another issue must corrupt the measurements. . . . .	87

---

---

Fig.3.14	Measurement series 08 - An exchange of the clamp flange screws should provide a distinct force to the mounting unit. Additionally the force can be enhanced without forcing cracking due thermal expansion issues. . . . .	88
Fig.3.15	Measurement series 09 - This series should show differences of untreated material and pre-dried membranes. Due to No significant declarations can be stated though. The yellow points reveal a damaged membrane. . . . .	89
Fig.3.16	Measurement series 10 - Blank value evaluation for the calculation of the absolute diffusion rates of the GREC membranes. The average value including it's SD will be substracted from each's final phase series mean value. . . . .	90
Fig.3.17	Buffer solutions for pH-dependent investigation on GREC membrane permeability. . . . .	92
Fig.3.18	Measurement series 11 - First attempt to seriously ascertain significant permeability rates. . . . .	93
Fig.3.19	Measurement series 12 - Second experiment similar to the priorly showed measurement series, including R1566 as an analyte instead. . . . .	94
Fig.3.20	Measurement series 13 - Exchange of the diffusive species for the first time using a potassium hydrogen phthalate buffer with pH 4.01. . . . .	95
Fig.3.21	Measurement series 14 - Analyte specific pendant to the pH-acidic R1570 measurement series. . . . .	96
Fig.3.22	Measurement series 15 - Adding a pH 9.00 buffer to the upper cell to get an idea of the influence to the R1570 membrane. . . . .	97
Fig.3.23	Measurement series 16 - Visualization of the data points of R1566 exposed to a mixture of boric acid, sodium hydroxide and potassium chloride (pH 9.00 buffer). . . . .	98
Fig.3.24	Measurement series 17 - Illustration of the reference material (PET), used in solar panel fabrication. . . . .	99
Fig.3.25	Visualization of the adsorption rates measured via rapid cells at RT. . . . .	100
Fig.3.26	Zeta-potential analysis of the untreated laminates. . . . .	102
Fig.3.27	Zeta-potential analysis of the chemCu treated laminates. . . . .	103
Fig.3.28	Zeta-potential analysis of the galvCu treated laminates. . . . .	104
Fig.3.29	Zeta-potential analysis of the CuCl <sub>2</sub> treated laminates. . . . .	105
Fig.3.30	Zeta-potential analysis of the H <sub>2</sub> O <sub>2</sub> treated laminates. . . . .	106
Fig.3.31	Zeta-potential analysis of the H <sub>2</sub> SO <sub>4</sub> treated laminates. . . . .	107
Fig.3.32	Zeta-potential analysis of the NaOH treated laminates. . . . .	108

---

---

Fig.3.33	IR spectrum of the GREC R1566. . . . .	109
Fig.3.34	IR spectrum of the GREC R1570. . . . .	110
Fig.3.35	Typical functional groups present in the epoxy laminate systems. <sup>[36]</sup>	111
Fig.3.36	IR spectra of R1566 laminate treated with industrial chemicals. . .	112
Fig.3.37	IR spectra of R1570 laminate treated in industrial chemicals. . . .	113
Fig.3.38	IR spectra of R1566 laminate treated with standard chemicals. . .	114
Fig.3.39	IR spectra of R1570 laminate treated with standard chemicals. . .	115
Fig.3.40	Typical constituents of FR-4 laminates. . . . .	116
Fig.3.41	Diglycidyl ether bisphenol A (DGEBA). . . . .	116
Fig.3.42	10-dihydro-9-oxa-10-phosphaphenanthrene-10-oxide (DHP-DOPO), tetrabromobisphenol A (TBBPA) and dicyanodiamide (DICY). . . . .	116
Fig.3.43	SEM image (P11) of a copper substrate, zinc-coated in a 1 M ZnCl <sub>2</sub> solution, containing 26 mg PEG and 45 mg TBAI. The time for deposition was 120 min at 0.7 V and 11 mA. The overall surface is appropriate with except of some preferably deposited volumes between the drillings. In a 1000x magnification, inhomogeneous depositions and polishing rills are observable. . . . .	117
Fig.3.44	SEM image (P12) of a copper substrate, zinc-coated in a 1 M ZnCl <sub>2</sub> solution, containing 20 mg PEG and 41 mg TBAI. The time for deposition was 120 min at 0.7 V and 11 mA. The overall surface is appropriate with partially very smooth areas. A closer look at a magnification of 1000x reveals clusters and polishing rills. . . . .	118
Fig.3.45	SEM image (P13) of a copper substrate, zinc-coated in a 1 M ZnCl <sub>2</sub> solution, containing 17 mg PEG and 36 mg TBAI. The time for deposition was 120 min at 0.7 V and 17 mA. The surface is pock-marked and denotes, that a lower amount of brightener is enforcing the roughness. At higher magnifications, again striations as a result of fabrication are observable. . . . .	119
Fig.3.46	SEM image (P14) of a copper substrate, zinc-coated in a 1 M ZnCl <sub>2</sub> solution, containing 21 mg PEG and 41 mg TBAI. Additionally, 7 ml dimethylketone (acetone) were added. The time for deposition was 119 min at 0.7 V and 16 mA. Despite the presence of a few clusters the surface exhibits superior smoothness. An mag. 100x reveals the zinc pustules sticking out the surface. . . . .	120
Fig.3.47	EDX spectra showing chemical composition and mass fractions at chosen locations. . . . .	121

---

---

Fig.3.48	Curves for the measurement of voltage and current. The top diagram illustrates the system Cu/Zn and the bottom diagram the system Au/Zn, respectively. . . . .	122
Fig.5.1	Gravibox, a vessel for drying agent, having a removable slitted cap to provide access to humidity to pass by. . . . .	127
Fig.5.2	A drying tower, providing the possibility to label and sort membranes of certain materials. In the lower part, different drying agents can be deployed. The removal of a membrane of interest is a process of ease by just unlocking and rotating the corresponding tray. . . . .	128
Fig.5.3	Deformed O-rings as a result of thermal treatment in a drying cabinet. . . . .	129
Fig.5.4	To mount or separate both cell halves, a lubricant simplifies the process. The finally chosen lubricant is visualized. . . . .	130
Fig.5.5	Flange (face-to-bottom) to mount gaskets and membranes layer by layer. . . . .	131
Fig.5.6	Half-section image of the diffusion cell showing fully assembled cells and the Gravibox encapsulating drying agent. . . . .	134
Fig.5.7	Calibration standards used in $\zeta$ -potential analysis. . . . .	135
Fig.5.8	Cleaning procedures within the SurPASS <sup>TM</sup> 3 software. . . . .	137
Fig.5.9	Adhesive tape to adhere sample membranes. . . . .	138
Fig.5.10	Sample brackets with adhered analyte material. . . . .	138
Fig.5.11	Measuring cell parts including GREC membranes, adhered on sample brackets in the corresponding sealings. The background shows the cutting board for trimming adhesive tape and membranes. . . . .	139
Fig.5.12	Micrometer - 0.5 mm thread. One graduation line therefore equals 25 $\mu$ m. . . . .	140
Fig.5.13	Screenshot of the software indicating how values/curve should look like. . . . .	141
Fig.5.14	Finished acquisition of the isoelectric point at pH 3.28. . . . .	142
Fig.5.15	Measuring periphery showing electrodes and hoses. The waste hose is depicted in fluid disposal function. . . . .	143
Fig.5.16	SurPASS <sup>TM</sup> 3. . . . .	144
Fig.5.17	List of drying agents including several properties. <sup>[15]</sup> . . . . .	145
Fig.5.18	Selected images of CAF, abstracted from literature <sup>[10, 32, 33]</sup> . . . . .	147
Fig.5.19	Failures associated with the epoxy/glass interface. <sup>[16]</sup> . . . . .	148
Fig.5.20	Selected pictures of the diffusion cells. . . . .	149

---



Fig.5.21 Images of the diffusion cell. . . . . 150

# Tables

1.2	Several properties affecting the zeta potential at the solid-liquid interface. <sup>[26]</sup> . . . . .	12
1.4	Illustration of isoelectric points at different pK- and zeta potentials, revealing surface type behavior. <sup>[26]</sup> . . . . .	13
1.6	Basic electronic components mounted on PCBs. Note that this is just an abstract of the most common components. . . . .	15
1.9	An abstract of electrochemical series with respect to copper and associated counter ions. <sup>[19, 27]</sup> . . . . .	23
2.1	Overview of reviewed industrial chemicals in electrokinetic potential analysis. . . . .	62
3.1	Final mean values of the max. adsorption levels including standard deviations. The values are derived by normalizing 96 h measurement data to 24 h. . . . .	68
3.3	Summary of facts of the zeta potential analysis, containing conditioning agents, acidity and IEP values. . . . .	72
3.5	Difference in mass after drying of membranes over MS 4 Å/ CaCl <sub>2</sub> in vacuum for 24 h. . . . .	74
3.7	Difference in mass after drying of membranes over MS4Å/ CaCl <sub>2</sub> in vacuum for several days. . . . .	75
3.9	Functional groups and wave numbers that might be present in the GRECs. <sup>[36]</sup> . . . . .	110